SCIENZE DELL'INGEGNERIA CIVILE

SCUOLA DOTTORALE / DOTTORATO DI RICERCA IN

XXVIII

CICLO DEL CORSO DI DOTTORATO

DEFINITION OF SEISMIC INPUT FOR STRUCTURAL SAFETY EVALUATION. TWO CASE STUDIES: Seismic response of concrete dams; dynamic soil-structure interaction of the Leaning Tower of Pisa

Titolo della tesi

Dott.Ing. Gabriele Fiorentino

Nome e Cognome del dottorando firma

Prof. Camillo Nuti

Docente Guida/Tutor: Prof. firma

Prof. Aldo Fiori

Coordinatore: Prof. firma

Collana delle tesi di Dottorato di Ricerca

In Scienze dell'Ingegneria Civile

Università degli Studi Roma Tre

Tesi n° 58

Sommario

La definizione dell'input sismico è un punto fondamentale per la valutazione della risposta dinamica delle strutture. Strutture strategiche quali le dighe o edifici monumentali che fanno parte del patrimonio architettonico necessitano che l'input sismico venga valutato con uno studio ad hoc, specialmente per un territorio caratterizzato da una sismicità medio-alta quale quello italiano. Nella presente tesi di dottorato viene presentato un metodo "ibrido" per la valutazione della pericolosità sismica, attraverso il quale combinando i tradizionali approcci probabilistico e deterministico si ottiene un terremoto di scenario. I parametri geofisici di questo evento sismico vengono quindi utilizzati per la selezione di accelerogrammi spettro-compatibili. La procedura proposta è stata quindi applicata a due casi studio di riferimento: nel primo caso a due dighe in calcestruzzo, per le quali è stata calcolata la risposta dinamica con un approccio step-by-step, partendo da analisi semplificate di scorrimento alla base fino ad arrivare ad analisi accurate in 3D con la valutazione del danno atteso. Nel secondo caso è stata valutata la risposta dinamica della Torre pendente di Pisa, dapprima analizzando gli studi esistenti ed individuandone le criticità, quindi definendo l'input sismico alla base tenendo in considerazione l'interazione suolo-struttura e le prove geofisiche eseguite nella Piazza dei Miracoli.

Abstract

The definition of the seismic input is an essential step for the evaluation of the dynamic response of structures. Strategic structures like dams or monumental buildings which are part of the architectural heritage require a specific study in order to evaluate the seismic input, especially in a country with medium-high seismicity like Italy. This work uses a hybrid approach for the evaluation of the seismic hazard, by matching the probabilistic and deterministic methods in order to obtain a controlling earthquake. The geophysical parameters of this event are then used for the selection and adjustment of spectrum-compatible accelerograms. The procedure is applied to two case studies: the first is represented by two concrete dams, for which the dynamic response is evaluated through a step-by-step method: starting from simplified analyses to obtain dam base sliding to more accurate analyses which can allow an estimate of the expected damage on the structure. The second case study the dynamic response of the Leaning Tower of Pisa is assessed, first through an identification of the critical issues in the existing studies on the topic, then by defining the seismic input considering soil-structure interaction and the recent geophysical tests performed in the Square of Miracles.

Contents

FIGURES INDEX ..... **XI**

TABLES INDEX ..... **XXII**

1 INTRODUCTION **1**

1.1 AIM OF THE STUDY 1

1.2 THESIS LAYOUT 3

PART I - DEFINITION OF SEISMIC INPUT **5**

2 SEISMIC RISK AND STRUCTURES **5**

2.1 SEISMIC RISK 5

2.2 SEISMIC RISK IN ITALY 9

2.3 SEISMIC HAZARD AND STRATEGIC STRUCTURES 9

2.4 SEISMIC HAZARD AND ARCHITECTURAL HERITAGE 12

3 PROCEDURE TO EVALUATE SEISMIC INPUT **19**

3.1 INTRODUCTION 19

3.2 PSHA VS DSHA - HYBRID APPROACH 22

3.3 PROBABILISTIC SEISMIC HAZARD ASSESSMENT 24

3.4 CRISIS 2014 PROCEDURE 49

3.5 SEISMIC HAZARD MODELS FOR ITALY: MPS04-S1 AND SHARE PROJECT 50

3.6 DISAGGREGATION 54

3.7 DETERMINISTIC SEISMIC HAZARD ASSESSMENT 60

3.8 VERTICAL SPECTRA AND V/H RATIO 64

4 SELECTION OF ACCELEROGRAMS 67

4.1 THE FINAL STEP OF HYBRID APPROACH 67

4.2 SEISMIC CODES REQUIREMENTS 72

4.3 SCALING REAL ACCELEROGRAMS 73

4.4 SPECTRAL MATCHING 82

PART II - SEISMIC RESPONSE OF CONCRETE DAMS 85

5 INTRODUCTION 85

5.1 ITALIAN CODE DAMS CLASSIFICATION 88

5.2 ITALIAN CODE SEISMIC REQUIREMENTS 90

5.3 ICOLD BULLETIN 148 93

5.4 SELECTION OF A RETURN PERIOD 97

6 DEFINITION OF SEISMIC INPUT 98

6.1 EVALUATION OF SEISMIC HAZARD FOR 4 SITES 98

6.2 ANALYSIS OF THE SEISMICITY OF THE SITES 99

6.3 UNIFORM HAZARD SPECTRA 107

6.4 DISAGGREGATION 112

6.5 SCENARIO EARTHQUAKES (DSHA) 118

6.6 SETS OF SCALED AND MATCHED ACCELEROGRAMS 121

7 SIMPLIFIED ANALYSES - EVALUATION OF BASE SLIDING 125

7.1 FOUNDATION-DAM-RESERVOIR INTERACTION: 126

7.2 BASE SLIDING: NUTI- BASILI METHOD (2009) 131

7.3 APPLICATION OF THE METHOD TO A CASE STUDY 135

8 SAFEDAM 146

8.1 A PROBABILISTIC PROGRAM TO EVALUATE DAM BASE SLIDING 146

8.2 SELECTION OF RANDOM VARIABLES 147

8.3 EQUIVALENT STATIC ANALYSIS 148

8.4 DYNAMIC ANALYSES 151

8.5 APPLICATION TO THE CASE STUDY 152

8.6 CONSIDERATIONS 154

9 ACCURATE ANALYSES 156

9.1 CASE STUDIES 157

9.2 FINITE ELEMENT MODEL 158

9.3 PRE-SEISMIC STATE 164

9.4 LINEAR ANALYSES 167

9.5 CHOICE OF ACCELERATION TIME HISTORIES 168

9.6 DISPLACEMENT TIME HISTORIES COMPARISON 169

9.7 EXPECTED DAMAGE 171

PART III - DYNAMIC SOIL-STRUCTURE INTERACTION OF THE LEANING TOWER OF PISA 179

10 INTRODUCTION 179

10.1 AIM OF THIS PART 179

10.2 GEOMETRY OF THE TOWER 182
10.3 ITALIAN GUIDELINES - REDUCTION OF RISK OF CULTURAL HERITAGE 183
10.4 SEISMIC SAFETY ASSESSMENT ACCORDING TO ITALIAN GUIDELINES 184
11 PAST STUDIES ON THE SEISMIC RESPONSE OF THE TOWER 186
11.1 GRANDORI & FACCIOLI (1993) 186
11.2 ISMES (1995) 188
11.3 MACCHI & GHELFI (2006) 192
12 GEOPHYSICAL TESTS 193
12.1 THE GROUND UNDERLYING THE TOWER 193
12.2 EXISTING TESTS 194
12.3 AMBIENT VIBRATION TESTS 197
13 FOUNDATION GEOMETRY AND MODEL 213
13.1 INTRODUCTION 213
13.2 SOIL-STRUCTURE INTERACTION 217
13.3 EXPERIMENTAL MODAL FREQUENCIES 218
13.4 SHEAR MODULUS AT SMALL DEFORMATIONS 223
13.5 WOLF FORMULATION 223
13.6 EVALUATION OF DYNAMIC IMPEDANCES 228
14 MODAL ANALYSIS 230
14.1 SIMPLIFIED MODEL (SAP 2000) 230
14.2 MODAL FREQUENCIES 231

14.3 MODAL SHAPES 232
14.4 MODEL UPDATING 235
15 SEISMIC INTENSITIES EXPECTED IN PISA 238
15.1 GRANDORI & FACCIOLI (1993) 238
15.2 SCENARIO EARTHQUAKES 240
15.3 SELECTION OF ACCELEROGRAMS 250
16 SITE RESPONSE ANALYSIS 255
16.1 INTRODUCTION 255
16.2 DECAY CURVES 257
16.3 ANALYSIS RESULTS 259
17 DYNAMIC RESPONSE OF THE TOWER 262
17.1 TYPE OF ANALYSIS AND RESULTS 262
18 CONCLUSIONS 264
REFERENCES 269

Figures index

Fig. 2.1 Number of deaths caused by earthquakes in 2012 (Daniell, 2012) 5

Fig. 2.2 Direct economic losses in each 2012 CATDAT earthquake (Daniell, 2012) 6

Fig. 2.3 Map of Fujinuma Dam, Fukushima Nuclear Power Plant and the epicenter of the earthquake with MCS intensities (modified from USGS, 2016) 10

Fig. 2.4 Collapse of Fujinuma dam, Japan 2011 11

Fig. 2.5 Collapse of the frescoed vaults in Assisi, 1997 13

Fig. 2.6 Bell Tower of Nocera Umbra cathedral: after collapse (left) after reconstruction (right) 13

Fig. 2.7 Collapse of the Dome of the Church of Anime Sante: Before (left) and after the earthquake (right) 14

Fig. 2.8 Collapse of the facade of the Town Hall of Sant'Agostino, May 2012 15

Fig. 2.9 Collapse of the Bell Tower of Novi (Modena), Before the earthquake (left) and after (right) 16

Fig. 3.1 Proposed procedure to define seismic input 19

Fig. 3.2 ZS9 Seismogenic zoning for Italian territory (Meletti et al. 2008) 27

Fig. 3.3 Hazard curves depending on seismic sources considered 28

Fig. 3.4 Number of earthquake vs Magnitude for Zone 923 30

Fig. 3.5 Gutenberg- Richter relation for zone 923 30

Fig. 3.6 Comparison between GMPEs for Mw 6 and spectral period T=0,1 s 40

Fig. 3.7 Comparison between GMPEs for Mw 6 and spectral period T=1 s 40

Fig. 3.8 Comparison between deterministic spectra for Mw 6, R=10 km 41

Fig. 3.9 Comparison between deterministic spectra for Mw 6, R=50 km 41

Fig. 3.10 PGA Hazard Curve 43

Fig. 3.11 Hazard Curve for structural period T=0,2 s 44

Fig. 3.12 Expected PGA for Italy, P=10% in 50 years (T_R=475 years) (INGV) 45

Fig. 3.13 Expected PGA for Site C, T_R=475 years (INGV) 46

Fig. 3.14 Site C: Elastic Horizontal response spectrum (NTC 2008), T_R=475 years 47

Fig. 3.15 475 years Uniform Hazard Spectra for Site C 48

Fig. 3.16 NTC08 and MPS04 response spectra for different T_R (NTC 2008) 51

Fig. 3.17 Seismic Hazard Maps fpr PGA from MPS04 and SHARE (Meletti 2014) 53

Fig. 3.18 Comparison: NTC08 spectrum and UHS from MPS04 and SHARE 54

Fig. 3.19 Disaggregation for PSA=0,59 g, T=0,1 s 57

Fig. 3.20 Contribution to hazard by Magnitude M for PSA, T=0,1 s 58

Fig. 3.21 Contribution to hazard by Distance R for PSA, T=0,1 s 58

Fig. 3.22 Disaggregation for PSA=0,35 g, T=1 s 59

Fig. 3.23 Contribution to hazard by Magnitude M for PSA, T=1 s 59

Fig. 3.24 Contribution to hazard by Distance R for PSA, T=1 s 60

Fig. 3.25 Controlling earthquakes for site C - 475 years 62

Fig. 3.26 Comparison between UHS and deterministic spectra - SP96 63

Fig. 3.27 Comparison between UHS and deterministic spectra - AB10 64

Fig. 3.28 Effect of soil condition on V/H ratio - SP96 GMPE *65*

Fig. 4.1 Evaluation of an artificial accelerogram with Belfagor (Mucciarelli, 2004) *69*

Fig. 4.2 Main window of the software REXEL (Iervolino, 2010) *78*

Fig. 4.3 Main window of In-Spector (Acunzo, 2014) *80*

Fig. 4.4 Main window of Seismomatch (*83*

Fig. 5.1 Classification of worldwide dams by purpose (ICOLD) *85*

Fig. 5.2 Classification of worldwide dams by dam type (ICOLD) *86*

Fig. 5.3 Map of existing Large Dams in Italy (ITCOLD) *87*

Fig. 5.4 Example of gravity dam *88*

Fig. 5.5 Example of arch dam *89*

Fig. 5.6 Example of arch-gravity dam *90*

Fig. 6.1 Four Italian Dam sites selected for Seismic Hazard Assessment *98*

Fig. 6.2 Composite and individual seismogenic sources for Site A, Piemonte *100*

Fig. 6.3 Seismogenic zones; historical and instrumental seismicity for Site A *101*

Fig. 6.4 Composite and individual seismogenic sources for Site B, Toscana *102*

Fig. 6.5 Seismogenic zones; historical and instrumental seismicity for Site B *102*

Fig. 6.6 Composite and individual seismogenic sources for Site C, Abruzzo *103*

Fig. 6.7 Seismogenic zones; historical and instrumental seismicity for Site C *104*

Fig. 6.8 Composite and individual seismogenic sources for Site D, Calabria *105*

Fig. 6.9 Seismogenic zones; historical and instrumental seismicity for Site D *106*

Fig. 6.10 Geographical coordinates and seismogenic zoning ZS9 in CRISIS 2014 *107*

Fig. 6.11 Definition of recurrence relation parameters in CRISIS 2014 *108*

Fig. 6.12 Definition of GMPE in CRISIS 2014 *108*

Fig. 6.13 Probabilistic response spectra for site A *110*

Fig. 6.14 Probabilistic response spectra for site B *110*

Fig. 6.15 Probabilistic response spectra for site C *111*

Fig. 6.16 Probabilistic response spectra for site D *111*

Fig. 6.17 Disaggregation for Site A: PGA (top), PSA 0,2s (middle), PSA 1s (bottom) *114*

Fig. 6.18 Disaggregation for Site B: PGA (top), PSA 0,2s (middle), PSA 1s (bottom) *115*

Fig. 6.19 Disaggregation for Site C: PGA (top), PSA 0,2s (middle), PSA 1s (bottom) *116*

Fig. 6.20 Disaggregation for Site D: PGA (top), PSA 0,2s (middle), PSA 1s (bottom) *117*

Fig. 6.21 Comparison probabilistic/deterministic spectra for site A *119*

Fig. 6.22 Comparison probabilistic/deterministic spectra for site B *120*

Fig. 6.23 Comparison probabilistic/deterministic spectra for site C *120*

Fig. 6.24 Comparison probabilistic/deterministic spectra for site D *121*

Fig. 6.25 Site D: response spectra of the accelerograms scaled with REXEL *122*

Fig. 6.26 Site D: response spectra of the accelerograms modified with Seismomatch *123*

Fig. 6.27 Comparison between scaled and matched accelerogram #6335 *124*

Fig. 7.1 Dam-reservoir dynamic interaction according to Westergaard *127*

Fig. 7.2 Fenves and Chopra method: Dam-reservoir interaction *128*

Fig. 7.3 Fenves and Chopra method: Dam-foundation interaction *130*

Fig. 7.4 Nuti-Basili model for SDOF non-linear system (Nuti and Basili, 2009) *133*

Fig. 7.5 Plot of μ vs β as presented by Nuti and Basili (Nuti and Basili, 2009) *135*

Fig. 7.6 Highest block of the gravity dam (left) and simplified model (right) *136*

Fig. 7.7 SDOF equivalent system proposed by Nuti and Basili (2009). *137*

Fig. 7.8 SDOF system modeled in Opensees *137*

Fig. 7.9 Response for the accelerogram 006335: (top) relative displacement of nonlinear SDOF compared with a linear one; (bottom) plot of the base sliding. *139*

Fig. 7.10 Base displacement obtained with the 56 analyses for sites A, B, C, D *140*

Fig. 7.11 β-μ points compared with the Nuti and Basili correlation curve. *144*

Fig. 8.1 Relative frequency of Sliding Safety Factors *151*

Fig. 8.2 Equivalent linear and non-linear response (top), residual base sliding (bottom) *152*

Fig. 8.3 Synthetic results of equivalent static analyses *153*

Fig. 8.4 Synthetic results of dynamic analyses *154*

Fig. 9.1 Front view of the gravity dam *157*

Fig. 9.2 Front view of the arch-gravity dam *158*

Fig. 9.3 Finite element model of the gravity dam *159*

Fig. 9.4 Finite element model of the arch-gravity dam *159*

Fig. 9.5 Model of the gravity dam including the foundation *162*

Fig. 9.6 Model of the arch-gravity dam including the foundation *162*

Fig. 9.7 Reservoir model for arch gravity dam in Abaqus *163*

Fig. 9.8 Winter (left) and summer (right) thermal effects for the arch-gravity dam *165*

Fig. 9.9 Pre-seismic state for the gravity dam *166*

Fig. 9.10 Pre-seismic state for the arch-gravity dam *167*

Fig. 9.11 Selected accelerograms for accurate analyses *169*

Fig. 9.12 Crest Displacement time histories for central block of gravity dam *170*

Fig. 9.13 Crest Displacement time histories for central block of arch-gravity dam *170*

Fig. 9.14 Tensional (a) and compressive (b) behavior of the material (Lee and Fenves, 1998) *172*

Fig. 9.15 Damage on the gravity dam - Site A: DS wall (top) and US wall (bottom) *174*

Fig. 9.16 Damage on the gravity dam - Site D: DS wall (top) and US wall (bottom) *175*

Fig. 9.17 Damage on the arch-gravity dam - Site A: DS wall (top) and US wall (bottom) *176*

Fig. 9.18 Damage on the arch-gravity dam - Site D: DS wall (top) and US wall (bottom) *177*

Fig. 10.1 History of the inclination of the Tower (Burland 2009) *179*

Fig. 10.2 Intervention of under-excavation under the Tower (Burland 2009) *180*

Fig. 10.3 Elevation and section of the Tower, N-S direction ([74][79]) *182*

Fig. 11.1 Finite element model (Grandori e Faccioli 1993) *187*

Fig. 11.2 Vibrodyne used by ISMES for the test (1995) *189*

Fig. 11.3 Modal shapes obtained by ISMES (1995) *190*

Fig. 11.4 Finite element model built by ISMES (1995) *191*

Fig. 12.1 Soil profile of the ground underlying the Tower (Burland, 1994) *194*

Fig. 12.2 Comparison of Vs obtained with geophysical tests in the last 25 years *195*

Fig. 12.3 Propagation of body waves in a linear elastic medium *197*

Fig. 12.4 Propagation of surface waves in a linear elastic medium *198*

Fig. 12.5 Geometric dispersion of Rayleigh waves (Foti et al. 2015) *199*

Fig. 12.6 Inverse problem (modified from Foti et al. 2015) *201*

Fig. 12.7 Acquisition system for the Array 2D test *202*

Fig. 12.8 Array 2D test performed in the Square of Miracles, November 2015 *203*

Fig. 12.9 installation of a seismic station close to the Tower *203*

Fig. 12.10 Acquisition phase for station A *204*

Fig. 12.11 Array Transfer function (left) and experimental dispersion curve (right) *206*

Fig. 12.12 Soil profile and dispersion curve obtained with Geopsy *207*

Fig. 12.13 Comparison between geophysical tests including Array 2D results *208*

Fig. 12.14 H/V test performed in the Square of Miracles, November 2015 *210*

Fig. 12.15 Fourier spectra of records (left) Directionality of passive sources (right) *210*

Fig. 12.16 Resonance peaks of H/V spectral curve for a single station *211*

Fig. 13.1 Section of foundation ring (Burland 1994) *213*

Fig. 13.2 Condition of the basement of the Tower before the works by Gherardesca (1838) *214*

Fig. 13.3 Works for the consolidation of the Catino *215*

Fig. 13.4 Connection between the foundation and the Catino (Burland, 2009) *216*

Fig. 13.5 Fondazione della torre e catino di base, configurazione attuale *216*

Fig. 13.6 Schematization of soil-structure interaction (Mylonakis, 2006) *217*

Fig. 13.7 Position of the sensors on the Tower (left) and on the ground (right) *219*

Fig. 13.8 Response recorded on the Tower by sensors S1, S2, S3 *220*

Fig. 13.9 CWT of the recorded tower response *221*

Fig. 13.10 Vertical response due to the vertical mode (Filter 2-4 Hz) *222*

Fig. 13.11 Vertical response due to the bending mode (Filter 0,8-1,2 Hz) *222*

Fig. 13.12 Standard lumped parameter model - Wolf (1994) *223*

Fig. 13.13 Parameters of spring-dashpot-mass model (Wolf, 1994) *224*

Fig. 13.14 Plot of $k(a_0)$ vs a_0 - Horizontal translation *226*

Fig. 13.15 Plot of $k(a_0)$ vs a_0 - Vertical translation *226*

Fig. 13.16 Plot of $k(a_0)$ vs a_0 - Rocking *227*

Fig. 13.17 Plot of $k(a_0)$ vs a_0 - Torsion *227*

Fig. 14.1 Scheme of the FE model *231*

Fig. 14.2 First modal shape - Horizontal, direction E-W *233*

Fig. 14.3 Second modal shape - Horizontal, direction N-S *234*

Fig. 14.4 Third modal shape - Vertical *234*

Fig. 14.5 6th modal shape - torsional *235*

Fig. 15.1 Correlation between PGA and MCS intensity (modified from Sabetta) *239*

Fig. 15.2 Response spectrum obtained by Grandori e Faccioli (1993) *240*

Fig. 15.3 1Uniform Hazard Spectra - 130 years return period *241*

Fig. 15.4 Uniform Hazard Spectra - 500 years return period *241*

Fig. 15.5 Disaggregation for PSA 1s, TR=130 years *243*

Fig. 15.6 Disaggregation for PSA 0,3s, TR=130 years *243*

Fig. 15.7 Disaggregation for PSA 1s, TR=500 years *244*

Fig. 15.8 Disaggregation for PSA 0,3s, TR=500 years *244*

Fig. 15.9 Gutenberg-Richter relation for zone ZS916 *246*

Fig. 15.10 Comparison between spectra - 130 years *247*

Fig. 15.11 Comparison between spectra - 500 years *247*

Fig. 15.12 V/H ratio for the response spectra of the Scenario earthquakes *249*

Fig. 15.13 Comparison Horizontal/vertical spectra - 130 years *249*

Fig. 15.14 Comparison Horizontal/vertical spectra - 500 years *250*

Fig. 15.15 Selected scaled accelerograms - Horizontal - TR=130 years *251*

Fig. 15.16 Selected scaled accelerograms - Vertical- TR=130 years *252*

Fig. 15.17 Selected scaled accelerograms - Horizontal - TR=500 years *252*

Fig. 15.18 Selected scaled accelerograms - Vertical - TR=500 years *253*

Fig. 15.19 Acceleration Time history on rigid soil - CAG *254*

Fig. 16.1 Source-to-site travel path of body waves (Kramer, 1994) *255*

Fig. 16.2 Source-to-site travel path of body waves (Yoshida, 2015) *256*

Fig. 16.3 G/G_0 decay curve for Pisa clays *258*

Fig. 16.4 D/γ curve for Pisa clays *259*

Fig. 16.5 Non-linear amplification function *260*

Fig. 16.6 Response spectra of the accelerograms at ground level - T_R=500 yrs *261*

Fig. 16.7 Ground surface time history acceleration - Event Umbria-Marche CAG *261*

Fig. 17.1 Acceleration time history of node 30 - Event Umbria-Marche CAG *263*

Fig. 17.2 Displacement time history of node 30 - Event Umbria-Marche CAG *263*

Tables index

Tab. 3.1 EC8 Site Classification *35*

Tab. 3.2 Parameters of the considered GMPEs *39*

Tab. 3.3 Controlling earthquakes based on disaggregation *62*

Tab. 5.1 Definition of Design Earthquakes for SEE *95*

Tab. 6.1 Case studies sites for the evaluation of seismic input *99*

Tab. 6.2 Controlling earthquakes for the case studies *118*

Tab. 6.3 Intervals of Magnitude and distance for REXEL *122*

Tab. 7.1 Results of simplified analyses *141*

Tab. 7.2 Statistical parameters of the base residual displacement for the different groups of signals *143*

Tab. 11.1 Parametri terreno Grandori e Faccioli (1993) *186*

Tab. 11.2 Caratteristiche meccaniche del modello (Grandori e Faccioli 1993) *188*

Tab. 11.3 Numerical results by Grandori e Faccioli (1993) *188*

Tab. 11.4 Results of dynamic test by ISMES (1995) *189*

Tab. 11.5 Results obtained with two numerical models by ISMES *191*

Tab. 11.6 Position of the centroids of each Ordine, after Macchi e Ghelfi (2002) *192*

Tab. 12.1 Ranges of parameters to constraint the problem *206*

Tab. 13.1 List of the considered seismic events. *220*

Tab. 13.2 Comparison of results from different authors *221*

Tab. 13.3 Values of $k(a_0)$ for the identified modes *228*

Tab. 13.4 Values of the dynamic impedances (units: kN/m^2) *229*

Tab. 14.1 Comparison between numerical and experimental frequencies. *232*

Tab. 14.2 Comparison between experimental frequencies and numerical results after model updating. *236*

Tab. 14.3 Comparison between the results of numerical analyses by various authors *236*

Tab. 15.1 Correlation between MCS intensity/T_R/PGA *239*

Tab. 15.2 Selection of controlling earthquakes *245*

Tab. 15.3 Search parameters for ITACA database *250*

Tab. 15.4 Parameters used for the scaled accelerograms - 130 years return period *253*

Tab. 15.5 Parameters used for the scaled accelerograms - 500 years return period *254*

Tab. 17.1 Maximum acceleration and displacement results - 8th Ordine *262*

1 Introduction

1.1 Aim of the study

Recent earthquakes occurred in different areas of the world highlighted the fragility of existing structures and infrastructures. Seismic risk is particularly high for some structures, as strategic structures like hospitals, electric power plants and dams whose collapse could result in a large number of casualties or high economic losses.

Another category of structures whose seismic risk has to be assessed carefully are architectural heritage buildings, First of all because of their historical and artistic value; and then because they are characterized by high fragility of the building itself or of the soil-foundation-structure system. They are often located in highly seismic areas.

For different reasons, for both categories Codes and guidelines, as well as the technical literature require to perform specific studies in certain conditions in order to define the seismic input at a given site. Today the most used methods to evaluate the Seismic Hazard at a site are the Probabilistic approach (PSHA) and the deterministic approach (DSHA). According to some authors, better results can be achieved combining together these two methods. This "hybrid" method can be used to select real acceleration time histories, which are scaled or adjusted in order to obtain spectrum-compatible records. There is a wide range of computer programs that help to obtain these time histories, which can be used to perform non-linear dynamic analyses on structures.

The aim of this research work is to discuss the application of this method to two real case studies providing seismic actions having a strong connection with the seismo-tectonic conditions of the sites under analysis.

The majority of the existing concrete dams was designed and constructed following seismic design criteria which now are considered obsolete. For this reason they need to be re-assessed with analyses that take into account the most advanced numerical techniques and scientific methods. In this work the Seismic Hazard Assessment was performed at four sites

in Italy characterized by a different level of seismicity, then acceleration time histories were selected using two different methods. Initially, for each site a dynamic non-linear analysis was performed to evaluate the base displacement of a dam, modeled as a simplified SDOF system. Subsequently, a gravity dam and an arch-gravity dam were taken into account as case studies for applications. Both structures were studied by means of 3D models, performing non-linear dynamic analyses and evaluating the expected damage.

One of the purposes of this study is to show the importance of the procedure to assess the seismic hazard in the framework of a step-by-step approach for the evaluation of the seismic safety of dams. The process starts from simplified analyses which can be useful to perform a rapid analysis of damage, to then move to more complex analyses which can provide all the parameters needed to state whether a concrete dam is safe or not.

The seismic behavior including soil-foundation-structure interaction of the Leaning Tower of Pisa was object of studies that date back to the end of the 20th century. The foundation of the Tower was consolidated from 1999 to 2001 by means of under-excavation, and the circular ring at the base known as "Catino" was rigidly connected to the foundation, so the boundary conditions of the foundation are changed. For these reasons it was necessary a study to evaluate the dynamic behavior of the Tower. First the hybrid method for the evaluation of the Seismic Hazard was applied to the site of the Square of Miracles in Pisa, in order to obtain the seismic input in terms of response spectra and accelerograms.

According to the Italian Guidelines on cultural heritage, for monuments like the Tower of Pisa a specific seismic hazard assessment has to be

performed. This should take into account the site's specific geologic and geotechnical conditions.

A modal analysis along with a sensitivity analysis was performed to find the modal frequencies of the Tower. These were then compared with the experimental ones while a model updating of the frequencies was done.

In the Square of Miracles in Pisa the soft soil layers underlying the square have a great influence on the amplification of the ground motion. The study of the geophysical tests conducted in the past years and the execution of an Array 2D test performed in November 2015 gave the possibility to create a dynamic profile of the ground up to a depth of 100 meters, and to obtain the motion at the ground level, which was applied on the Tower to evaluate its dynamic response.

1.2 Thesis layout

This work is divided into three parts: in the first part, formed by chapters 2 to 4, the proposed procedure for defining the seismic input is discussed. Chapter 2 contains an introduction on the seismic risk for strategic structures and architectural heritage. Chapter 3 gives a brief overview of the method used, Chapter 4 introduces the hybrid approach to define response spectra and the description of the methods used to select accelerograms.

The second part of the thesis, from chapter 5 to 9, contains the application of the hybrid approach to two concrete dams. Chapter 5 introduces the provisions of Italian Code and ICOLD Bulletin, in chapter 6 the seismic input in terms of response spectra and accelerograms is defined. Chapter 7 and 8 contain applications of the method to simplified analyses of dams with the purpose to evaluate dam base sliding. Finally, chapter 9

discusses the dynamic response of dams with accurate analyses (3D FEM models).

In the third part, from chapter 10 to 17, the assessment of the dynamic soil-structure interaction of the Leaning Tower of Pisa is discussed. Chapter 10 starts with an introduction on seismic Codes and on the history of the works made on the Tower. Chapter 11 investigates past studies on the seismic response of the Tower, while chapter 12 discusses the past and recent geophysical tests performed in the Square of Miracles. In chapters 13, and 14 is presented the study of the interaction between the soil and structure, the modal analysis and the results of the model updating, together with the results obtained from the analysis of experimental records. In chapter 15 the seismic input expected in Pisa is evaluated in terms of response spectra and accelerograms, while in chapters 16 and 17 the results of the site response analysis and of the dynamic response of the Tower are discussed.

Chapter 18 presents a final summary of the work done, some conclusive remarks and possible future developments.

PART I - DEFINITION OF SEISMIC INPUT

2 Seismic risk and structures

2.1 Seismic Risk

The great number of casualties due to earthquakes has highlighted the high fragility level of the existing structures and infrastructures. Earthquakes cause each year a mean annual death toll of 21.800 casualties worldwide. From 1975 to 2005 the number of disasters has increased by about 400%, also depending on the rise in the population and urbanization.

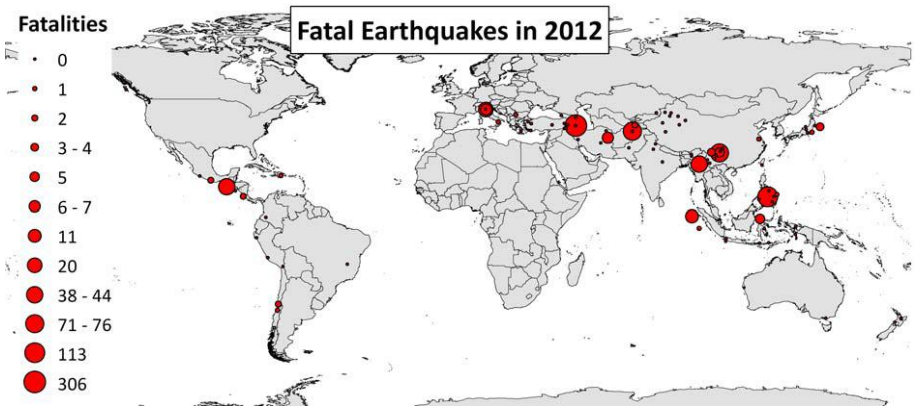

Fig. 2.1 Number of deaths caused by earthquakes in 2012 (Daniell, 2012)

According to 2012 report by CATDAT, a database of the damaging earthquakes, the number of total fatalities occurred that year was between 690 and 727, a quite low number in comparison to the mean annual death toll. Another important fact is related to economic losses. According to [1] a median value of 20,24 billions USD was estimated as amount of the total direct economic losses worldwide.

The highest economic losses in 2012 in the world were caused by the Emilia-Romagna earthquakes (M 5,8 and M 6) occurred in May 2012, with a median value of 17,5 billion USD of direct losses (Fig. 2.2). This large amount of losses is due mainly to two causes:

1. Earthquakes occurred in a highly industrialized area, which is characterized by a high density of factories and industrial plants.
2. The region had little to no seismic zoning under the Italian Codes until 2003. Therefore the majority of industrial plants were built without using appropriate design details against earthquakes.

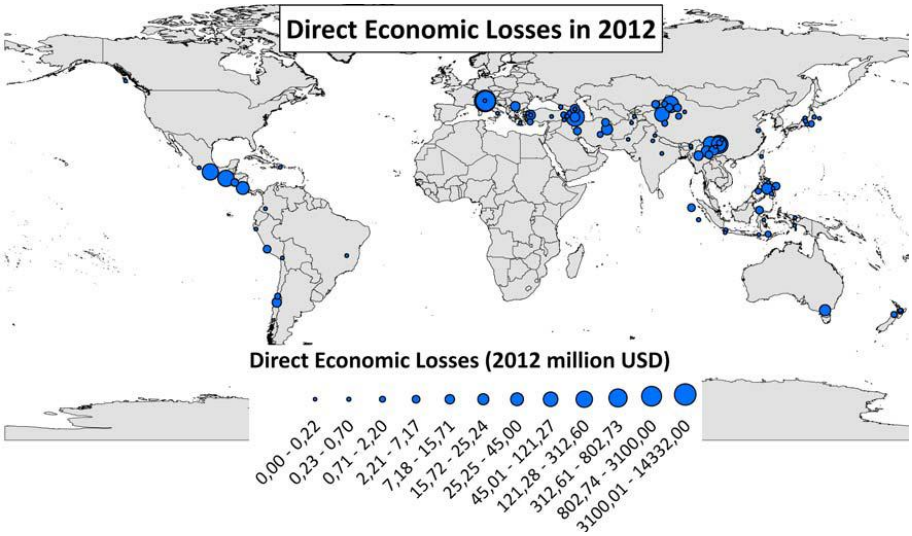

Fig. 2.2 Direct economic losses in each 2012 CATDAT earthquake (Daniell, 2012)

2.1.1 Definition of seismic risk

The definition of Risk and Hazard are often confused with each other, but it could easily be recognized that between these two concepts there is a cause and effect relationship, as indicated for example in [2]. Hazard could be an event which has the potential to create loss. Conversely, Risk

depends on the actual exposure of something which has a human value. The Risk can be evaluated as the combination of the probability of an hazardous event and its negative consequences.

According to these definitions, Seismic Risk is defined as the amount of damage expected at a given site as a consequence of a seismic event in a given time period, depending on the seismicity of an area, on the resistance of buildings and on anthropization. The traditional form to express the seismic risk is:

$$R = H \cdot V \cdot E$$

Where:

- H is the Seismic Hazard
- V is the Vulnerability
- E is the Exposure

Since it is not possible to act on the Hazard and the Exposure, the reduction of seismic Risk is generally performed by reducing the vulnerability of buildings during construction or by retrofitting the existing structures. Another issue is to reduce the probability of damages due to secondary hazards, such as landslides, liquefaction or tsunamis triggered by the earthquake.

2.1.2 Seismic Hazard

The seismic hazard is defined as the probability of occurrence of a given level of seismic intensity at a given site in a defined time period. The seismic intensity can be expressed as local intensity (e.g. X degree of the MCS scale), magnitude or ground motion acceleration, and it represents a measure of the seismicity of an area.

As we will see in the next chapter, there are two approaches to evaluate the Seismic Hazard, namely the Probabilistic Seismic Hazard Assessment (PSHA) and the Deterministic Seismic Hazard Assessment (DSHA).

2.1.3 Vulnerability

The vulnerability is the capacity of buildings to report damages due to an earthquake. The collapse of buildings is the main cause of death during earthquakes.

The Italian Code, D.M. 14/1/2008 (NTC2008), gives prescriptions for the expected behavior of buildings for different levels of seismic intensity. A structure should not be damaged for a low level of seismicity, should not have structural damages for a medium level of seismicity and should not collapse for high seismicity levels, also if major damage can occur.

The vulnerability is the element of seismic risk which can be modified, increasing the resistance of existing constructions. In fact it is possible to lower the vulnerability of buildings with interventions which can improve their capacity to resist to earthquakes suffering minor damages.

2.1.4 Exposure

The exposure estimates the value of objects and people subject to the seismic action and therefore exposed to the seismic risk. For the system of civil protection one of the priorities in case of earthquake is the safeguard of human lives. For this reason it is very important to estimate the number of people involved in such an event, and to evaluate quickly the number of casualties.

This is a complex operation because the estimate depends on a great number of factors, as the type of buildings (residential, industrial, etc), the

hour of the earthquake (day, night), the possibility to hide or to escape somewhere.

In Italy, another aspect of the exposure is the presence of an incredible cultural heritage, formed by the built heritage of the historical centers of Italian cities and small towns.

2.2 Seismic risk in Italy

Italy is characterized by a medium-high level of seismicity (for frequency and intensity), in fact it is one of the European countries with the highest levels of seismicity, because it is placed at the boundary between the African and the Eurasian plates. The vulnerability is very high, due to a fragility of the built heritage, and a very high exposure due to very high density of population and the presence of a cultural, architectural and historical heritage which is unique in the world.

Therefore Italy is a country with a very high seismic risk in terms of victims, damages to the built heritage and direct and indirect costs expected after an earthquake.

2.3 Seismic Hazard and Strategic structures

The evaluation of the seismic hazard is especially important for strategic structures, whose collapse could cause very high damage to goods and a very high death toll. Some examples of strategic structures are highway bridges, nuclear power plants and large dams.

The 2011 Tohoku earthquake (M_w 9,1) was one of the largest and most destructive seismic events of the last years. As it is well known the Tsunami caused the failure of the cooling system at the Fukushima Daiichi Nuclear Power Plant, resulting in an overheating of the nuclear

reactor and the raising of radiation levels inside (1.000 times the normal levels) and outside (8 times the normal levels) the plant.

With regard to dams, the same earthquake caused the collapse of an earth dam with a height of 18 meters, with a reservoir volume of 1,5 million m^3 (See Fig. 2.4). The resulting flood destroyed the village of Naganuma, where 5 houses were washed away, and 8 people lost their lives, as it is reported in [4] and [6]. In the two months after the earthquake, approximately 400 dams were inspected in Japan, and the experts found that the structures had withstood severe ground motions and retained the water, as reported in [4], while minor or moderate damage was found.

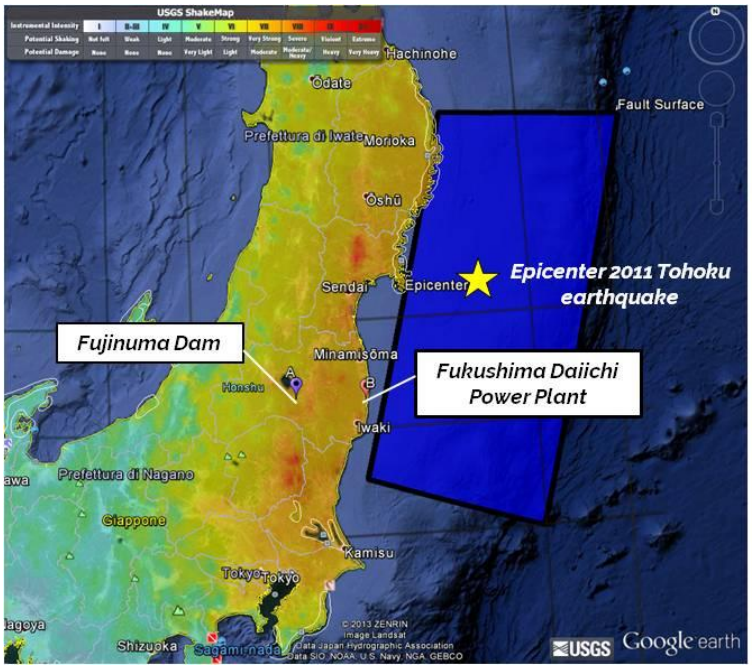

Fig. 2.3 Map of Fujinuma Dam, Fukushima Nuclear Power Plant and the epicenter of the earthquake with MCS intensities (modified from USGS, 2016)

Fig. 2.3 shows the seismic intensity map of the East Coast of Japan, highlighting the positions of the Fujinuma ike Dam and of the Fukushima Nuclear Power Plant.

Until today there have been no collapses of concrete dams due to earthquakes, but some of these structures were seriously damaged, suffering from sliding at the base of the structure, joint opening, collapse of appurtenant structures.

Fig. 2.4 Collapse of Fujinuma dam, Japan 2011

Focusing on Large dams, it is possible to point out that both the recent guidelines of the Italian Code on Dams (2014) and ICOLD (International Committee On Large Dams), the international NGO which is a point of reference in the field on dam engineering, publishing bulletins and guidelines, recommend to evaluate the seismic input for Large dams with appropriate Seismic Hazard studies, instead of using standard Code Spectra.

In fact, as it will be described in sections 5.2 and 5.3, both require a specific seismic hazard evaluation for the dams whose collapse could cause a high risk for the community.

The intensity of the recommended seismic action is very high: For a collapse limit state the return period is:

- 2.500 years for a new dam and 1950 years for an existing dam according to the guidelines of the Italian Code.
- 10.000 years for ICOLD bulletin 148

It is then clear that the seismic hazard must be evaluated with an appropriate study, taking into account all the parameters which could influence the expected intensity at the site.

2.4 Seismic Hazard and Architectural heritage

Italy is the country which has the greatest number of UNESCO world heritage sites in the world, with a total of 47 sites including, as examples, the historic centre of Rome, Piazza del Duomo in Pisa, the city of Venice and its lagoon, and the archeological areas of Pompei (Campania) and Agrigento (Sicily), as reported in [7].

It is straightforward that all these areas and monuments have an extraordinary value, which has to be protected from anthropic, environmental and natural risks. Meanwhile, earthquakes produce great damages to the cultural heritage due to the high level of seismic hazard, together with the fragility which characterizes old masonry constructions, and in particular vaults and domes, high structures such as clock and bell towers, pitched roofs, tympanums and apses of churches.

A recent work by Parisi and Augenti [8] summarizes the damages caused by recent earthquakes in Italy and in the rest of the world.

Fig. 2.5 Collapse of the frescoed vaults in Assisi, 1997

Fig. 2.6 Bell Tower of Nocera Umbra cathedral: after collapse (left) after reconstruction (right)

In the last twenty years, three earthquakes in Italy caused a great number of casualties and major damage to the cultural heritage. From May 1997 to April 1998 an earthquake cluster (M_w 5,7-6) hit the regions of Umbria

and Marche, causing 11 casualties, and damaging important monuments. The largest number of deaths and damages had been in the villages of Cesi, Collecurti, Montesanto, Annifo Villa. In Assisi the dome of the upper Basilica of San Francesco collapsed, causing the death of 4 people and the damage of the vaults, some painted by Giotto and Cimabue (See Fig. 2.5). In Nocera Umbra there were several damages in the historical centre, where the bell tower collapsed (See Fig. 2.6). Only in Umbria a total of 2316 monumental buildings were damaged.

The 2009 L'Aquila earthquake came after a sequence of tremors lasting from January to March, beginning with the M_w 6,3 mainshock on April 6th. The sequence caused 308 deaths and 1600 injured. Over 80.000 buildings were inspected and 30,6% of them were found to be unfit for use. Experts checked 1800 monumental constructions, 55,1% of them were strongly damaged or collapsed. Many others historical buildings, such as the church Basilica di Santa Maria di Collemaggio and the Church of the Anime Sante (See Fig. 2.7).

Fig. 2.7 Collapse of the Dome of the Church of Anime Sante: Before (left) and after the earthquake (right)

Today, while the majority of the modern buildings of the town have been reconstructed, and the 55% of the private buildings of the historical centre was reconstruct or consolidated, as the reconstruction of public buildings is extremely slow, as reported in [10].

The 2012 Emilia-Romagna earthquakes were a series of seismic events which took place from May to June, with seven events with $M_w > 5.0$. Two mainshocks hit the area on 20 and 29 May, causing respectively 7 and 19 casualties, 350 injured, 14.000 homeless people and heavy damage to industrial and historic buildings.

The maximum values for horizontal and vertical PGA were recorded as 0,26g and 0,31g. These earthquakes caused the interruption of business activities in the epicentral area, because of the high level of damage of the industrial plants. While 20 May event had a moderate impact on the

Fig. 2.8 Collapse of the facade of the Town Hall of Sant'Agostino, May 2012

Fig. 2.9 Collapse of the Bell Tower of Novi (Modena), Before the earthquake (left) and after (right)

cultural heritage, 29 May event caused major damage to historical buildings. Two examples of buildings damaged by the earthquake are the Town Hall of Sant'Agostino, in the province of Ferrara (See Fig. 2.8) and the partial collapse of the Bell Tower of Novi, in the province of Modena.

From the experiences of the events of Umbria-Marche (1997-1998) and L'Aquila (2009) it was clear that the evaluation of seismic risk for historical structures has many differences from the assessment of modern structures. In fact, for modern structures the current approach is to consider a seismic input with a probability of occurrence of 10% in 50 years, the normal reference period for a civil construction, resulting in a return period of the seismic action of 475 years.

Considering such a return period could not be appropriate for historical buildings, because the concepts included in the Codes are based mainly on modern structures, while historical buildings are generally built

following criteria which are not based on the principles of the materials and structure mechanics, but on proportions and building techniques known as *Regole dell'Arte,* which were based on past building experiences, intuition and a great knowledge of the materials used. Many of these structures are made of old masonry, which can be particularly weak for seismic actions. Therefore, retrofit solutions for these buildings have to be designed carefully, trying to find a balance between earthquake protection and life safety and the conservation of the cultural heritage.

There are other factors to take into account for historical buildings, as reported in [9]. For example it is possible that buildings with great architectural or historical value could be rarely used. In this case it can be necessary to prevent the collapse of the structure, while life safety and immediate use of the building are not a priority. Otherwise, there are structures with a minor importance which can be public buildings, for which life safety and immediate use are necessary.

In [9] the authors proposed a method to define seismic input, evaluating Code response spectra by dividing the usual return period (i.e. 475 years) for some coefficients γ ranging from 0,5 to 2, increasing or decreasing the seismic input. This factors are function of the intended use of the building, its historical and architectural value.

In 2011 the Italian Government proposed a Directive which contained the guidelines for the "Evaluation and the reduction of the seismic risk for the cultural heritage" [11], referring to the existing Italian Code. In presence of soft heterogeneous soil, and depending on the different stiffness and continuity of shallow soil layers, and on topographic discontinuities there may be ground motion amplification effects, both in terms of maximum accelerations and frequency content.

In this document it is stated that in these cases it is necessary to perform specific analyses of local seismic response, taking into account the available studies on local seismic response and micro-zoning.

If conversely the stratigraphic and topographic conditions fall in the categories described in paragraph 3.2.2 of Italian Code [12], it is possible to use the response spectra defined by the Code.

3 Procedure to evaluate seismic input

3.1 Introduction

Aim of the procedure used in this work is to define the seismic input, first in terms of response spectrum, then in terms of acceleration time histories, which are useful to perform nonlinear dynamic analyses. A flowchart of this procedure is displayed in Fig. 3.1.

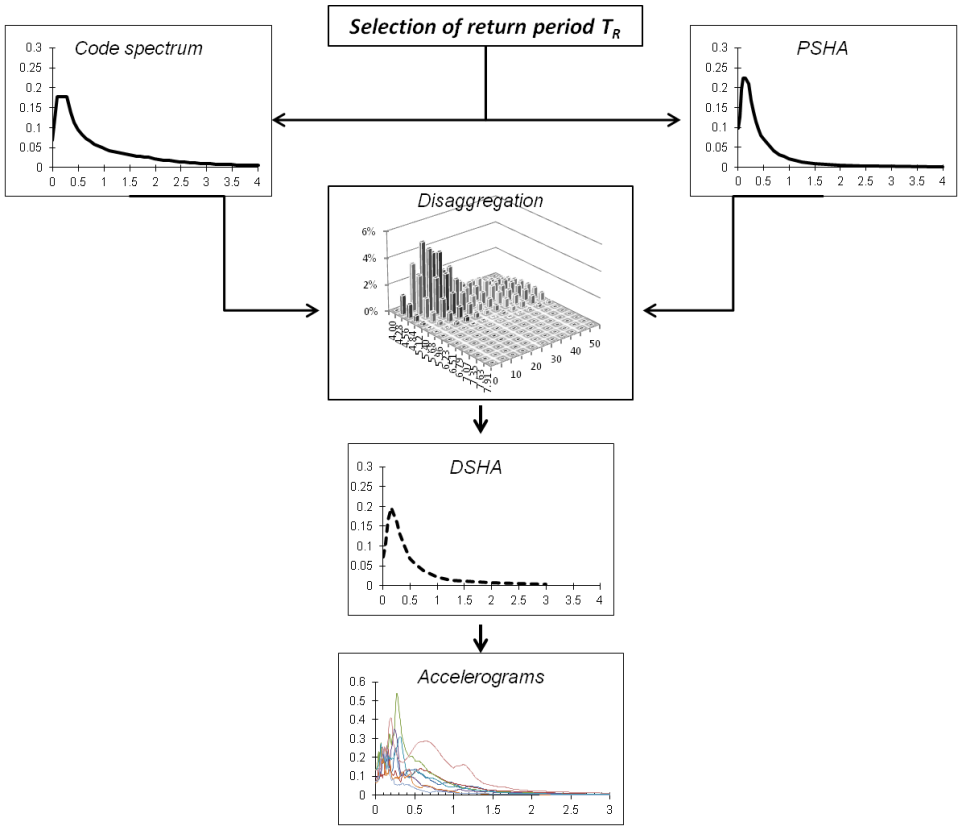

Fig. 3.1 Proposed procedure to define seismic input

The procedure starts with the assessment of a Uniform Hazard Spectrum on rigid soil, which can be evaluated through a Probabilistic Seismic Hazard Assessment, or taken by the Code. In order to evaluate UHS it is necessary to choose an appropriate Return Period T_R, corresponding to a given probability of exceedance of the ground motion intensity level in a given reference period. The PSHA and the Code spectra can be compared to see if there is consistency.

As we will see, the Uniform Hazard Spectra include the contribution to the Hazard of all the sources involved in calculations. Therefore, they provide no information about earthquakes which have produced the spectral accelerations. Disaggregation of the Hazard allows to obtain the M-R combinations which are more likely to produce the expected level of ground motion intensity at the site for a given spectral period, depending on the structure that has to be analyzed.

The disaggregation of the hazard has to be validated by means of a comparison with the historical seismicity of the area of interest, which is generally synthesized in seismic catalogues that include all the historical earthquakes in a certain region.

Searching in the seismic catalogue, which can be reported in a GIS map, one or more Scenario earthquakes can be selected. The Magnitude and the Distance of the Scenario earthquakes have to be close to the value of Magnitude and Distance indicated by Disaggregation of Hazard.

The M-R combination of the Scenario Earthquake is used to generate a **Deterministic Spectrum,** obtained by using deterministically a chosen Ground Motion Predictive Equation (GMPE), which provides the values of a given ground motion intensity parameter (e.g. PGA - Peak Ground Acceleration) as function of M, R, and often also site condition and style of faulting.

Today many GMPEs have been developed for different regions in the world, following different approaches. Some examples of the most recent equations are presented in 3.3.3.

A GMPE, when used deterministically, provides the median value of the intensity parameter, which is the 50-th percentile of the distribution. In the cases proposed in this work the assessment is done referring to the collapse limit state, which generally produces very high levels of seismic intensity. When evaluating the probabilistic response spectrum the uncertainty in the definition of the intensity parameter is automatically taken into account.

If a comparison is made between the two response spectra obtained with the different methods, the Deterministic spectrum would be surely lower than the probabilistic spectrum. Therefore, it is necessary to add to the median value of the deterministic spectrum a certain number of standard deviations σ in order to make the two spectra comparable.

The deterministic spectrum thus obtained is related to a certain couple of M-R values, that could be easily used to search appropriate sets of acceleration time histories on recording databases which are available today. In fact, the final step of the procedure is the selection of spectrum-compatible acceleration time histories.

There are three types of seismic records: Artificial, synthetic and natural accelerograms. Within the framework of the proposed procedure only natural accelerograms are used to perform dynamic analyses because, as it will be discussed in section 4.1, natural accelerograms for obvious reasons better describe real seismic events. Nowadays almost all National Codes and guidelines require to perform analyses using spectrum-compatible records. There are two methods to obtain this compatibility: Scaling and Matching. In this work the sets of accelerograms are obtained

using three computer programs: for dams, accelerograms are obtained with REXEL (scaling) and with Seismomatch-RSPmatch (matching), while for the Tower of Pisa the software In-Spector (scaling) was used.

3.2 PSHA vs DSHA - hybrid approach

Historically, the first method used to evaluate the seismic hazard was the Deterministic Seismic Hazard Assessment (DSHA). This method is based on the selection of a *Controlling Earthquake*, which is selected choosing a seismic event included in the seismic catalogue, on the basis of the seismo-tectonic conditions in the area of the study. The main disadvantage of this method is that it does not provide informations on the probability of occurrence of this earthquake and on the uncertainties.

In the last years the Probabilistic Seismic Hazard Assessment (PSHA) has gradually took over the DSHA, because it can integrate the seismicity of all the seismogenic zones, including the uncertainties on magnitude, distance, Site conditions and style of faulting giving as result the probability of exceedance of a given level of Ground Motion Intensity.

Nevertheless, PSHA has a drawback: since it aggregates the hazard of near and far seismicity sources, there is a lack of information on which earthquake caused the resulting ground motion intensities.

With regard to uncertainty, DSHA considers the scatter by simply adding a certain number of standard deviations to the median value, while PSHA integrates all the possible combinations of all the parameters affecting the Ground Motion Predictive Equations (GMPEs) including the scatter in the calculations.

As reported in [13], for many years the field of earthquake engineering was divided between supporters of one method or another, each faction trying to demonstrate the superiority of its approach.

Today there are proposal to overcome this dichotomy by proposing methodologies to obtain the seismic input which combine the advantages of the two existing methods. In this work a *hybrid* approach is used as proposed by Sabetta et al. [14], and the procedure can be summarize as follows:

1. **PSHA**: Evaluation of the Uniform Hazard Spectra on rigid soil based on the hazard curves for a chosen return period, depending on the considered Limit State. This can be done using computer programs as CRISIS 2014. Evaluation of the Code spectra for the same return period.
2. **Disaggregation** of the seismic hazard, selection of M-R combinations which produces the maximum spectral acceleration.
3. **DSHA**: on the basis of the disaggregation of hazard, the seismic catalogue and the analysis of the active faults and seismic sources near the site, one or more controlling earthquakes can be selected choosing from a seismic catalogue. Response spectra are computed using a predictive equation.
4. **Comparison** between spectra obtained with the two different methods, selection of Design Spectra.

In the following sections the procedure described above will be discussed, focusing on most critical choices involved in the process, as the selection of appropriate predictive equations, the issue of uncertainties and upper bounds.

For each of the steps an application on a realistic site in Italy will be provided. The case study (i.e. site) chosen for this purpose is located in Abruzzo, and it is named Site C since it will be used also in the second part (See details in section 6.1) together with other three sites. The

probabilistic assessment will be done considering a 10% probability of exceedance in a reference period of 50 years, which corresponds to a return period of 475 years, usually considered as reference return period to make comparisons between hazard estimations.

The scale of magnitude used in this work is the *Moment Magnitude Scale*, also denoted as M_W or M. In the following sections, if not specified, the notation M indicates this magnitude scale.

3.3 Probabilistic Seismic Hazard Assessment

Probabilistic Seismic Hazard Assessment (PSHA) is a method that allows to evaluate the Seismic Hazard Curves at a site, which provide the probability of exceedance for different levels of strong ground motion, at a given site in a given time period. The method permits to include the effects of far or near single seismic sources. From this curves it is possible to obtain Uniform Hazard Spectra.

The method was presented by professor A.C. Cornell in a paper called "Engineering seismic risk analysis" [14]. Within the PSHA framework it is possible to identify and combine in a rational manner all the uncertainties due to the dimension, position, earthquake occurrence rate and variation of the ground motion parameters.

Differently from the Deterministic Seismic Hazard Assessment, seismic hazard is not based on a particular seismic event (or *Scenario Earthquake*), but takes into account all the seismic events which can produce an effect on the given site.

Cornell's method is based on 3 hypothesis:

a) The occurrence of a given seismic event is a Poisson process (events are independent and stationary in time).

b) Magnitude of the event follows an exponential probability distribution.

c) Seismicity is uniformly distributed on each seismic source.

Poisson process

According to hypothesis a) of the PSHA method the occurrence of seismic events is described by a Poisson process. The probability to have a given number *n* of events in a given time of duration *t* is expressed by the Poisson probability distribution:

$$p[N=n]=\frac{(\lambda_m t)^n e^{-\lambda_m t}}{n!} \qquad n=0,1,2,...$$

Where λ_m is the average occurrence rate of the seismic events. From the structural engineering point of view, it is important to evaluate the probability to have at least one seismic event with Magnitude greater or equal to a given value of Magnitude *m* in a given time period, corresponding to the reference period (lifetime) of a structure V_R.

Applying the definition of the Poisson probability distribution, and considering that $\lambda_m=1/T_R$, it is possible to obtain the following relations:

$$P[N\geq 1]=1-P[N=0]=1-e^{-\lambda_m t}==1-e^{-\frac{V_R}{T_R}}$$

$$P[N\geq 1]=1-e^{-\frac{V_R}{T_R}}$$

With this expression it is possible to evaluate the probability to have a seismic event with a return period T_R in the lifetime V_R. If the following values are considered T_R=475 and V_R=50, the result obtained is the same as the value reported in the Italian Code:

$$P[N\geq 1]=p=10\%$$

By inverting the expression it is possible to obtain the return period:

$$T_R = \frac{-V_R}{\ln(1-p)}$$

Minimum informations required to apply the method are the *recurrence relation*, an estimate of the average level of seismic activity for each of the seismic sources, and the *Predictive Equation*, an expression that relates the Ground Motion Intensity parameters to the Magnitude and Distance of a seismic event from a given site.

The Standard procedure for the PSHA consists of 4 steps:

1. Identification and characterization of seismic sources.
2. Evaluation of the parameters of the recurrence relation.
3. Selection of a Ground Motion Predictive Equation (GMPE).
4. Evaluation of the Hazard Curves and Uniform Hazard Spectra.

3.3.1 Identification and Characterization of seismic sources

The available informations on geological and seismo - tectonic features of the region of interest, together with the data contained in the seismic catalogues, are used to identify and characterize the seismic sources.

In Italy, INGV (National Institute of Geophysics and Volcanology) has worked on the seismic zoning of the entire Italian territory, defining the ZS9 seismogenic zoning [16]. Within this framework, Italy has been divided in 36 zones, where earthquakes have the same probability of occurrence in every point of the area (See Fig. 3.2). The first step of the method is therefore to select all the seismic sources which fall in a circular area of radius R, which can be chosen equal to 100 km.

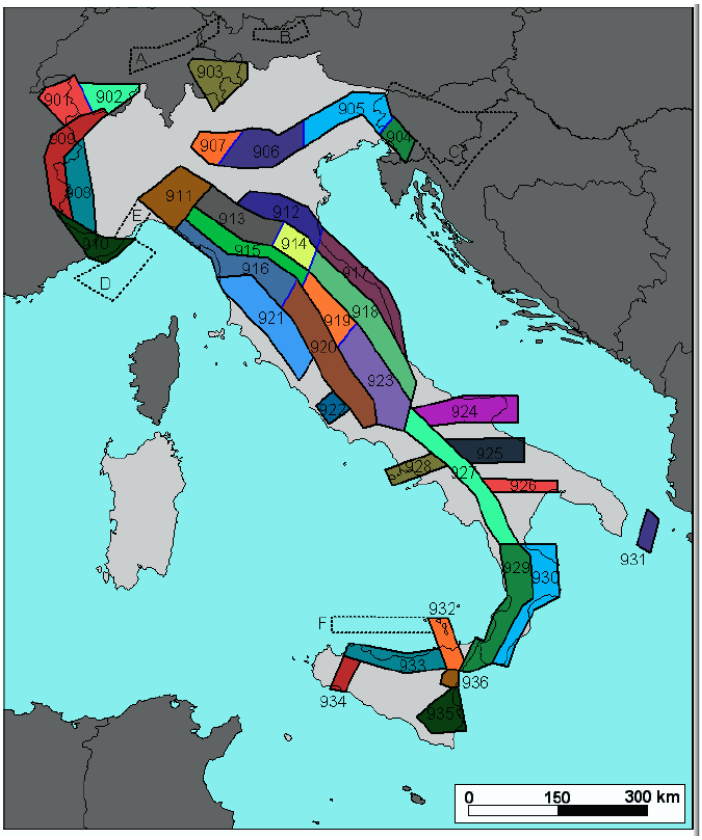

Fig. 3.2 ZS9 Seismogenic zoning for Italian territory (Meletti et al. 2008)

In fact Ordaz [17] performed the evaluation of the seismic hazard for a site placed at the center of a circular seismic zone, characterized by uniform seismicity and parametric values of radius; R=10, 30, 100, 200 km.

Fig. 3.3 shows the results obtained for the different cases. For a given site, there is a sort of *cone of vision* for the site, so just a part of the seismic source contributes to hazard. It is possible to observe that there is a great difference between a seismic source with R=10 km, and one with R=30 km.

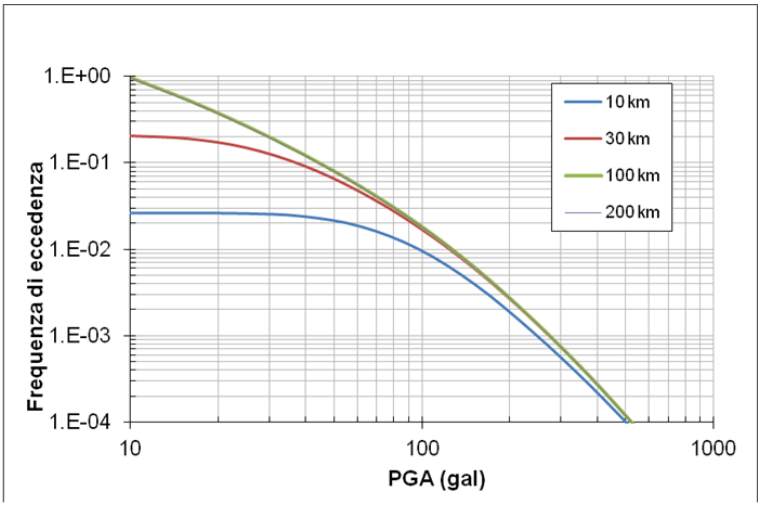

Fig. 3.3 Hazard curves depending on seismic sources considered

Comparing this last source with the R=100 km source, we can see the over 100 gal (cm/s^2) the contribute to hazard is almost the same, fact that is yet more evident comparing R=100 km source with R=200 km source. Therefore, it is possible to conclude that with the given parameters, only the area within 100 km from the site gives its contribution to seismic hazard.

3.3.2 Recurrence relations

It is well known that Gutenberg and Richter [18] showed that there is a logarithmic relation between the cumulative frequency of earthquakes and their Magnitude:

$$\log \lambda_m = a - bm$$

This relation includes the informations about all the earthquakes of a given seismic zone, giving the exceedance rate λ_m of each Magnitude value, while a and b are parameters to determine with a linear regression analysis. A Truncated G-R relation is often used in common practice,

taking into account the fact that seismic sources cannot generate earthquakes with magnitude major than a certain value M_{max}, and that earthquakes with $M<M_0$ are not important for engineering purposes.

Parameter *a* represents the seismic activity (the higher is, the greater is the seismicity), while *b* defines the relative probability to have large or small earthquakes. The reciprocal of λ_m is the return period T_R, that is the average time period between events with Magnitude major than a given value *m*.

Earthquake data are described in seismic catalogues, where for each seismogenic source it is possible to identify all the main informations about the seismic events.

Taking into account the relation, by composition with the exp function we obtain:

$$\lambda_m = 10^{a-bm} = e^{\ln 10(a-bm)} = e^{\alpha-\beta m}$$

So we obtain β=bln10 and α=aln10. This expression shows that the Earthquake Magnitude follows an exponential distribution, that is possible to write as follows:

$$f_M(m) = \beta \cdot e^{-\beta m}$$
$$F_M(m) = 1 - e^{-\beta m}$$

Where f_M is the probability density function and F_M is the cumulative probability distribution.

The Gutenberg-Richter relation is based on the fact that the number of earthquakes in a given region decreases with Magnitude. This is shown in Fig. 3.4 for zone 23, where is possible to observe that, for example, for M 4,5 there are more than 50 earthquakes, while for M 7 there is only one.

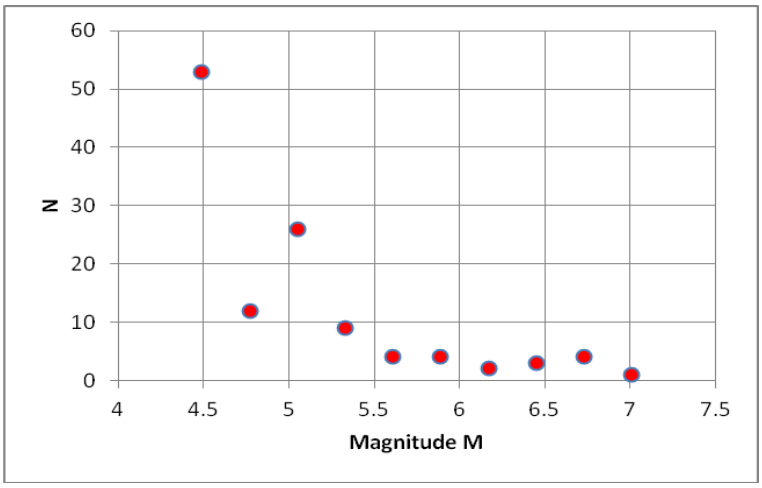

Fig. 3.4 Number of earthquake vs Magnitude for Zone 923

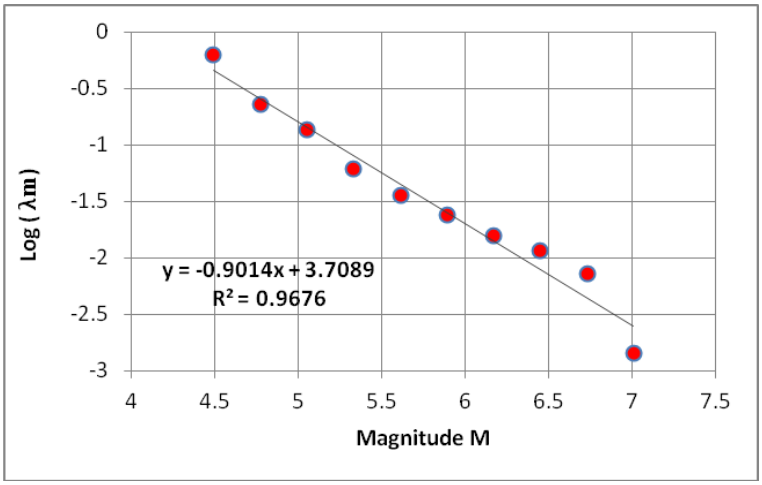

Fig. 3.5 Gutenberg- Richter relation for zone 923

If the number of earthquakes is divided for the years of the catalogue in which these events were observed (*Completeness Interval*), the annual relative frequency is obtained. This frequency is summed for all zones and plotted in logarithmic value versus the Magnitude, obtaining the Gutenberg- Richter relation for the zone as depicted in Fig. 3.5. The linear

relationship is highlighted by the linear regression, which parameters will be used for the probabilistic assessment.

3.3.3 Selection of Predictive Equations

Ground Motion Predictive Equations (GMPEs) represent the Ground Motion model, giving the intensity of the Ground Motion (e.g. PGA/PSA) as function of Magnitude and source-to-site Distance. Other parameters which can affect local intensity are the soil type (e.g. rock, shallow or deep alluvium deposits), or the style of faulting (e.g. Normal, Reverse, Strike-Slip).

The parameter chosen in this work to measure the seismic local intensity is the spectral acceleration, or S_a, which is function of the frequency f (or period T) and damping ratio ξ of the oscillator, so it is possible to write it as $S_a(f, \xi)$.

Generally GMPEs are expressed with an equation:

$$\ln(S_a) = g(M, R, \theta) + \varepsilon \cdot \sigma_{\ln S_a}$$

Where g is the functional form used to predict the Ground Motion intensity parameter, σ_{lnSa} is the standard deviation of ln (S_a). θ is a variable depending on the soil conditions and style of faulting at the site. ε is the Ground Motion randomness, which will be better explained in section 3.6.

Strong Motion Intensity parameters generally increase with Magnitude, decrease with epicentral distance, and for low velocity soil are higher than for rock sites. Nowadays many GMPEs are available, each one has been defined referring to a particular region or country.

In this section are given some examples of predictive equations. The choice of these specific relations is due to the fact that these GMPEs are

at the base of the Hazard models existing for Italy. In fact, SP96 was used to develop project S1 of INGV from which derive the spectral shapes used in the Italian Code, ITA10 was also connected to Italian data, while AB10 and CF08 were implemented in project SHARE. A comparison between these hazard models is done in section 3.5.

- SP96, relation by Sabetta and Pugliese, 1996 [19];
- ITA10, relation by Bindi et al., 2011 [20];
- AB10, relation by Akkar & Bommer, 2010 [21][22][23][24];
- CF08, relation by Cauzzi & Faccioli, 2008 [25].

While the initial data are different for each equation, the procedures to obtain the relation is similar for all, adapting an analytical expression to strong motion records taken from accelerometric databases.

When real accelerograms are available, in general in areas with a high seismicity, it is possible to perform regression analyses on observed data. When there is a lack of observed data there are two options, namely the analysis of regression of simulated accelerograms (using real records for small earthquakes to constrain the distance parameter), or using hybrid methods, which are capable to describe complex source effects from observed data and modifying them for regional differences.

Within the framework of the Seismic Hazard Assessment, the input element which has strongly developed in the last twenty years are the predictive equations. This fact is due to the great number of strong motion data available today, because the accelerometric networks are developing all over the world, and also because recent studies use more complete functions to describe the attenuation of the ground motion. The availability of more data brought to larger values of dispersion, as will be described in the next sections.

Sabetta and Pugliese 1996

The predictive equation SP96 was obtained using a database of 190 horizontal and 95 vertical components of natural accelerograms recorded for 17 Italian earthquakes. The limits of the geophysical parameters used in this predictive equation are the following:

- **Spectral periods** range from 0,033 s to 4 s.
- **Magnitude**: The magnitude of the considered records ranges from 4,6 to 6,8. Magnitude scale used is M_S (surface waves magnitude).
- **Source-to-site Distance**: The type of distance used is epicentral distance. Based on the considered records the limitation for distance is R≤100 km.
- **Site condition:** the equation considered three types of soils: rigid soil or rock, shallow alluvium soils (H≤20 m), deep alluvium soils (H≥20 m).

Regression analysis of PGA and PGV and of the spectral ordinates was performed using the vertical component and the greater value between the horizontal components The response spectra was evaluated in terms of PGV with a damping ratio of 5%.

The functional form of the predictive equation is:

$$\log\left[PSV(T;M;R)\right] = a + bM + c\log\left(R^2 + h^2\right)^{1/2} + e_1 S_1 + e_2 S_2 \pm \sigma_{\ln y}$$

Where

- *PSV* is the Peak Spectrum Velocity;
- $f_1(M) = bM$ is the magnitude function;

- $f_2(R) = c\log(R^2 + h^2)^{1/2} + dR$ is the distance function, formed by a first term and a second term, which takes into account respectively the geometric attenuation and the inelastic attenuation or scattering
- S_1 and S_2 are two dummy variables, $S_1=S_2=0$ for rigid soil, $S_1=1$ for shallow alluvium, and $S_2=1$ for deep alluvium

Bindi et al. 2010

This predictive equation was developed within the framework of project S4-Italian Strong Motion Database, funded by the Department of Civil Protection (DPC), to improve the quality of the Italian Strong Motion database ITACA [26]. 1213 recordings from 218 earthquakes and 353 were considered, and by excluding stations with missed information on the moment magnitude, stations with one record only and earthquake recorded only by one station, they arrived to a final database of 769 records recorded in 99 seismic events in 150 different stations. This predictive equation included also the 2009 L'Aquila seismic events, which contributed to give informations on some combinations of M and R which were quite rare in the Italian database. Regarding seismic parameters used in this study, the following ranges of parameters were provided:

- **Spectral periods** ranging from 0,033 s to 4 s
- **Magnitude** ranges from M 4 to M 6,9
- **Source-to-site distance** was extended from to 200 km from 100 km of the first predictive equations by Bindi et al. (2010), ITA08. The type of distance used in this equation is the R_{JB} distance, which is defined as the minimum horizontal distance from the surface projection of the fault rupture.

- **Style of faulting** was considered for all the recordings, using 4 different types, namely Normal (593), Reverse (87), Strike Slip (61), Unknown (28). Therefore, the number of records with unknown style of faulting is quite low.
- **Site condition**: Conversely from SP96 and from ITA08, this study implemented the site classification of EC8, which is synthesized in Tab. 3.1.

Tab. 3.1 EC8 Site Classification

Class	Vs (m/s)
A	>800
B	360-800
C	180-360
D	<180
E	5 to 20 m of C or D

The functional form of ITA10 is:

$$\log_{10} Y = e_1 + F_D(R, M) + F_M(M) + F_S + F_{sof}$$

Where e_1 is a constant term, F_D is the distance function, including a term which decreases linearly with the distance to consider the inelastic attenuation, F_M is the magnitude function and F_S and F_{Sof} are respectively the functions which consider the site conditions and the style of faulting. In the following expressions M_{ref}, M_h and R_{ref} have to be determined.

$$F_D(R, M) = [c_1 + c_2 (M - M_{ref})] \log_{10} \left(\sqrt{R_{JB}^2 + h^2} / R_{ref} \right) - c_3 \left(\sqrt{R_{JB}^2 + h^2} - R_{ref} \right)$$

$$F_M(M) = \begin{cases} b_1 (M - M_h) + b_2 (M - M_h)^2 & \text{for } M \leq M_h \\ b_3 (M - M_h) & \text{otherwise} \end{cases}$$

Cauzzi and Faccioli 2008

This predictive equation spreads from the will of the authors to give more importance to the concepts of the capacity design, which considers a performance-based design of structures. Within this framework the relative displacement of the structure has become the main indicator of the seismic demand. Main methods which take into account the non-linear behavior must consider displacements related to spectral periods which overcome the classical range of periods 0-4 s. This is why the spectral periods considered in this project range from 0,05 s to 20 s.

The records were selected forming a new worldwide database which collects recordings with high quality standards, mainly recorded digitally (only 9 accelerograms are analog-type), selected on the basis of site conditions, and with minimum disturbances of the signal. The accelerograms selected come from databases of Iran, Japan, United States, and the strong motion of the Imperial College of London for Italy and Europe recordings. A total of 1155 earthquakes from 60 earthquakes were considered.

- **Spectral periods** range from 0.05 s to 20 s due to capacity design requirements.
- **Magnitude** of the selected records ranges from M 5 to M 7,2, the minimum value of magnitude was selected due to the results of disaggregation performed in Italy on a probabilistic base, showing that earthquakes with Mw<5 has low or no effect on the strong motion intensities.
- Also maximum **Source-to-site distance** was chosen on the basis of the disaggregation, and the maximum value of distance is 150 km. In this predictive equation the focal distance R was chosen.

- **Site classes** considered were taken from EC8 classification, with a contribution from different site condition as follows: Class A 6%, Class B 43%, Class C 38%, Class D 9%. The remaining 4% is from unknown site condition.
- **Style of faulting:** The predictive equation takes into account the focal mechanisms of the earthquake considered: Strike slip earthquakes are around 53,3%, Normal faults are 26,7% and Reverse faults are 20% of the total.

Akkar and Bommer 2010

Akkar and Bommer predictive equation is based on the concept of a pan-European predictive model, which considers the seismically active regions of Southern Europe (Italy, Greece, Spain), the Maghreb (North Africa) and the Middle East.

The data set considered 532 accelerograms from 131 earthquakes, and it is the same database of the predictive equation that Akkar and Bommer presented in 2007 (See [22] and [23] for references). That study aimed to provide predictive equations for displacement response ordinates to update the response spectra of Eurocode 8.

- **Spectral periods** range from 0.033 s to 3 s due to capacity design requirements. In the works made in 2007 the maximum period was 4 s.
- **Magnitude** of the considered signal ranges from M 5 to M 7,6. The distance metric used in that work was the R_{JB}.
- **Source-to-site distance** was chosen to be within 100 km

- **Site condition:** the predictive equation considers two types of soils: soft soils, defined by a V_{S30}< 360 m/s, and stiff soils, defined by V_{S30}>750 m/s.
- **Style of faulting:** there are two variables in the equations which allow to choose between Normal and Reverse faults.

This predictive equation has been updated in the last years , including some important features: first of all the data set was updated, considering 1041 records coming from 221 earthquakes, which are part of a databank extended and upgraded starting from the database of the SHARE [34] project.

The Magnitude range was extended, starting from M 4. The range of spectral period is also larger, from 0,01s to 4s. The distance of applicability was raised up to 200 km. In a parallel work also the predictive equation for the V/H ratio was developed.

The functional form of the predictive equation also developed, arriving to a more complex form which is considered not of interest of this work. The functional form of 2010 Akkar and Bommer Predictive equation is the following:

$$\log(PSA) = b_1 + b_2 M + b_3 M^2 + (b_4 + b_5 M)\log\sqrt{(R_{jb}{}^2 + b_6{}^2)} + b_7 S_S + b_8 S_A + \\ + b_9 F_N + b_{10} F_R + \varepsilon\sigma$$

This is the same form used in their 2007 work, but in 2010 model they derived the equations for the prediction of the pseudo-spectral acceleration. In this equation, SS and SA are two dummy variables which are equal to 1 respectively for soft soils and for stiff soil sites. In the same way, FN and FR are the dummy variables for the style of faulting.

A comparison between the parameters of the predictive equations discussed above are displayed in Tab. 3.2.

Tab. 3.2 Parameters of the considered GMPEs

	Database		M range		R range	Spectral periods (s)		Site class	Sof
GMPE	N_R	NE	Mmin	Mmax	Rmax	Min	Max		
SP96	285	17	4.6	6.8	100	0.033	4	rock, soft	-
ITA10	769	99	4	6.9	200	0.033	4	EC8	yes
CF08	1155	60	5	7.2	150	0.05	20	EC8	yes
AB10	532	131	5	7.6	100	0.033	3	rock, soft	yes

Predictive equations can be compared in order to show the attenuation of the ground motion intensity with distance. Fig. 3.6 and Fig. 3.7 show a comparison of the median values of the above described GMPEs, respectively for a spectral period T=0,1 s and a spectral period T=1 s. In both cases a Magnitude M 6 was used.

By observing Fig. 3.6, that is for small spectral periods, it is possible to distinguish two "groups" of equation at near source-to-site distances, one formed by ITA10 and SP96 equation, with smaller values of spectral accelerations, and the other by CF08 and AB10, which for small periods are dominant.

This fact is confirmed by evaluation of the median value of the response spectra computed with a deterministic approach for the same value of Magnitude, M 6, and for distances of 10 km and 50 km, displayed in Fig. 3.8 and Fig. 3.9.

For short distances the spectrum obtained with AB10 has larger values from PGA (T=0) up to T=0,6 s, CF08 has also large values for very short periods, up to T=0,2 s. For long periods the largest values are obtained with SP96 and AB10.

At large source-to site distances the entire range of periods is dominated by equations SP96 and AB10.

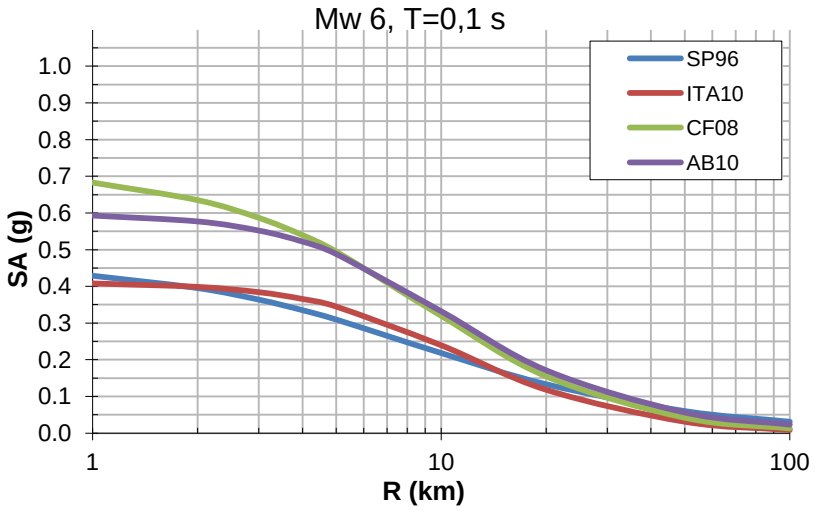

Fig. 3.6 Comparison between GMPEs for Mw 6 and spectral period T=0,1 s

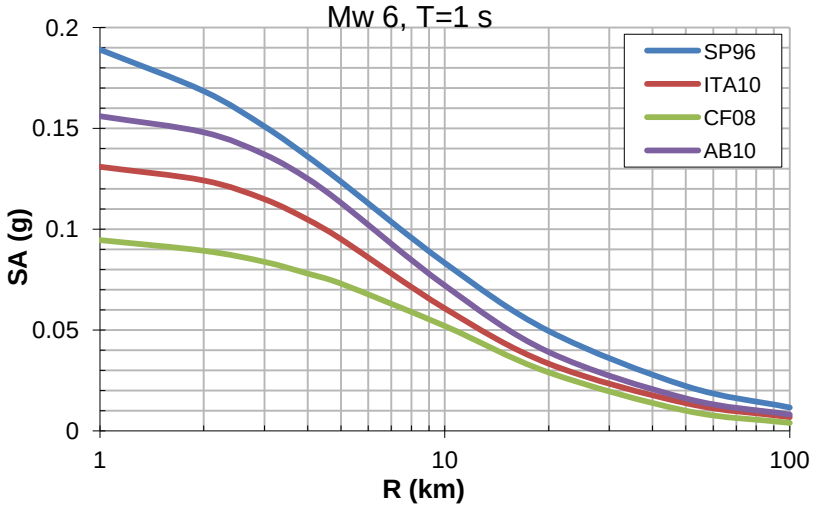

Fig. 3.7 Comparison between GMPEs for Mw 6 and spectral period T=1 s

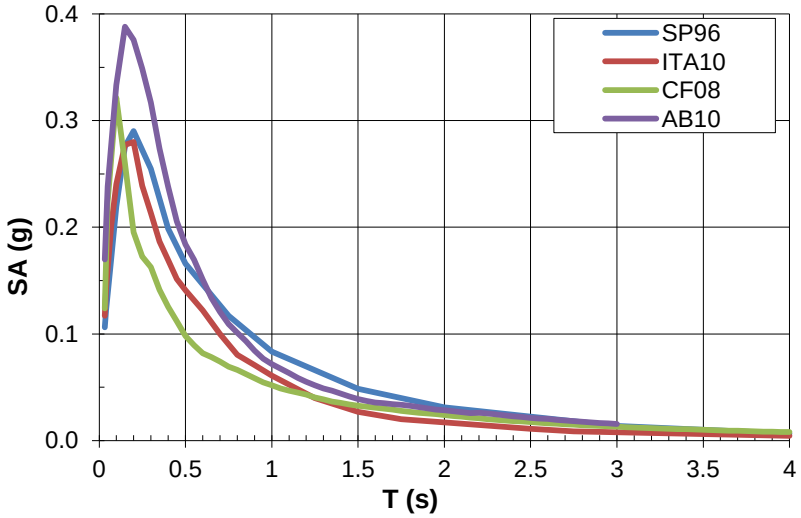

Fig. 3.8 Comparison between deterministic spectra for Mw 6, R=10 km

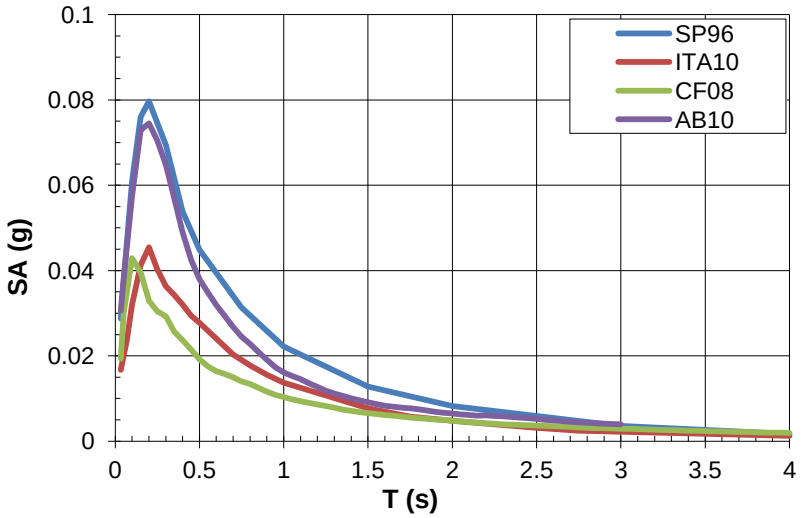

Fig. 3.9 Comparison between deterministic spectra for Mw 6, R=50 km

3.3.4 Hazard Curves and UHS

Procedure

For a given source or seismogenic zone, the probability that a parameter of Ground Motion $Y>y^*$ is:

$$P(Y > y^*) = \int_{M_0}^{M_{\max}} \int_{r_{\min}}^{\infty} P[Y > y^* \mid m, r] \cdot f_M(m) \cdot f_R(r) dm dr$$

Where:

- $f_M(m)$ is the probability density function of Magnitude.
- $f_R(r)$ is the probability density function of Source-to-site distance.

By aggregating over all N zones the exceedance annual rate $\lambda_{m,}$ the total exceedance annual rate is obtained, being:

$$\sum_{i=1}^{N} \lambda_{mi}$$

Obtaining:

$$P(S_a > x) = \sum_{i=1}^{N} \lambda_{mi} \int_{M_0}^{M_{\max}} \int_{r_{\min}}^{\infty} P[S_a > x \mid m, r] \cdot f_{Mi}(m) \cdot f_{Ri}(r) dm dr$$

Hazard curves are obtained solving the integral. Usually this is done using numerical integration, because in real cases the integral cannot be solved analytically. Computer programs as CRISIS 2014 [27] can solve the integral using numerical methods.

From the perspective of civil engineering is more interesting to evaluate the response spectrum, in order to apply the evaluation of the Seismic Hazard to actual structures.

As an example, the procedure to evaluate the response spectrum with a return period of 475 years (10% of exceedance in 50 years) from the Hazard Curves is described.

The software CRISIS 2014 evaluates a hazard curve for each spectral period. On the Hazard Curve (e.g. PGA Hazard Curve, for T=0) it is possible to identify the exceedance rate corresponding to a return period of 475 years, with its reciprocal:

$$\lambda_m = \frac{1}{475} = 0{,}0021$$

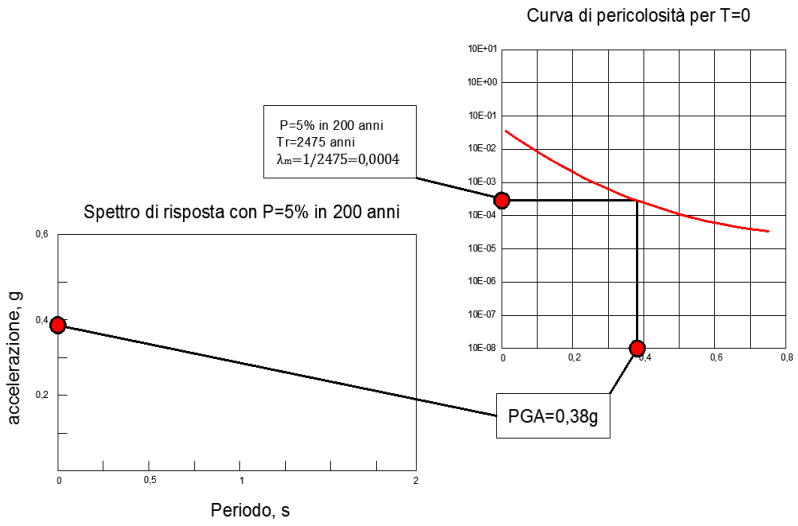

Fig. 3.10 PGA Hazard Curve

On the Hazard Curve the corresponding value of PGA can be identified. This value is reported on a plot of the spectral acceleration versus the Structural period (See Fig. 3.10).

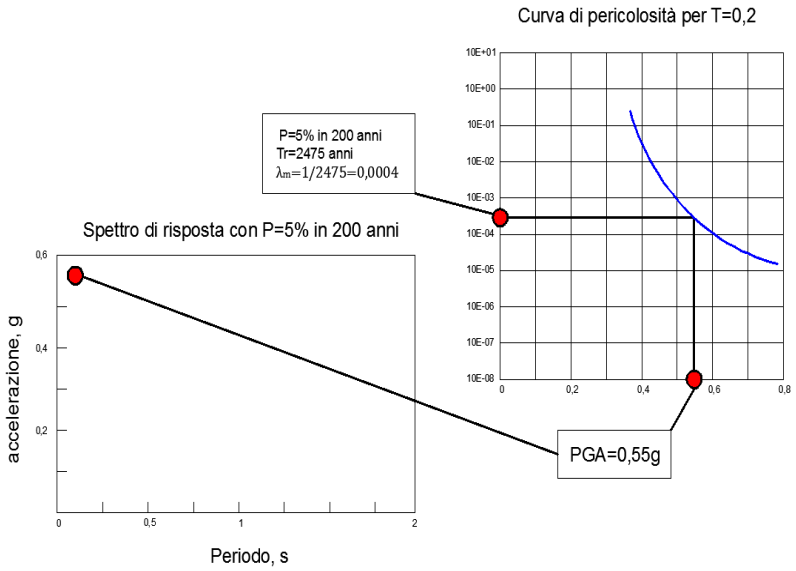

Fig. 3.11 Hazard Curve for structural period *T=0,2 s*

To obtain the second spectral ordinate the above described procedure must be repeated taking into account the Seismic Hazard Curve relative to the spectral period T=0,2 s (Fig. 3.11).

This spectrum is called Uniform Hazard Spectrum (UHS), because each point of the spectrum has the same probability of exceedance. UHS can be used to perform response spectrum analysis, or to obtain accelerograms useful for a time-history analysis.

3.3.5 Italian Code Spectrum

Italian Code for constructions (NTC 2008 or NTC08) requires at paragraph 3.2 to evaluate the seismic input relating to the "Reference Seismic Hazard" parameters at the site. On the basis of these parameters it is possible to evaluate the spectral shapes of the Limit States defined by the Code itself.

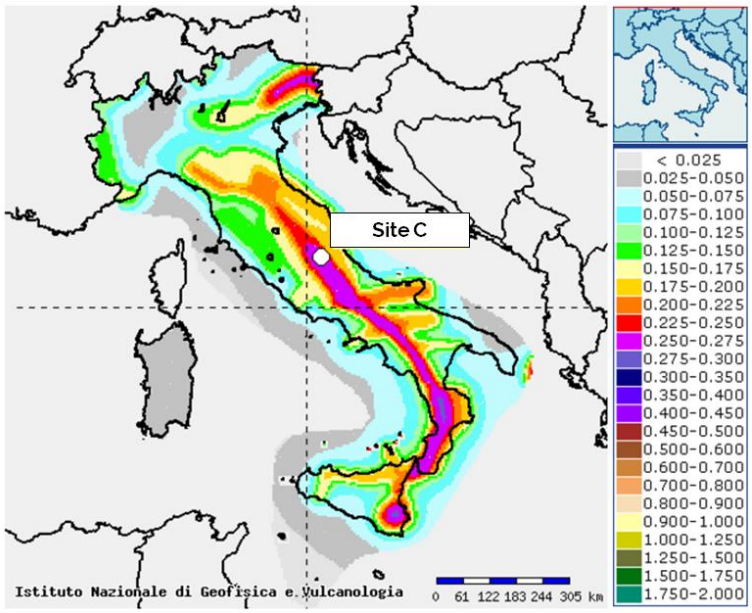

Fig. 3.12 Expected PGA for Italy, *P=10% in 50 years (T_R=475 years)* (INGV)

Within the framework of the Italian Code, the probability of occurrence of a seismic event with a given Ground Motion intensity in a time period V_R is called P_{VR}. The Response spectra given by the Italian Code are obtained by Uniform Hazard Spectra for the Italian territory.

The reference seismic hazard reported in the Code comes from a study made by INGV and commissioned by the Department of Civil Protection (DPC) which brings to the elaboration of the Seismic Hazard Maps for

Italy. INGV developed over the years 2004-2006 the project S1 [28], in which a probabilistic analysis of the seismic hazard was performed for a regular grid with a pitch of 5 km.

Fig. 3.12 shows the Italian Hazard map in terms of maximum horizontal acceleration expected, called *ag* in the Code, as reported in the website of the S1 project, for a P_{VR}=10% in 50 years corresponding to a return period of 475 years.

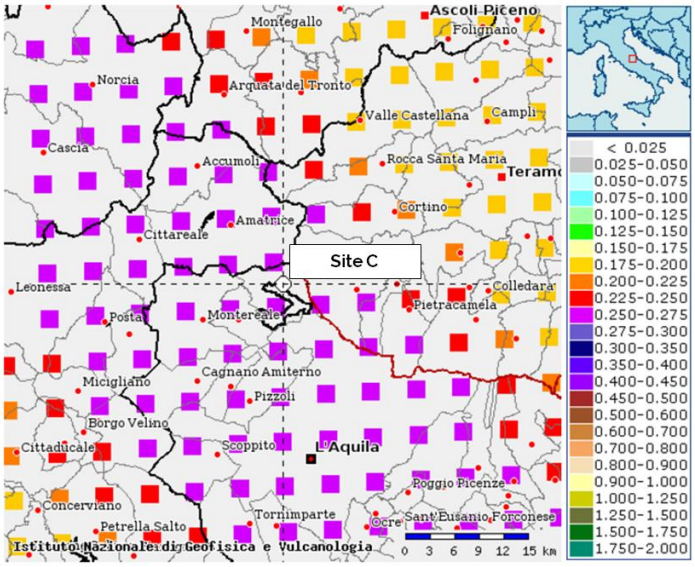

Fig. 3.13 Expected PGA for Site C, T_R=475 years (INGV)

In the map it is possible to note the areas with the highest hazard highlighted in purple, corresponding to an acceleration interval ranging from 0,25g to 0,275g.

Taking as an example Site C in Abruzzo, *ag* reaches a value of 0,25g, obtained from the interpolation of the four points on the grid closer to the site (See Fig. 3.13).

This value of *ag* corresponds to the spectral ordinate for T=0, that is the PGA, in the response spectrum given by the Code, which is displayed in Fig. 3.14.

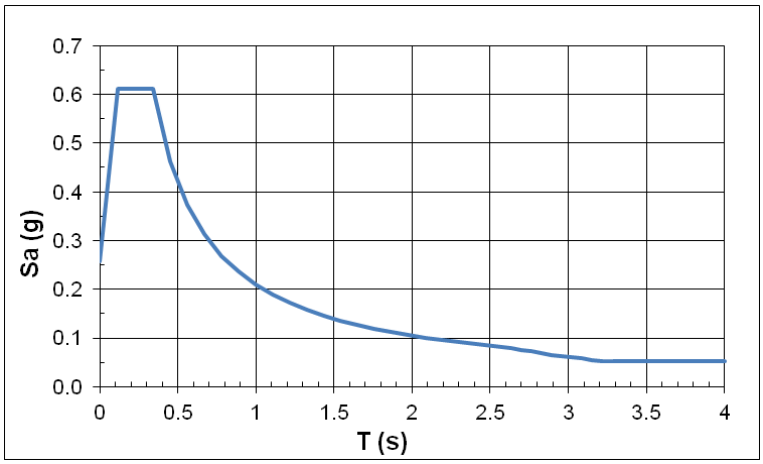

Fig. 3.14 Site C: Elastic Horizontal response spectrum (NTC 2008), T_R=475 years

3.3.6 Application

Fig. 3.15 shows the comparison between Uniform Hazard Spectra obtained for the case study with the software CRISIS 2014 using two different Ground Motion Predictive equations, SP96 by Sabetta and Pugliese and AB10 by Akkar and Bommer, and the Italian Code spectrum. The results presented are evaluated using a 475 years return period.

It is possible to observe that there is a good agreement between the Code spectrum and the other two spectra. The response spectrum obtained with Sp96 GMPE is greater than the Code spectra for all the periods, while there is a better match between the Code spectra and the response spectrum obtained with AB10 predictive equation. Code spectrum has a

"plateau", a smoothed part which takes into account the fact that in natural recordings there are a lot of peaks and valleys.

The nature of the Uniform Hazard Spectra will be more clear in section 3.7, in which a comparison between probabilistic and deterministic spectra is made.

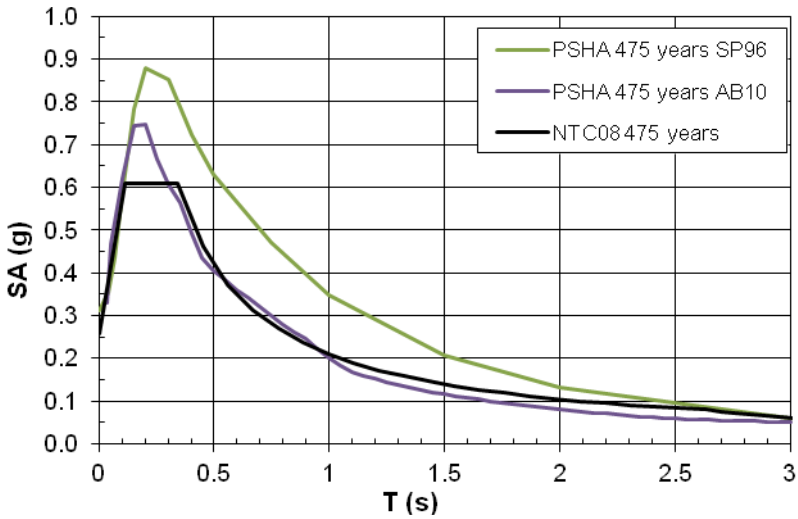

Fig. 3.15 475 years Uniform Hazard Spectra for Site C

3.3.7 Upper Bounds

Ground motion acceleration records show a great variability in the level of intensity, so the GMPEs, derived by regression analyses on a very large set of these records, can show a large scatter from the median values. Some authors, as Bommer [13], highlighted that a comparison between median values and median values +1 standard deviation can bring to differences of 80-100%. This fact can have effects both on PSHA and DHSA.

In PSHA, for high return periods the intensity parameters lie on the tail of the distribution, so that the values of intensity can theoretically increase without a limit, giving rise to physically unrealistic acceleration. For this reason it is necessary to introduce upper bounds, as is discussed in a report of the PEGASOS project (2004) [30] and in a paper by Sabetta et al.(2014) [14]. There are various methods to specify thresholds for predictive equations, for example truncating at a certain number of standard deviations [30]. Various proposals for the range of values for the threshold of truncation for the PSHA are available in literature, some stating that a physically correct value must range from 2 to 4,5 standard deviations [13]. In this work, for probabilistic assessment calculations, a threshold at 3σ was chosen.

In DSHA, the problem of assessing upper bounds is very important. First, it is needful to highlight that the DSHA method is not fully deterministic, as the GMPEs are derived with probabilistic calculations. In the framework of the hybrid approach here proposed, it is necessary to choose the appropriate ground motion randomness ε in order to compare the results obtained with PSHA and with DSHA.

While there is a trend to use the 84-percentile (that is the median +1σ) level of motion in the deterministic assessment, in the literature no indication is given on how to choose the ε, as reported by Sabetta et al. [31] and Krinitzsky [32], but its value must be chosen in order to match the spectra obtained with the probabilistic assessment.

3.4 CRISIS 2014 procedure

The software CRISIS 2014 [27], used in this work to assess the Seismic Hazard Curves, follows a different procedure to evaluate Hazard Curves in comparison with the method proposed by Cornell.

As an example, it is assumed to have a number *N* of seismogenic sources, each one at a distance r_i from the site, and the aim of the Seismic Hazard Assessment is to evaluate the Hazard of a site placed at a distance r_1 from source 1.

First a value of PGA (e.g. PGA=0,2 g) is chosen. By inverting the GMPE it is possible to evaluate the Magnitude $M_{0,2}$ which produces that level of ground shaking.

$$\log(PGA) = c_1 + c_2 M - c_3 \log(r^2 + h_0{}^2)^{1/2}$$

$$M_{0,2} = \frac{1}{c_2}\left[\log(0,2) - c_1 + \frac{c_3}{2}\log(r_1{}^2 + h_0{}^2)\right]$$

From the Gutenberg-Richter relation, the average annual exceedance rate for the earthquakes of the source 1 which have Magnitude $M_{0,2}$ can be obtained.

$$\lambda_{m1}(0,2) = 10^{(a-bM_{0,2})}$$

The procedure is repeated for several PGAs and is aggregated for all the seismogenic sources. The Hazard Curves are obtained from the exponential distribution (Poisson process)

$$P[a > a_i \mid t] = 1 - e^{-t\sum_{i=1}^{3}\lambda_{mi}}$$

3.5 Seismic Hazard models for Italy: MPS04-S1 and SHARE project

The SHARE project (Seismic Hazard Harmonization in Europe, see [33]) at the beginning of 2013 began to distribute the results of a probabilistic hazard model developed for Europe. The results include Seismic Hazard maps for various return periods for PGA and many spectral ordinates, Hazard Curves, Uniform Hazard Spectra and disaggregation of Hazard.

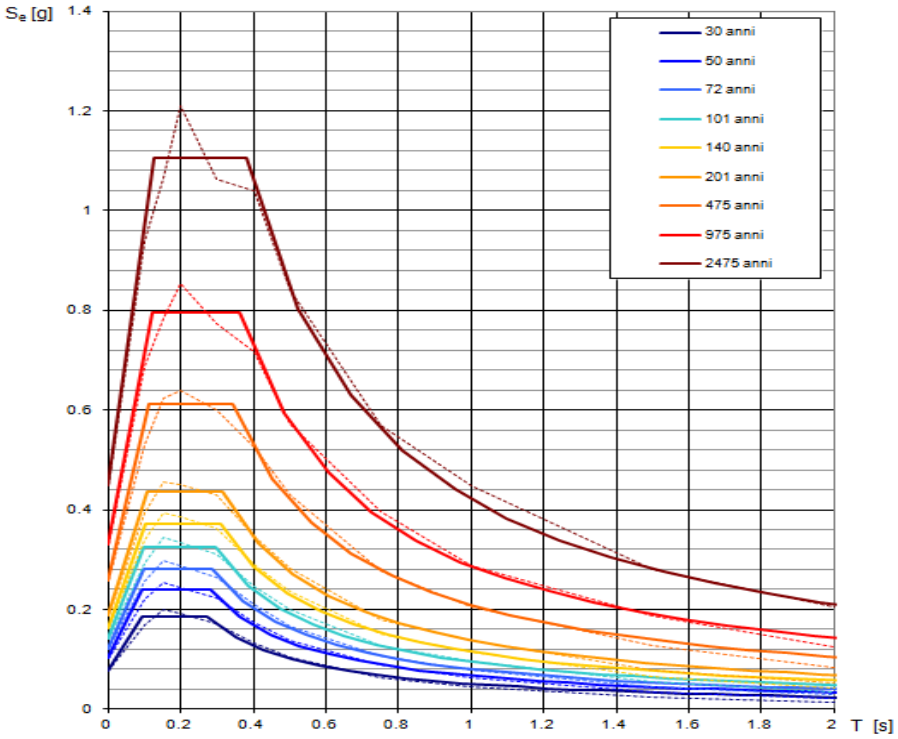

Fig. 3.16 NTC08 and MPS04 response spectra for different T_R (NTC 2008)

These results represent the most recent contribution to Hazard studies in Italy, since the last study conducted was project S1 of the model MPS04, developed by INGV and commissioned by the Department of Civil Protection (DPC) which has brought to the elaboration of the Seismic Hazard Maps for Italian territory. MPS04-S1 was developed after the revision of the seismic Code which took place after the earthquake in San Giuliano di Puglia [28]. The last Italian Directives (Ordinanza PCM 3274/2003, Ordinanza PCM 3519/2006) and then the Italian Code Norme Tecniche per le Costruzioni (NTC08) derive from this project, as shown in Fig. 3.16. The figure is taken from the Italian Code Excel program

Spettri-NTC which displays the comparison between the NTC08 and MPS04 response spectra for different return periods.

SHARE project is born from a declaration of European Program FP7, which pointed out that EC8 would gradually take over for national Codes, but its provisions were based mainly on national seismic hazard zonations. Seismic hazard in European countries was assessed in very different and often incompatible ways, so there was a need to harmonize the methodologies for seismic hazard zonation in Europe.

Some authors, for example Meletti et al. [34], tried to compare the results obtained by the different projects, since these differences affect the way to compute the seismic input according to EC8 and national Codes.

The Hazard Maps provided by project MPS04 and SHARE are displayed in Fig. 3.17 in terms of PGA for a probability of exceedance of 10% in 50 years, which corresponds to a return period of 475 years. From the comparison between the two maps, performed by Meletti in the same study, emerges that for PGA the values of the project SHARE are higher in many areas of Italy, but for other spectral ordinates, for example T=0,5 s and T=1 s the values obtained for SHARE project are lower.

This fact could be highlighted by making a direct comparison between the UHS obtained with the two methods, which is depicted in Fig. 3.18 for Site C and for a return period of 475 years.

SHARE response spectrum has larger values for PGA and for T<0,2 s, while MPS04 response spectrum has larger values for T>0,2 s. The main reasons for this important differences between were highlighted by Meletti et al. in the same work, stating the following facts: MPS04 is based only on one seismogenic zonation, which is ZS9, while SHARE project is based on three different models, considering ZS9, a model

including active faults and composite sources, and a model with scattered seismicity.

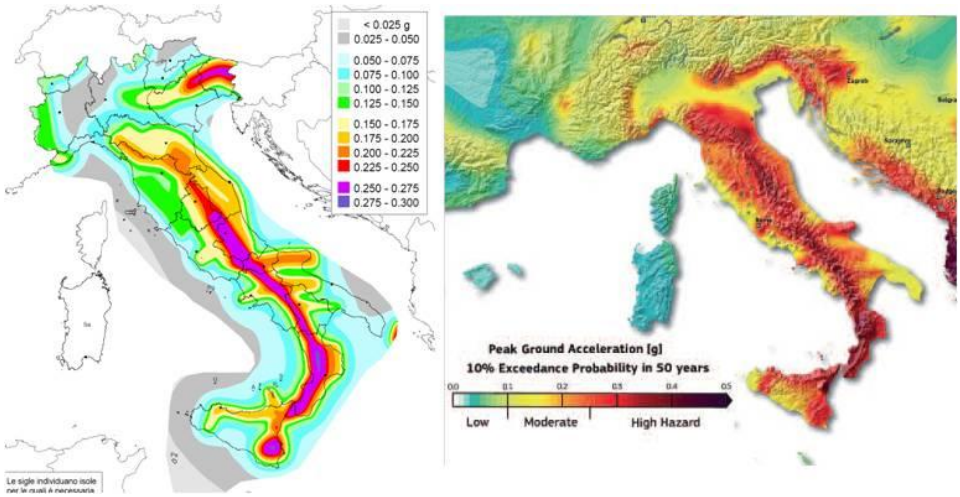

Fig. 3.17 Seismic Hazard Maps fpr PGA from MPS04 and SHARE (Meletti 2014)

SHARE used more updated seismic catalogues because is more recent, with better definitions of completeness intervals and maximum magnitude.

However, the main cause of the differences comes from the different predictive equations used by the models. MPS04 was based on the GMPEs of Sabetta and Pugliese, 1996, Malagnini et al., 2000, Marasca et al., 2002 and Ambraseys et al., 1996.

SHARE model is based on the predictive equation by Akkar and Bommer, 2010, Cauzzi and Faccioli, 2008, Zhao et al., 2006, and Chiou and Youngs, 2008.

It is important to observe that the attenuation models used in MPS04 defined the Ground motion parameters as the maximum value between the horizontal components, while SHARE takes the average value.

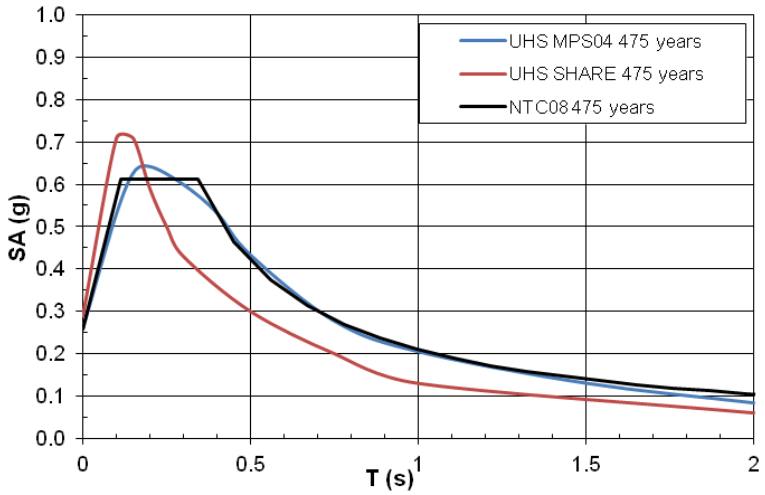

Fig. 3.18 NTC08 spectrum and UHS from MPS04 and SHARE for Site C

3.6 Disaggregation

3.6.1 Procedure

The evaluation of the Seismic Hazard with PSHA considers a great number of seismic intensities and seismogenic sources, providing an aggregated description of the Seismic Hazard, with the main drawback that the Uniform Hazard Spectra does not provide any information on which seismic event (e.g. earthquake with M 6.0, R=15 km) caused that local intensity.

When designing a structure, verification or decision-making it is often useful to define a *Design Earthquake*, as known as *Scenario Earthquake* or *Controlling Earthquake*, characterized by a Magnitude M and a distance R.

Disaggregation, with a method first introduced by McGuire [35] and Bazzurro and Cornell [36], allows to obtain a design earthquake

representing accurately the UHS. As described above, Ground Motion parameters depend mostly on M and R. The intensity level shows a great uncertainty, which can be represented by another random variable, ε, called ground motion randomness, which is the fraction of the standard deviation that must be added to the median value predicted by M and R.

It is possible to express the mean annual frequency of exceedance also as function of ε, as reported in the following equation:

$$P(S_a > x) = \sum_{i=1}^{N} \lambda_{mi} \int_{M_0}^{M_{\max}} \int_{r_{\min}}^{\infty} P\left[S_a > x \mid m, r, \varepsilon\right] \cdot f_{Mi}(m) \cdot f_{Ri}(r) \cdot f_{\varepsilon}(\varepsilon) dm dr d\varepsilon$$

To understand which values of M, R and ε give the largest contribution to hazard, it is needful to disaggregate the hazard by expressing the marginal distributions of M-R-ε, then dividing the corresponding annual frequencies by the total annual frequency.

The probability in the integrand function can be replaced with the following expression, where δ is the Dirac function, because the target of the method is to obtain M-R-ε sets which are equal to the target Ground Motion, not exceeding that:

$$P\left[(S_a > x | m, r, \varepsilon)\right] = \delta\left[\ln S_a(m, r, \varepsilon) - \ln x\right]$$

Marginal distributions of M, R and ε can be obtained by removing the corresponding terms from the integral:

$$f_m^{'}(m) = \sum_{i=1}^{N} \lambda_{mi} \iint \delta\left[\ln S_a(m, r, \varepsilon) - \ln x\right] \cdot f_{Ri}^{'} \cdot f_{\varepsilon}^{i} dr d\varepsilon$$

$$f_r^{'}(r) = \sum_{i=1}^{N} \lambda_{mi} \iint \delta\left[\ln S_a(m, r, \varepsilon) - \ln x\right] \cdot f_{Mi}^{'} \cdot f_{\varepsilon}^{i} dm d\varepsilon$$

$$f_{\varepsilon}^{'}(\varepsilon) = \sum_{i=1}^{N} \lambda_{mi} \iint \delta\left[\ln S_a(m,r,\varepsilon) - \ln x\right] \cdot f_{Ri}^{'} \cdot f_{Mi}^{i} dr dm$$

3.6.2 Application to the case study

The disaggregation of the hazard can be displayed aggregating in 1D M bins, or in 2D M-R bins, or in 3D M-R-ε bins. In probability theory, this three different representations of the disaggregation are called Probability Mass Function, respectively of M, M-R, M-R-ε.

In the following figures (From Fig. 3.19 to Fig. 3.24) are displayed the results for a disaggregation analysis conducted on the case study. The graphs show the most common parameters used in literature to discuss the results of disaggregation.

In Fig. 3.14 the contributions to the hazard for different values of Magnitude and Distance are displayed for spectral period T=0,1 s, which corresponds to a spectral acceleration of 0,59 g. Fig. 3.20 and Fig. 3.21 show respectively the contribution to hazard for different values of Magnitude M and for different values of distance D, obtained using the conditional probability of exceedance.

For this spectral period there is a larger contribution to hazard from Magnitudes in the range 5,7-6,2 at distances which fall in the range 10 km<R<20 km, but also small values of Magnitude (4,5-4,7) at near distances (R≤10 km) give a high contribution to the hazard.

Fig. 3.22 shows the disaggregation of hazard for spectral period T=1 s, corresponding to PSA=0,35 g. Fig. 3.23 and Fig. 3.24 show the contribution to hazard separately, in the same way as before. Observing the plot it is clear that in this case there is a very low contribution of near earthquakes with low values of Magnitude, while the values that give the major contribution to hazard are in the range 6,4-6,9 for Magnitude and

from 10 to 20 km for distance R, while there is a contribution also for farther distances (20-30 km).

It is then clear that spectral acceleration for small periods (0,1-0,3 s) are caused mainly by near earthquakes with low values of Magnitude, while spectral acceleration for higher periods (1-2 s) are caused by far earthquakes with larger values of Magnitude.

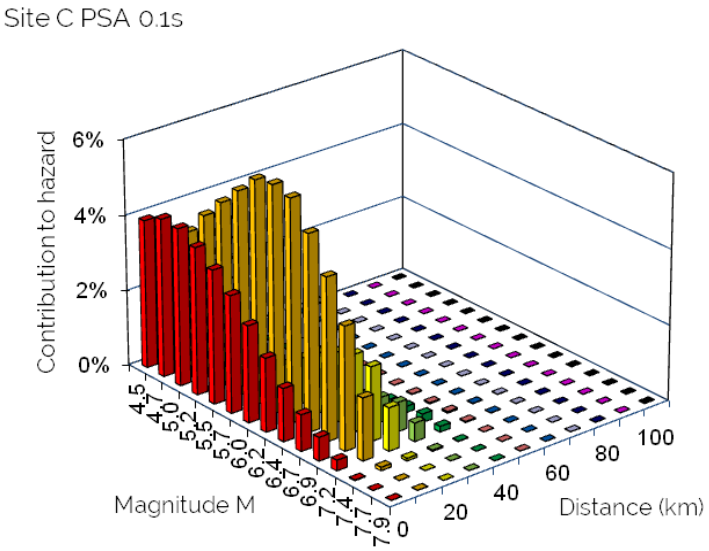

Fig. 3.19 Disaggregation for PSA=0,59 g, T=0,1 s for Site C

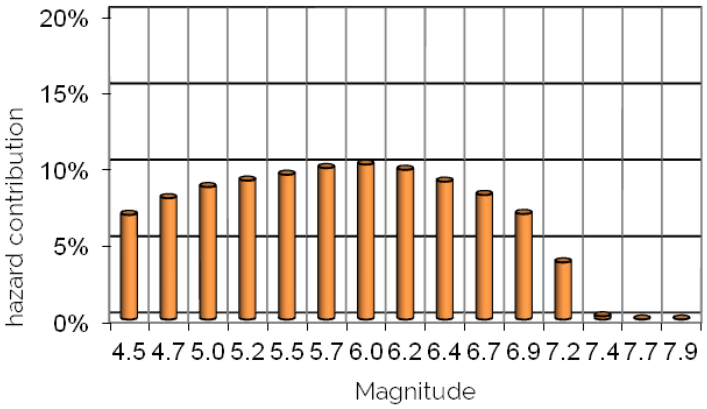

Fig. 3.20 Contribution to hazard by Magnitude M for PSA, T=0,1 s for Site C

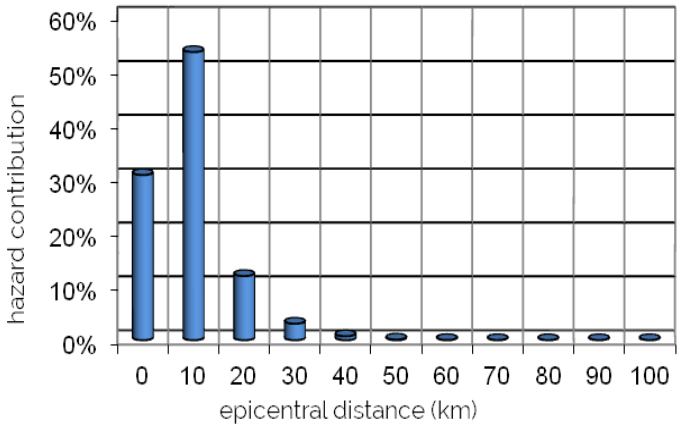

Fig. 3.21 Contribution to hazard by Distance R for PSA, T=0,1 s for Site C

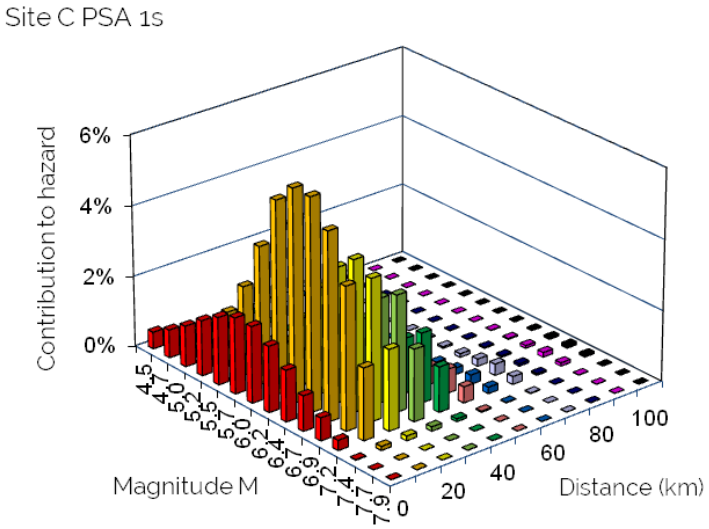

Fig. 3.22 Disaggregation for PSA=0,35 g, T=1 s for Site C

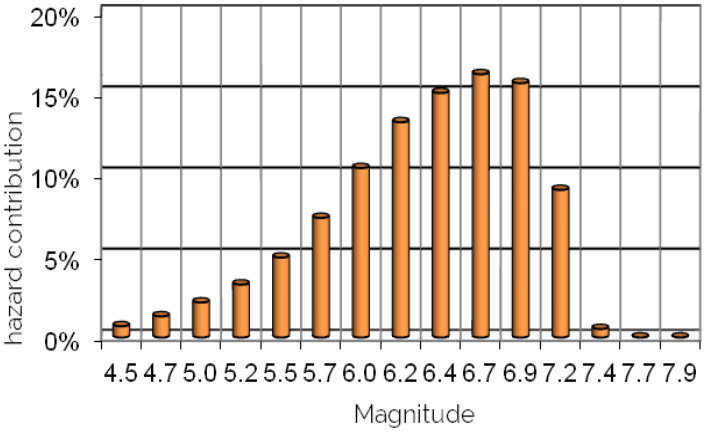

Fig. 3.23 Contribution to hazard by Magnitude M for PSA, T=1 s for Site C

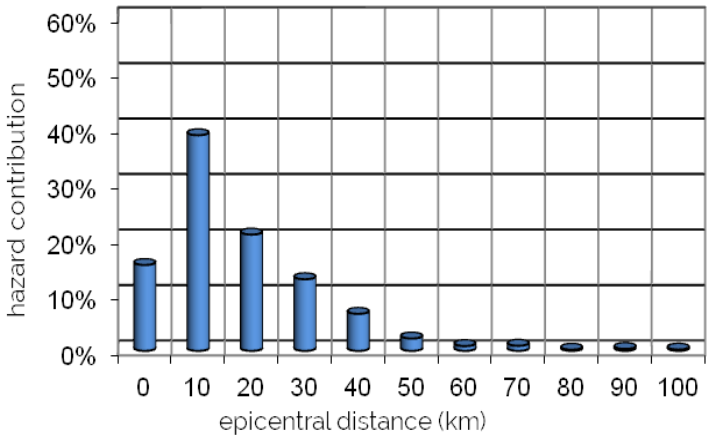

Fig. 3.24 Contribution to hazard by Distance R for PSA, T=1 s for Site C

3.7 Deterministic Seismic Hazard Assessment

3.7.1 Procedure

DSHA method has been used years before the PSHA. In the DSHA framework the procedure could be divided in 4 steps:

1. Identification and characterization of all the seismogenic sources which can cause a significant ground shaking at the site.
2. A *Scenario Earthquake* or *Controlling Earthquake* is selected, defined by a value of Magnitude M and one for the distance R. That is the seismic event which can cause the expected level of local intensity (e.g. PGA/PSA).
3. Selection of GMPE. In this case the equation is applied in a deterministic way, by simply substituting the values of M and R in the equation.

4. Seismic Hazard at the site is generally defined in terms of local intensity caused by the Scenario Earthquake.

In the design of structure which collapse could have disastrous effects, as nuclear power plants or large dams, DSHA could be very useful to identify the strongest level of intensity that could take place at a given site.

Some drawback can be highlighted in the DSHA method, mainly due to the lack of information on:

- The probability of occurrence of the Scenario Earthquake.
- The level of intensity of the ground shaking expected in a given time period (e.g. the lifetime of the structure).
- The definition of the uncertainties in the intensity prediction.

In fact GMPEs provide the median value of the local intensity, that is the 50th percentile, of the ground motion parameter. To obtain the desired level of seismic intensity for the Scenario Earthquake is often necessary to add a fraction ε of the standard deviation σ to the median value.

ε represents the influence of the random variability in the ground-motion prediction, and it may play a very important role in comparing probabilistic and deterministic assessments. Since the equations used to predict the ground motion are probabilistic, it is actually impossible to perform a fully deterministic evaluation of the seismic hazard.

3.7.2 Selection of controlling earthquakes for case study

The study of the regional seismicity, represented in Fig. 3.25 in a GIS map, has brought to the choice of three controlling earthquakes, which are reported in Tab. 3.3.

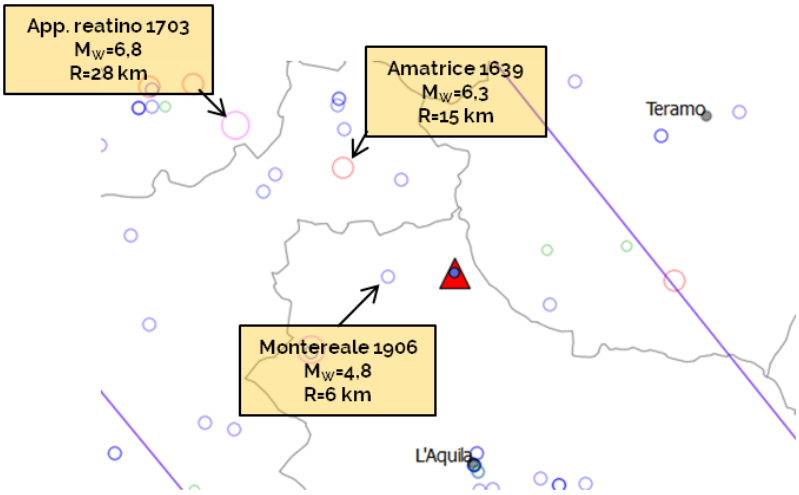

Fig. 3.25 Controlling earthquakes for site C - 475 years

The selection of the controlling earthquakes was made on the basis of the disaggregation of hazard, choosing seismic events which are consistent with the disaggregation results for the different spectral periods.

Tab. 3.3 Controlling earthquakes based on disaggregation for Site C

Controlling earthquake	Magnitude M	Distance R (km)
Amatrice 1639	6.3	15
Appennino reatino 1703	6.8	28
Montereale 1906	4.8	6.9

Deterministic spectra were evaluated for the case study with the predictive equations used in the assessment of the probabilistic spectra, namely SP96 and AB10 equations.

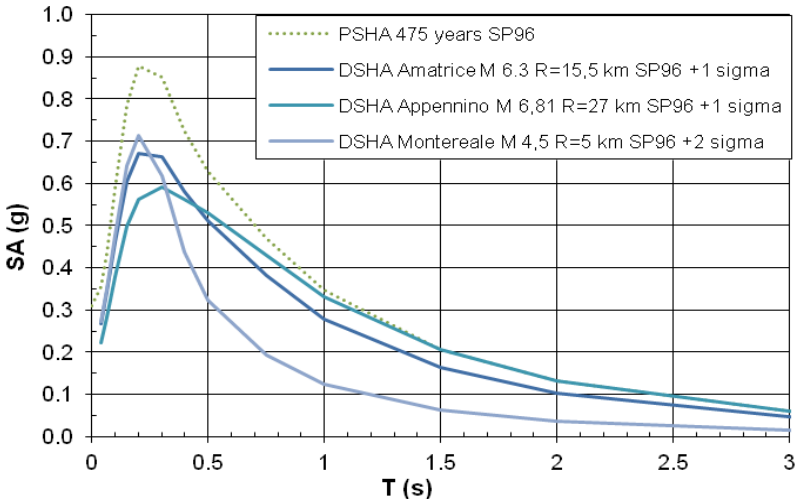

Fig. 3.26 Comparison between UHS and deterministic spectra - SP96 for Site C

Fig. 3.26 and Fig. 3.27 show a comparison between the probabilistic spectrum (dotted line) obtained respectively with SP96 and AB10 predictive equation (evaluated in section 3.3.4), and the deterministic spectra (solid lines) evaluated with the parameters of the controlling earthquakes. It is possible to notice that the probabilistic spectrum envelopes the spectral acceleration of the deterministic ones. This is a demonstration of the fact that the probabilistic assessment includes the contribution and the uncertainties of all the seismic sources. The comparison is made by adding a certain fraction of standard deviation σ to the median value given by the predictive equation, which ranges from 1σ to 2σ for SP96 predictive equation, and from 0,5σ to 1,5σ for AB10.

Focusing on the deterministic spectra, we can observe that for Montereale seismic event, which is a near earthquake with a small magnitude, the spectrum has a narrow shape for both GMPEs. For small periods the PSHA is ruled by this event, which has values higher than the other

DSHA spectra in the range 0.05s-0,2s. For T>0,2 s the PSHA spectrum is ruled by earthquakes with larger magnitudes and distances.

In the case of SP96, in the range of periods 0,2-0,4 s the spectrum of the Amatrice earthquake has higher values than the Appennino Reatino earthquake. For AB10 the far earthquake gives the major contribution to hazard for long periods (T>0,2 s)

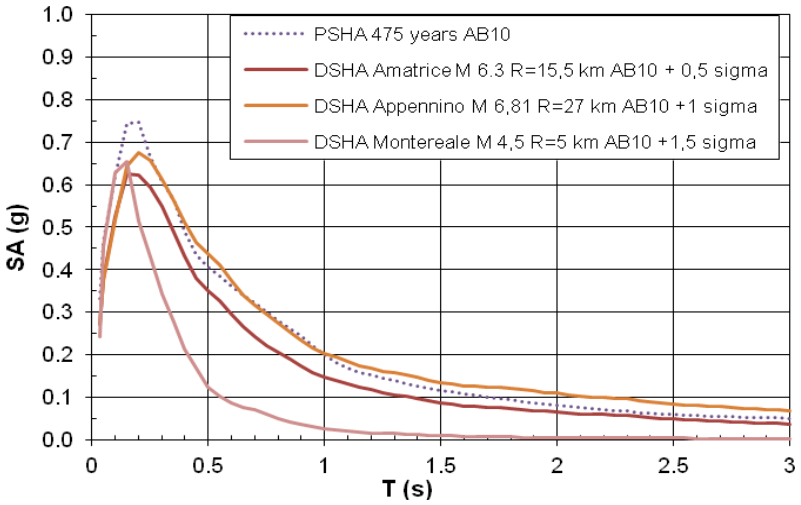

Fig. 3.27 Comparison between UHS and deterministic spectra - AB10 for Site C

3.8 Vertical spectra and V/H ratio

The issue of evaluating vertical spectra is nowadays becoming more and more relevant in Italy and in other seismic areas in the world. The lesson learned by recent earthquakes, as L'Aquila seismic event in 2009, demonstrates that many collapses of existing structures were due to the effects given by the vertical component of the Ground Motion.

A study by Di Sarno et al. [37], focused on the seismic response of RC columns subjected to horizontal and vertical Ground Motions, shows V/H

ratio of eight horizontal components (N-S, E-W) of four seismic stations in the near-field (R<10 km from the epicenter of the earthquake), 50% of which are greater than unity (V/H_{max}=1,164).

Conversely, at far field distances V/H ranges from 0,25 to 0,75. Thus, the well known rule introduced by Newmark and Hall [38] that suggested to compute the vertical component of motion by multiplying the horizontal component for 2/3, which was included in many Codes, is not adequate to be applied as a general law.

Moreover, some studies (see [30]) show that V/H ratio varies with Magnitude, Distance, site conditions and style of faulting, ranging from 0,3 to 1,8. Actual predictive equations show values that increase with Magnitude, decrease with distance, for small periods are higher on soil than on rock, for long periods are higher on rock than on soil, as is reported in [39]. As an example, Fig. 3.28 shows a comparison between values of V/H ratio computed with the GMPE by Sabetta and Pugliese for rock and shallow alluviums, for M 7 and R_{jb}=20 km.

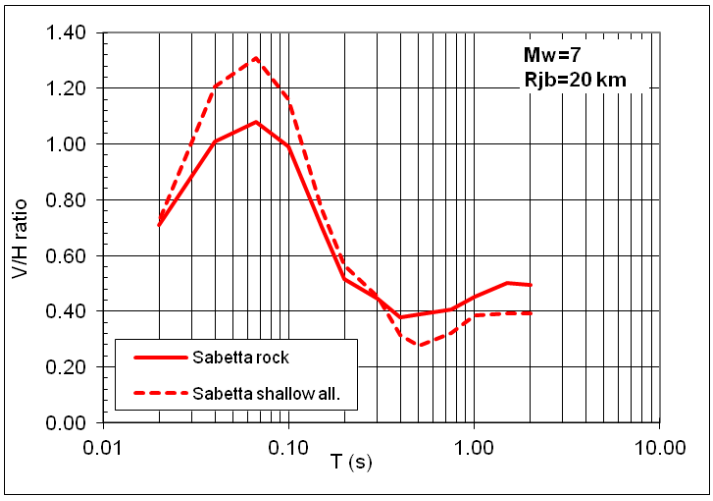

Fig. 3.28 Effect of soil condition on V/H ratio - SP96 GMPE

It is possible to notice that both for rock and for shallow alluviums there is a range of periods for which V/H ratio is greater than unity. Moreover, it is clear the dependence on the period and the differences between rigid and deformable soils.

The trend in recent literature studies is to evaluate the vertical response spectra using Predictive Equations to compute V/H ratios, then multiplying for the horizontal spectra. V/H ratio shows a peak between 0,05 and 0,1 sec and a minimum between 0,4 and 0,8 sec, increasing slowly for longer periods. Therefore, the horizontal component of the spectra must have a good resolution at short periods.

Seismic Codes, such as Eurocode 8 and NTC 2008, define simplified V/H spectral ratios which depends on PGA. This approach is not appropriate for site-specific hazard studies, for which scenario spectra obtained from disaggregation of hazard are required.

4 Selection of accelerograms

4.1 The final step of hybrid approach

Response spectra represent the most common tool to perform simplified linear analyses for the design of earthquake resistant structures and for existing structures assessment. This is a simplified procedure because the response spectrum is a synthetic plot which gives the maximum acceleration response of a number *n* of SDOF systems with different fundamental period.

There are some cases for which it is necessary to perform a fully dynamic analysis, using acceleration or displacement time histories applied to an appropriate non-linear model of the structure. It is straightforward that by using time histories it is possible to obtain a more detailed description of the motion response of the structure.

Some examples of such cases are:

- Buildings designed for a high degree of ductility;
- Structures characterized by high irregularities in plan or elevation;
- Structures with important higher modes;
- Critical structures, which collapse can cause unacceptable harm or disruption;
- Structure with base isolation.

Three main methods to obtain accelerograms are discussed here:

1. Artificial spectrum-compatible accelerograms;
2. Synthetic accelerograms with simulation of seismic source;
3. Real accelerograms recorded during earthquakes.

The procedure of selection of acceleration time series must be applied selecting time series characterized by the same parameters, such as Magnitude, Distance, Style-of-Faulting, directivity and site condition.

The necessity to use artificial or synthetic accelerograms could raise from the lack of time series having these features. Nevertheless, for non-linear analysis of structures there is less confidence that they capture these important features, as reported in a work by Al Atik and Abrahamson [40], so the use of real ground motion records must be preferred whenever is possible.

4.1.1 Artificial accelerograms

Artificial accelerograms can be generated by three types of sofwares. First type are **statistical based softwares**, like SIMQKE [41]. The method is based on the generation of a power spectral density function from the Design smoothed response spectrum, generating a sinusoidal time series with random amplitude and phase angles.

Final accelerograms are obtained by first summing all the sinusoidal motions and then modifying the response spectrum in order to match the target spectrum with an iterative procedure.

The main advantage of this method is that an almost perfect match with the target response spectra could be reached, but the signals obtained do not have any relation with the physical parameters of the earthquake (e.g. Magnitude, Distance). Moreover, they are characterized by an excessive energy content due to the high number of strong motion cycles.

Physical based softwares try to include this parameters in the procedure to obtain artificial accelerograms. They simulate point or linear seismic source. An example of this programs is Simnost, created by Sabetta and Pugliese [19] to obtain accelerograms to use as input data to obtain their

Ground Motion Predictive Equation. The input of this program are Magnitude, Distance and site conditions (Rock, Shallow or deep alluvium).

The main drawback of Simnost is that the result, given a certain Magnitude and a Source-to-site distance, may not be compatible with the elastic probabilistic response spectrum (e.g. Code spectrum).

There is a third method to generate artificial accelerograms, which combines the first two methods and tries to improve their advantages. An example of such a method is BELFAGOR [42], depicted in Fig. 4.1 derived by the program PhySimqke and it is divided into two parts: in the first part the method proposed by Sabetta and Pugliese is applied as in Simnost, starting from Magnitude, Distance and Site conditions. In the second part an iterative procedure modifies the amplitude distribution in the frequency domain to arrive to a complete match with the target spectra.

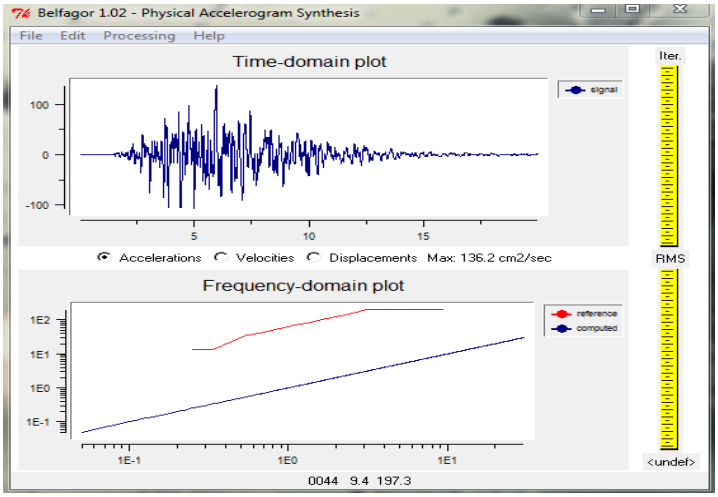

Fig. 4.1 Evaluation of an artificial accelerogram with Belfagor (Mucciarelli, 2004)

So doing an accelerogram which satisfies all the requirements of the Code is obtained, with two other advantages: the distribution of the arrivals of seismic waves is very similar to a real earthquake, and there is a slight variability in time domain between one generation and another, allowing to perform many analyses taking into account the variability of motion.

The iterative procedure is performed as follows:

- Generation of the acceleration time series;
- In frequency domain, the values of Fourier spectrum of the signal F(f) are corrected with the following equation:

$$F(f)_{i+1} = F(f)_i \cdot \frac{SRT(f)}{SR(f)_i}$$

Where SRT(f) is the value of the target response spectrum at the frequency f and $SR(f)_i$ is the corresponding value of the response spectrum at i-th iteration. Spectral amplitudes are combined with values of the phases of the non-stationary signal simulated at the beginning to obtain the resulting signal in time domain.

4.1.2 Synthetic accelerograms

Synthetic accelerograms are generated from models which simulate earthquake source including effects due to path and site. This methods generally require the experience of an expert in engineering seismology in order to set all the parameters necessary to characterize the earthquake source, and in the process is involved a high degree of expert judgement.

4.1.3 Real ground motion records

As above described, real accelerograms are preferred over artificial and synthetic accelerograms, and nowadays an increasing number of countries

and organizations have prepared databases which include all the records of that country or region.

Examples of these databases are:

- ITACA (ITalian ACcelerometric Archive), realized by INGV, which contains all the waveforms of Italian events, that is the database used in this work;
- PEER Ground Motion database, realized by PEER (Pacific Earthquake Engineering Research Center);
- SHARE (Seismic Hazard Harmonization in Europe) project. SHARE assembled a strong motion database from preexisting strong motion databases. The database consists of accelerograms gathered from the European strong-motion database (ESMD), which is formed by: the Turkish national strong-motion database (T-NSMP), the Next Generation Attenuation database (NGA), the KIK-Net database, the global worldwide database compiled by Cauzzi and Faccioli (C&F), the Internet Site for European Strong-motion Data (ISESD), and the Italian Accelerometric Archive (ITACA) database.

Real records selected from Databases can be used as natural accelerograms, but in order to match the target response spectrum they must be scaled or matched using appropriate methods.

Within the framework of the Seismic Hazard Assessment discussed in this work, the Scenario Earthquake is defined by means of M-R values. The selection of real records must take into account the most important parameters of the Scenario Earthquake, which are Magnitude and Distance. Regarding site conditions, databases provide all the

informations about the soil type of the seismic stations where the chosen signals were recorded.

4.2 Seismic Codes requirements

4.2.1 Italian Code (NTC) and EC8

The Italian Code in section 3.2.3.6 gives provisions for using acceleration time histories to perform dynamic analyses. The three translational component of motion recorded by the instrument are called a *group* of accelerograms. Both operational and collapse limit states can be verified using acceleration time histories, which can be artificial, synthetic or natural records.

Regarding **artificial accelerograms**, there are some requirements for the duration of the time history: the pseudo-stationary part of the record must have a duration greater or equal than 10 sec; The entire duration must be least 25 sec. The average elastic response with a 5% damping ratio spectra of the chosen records must be consistent with the design spectra. The deviation between the two ordinates has to be less than 10%, within the largest of the following intervals:

- max (0,15s ÷ 2,0s, 0,15s ÷ 2T) for Collapse Limit State;
- 0,15 s ÷ 1,5 T for Operational Limit State.

The use of **synthetic accelerograms**, with simulation of the fault mechanism and propagation is allowed, provided that the hypothesis on the seismogenic characteristics of the source and of the propagation medium are appropriate.

The use of **natural accelerograms** is allowed, provided that their choice represents correctly the seismicity of the site and it is justified on the basis of the seismogenic characteristics of the source, of the site condition,

Magnitude, Source-to-site distance and of the PGA. These accelerograms must be selected and scaled in order to match the Code response spectra in the range of the relevant periods for the given structure.

Section 7.3.5 of the NTC contain the requirements to perform non-linear dynamic analyses. Both in the linear and non-linear field the two horizontal components and the vertical are applied at the same time, forming a *group* of accelerograms.

If a set of 7 accelerograms is used to perform the assessment of the structure, the effects on the structure are represented by the average values of the most unfavorable effects obtained with the analysis. If fewer accelerograms are used the effects are represented by the most unfavorable values.

The Code does not allow to use less than 3 groups of accelerograms. If there is the need to assess the effects of the spatial variability of the Ground Motion, the analysis has to be performed by imposing at the base of the structure different accelerograms but mutually consistent and derived from an appropriate response spectra. The effects on the structure must be combined with the following expression:

$E_x+0.3E_y+0,3E_z$

4.3 Scaling real accelerograms

4.3.1 Methodologies for selection and scaling

Selection in terms of strong-motion parameters

In the majority of cases, not only in the case of Italy, Seismic Codes provisions for the selection of accelerograms are based on the compatibility with the Code response spectrum, which is a Uniform Hazard Spectrum. Therefore, sometimes there is the need to select or

scale natural ground motion recordings in order to match a spectrum like this.

A single parameter which can help in searching and scaling of these parameters is $D_{RMS,}$ which is defined as the root-mean-square deviation of the observed spectrum from the target design spectrum:

$$D_{RMS} = \frac{1}{N}\sqrt{\sum_{i=1}^{N}\left(\frac{SA_0(T_i)}{PGA_0} - \frac{SA_S(T_i)}{PGA_S}\right)^2}$$

Where N is the number of spectral periods for which the response spectrum is evaluated, $SA_0(T_i)$ is the spectral acceleration from the chosen signal at period T_i, $SA_s(T_i)$ is the target spectral acceleration at period T_i; PGA_0 and PGA_s are respectively the peak ground acceleration of the record and the anchor spectral ordinate of the target spectrum.

Obviously, when comparing two response spectra the accuracy of the matching process is expressed by the value of D_{RMS}: if this value is small there is a good agreement between the record response spectrum and the target spectrum. This parameter can give better estimates on the quality of record selection in comparison with the method which matches on the basis of spectral intensities (i.e. minimizing the area below the spectrum).

Bommer and Acevedo [43] suggest maximum values of D_{RMS} of 0,1 if the aim is to obtain a response spectra based on spectral ordinates, while the value could arrive to 0,2 if the search of accelerograms was performed using seismological criteria, that is using the results of a Seismic Hazard Assessment.

The main drawback of this method is that a good match can easily be obtained also for records which have spectral ordinates significantly above or below the target spectrum.

The method based on D_{RMS} constraints the spectral ordinates so the quality of the match is higher. This method has one main disadvantage, that it does not take into account for the duration of the strong motion record. In fact, some Codes have stated a minimum duration for the strong motion records, while the problem is that in literature there are many different ways to measure duration.

Selection in terms of geophysical parameters

There are cases in which a Seismic Hazard Assessment which takes into account a specific site or area exists, and for this site is available a controlling earthquake obtained with DSHA. As it was described in previous sections, the controlling earthquake is defined by Magnitude M, a distance R and often the site soil condition and the style of faulting.

So in this case there are at least two parameters to be used as input for the search process and selection of accelerograms, which are M and R. If a search is performed in a strong motion database for records matching the exact parameters of the controlling earthquake, it is unlikely to find a good number of recordings because the search has been too specific.

Conversely, it is more appropriate to perform a search in a certain range of Magnitude and Distance.

Influence of Magnitude

In literature there is a general agreement on the fact that Magnitude is a necessary parameter to select strong motion records, since it has influence on the duration of the ground motion and on the shape of the spectrum and today it is recommended to select records which have a maximum scatter of 0,2-0,25 units of Magnitude from the controlling earthquake. The search window could initially be larger, then it is possible to shorten it if a sufficient number of records is found.

Influence of Distance

Many studies stated that spectral shapes are less sensitive to distance than to magnitude. Therefore it is possible to use wider search windows than for the Magnitude. The main disadvantage in extending the search window is that the final dispersion of data is very large, so the search window for distance should be increased gradually in order to find an appropriate number of records.

Influence of Site Classification and style of faulting

When searching for natural strong motion records also site classification could play an important role in defining the most appropriate spectral shapes. The main obstacle to the introduction of this parameter in the search is that site condition are available only for few sites in the world.

Moreover, for sites which have a site classification is defined V_{S30}, which is the velocity of the shear waves at 30 meters depth, but also the soil layers underlying the first 30 meters are important.

As for the previous cases, if enough signals could be identified with a more restrictive search, this could be better for the selection of good quality records.

Regarding the Focal mechanisms, there is agreement in literature on the fact that Reverse faulting can produce larger ground motion intensities in comparison with Normal and Strike-Slip faulting.

Scaling factors

There are various reasons why scale factor used to adjust the real accelerograms selected must have an upper and a lower bound, in order to avoid obtaining unrealistic ground motion records. Also if techniques exist to adjust the accelerograms to the target spectra, it is more advisable

to search for records which are similar to the target spectra without modifications.

An acceptable range for the Scale factors is 0,25-4, but some authors prefer to choose SF ranging from 0,5 to 2, although it could be an excessive limitation of the range.

4.3.2 Scaled accelerograms: REXEL

The software REXEL v3.5 [44], which main window is depicted in Fig. 4.2, allows the selection and scaling of spectrum-compatible real accelerograms. The compatibility can be reached either using the response spectra of NTC08, EC8, or for user-defined response spectra.

The real accelerograms are selected from the European Strong Motion Database (ESDB), or ITACA, or SIMBAD [45]. The program allows to do all the operations that must be done in order to define the response spectrum, the selection and scaling of the natural records by its interface, without any independent choice if the Code spectra are used.

In the first step of the program it is possible to define all the features of the NTC08 or EC8 response spectra, starting from the geographical coordinates of the chosen site, the reference period of the structure, the return period of the seismic input.

In the second step it is possible to define the range of geophysical parameters (Magnitude, Distance and site condition) which will be used to search in all the available databases for real accelerograms. These accelerograms will be scaled to obtain combinations of 7 accelerograms whose average spectrum matches the target spectrum. The range of spectral periods and the tolerances can be defined by the user. The analysis could be executed including from 1 to 3 components of motion,

depending on the will to perform 1D, 2D or 3D analysis including the vertical component.

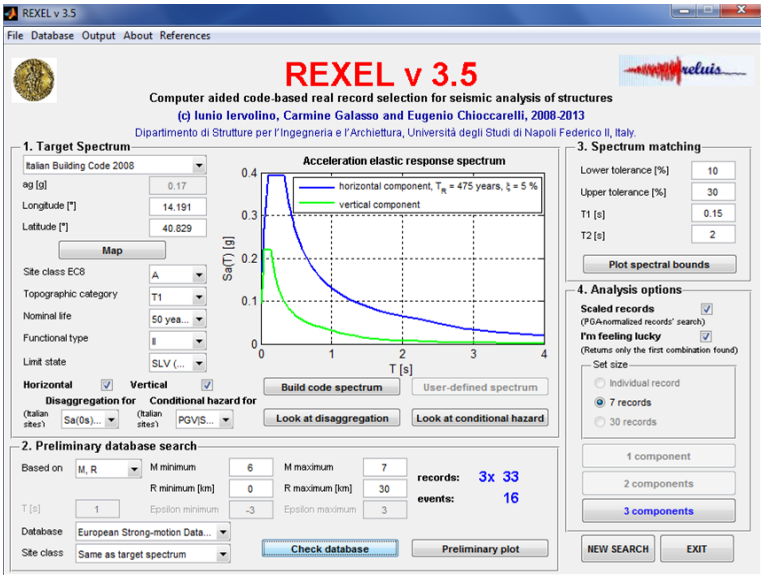

Fig. 4.2 Main window of the software REXEL (Iervolino, 2010)

The procedure implemented by REXEL is based on the parameter δ_i, which gives a measure of the scatter between the spectrum of a single record and the target spectrum:

$$\delta_i = \sqrt{\left(\frac{1}{N} \sum_{i=1}^{N} \left(\frac{Sa_j(T_i) - Sa_{ref}(T_i)}{Sa_{ref}(T_i)} \right)^2 \right)}$$

Where $Sa_j(T_i)$ is the pseudo-acceleration ordinate of the spectrum of the real accelerogram for spectral period T_i, $Sa_{ref}(T_i)$ is the value of the target spectrum at the same period T_i. The real accelerograms are then ordered in ascending order of δ_i so that the first combination (found with the option "I'm feeling lucky") are that with the smallest dispersion compared to the target spectrum.

In many cases, this type of procedure could be easier and faster to use than those used by similar programs. The automatic procedure implemented in the software allows also to inexpert users to successfully use the program without major obstacles.

A drawback of the program is that the user is not free to introduce accelerograms selected by himself, resulting in a rather "standard" procedure. Moreover, sometimes for certain spectral or geophysical parameters it is difficult for the program to find valid combinations. It could happen for example for very long return periods as 1950 or 2500 years, like the ones used for the assessment of dams, or for very high values of magnitude, for which there are less accelerograms in the databases.

An application of this software will be shown in the second part of the thesis, in section 6.6.

4.3.3 Scaled accelerograms: In-Spector

The software In-Spector [46] by Acunzo, Pagliaroli and Scasserra was created with the aim to provide a tool which can help engineers and technicians to obtain spectrum-compatible scaled accelerograms.

The use of the software, declared in the paper itself, is oriented to "expert users", which must be familiar with the procedures of natural accelerograms selection. This is due to the fact that conversely to other programs that allow to manage natural accelerograms, this program permits to introduce real accelerograms selected by the user, thus creating a fully customized analysis. The main steps of the program are the following:

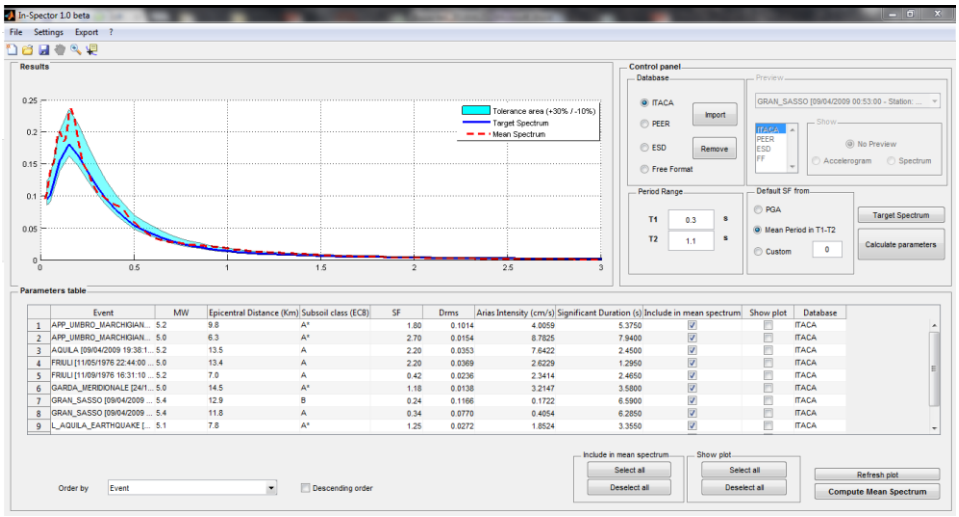

Fig. 4.3 Main window of In-Spector (Acunzo, 2014)

1. Pre-selection of the real accelerograms made by the user. This can be made searching for records in one of the databases available online, such as ITACA (for Italy), European Strong Motion Database, PEER etc… The geophysical parameters used to perform the search are the Magnitude and Distance which are defined by the controlling earthquake obtained with the Seismic Hazard Assessment.
2. Definition of the target spectrum. This could be either a Code spectrum, a Uniform Hazard Spectrum or a deterministic spectrum evaluated on the basis of the controlling earthquake.
3. The software computes the response spectrum and consequently the parameter D_{RMS} discussed in 4.3.1 for all the selected records in a given range of periods, which contains the fundamental period of the structure to be analyzed.
4. The software evaluates the Scale Factor F_S to apply to each record in order to obtain an average spectrum that matches the target

spectrum respecting the given tolerances. The software allows to exclude from the analysis the records which have excessive values of the scale factor, or to change manually the scale factor of each single accelerogram finding a new combination that matches the target spectrum. The Scale Factor F_S can be defined in terms of PGA as follows:

$$F_s = \frac{PGA_S}{PGA_0}$$

Where PGA_S is the anchor point of the target spectrum and PGA_0 is the peak ground acceleration of the natural accelerogram. The scale factor can be also defined in terms of spectral accelerations:

$$F_S = \frac{SA_S(T)}{SA_0(T)}$$

Where $SA_S(T)$ is the spectral acceleration of the target spectrum for period T and $SA_0(T)$ is the spectral acceleration for the same period T.

5. It is then possible to export all the results, in terms of accelerograms and response spectra in txt or xml format.

The main advantage of this software is that all the selection choices can be made in a way which is independent from the software itself. Each user can thus apply his own judgement, which is fundamental when studying particular structures. Obviously the user must be expert in selecting the input accelerograms. The main window of the software is shown in Fig. 4.3.

An application of this software was made in this study for the evaluation of the ground motion on the Leaning Pisa Tower, which will be discussed in section 15.3.

4.4 Spectral matching

As discussed above, Codes generally require that the accelerograms had a good agreement with the ordinates of the design response spectrum. The number of the accelerograms to consider is matter of discussion, since real strong motion recordings show a great variability also between signals of the same event recorded by close stations. Therefore, there is a need to consider a certain number of accelerograms.

The Codes provisions state that it is possible to consider a set of three accelerograms, taking as structural response the maximum of the effects produced by the records. This provision spreads by the will to reduce the computational cost.

Nevertheless, as mentioned in section 3.3 when discussing the PSHA, Uniform Hazard Spectra, including Code spectra, include the uncertainties of the GMPEs in terms of local intensity. Therefore, considering the maximum value of the effects produced by three accelerograms would bring to consider twice the uncertainties, and obtain a too conservative design choice.

By a seismological point of view, it seems more appropriate to select seven accelerograms and use the average response obtained from a dynamic analysis. The number of seven accelerograms has been identified by a study by Shome et al., 1998 [47], which demonstrated that an acceptable low dispersion is produced when considering seven accelerograms. as a consequence, today many national Codes require to perform dynamic analyses using 7 accelerograms.

4.4.1 Matched accelerograms: RSPMatch-SeismoMatch

Seismosoft created a software [48], based on the method introduced by some authors (for example Hancock [49]) which can adjust the selected

records in order to reach spectrum-compatibility. The methodology used by this program modifies a time history in the time domain in order to create a spectrum-compatible record by adding particular wave packages, called *wavelets*, to the parts of the record which have a significant dispersion in comparison with the target spectrum.

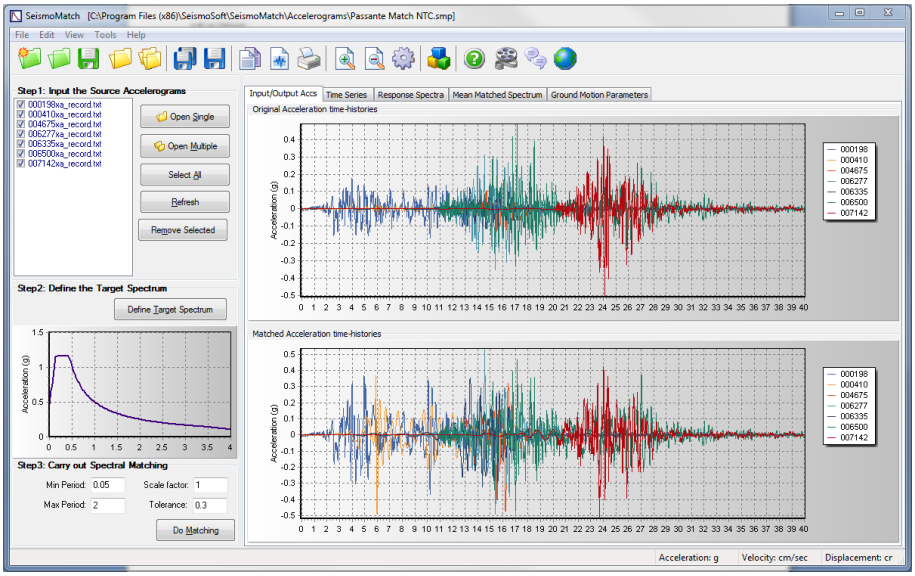

Fig. 4.4 Main window of Seismomatch (

The program operates in three steps:

a) Evaluation of the response of an elastic SDOF system giving as input the selected real accelerogram, for each period and for the chosen damping ratio.
b) The program compares the maximum response of the SDOF system with the reference acceleration and evaluates the scatter.
c) The wavelet package is added to the selected record correcting the phase angle so that the new record peak corresponds to the amplitude of the target spectra.

The authors of this program corrected the initial method proposed by Lilhanand and Tseng, 1987 [50]: in fact the wavelet functions proposed by these authors modified velocity and displacement of the time series, so it was necessary a correction which could change the spectrum-compatibility.

An application of this software to the dynamic response of dams is presented in section 6.6

Part II - Seismic response of concrete dams

5 Introduction

Dams are very large structures which are multi-purpose: the main purposes why dam are built are for irrigation and for hydropower uses. Other uses are water supply and flood control. The multi-purpose vocation of this structures has been investigated by ICOLD [51], the International Commission which publishes guidelines and report on dams. Almost 40.000 dams in the world were examined.

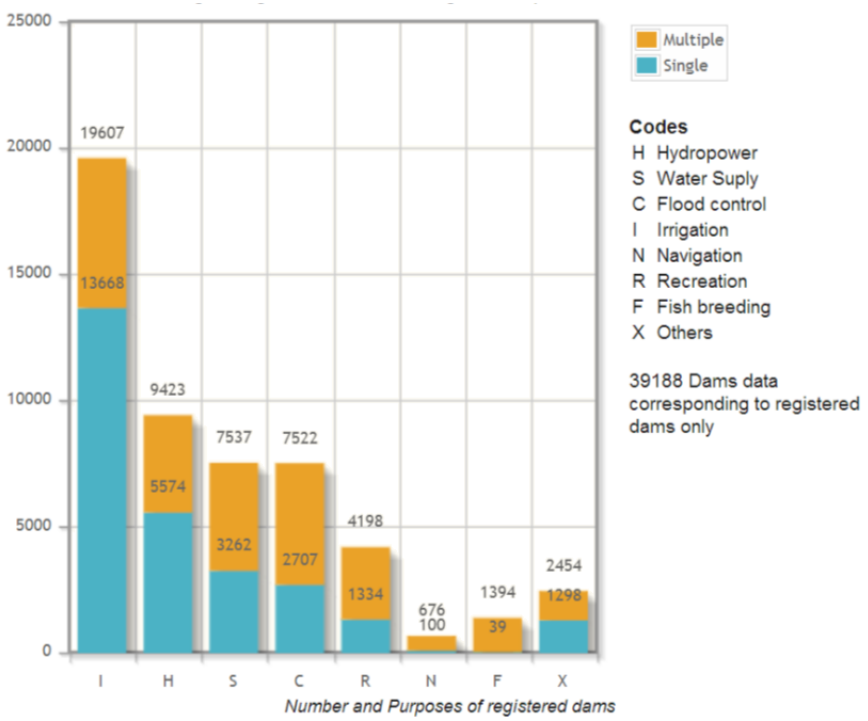

Fig. 5.1 Classification of worldwide dams by purpose (ICOLD)

From an engineering point of view, dams are multi-disciplinary structures, as they are studied by structural, geotechnical and hydraulic

engineers. The same study conducted by ICOLD on registered dams stated the majority of the existing dams are earth dams, while concrete dams represent around a 22% of the total, as depicted in Fig. 5.2.

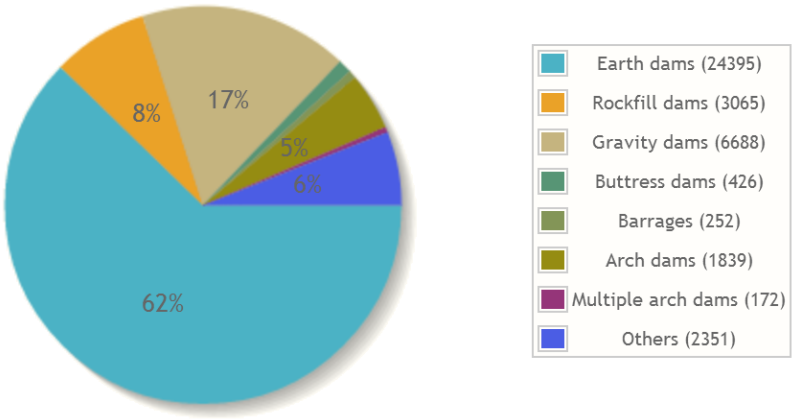

Fig. 5.2 Classification of worldwide dams by dam type (ICOLD)

Concrete dams are a relevant part of the great number of Large dams in Italy, in fact there are approximately 200 concrete dams over a total number of 542 dams (See Fig. 5.3). Therefore the percentage of concrete dams in Italy is greater than in the rest of the world. The majority of them have been designed and built following Design criteria which today are considered obsolete, so it is necessary to perform analyses which use modern numerical analysis techniques and updated to present scientific knowledge.

There are more than 500 dams in Italy, and around 200 are concrete dams: there are around 130 concrete gravity dams and around 90 arch dams, divided into simple arch, double curvature arch and arch-gravity dams, as reported in [52].

For most of them a seismic safety evaluation is necessary in the light of the forthcoming Italian Code on Dams. Non-linear dynamic analyses become a useful tool for dams which were designed considering seismic forces lower than the ones expected today.

Fig. 5.3 Map of existing Large Dams in Italy (ITCOLD)

In this work some results obtained for simplified analyses performed on an equivalent SDOF system are presented. Then the results of accurate analyses performed on two different concrete dams, an arch-gravity dam and a gravity dam are discussed. The problem of the correct evaluation of seismic actions for this high risk structures is also introduced. Part of these results were published in some papers presented at 2ECEES (The Second European Conference on Earthquake Engineering and Seismology, see [53]), and at the Conference "Giornate AICAP" of the Italian Association of Reinforced and Pre- tensioned Concrete (See [54]).

5.1 Italian Code dams classification

Concrete dams are divided by the Italian Code on Dams into two classes:

1. Gravity dams
2. Arch dams

An example of gravity dam is depicted in Fig. 5.4. Gravity dams are defined by the Code as structures with a rectilinear planimetric axis or with a slight curvature, which generally have filled triangular sections, divided into blocks by permanent joints, which have the purpose to prevent crack openings due to thermal or shrinkage. Gravity dams use their own weight to resist to hydrostatic forces, so the single blocks show a cantilever behavior. In gravity dams the joints do not have a structural function.

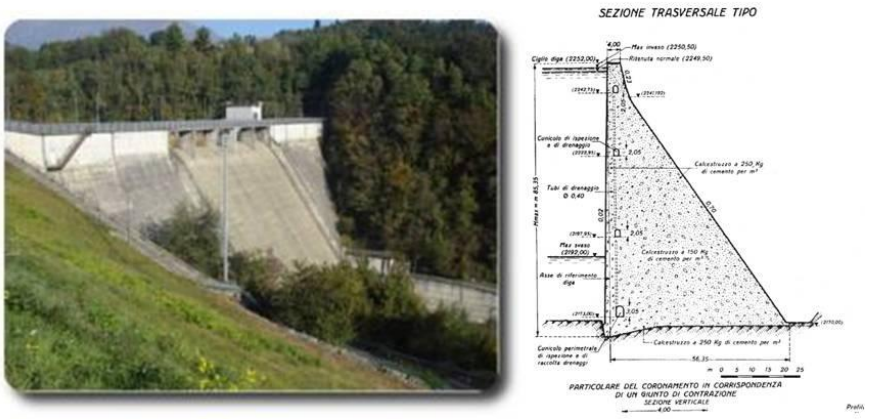

Fig. 5.4 Example of gravity dam

Arch dams (See Fig. 5.5) are defined in the Italian Code as "monolithic structures, with curved horizontal sections and with abutments standing on rock". Arch dams could have a very low thickness, and in this case the

horizontal forces are opposed by the arch effect due to the curvature of the wall.

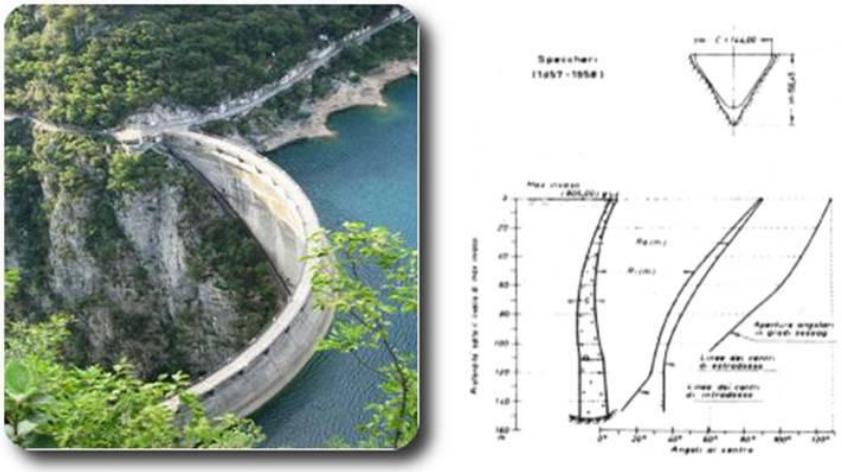

Fig. 5.5 Example of arch dam

In case of arch dams which have a considerable thickness it is more appropriate to define those structures as "arch-gravity" dams (See Fig. 5.6), because for these structures the weight plays an important role in resisting to horizontal forces, so the dam resist both for arch and for cantilever effects.

In the case of arch and arch-gravity dams, the joints have a static function, because they have to resist and to spread the compression forces from one block to another.

Fig. 5.6 Example of arch-gravity dam

5.2 Italian Code seismic requirements

Italian Code for dams are the recent *Technical Guidelines for design and construction of Dams*, approved in 2014 [55]. The proposal can be applied to all dams on Italian territory with height greater or equal than 10 meters and with a reservoir volume greater than 100.000 m^3.

The purpose of the Code is to ensure, also in case of extreme seismic events, the maintenance of the reservoir level and the functionality of the spillways, tunnels and all the parts necessary to empty the reservoir. For strategic dams Italian Code prescribes the maintenance of the full functionality of the dam and appurtenant structures.

For the definition of the Limit States, the guidelines define the following critical conditions:

1. Normal operations;
2. Repairable damages, without uncontrolled release of water;
3. Non-repairable damages, without uncontrolled release of water;

4. Damages which cause uncontrolled release of water, or the risk to have human losses;
5. Collapse of the structure.

The corresponding Limit State, consistent with NTC2008, are:

- Operation Limit State, defined by the exit from condition 1;
- Damage Limit State, defined by the passage from condition 2 to 3;
- Life Safety Limit State, defined by the reach of condition 4;
- Collapse Limit State defined by the reach of condition 5.

Section C.7.7 of the Code for Dams contains the requirements to evaluate seismic actions. As in the Code for standard constructions, these are defined on the basis of the reference seismicity of the construction site.

When there is a lack of seismo-tectonic and seismic hazard studies the spectral shapes defined by NTC have to be used. The use of accelerograms is allowed, provided that they are consistent with the seismic hazard of the site.

If the parameter *ag* (that is PGA) is greater than 0,15g for a 475 years return period, seismic input has to be evaluated on the basis of a seismo-tectonic study of the site. The results obtained with this study should not be minor than the values required by the Code.

As described above in the NTC is very important to define the Reference period of the structure, called V_R, defined as:

$$V_R = V_N \cdot C_U$$

Where V_N is the nominal life of the structure while C_U is the coefficient of use. The Code defines two types of dam, depending on their dimensions and on the reservoir capacity:

- Normal dams: have height not greater than 15 m and with a reservoir capacity not greater than 1.000.000 m^3.
- Strategic dams: have height greater than 15 m and a reservoir with a volume greater than 1.000.000 m^3.

Strategic dams are defined as dams which functionality has great importance for purposes of civil protection. If there is no specific classification, strategic dams are all the dams which serve hydroelectric power stations or to store drinkable water.

Dams important for the effects of the collapse are defined as the remaining large dams.

Dams of normal importance: all the other dams (generally small dams)

In the Italian Code for Dams there are two tables to define the return period. Table C2 provides the Reference period for each class of dams, as function of the "Nominal life" V_N and the coefficient of use C_U.

Tab.C2

Dighe:	V_N (anni)		C_U	V_R (anni)	
strategiche	≥ 100		2,0	*200*	
rilevanti	$\geq 50^{(1)}$	$\geq 100^{(2)}$	1,5	$75^{(1)}$	$150^{(2)}$
Imp. normale	≥ 50		1	50	

(1) dighe di dimensioni contenute
(2) grandi dighe

Based on the probability of exceedance defined by the Italian Code, the return periods to define the seismic input are provided by table C4:

Tab.C4 *Periodi di ritorno dell'azione sismica T_R (anni)*

Dighe:	SLO P_{VR} (%)=81		SLD P_{VR} (%)=63		SLV P_{VR} (%)=10		SLC P_{VR} (%)=5	
Strategiche	*120*		*200*		*1900*		*2475*	
Rilevanti	45(1)	90(2)	75(1)	150(2)	710(1)	1425(2)	1460(1)	2475(2)
Imp. normale	30		50		475		975	

(1) dighe di dimensioni contenute
(2) grandi dighe

For a strategic dam, the return period can be computed applying the equation seen in section 3.3. The parameters to compute V_R are the following:

- V_N= 100 years
- C_U=2
- V_R=200 years

The corresponding return period for the Collapse Limit State, related to a probability of exceedance P_{VR}=5% in V_R=200 years is:

- 1950 years for existing dams
- 2475 years for new dams

5.3 ICOLD Bulletin 148

5.3.1 Classification of dams

ICOLD Bulletin 148 [56] is a 2010 revision of ICOLD Bulletin 72, first published in 1989. Its title is *Selecting seismic parameters for Large Dams - guidelines* and contains the provisions to evaluate the seismic parameters of Large dams.

The guidelines accurately describe the following topics, necessary for the assessment of the seismic parameters: Primary factors to take into account in the evaluation of the seismic hazard; selection of the seismic events for the analysis; selection of seismic parameters; factors that influence the selection.

According to ICOLD classification, a dam is a Large dam if it is higher than 15 meters, or the height ranges from 10 to 15 meters and satisfies one of these conditions:

- Length greater than 500 meters;
- Volume of the reservoir greater than 1.000.000 m^3;
- Flow rate of the outlet spillway greater than 2.000 m^3/s.

Then the Bulletin describes the steps for the Seismic Hazard Assessment: Identification of the possible seismogenic sources; evaluation of the features of all the potential source, like geologic conditions, Magnitude and Activity rates.; Predictive equations. According to the Bulletin, the procedure must be detailed, but the level of deepening of study must be appropriate to site condition, dimensions of the dam, the destination of the structure and to the consequences of damages or of a total collapse. Studies on local geology have to be extended up to 100-300 km, while seismicity studies must start by a minimum of 100 km. When available, real seismic recordings have a great importance.

5.3.2 Selection of Design earthquake

The definition of the Design Earthquake allows to evaluate the parameters that will be applied in the analysis step (e.g. Magnitude, acceleration, spectral ordinates, duration etc etc). These parameters are usually estimates through an Hazard Assessment, using a deterministic or

probabilistic assessment. Bulletin 148 considers 3 types of Design earthquakes:

- SEE: Safety Evaluation Earthquake.
- OBE: Operating Basis Earthquake.
- RTE: Reservoir- Triggered Earthquake.

SEE

This is a seismic event for which it is possible to accept a certain level of damage, but there must be no uncontrolled release of water from the reservoir. The intensity of this event could be assessed using a probabilistic or a deterministic approach. For dams which collapse is associated to a high risk, SEE is described by a ground motion intensity caused by an earthquake with a return period of 10.000 years, in a probabilistic approach for risk classes High and Extreme, while for different risk classes the return period could be lower (1.000 or 3.000 years). If SEE is evaluated by means of a deterministic approach, the Design Earthquake must be the Maximum Credible Earthquake (MCE), which was defined by ICOLD in Bulletin 46 as the largest earthquake that can occur in a certain region. Seismic intensities associated to MCE are generally defined as the upper limit of ground shaking expected in a given area.

Tab. 5.1 Definition of Design Earthquakes for SEE

Approach	Earthquake
Probabilistico	T_R=10.000 anni
Deterministico	MCE

OBE

OBE is a seismic event for which no significant damages must occur to the dam. Generally it is evaluated using a probabilistic approach. Theoretically OBE could be determined with an economic analysis, but this is not feasible sometimes. Often a return period of 145 years (i.e. P_{VR}=50% in 100 years). In case of earthquakes which have intensities lower than OBE the dam and the appurtenant structures must remain operational and suffer for easily repairable damages.

RTE

RTE represents the maximum level of ground shaking which could be triggered by operations of filling or emptying of the reservoir, or just by its presence. Also this type of shaking could be evaluated with a deterministic or probabilistic approach. ICOLD dedicated an entire Bulletin on this topic, that is Bulletin 137 with the title "Reservoirs and seismicity- State of knowledge". Reservoir-Triggered Seismicity (RTS) is generally related to dams higher than 100 meters or with very large reservoirs (V> 500 millions m^3) and to new dams situated in seismic area

Although there is a debate regarding the causes of a RTE, one of the certainties is that a possible event could happen if there are active faults in the area of the reservoir. Also if all the faults or seismic sources existing in the area are tectonically inactive, the possibility to have a RTE cannot be excluded, if the geology and local and regional seismicity suggest that the area could be subjected to RTS. Depending on the position of the dam and on seismo-tectonic site conditions, RTE could present an intensity level lower, equal or greater than OBE, but RTE cannot be greater than SEE.

5.4 Selection of a return period

As it was described in sections 5.2 and 5.3, the Italian Code and the ICOLD Bulletin 148 require to compute the seismic hazard with very high return periods, namely 2.500 years (Italian Code) and 10.000 years (ICOLD) for new dams. A comparison between response spectra evaluated with these return periods with the same Ground Motion Predictive Equation, in this case the relation by Akkar and Bommer, show that for TR=10.000 years acceleration obtained are around 30% greater than for 2.500 years return period.

Seismic actions proposed by Italian Code are in any case very high. In the following sections it will be described the case of existing dams, so it seems more appropriate to use the return period given by Italian Code to define seismic input for existing dams, for which there is a return period of 1950 years.

6 Definition of seismic input

6.1 Evaluation of seismic hazard for 4 sites

Italy is a country which has a very diversified territory, by the seismological point of view. For this reason, a study which has the purpose to give a fast overview of the dynamic response of concrete dams in Italy must take into account different areas, which could better represent the various seismological conditions of the territory.

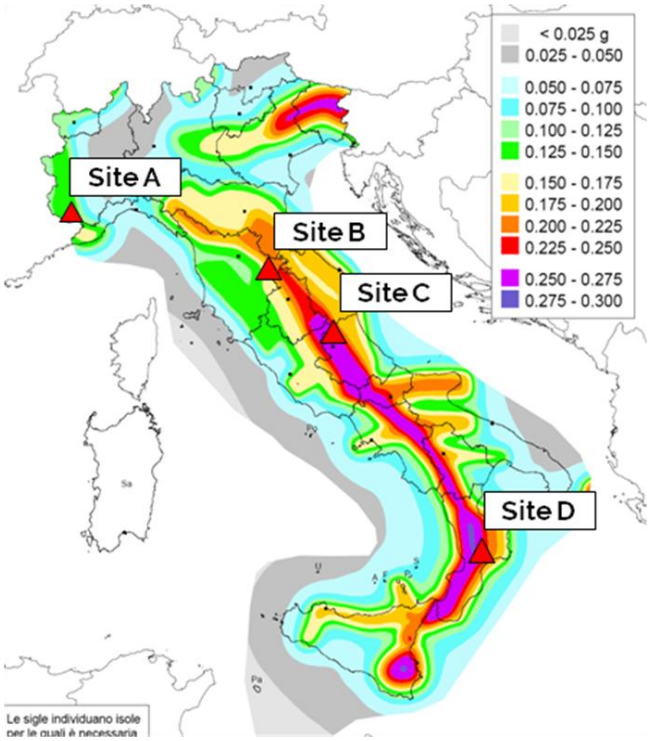

Fig. 6.1 Four Italian Dam sites selected for Seismic Hazard Assessment

In this work "high seismicity areas" are defined as areas with have a Peak Ground Acceleration ag>0,15g for a return period of 475 years, as reported by Italian Code. At this purpose four sites, selected in four

different Regions of Italy (Piemonte, Toscana, Abruzzo, Calabria), representing four Large dam sites in Italy are presented. These sites are reported in Tab. 6.1 and displayed in Fig. 6.1 on the Seismic Hazard map of Italy MPS04, where is possible to note the large differences between the intensity levels of one site to the other. For each of these sites the Italian Code requires a Seismic Hazard Assessment based on the seismo-tectonic features of the area, so it is necessary a specific seismic study. Sites are ordered from A to D in order to have increasing seismicity, so that Site A has the lowest intensity while Site D has the highest intensity. Tab. 6.1 reports also the PGA for each site computed with a return period of 1950 years. The PGAs so obtained range from 0,25g of Site A to 0,46g of Site D.

Tab. 6.1 ***Case studies sites for the evaluation of seismic input***

Site	Region	ag for Tr=475 years	ag for Tr=1950 years
A	Piemonte	0,15g	0,25g
B	Toscana	0,22g	0,35g
C	Abruzzo	0,26g	0,42g
D	Calabria	0,27g	0,46g

6.2 Analysis of the seismicity of the sites

The first step in a Hazard Assessment is the study of the seismicity of the area. For each of the four sites were taken into account the main seismogenic sources and the historical and instrumental seismicity in an area with a radius of 100 km from the chosen site. In the following figures for each site will be displayed:

- The individual or composite sources (faults, folds etc…), given by the DISS project (Database of Individual Seismogenic Sources), which can be displayed on Google Maps, published by INGV in

2015 [57]. Within this framework, yellow empty boxes indicate an individual source, while full orange boxes indicate composite source. Moreover, the seismic events of the Italian seismic catalogue are provided [58].

– The seismogenic zones included in ZS9 zoning, and historical and instrumental earthquakes reported in the Italian seismic Catalogue. In the figures the epicenters of the earthquakes are represented by circles, with dimensions proportional to Magnitude Mw of the earthquakes. These are displayed in an Open-source GIS program, Quantum GIS [59].

Site A

Site A, in Piemonte Region, is situated in an area, the western Alps, with a moderate seismicity, and few geological/geomorphologic observations of recent deformation.

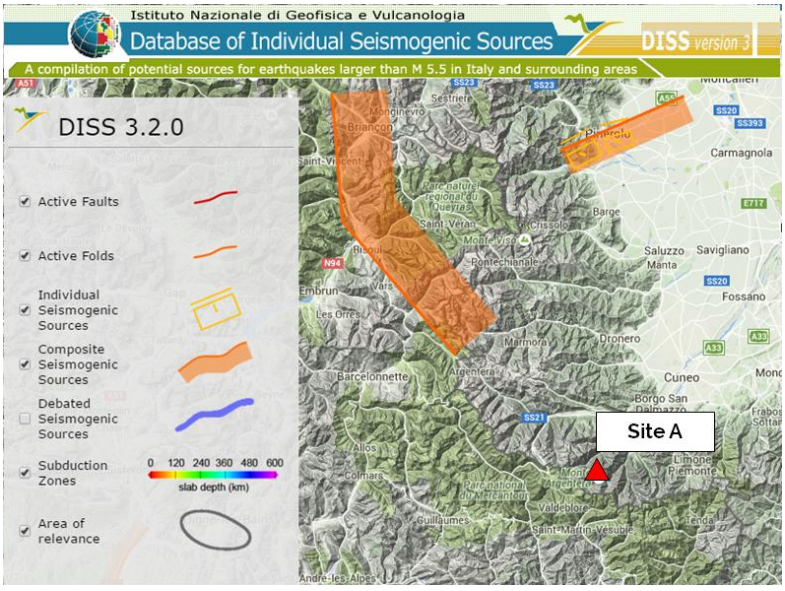

Fig. 6.2 Composite and individual seismogenic sources for Site A, Piemonte

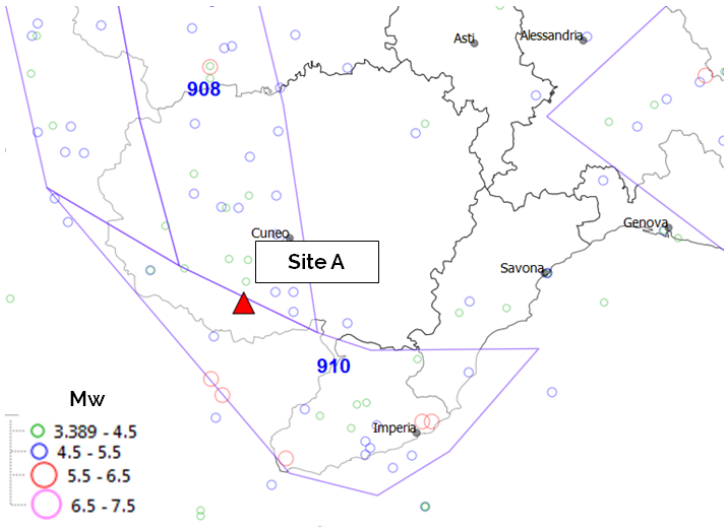

Fig. 6.3 Seismogenic zones; historical and instrumental seismicity for Site A

Fig. 6.2 shows that there are two main seismogenic sources, The Pinerolo Source (ITIS073), associated to the seismic event of April 16, 1808, With Magnitude M 5,6, which is one of the largest events occurred in historical/instrumental time in this portion of the western Alps foothills. The other one is Brianconnais (FRCS001) composite source, which lies at the southwestern border of Switzerland and belongs to Valais system, and shows a number of earthquakes in magnitude range 4,5<M<5.

Site B

Site B is located in an area with seismicity ranging from moderate to medium, with a high density of earthquake in the range of Magnitude 4,5<M<5, fact confirmed also by Fig. 6.5. A very extended composite source, ITCS037 Mugello-Città di Castello-Leonessa more than 200 km, runs from the North-West of Tuscany (Pistoia) to the North East part of Lazio (Nera valley). Historical and instrumental catalogues show seismic events with a maximum magnitude ranging from M 5,4 to M 6. Similar

seismic events in terms of Magnitude are produced also by other seismic sources close to the Site, as the Anghiari and Monterchi sources (M_{max} 5,9) and Selci Lama (M_{max} 5,6) as displayed in Fig. 6.4.

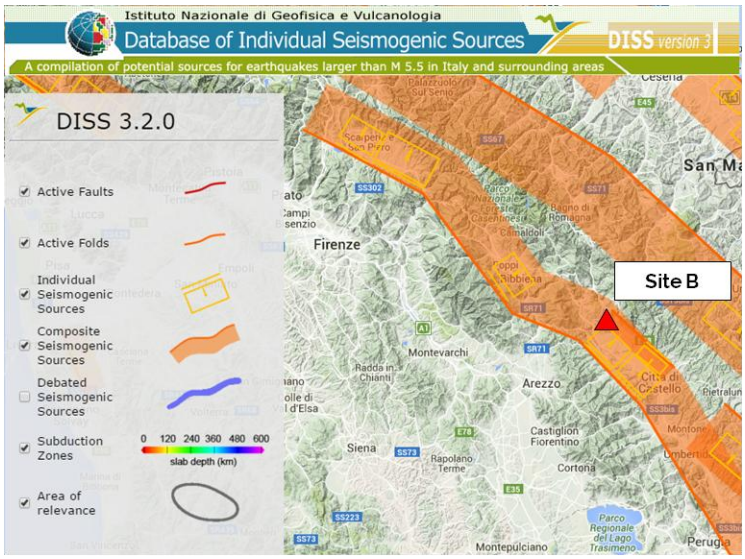

Fig. 6.4 Composite and individual seismogenic sources for Site B, Toscana

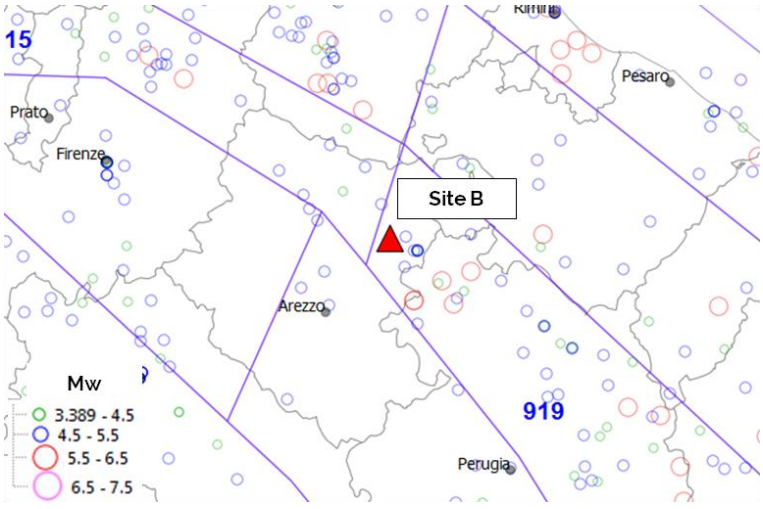

Fig. 6.5 Seismogenic zones; historical and instrumental seismicity for Site B

Site C

Site C shows a medium to high level of seismicity. The site is located on an active fault, "Campotosto Lake 2", which is related to the composite source of Colfiorito-Campotosto, which crosses the regions of Umbria-Marche and arrives up to the Gran Sasso. This source has generated earthquakes ranging from M 5,5 to M 6,8, and was the locus of one of a large aftershock of L'Aquila Earthquake, occurred on April 9, 2009. As depicted in Fig. 6.7 in the region that lies at north-west respect to the site there is a significant presence of earthquakes in the range 5,5-6,5.

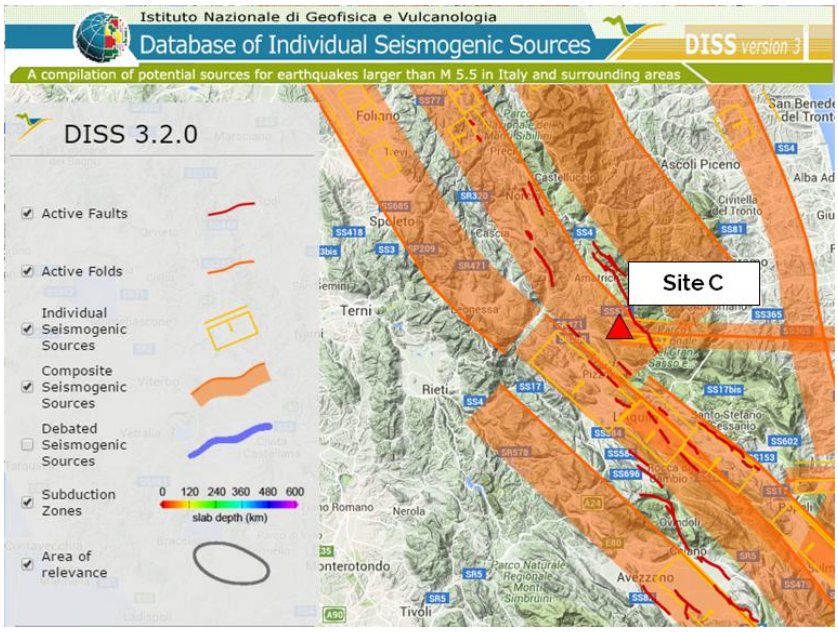

Fig. 6.6 Composite and individual seismogenic sources for Site C, Abruzzo

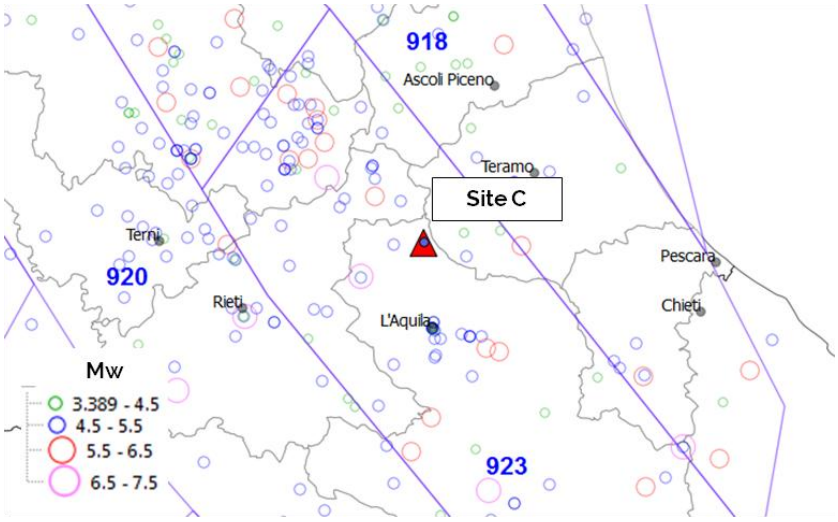

Fig. 6.7 Seismogenic zones; historical and instrumental seismicity for Site C

Other Composite sources are that of Campotosto Lake- Montesilvano, which produces a seismic event with M 5,7, the Bore-Montefeltro-Fabriano-Laga source, with earthquakes ranging from 5,8 to 6,2. The source of Borbona-L'Aquila-Aremogna, with earthquakes ranging from M 5,2 to M 6,6.

Finally some individual sources was identified, namely the Isola del Gran Sasso source, the Montereale Basin source, and the Paganica source, that generated the destructive April 6, 2009 L'Aquila earthquake mainshock, which had a Magnitude M_w 6,3.

Site D

Site D is located in one of the Regions of Italy characterized by a high level of seismicity, with a great number of earthquakes which have magnitude M> 6,5, as displayed in Fig. 6.9. The Composite source of the Savuto River valley, between the cities of Cosenza and Lamezia Terme, generated seismic events that reach magnitude M 7, as the earthquake of

September 8, 1905. Another composite source which produces very high intensity levels is the composite source of Caraffa-Squillace valley, located in the western part of Calabria region, with earthquakes ranging from Mw 6,1 to Mw 7,1. Castiglione-Cosentino source is an individual source included in the system of the above described Caraffa-Squillace source, which generated earthquakes with magnitude M 5,8-5,9. Another composite source is Crotone-Rossano source, which caused a M 6,5 earthquake on 8 march 1832.

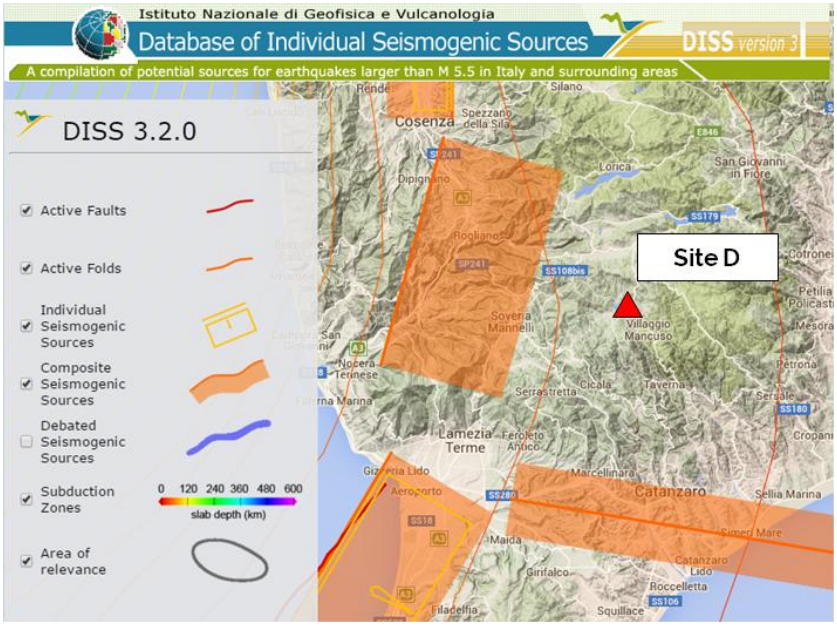

Fig. 6.8 Composite and individual seismogenic sources for Site D, Calabria

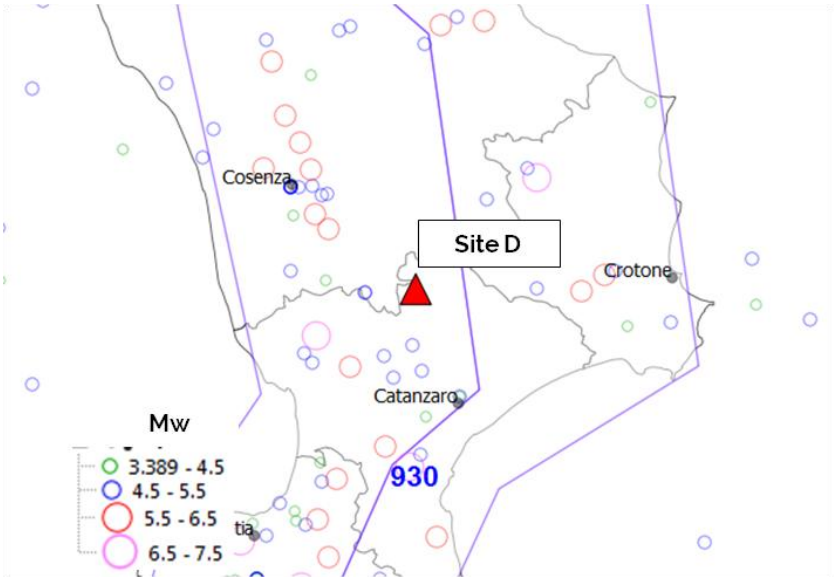

Fig. 6.9 Seismogenic zones; historical and instrumental seismicity for Site D

The Individual source of Sant'Eufemia, located up north the town of Vibo Valentia, was responsible of one of the strongest seismic events ever happened in Italy, that is the 8 September 1908 Calabria earthquake, which had a magnitude Mw 7,5 according to some studies and caused 557 casualties in Capo Vaticano, which had the strongest level of damage (MCS XI), Tropea and Vibo Valentia.

Seismic sources for site D obtained from DISS Database are depicted in Fig. 6.8.

6.3 Uniform Hazard Spectra

As input of the Probabilistic Seismic Hazard Assessment the geographical coordinates of the four sites, the return period and the Italian seismic zoning ZS9 are the data needed Fig. 6.10.

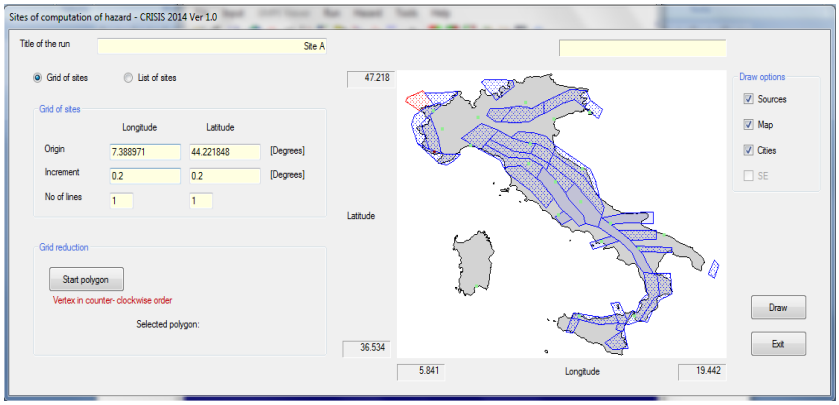

Fig. 6.10 Geographical coordinates and seismogenic zoning ZS9 in CRISIS 2014

It is possible to perform the probabilistic assessment using the software CRISIS 2014 [27], already mentioned in the first part of this work. The first step is to load the geographical coordinates of the four sites. Files with the map of Italy and of the seismic zoning can be uploaded in the program. Then it is necessary to insert the parameters of the recurrence relations computed making a regression analysis on the data available in the Italian Seismic catalogue CPTI11, in the section depicted in Fig. 6.11.

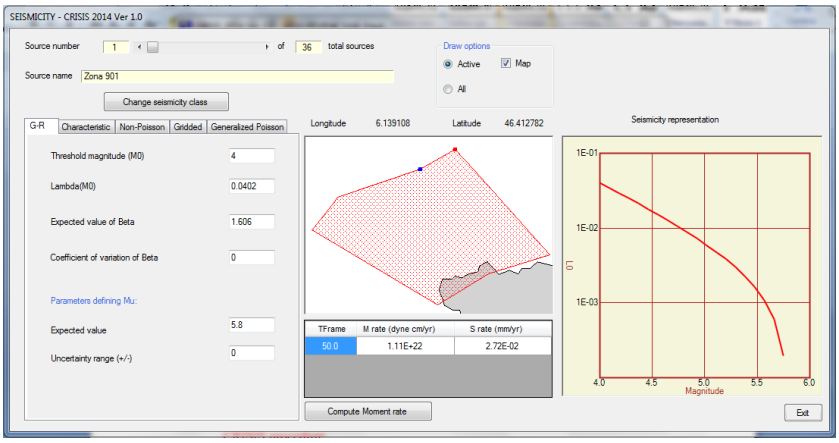

Fig. 6.11 Definition of recurrence relation parameters in CRISIS 2014

It is then possible to define various GMPEs to perform the analysis.

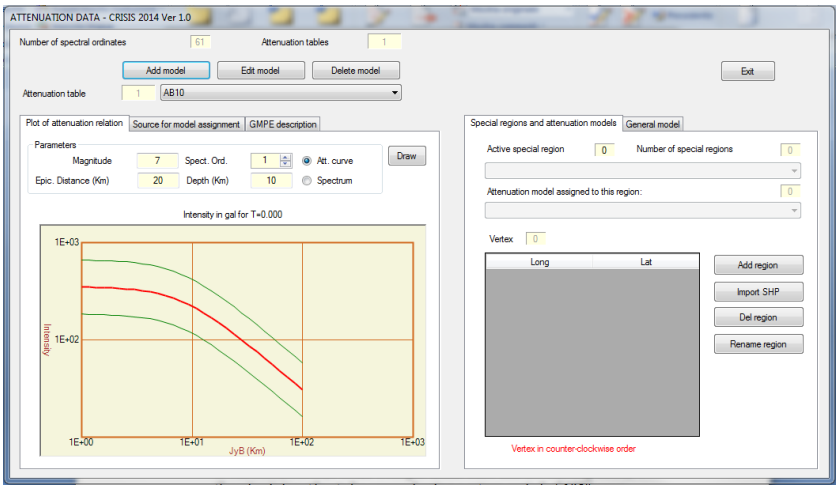

Fig. 6.12 Definition of GMPE in CRISIS 2014

As it was stated before, For the Collapse Limit state and for existing dams, the seismic input has to be assessed using a return period of 1950 years. This time period is longer than the completeness interval of the Italian Seismic Catalogue, which for most of the seismogenic zones is

less than 1000 years. To solve this problem in this part of the work the maximum magnitude was increased by 0,5 Units of M.

For very high return periods, the values of acceleration can reach values which can be physically unrealistic, as it was described in section 3.3.7. In order to solve the problem a threshold in the Ground Motion Predictive Equation was introduced, truncating the equation at 3σ.

The following figures (Fig. 6.13) show the comparison between three Uniform Hazard Spectra. The spectrum depicted in black is the Italian Code response spectrum for a return period of 1950 years. The spectrum in green is the UHS obtained with CRISIS 2014 with the 1996 predictive equation by Sabetta and Pugliese (SP96 in figures), the orange line is the UHS obtained with CRISIS 2014 with the 2010 predictive equation by Akkar and Bommer (AB10 in figures).

It can be pointed out that for sites A and B (low to medium seismic intensity) the values obtained with SP96 spectrum are smaller than the values obtained with AB10 for T<0,15 s, for T>0,15 s AB10 values are smaller, while for sites C and D SP96 values are larger for T<0,25 s, while for T>0,25 s AB10 values are smaller.

It is possible to highlight the good agreement between the Code response spectrum and the response spectra evaluated with CRISIS 2014. Figures show that PSHA spectra are always larger than the Code spectrum in the branch which has constant acceleration.

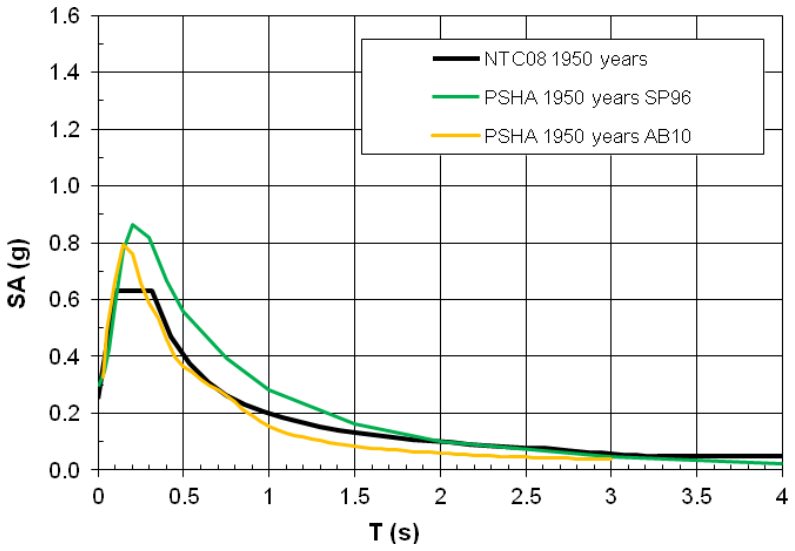

Fig. 6.13 Probabilistic response spectra for site A

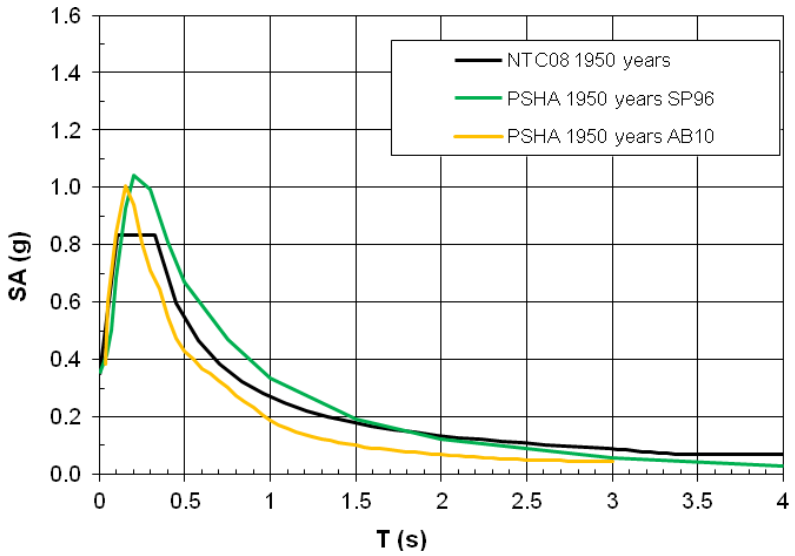

Fig. 6.14 Probabilistic response spectra for site B

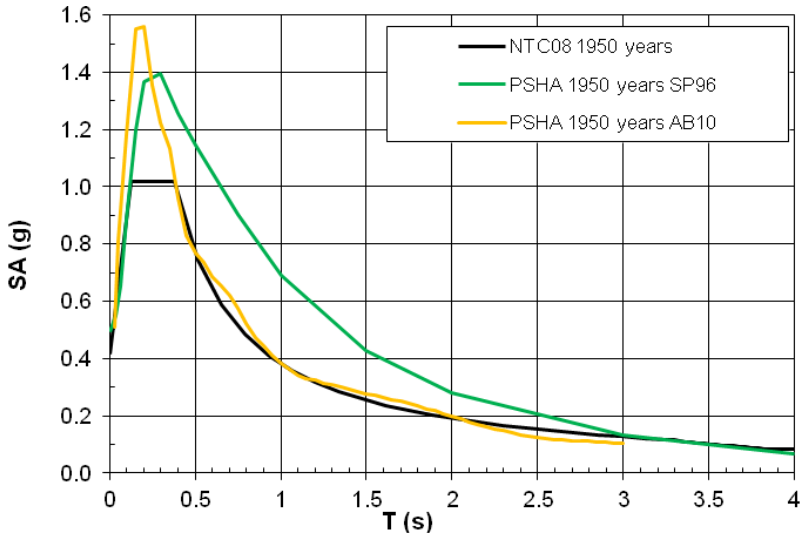

Fig. 6.15 Probabilistic response spectra for site C

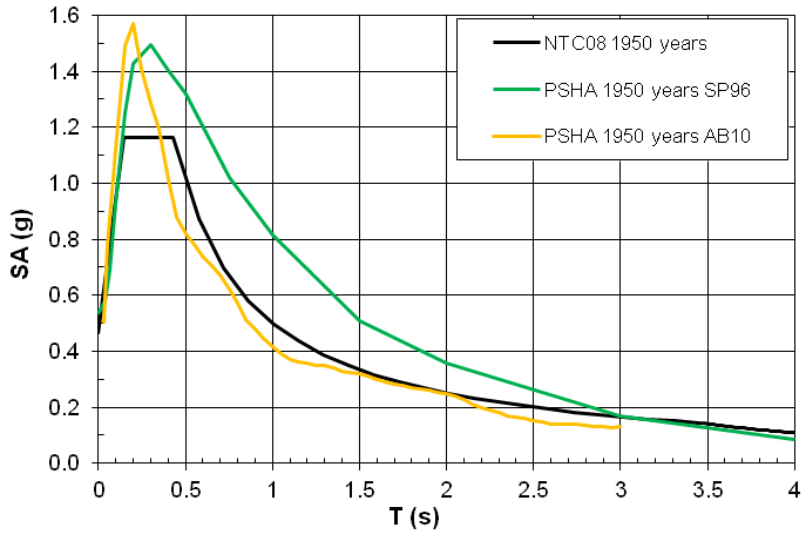

Fig. 6.16 Probabilistic response spectra for site D

6.4 Disaggregation

As described in section 3.6 the Uniform Hazard Spectra are useful to perform direct spectral analyses, while they don't give any information on the seismic events which generated them, so it is necessary to perform the disaggregation of the hazard, which CRISIS provides as output of the analysis.

A disaggregation analysis provides a 3D plot of the probability of occurrence of a given value of intensity, versus the Magnitude and Source to site distance of the seismic event.

Each plot is referred to a specific period of the response spectra: for example, there is a plot which provides the contribution to hazard for the PGA, that is the combination of Magnitude and Distance which produces the maximum Ground Motion at the soil, and it could be evaluated also the combination of M and R which produces the maximum spectral acceleration relative to the structure that is the object of the analysis.

In the following figures (Fig. 6.17, Fig. 6.18, Fig. 6.19, Fig. 6.20) the disaggregation plots for the four sites A, B, C, D are reported for the PGA and for the spectral periods T=0,2 s and T=1 s.

Observing the disaggregation plots it is possible to notice the similarities between the results for PGA and for PSA at T=0,2 s, for all the sites. For Site A the contribution to the hazard for these spectral periods is more likely produced by small to medium values of Magnitude (M 4.3-6) and by near earthquakes (5 km<R<10 km). For Site B it is possible to make similar observations, with higher Magnitudes (M 4.3-6) and the same range of distances.

For Sites C and D it is possible to observe a considerable increase in level of Magnitude, which is in the range M 5.7-6.8 for Site C and M 6-7.1 for site D, while there is a major contribution of far sources.

This fact can be better observed looking at the disaggregation for PSA 1s, in which there are increasing contributions from sources at distances up to 50 km. It is then confirmed a well known fact in seismology, which states that for increasing levels of seismic intensity the seismicity is ruled by largest values of Magnitude and largest distances.

For Concrete dams it is possible to evaluate the fundamental period of the dam as function of its height and of the elastic modulus of concrete with a simplified expression, proposed by Fenves and Chopra [60]:

$$T = \frac{12H}{\sqrt{E_C}} = 0{,}21s$$

Where:

- H=100 m is the height of the dam;
- E_C= 31447 MPa is the elastic modulus of concrete.

This fundamental period can be used as preliminary spectral period to find values in the disaggregation plot to find a controlling earthquake, using the disaggregation plot at 0,2 s.

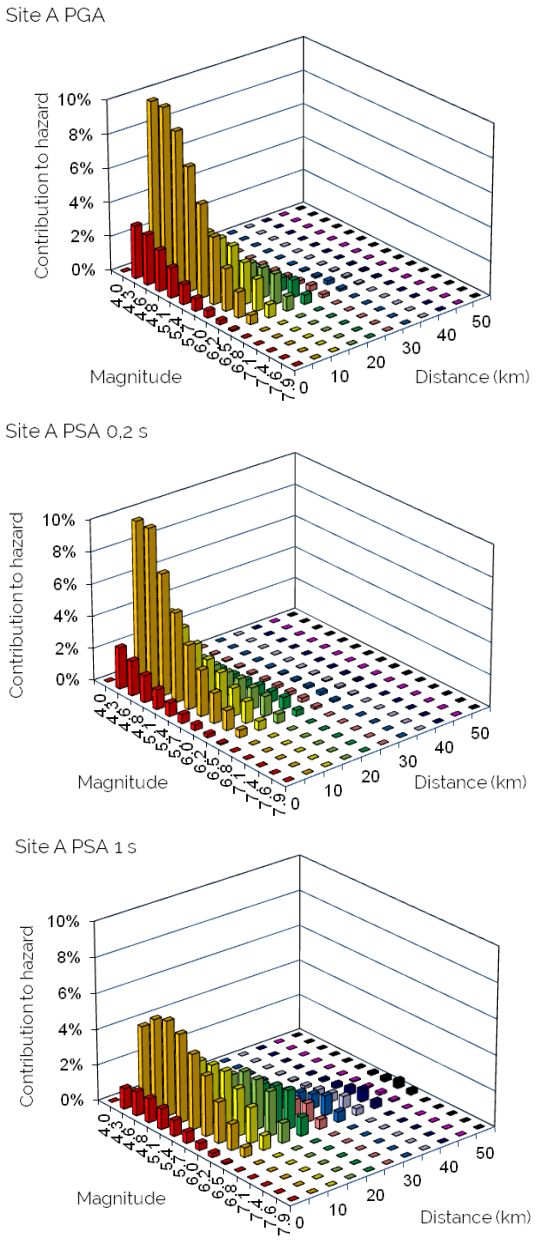

Fig. 6.17 Disaggregation for Site A: PGA (top), PSA 0,2s (middle), PSA 1s (bottom)

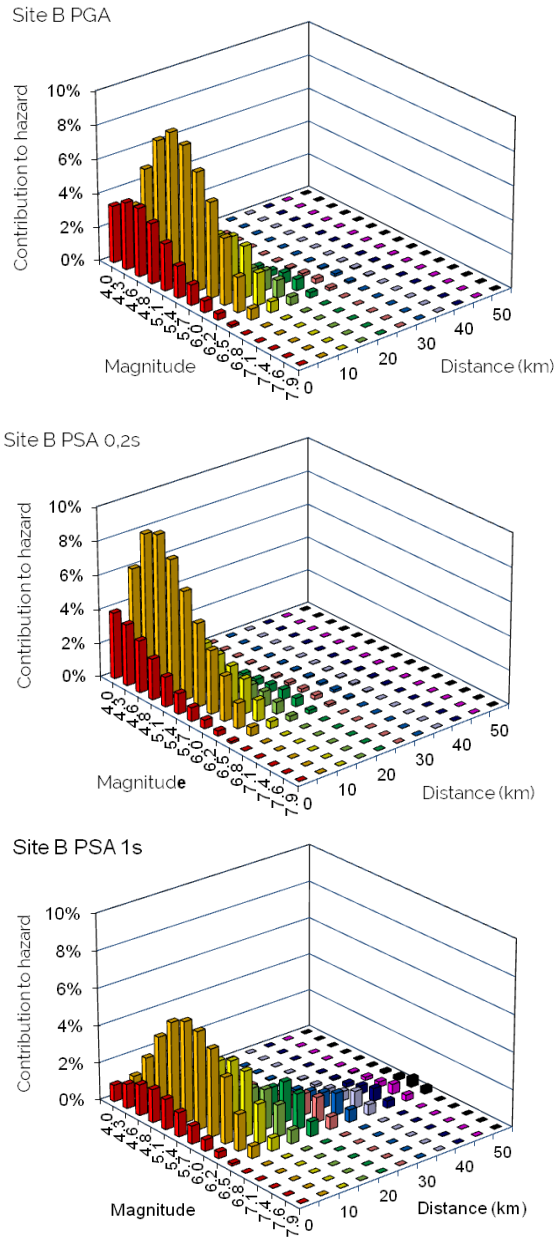

Fig. 6.18 Disaggregation for Site B: PGA (top), PSA 0,2s (middle), PSA 1s (bottom)

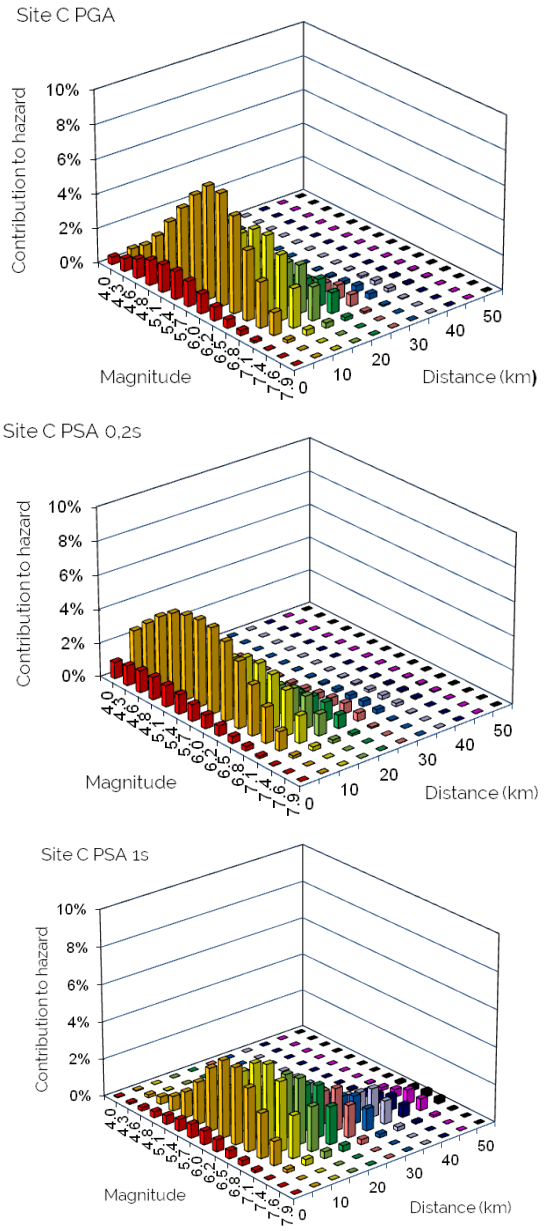

Fig. 6.19 Disaggregation for Site C: PGA (top), PSA 0,2s (middle), PSA 1s (bottom)

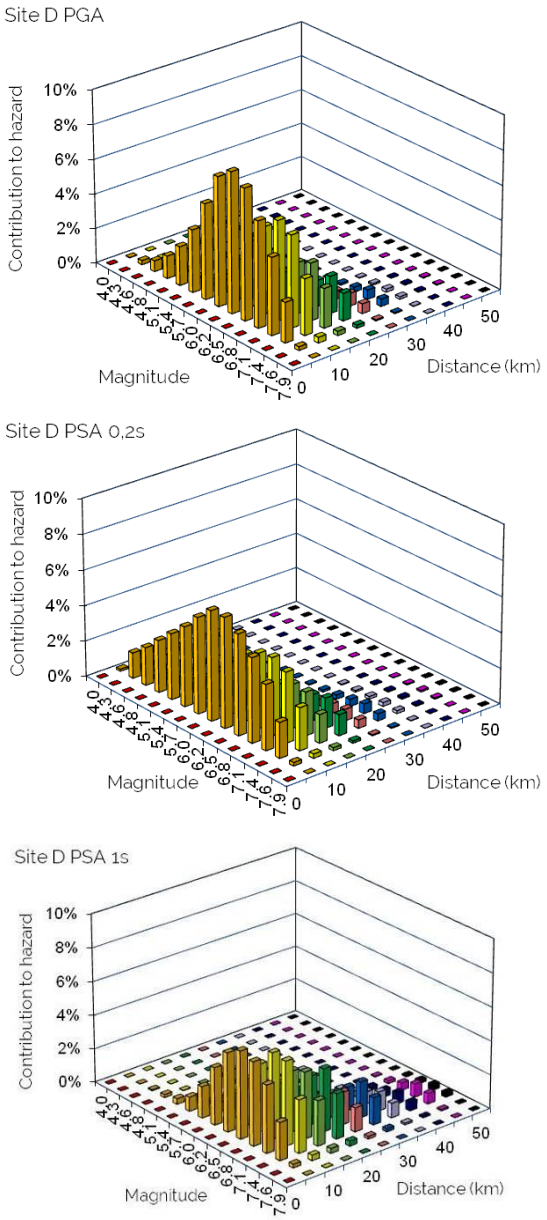

Fig. 6.20 Disaggregation for Site D: PGA (top), PSA 0,2s (middle), PSA 1s (bottom)

6.5 Scenario Earthquakes (DSHA)

As seen in section 6.2, a preliminary examination of the historical and instrumental seismicity can be made for each site, searching in the Database of Individual Seismogenic Sources and in the seismic catalogue CPTI11. Comparing the findings of this examination with the results of the disaggregation a controlling earthquake for each of the case studies can be identified.

For one of them, Site C, we found a recent controlling earthquake with time history records, which is the record of the mainshock of 2009 l'Aquila Earthquake, recorded by AQG seismic station, that is characterized by a site class B according to EC8, since measured velocity of shear waves is Vs=696 m/s. For the other cases, we chose historical earthquakes in the Italian Seismic Catalogue CPTI11. The controlling earthquakes chosen are displayed in Tab. 6.2 for all the case studies.

Tab. 6.2 Controlling earthquakes for the case studies

Site	Controlling earthquake	Magnitude M	Distance R (km)
A	Alpi Marittime 1644	5.8	22
B	Monterchi 1352	6.0	16
C	L'Aquila 2009	6.3	15
D	Calabria 1638	7.0	22

Deterministic response spectra are evaluated by substituting in the chosen GMPEs the values of M and R of the controlling earthquakes. In this case we use the GMPEs SP96 and Akkar & Bommer 2010. The scatter in the ground motion values can have a great influence on the evaluation of the parameters. In order to make the deterministic spectra comparable with the probabilistic ones, fraction of σ ranging from 1,5 to 2 (i.e. ε) were added to the median values obtained with the predictive equations.

Such high values of ε are justified, because in the case of dams a return period of 1950 years is considered, so it can be stated that there is a larger uncertainty on expected values than for normal values of return period.

Following figures (Fig. 6.21, Fig. 6.22, Fig. 6.23, Fig. 6.24) show a comparison between probabilistic and deterministic response spectra. PSHA spectra are depicted with dotted lines, DSHA are depicted with solid lines. It is possible to point out that there is a good agreement with probabilistic spectra, and this is achieved in the hybrid approach by selecting a value of ε that modifies the deterministic spectrum in order to match the probabilistic one.

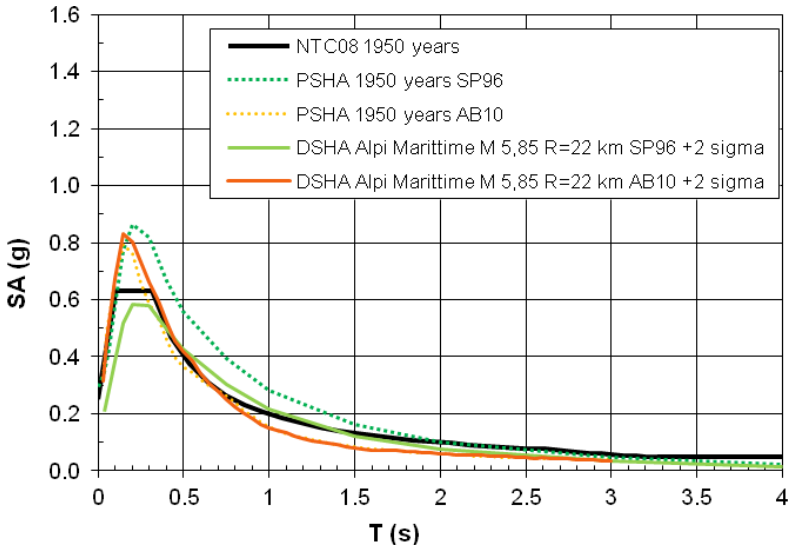

Fig. 6.21 Comparison probabilistic/deterministic spectra for site A

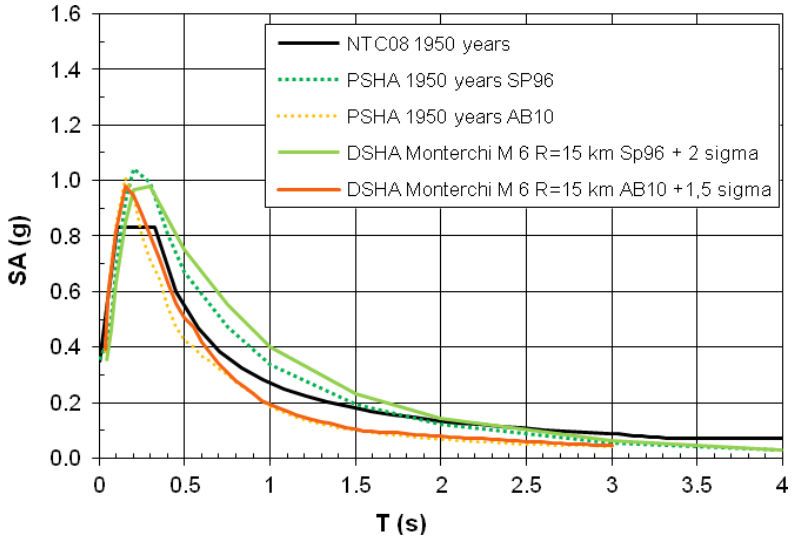

Fig. 6.22 Comparison probabilistic/deterministic spectra for site B

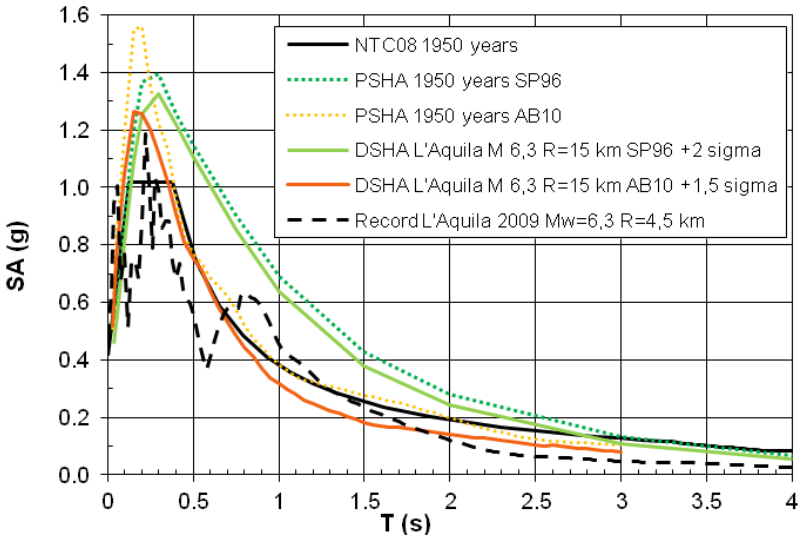

Fig. 6.23 Comparison probabilistic/deterministic spectra for site C

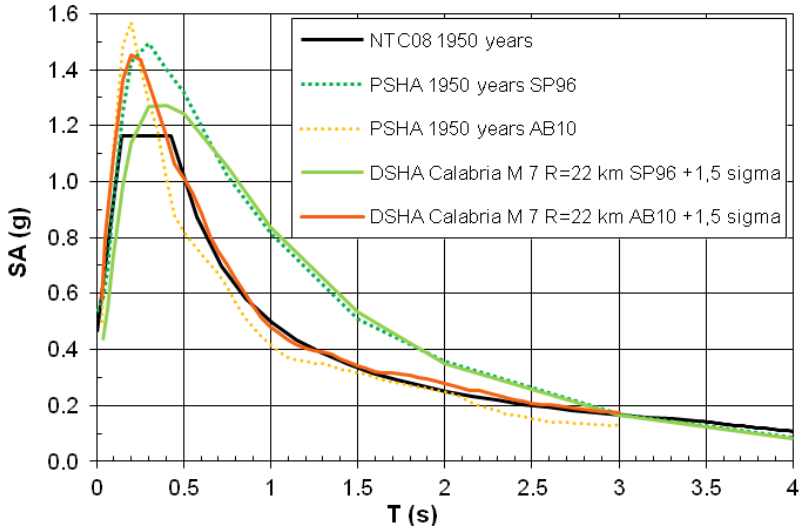

Fig. 6.24 Comparison probabilistic/deterministic spectra for site D

6.6 Sets of scaled and matched accelerograms

The next step in the procedure is the selection and modification of accelerograms with the purpose to understand how the different methodologies of selection and generation of accelerograms affect the response of dams.

For each of the sites were selected two sets of accelerograms:

- A first set of seven accelerograms extracted with the software REXEL, which selects natural accelerograms from various databases, as discussed in section 4.3.2. Then the natural recordings are scaled in order to match the target response spectrum. The parameters used in REXEL to select the natural recordings are reported in Tab. 6.3.

Tab. 6.3 Intervals of Magnitude and distance for REXEL

Site	Magnitude range	Distance range
A	5.7-6.5	0-30
B	6-6.5	0-40
C	6.2-7	0-30
D	6-7.5	10-30

– The second set was obtained starting from the same set of natural accelerograms selected with REXEL, but differs from the former because the recordings were modified with wavelets. The software used in this case is Seismomatch, discussed in section 4.4.1.

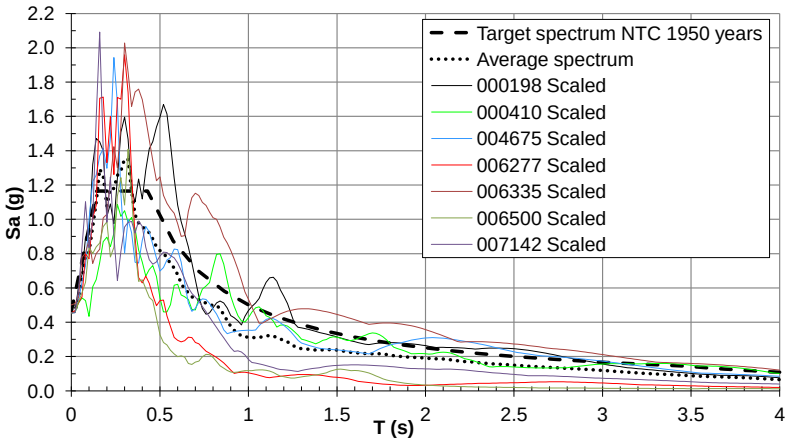

Fig. 6.25 Site D: response spectra of the accelerograms scaled with REXEL

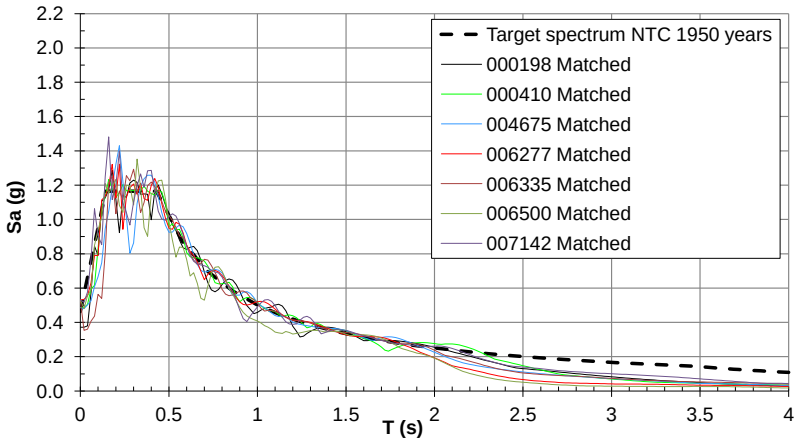

Fig. 6.26 Site D: response spectra of the accelerograms modified with Seismomatch

In both cases the target spectrum used was the Italian Code response spectrum with a return period of 1950 years. Fig. 6.25 and Fig. 6.26 show the results obtained with this methods for site D. It is clear from the images that scaled accelerograms show a high dispersion, in fact the scatter from the target spectra is quite large. The average spectrum (dotted line) is slightly lower than the target spectrum but remains in the limits imposed by the Code.

Regarding matched spectra, it is possible to observe that each natural recording is modified in order to match the target spectra. In this case using 7 accelerograms could be redundant, since the frequency content of the matched accelerograms is very similar.

As an example in Fig. 6.27 it is reported the comparison between the scaled and the matched version of one of the signals selected.

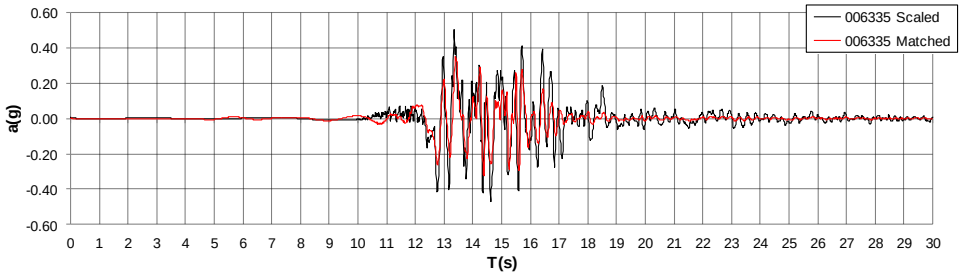

Fig. 6.27 Comparison between scaled and matched accelerogram #6335

7 Simplified analyses - evaluation of base sliding

Concrete gravity dams are formed by vertical blocks, casted in different moments, which resist to horizontal loads by means of their weight. As mentioned in section 6, the vertical joints between blocks have no structural function, therefore it is possible to make the assumption that each block is independent from the others. Therefore, it is possible to study the dynamic behavior of a block with 2D simplified analyses showing the behavior of the dam in section. These methods have the advantage to provide results in short times but are not reliable when tridimensional effects are relevant.

One of this cases is represented by dams built in narrow valleys or with a non-linear path in plan, as for example arch or arch-gravity dams. For this dams accurate analysis have to be performed, which take into account the interaction between structure, reservoir and foundation and also the non-linear behavior in the three dimensions.

Some studies stated that the base sliding is the most probable failure mechanism which can produce the collapse in a concrete gravity dam (See [61]). Stability against the base sliding in one of the main requirements when designing and assessing the seismic safety of a dam. Sliding can occur in any weak plan, inside the dam, the soil or at the interface between the two materials. For dams the weak part lies at the interface between the foundation rock and the dam concrete.

There is a great number of methodologies to evaluate dam safety against sliding, the most used is based on limit analysis, which consist in controlling that the resisting forces are greater than the forces that cause sliding of a certain quantity which is quantified by the Sliding Safety Factor (SSF).

When the purpose of the work is to evaluate the entity of the base displacement produced by an earthquake, that type of approach has to be rejected, and it is better to introduce methods based on the behavior of the dam in the time domain. The base "slip" has to be evaluated for existing dams designed with seismic actions which were lower than the current Codes provisions.

Despite the fact that sliding is considered a critical behavior, it can also bring a positive effect on the dam. Small displacements which happens during a seismic event can produce a dissipation of energy which is sometimes beneficial to the tensional field in the dam.

In the following sections are presented the main methods used in this work to evaluate the interaction between the dam, the reservoir and the foundation, then a method to evaluate the base sliding will be discussed, and it will be applied on a simplified dam model using the seismic input defined for four sites in chapter 6.

7.1 Foundation-dam-reservoir interaction:

7.1.1 Westergaard method (1933)

A paper published by Westergaard in 1933 introduced a method to evaluate the hydrodynamic pressure acting on the dam due to the presence of the water in the reservoir. This work was based on the hypothesis of rigid dam and uncompressible fluid.

The distribution of pressures on the upstream wall of the dam had a parabolic trend, which is depicted in Fig. 7.1. It is possible to think at the pressures distribution as a certain part of the water in the reservoir is moving together with the dam, so it is possible to estimate a volume of water which is capable of generating an inertial force equivalent to the

hydrodynamic pressure. By simplifying it could be possible to think at this volume of water as it was an "added mass" attached to the dam.

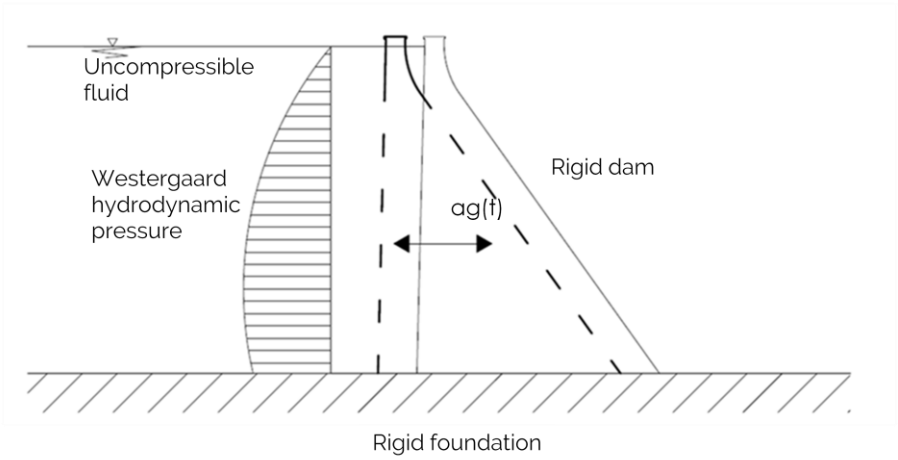

Fig. 7.1 Dam-reservoir dynamic interaction according to Westergaard

7.1.2 Fenves and Chopra method (1986)

Some authors, including Chopra, tried to develop a procedure to evaluate the seismic response of the dam considering the interaction of the dam with the water in the reservoir and with the foundation.

Previously, in a work made in 1978 he observed that the fundamental vibration mode of a dam is the one which causes the largest effects on the structure. Following this approach, the dam can be modeled as an equivalent SDOF system.

As a conclusion of this work, together with Fenves they published on ASCE journal a work with the title "Simplified analysis for earthquake resistant design of concrete gravity dams" [60]. This work evaluated the response of the dam in three steps, referring to:

– The fundamental vibration mode of the dam (and higher modes);

- The dam-reservoir interaction;
- The dam-foundation interaction.

The main advantage of this method is due to the introduction in the method of the interactions with the reservoir and with the foundation. These interactions were considered separately and then combined.

The sections of gravity dams are quite similar to each other, therefore a modal shape which can be used for the majority of the case studies has been proposed. On the basis of this modal shape the authors proposed an equivalent static force which is able to reproduce the effects associated to the first vibration mode.

Another work by the same authors proposed also a method to take into account the effects of higher modes on the dam response. In both cases the advantage of the method is that a static load distribution equivalent to the seismic action to be applied to the dam is provided.

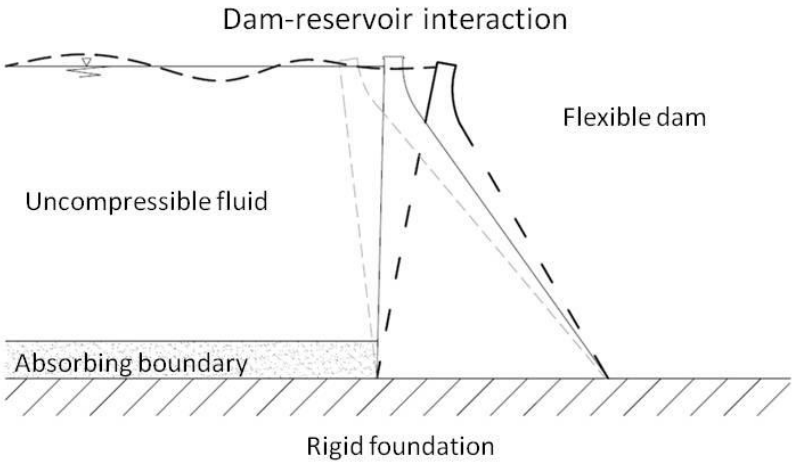

Fig. 7.2 Fenves and Chopra method: Dam-reservoir interaction

Since the method proposed is linear, the static force distributions include the contribution of the dam-foundation and dam-reservoir interactions by means of the superposition principle.

The dam-reservoir interaction, depicted in Fig. 7.2 is based on the hypothesis of flexible dam and rigid foundation. The water modifies the response of the structure introducing an external force which can be added to the component given by the ground motion, a change of the mass of the system and a modification in the damping of the SDOF system. This last feature is due to *radiation damping*, that is the partial absorption of hydrodynamic pressure waves by the sediments invariably deposited at the bottom and sides of the reservoir, or by the rock underlying the reservoir.

The dam foundation interaction considered by Fenves and Chopra is depicted in Fig. 7.3. Dam's foundations are generally formed by rocks with good mechanical features, suggesting that the deformability of the foundation is limited. The hypothesis done is that there is a rigid motion at the base of the dam.

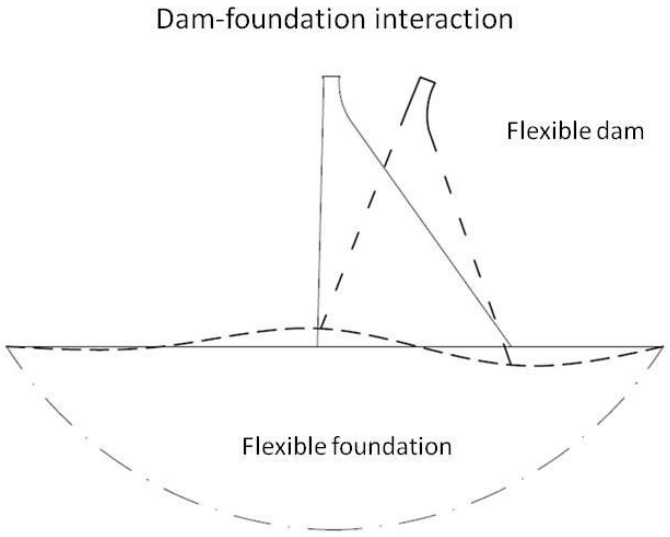

Fig. 7.3 Fenves and Chopra method: Dam-foundation interaction

A particular aspect which characterizes dam behavior is the low contribution of the first mode to the participating mass, so it could be needful to take into account the contribution of higher modes. The method by Fenves and Chopra provides a simplified method also to evaluate this contribution. Then the responses obtained for the first mode and higher modes must be combined using SRSS or ABSUM methods. When performing a first analysis the contribution of the first modes could be neglected.

It is then possible to point out that if the interactions of the dam with the foundation and the reservoir are considered, the parameters of the oscillator can be modified in order to take into account these interactions.

Considering the interactions brings to a SDOF system which has a larger mass, that takes into account also for the hydrodynamic pressure of the water in the reservoir, a lower stiffness due to the flexibility of the

foundation and a larger damping, resulting in an equivalent fundamental period T_{eq} which is different from the period obtained with the rigid dam. Consequently, if the period changes also the spectral acceleration is different.

7.2 Base sliding: Nuti- Basili Method (2009)

7.2.1 Introduction

The method proposed by Nuti and Basili [62] had the purpose to provide a simplified method to evaluate the base sliding of concrete gravity dams using regression curves, without the need to perform non-linear analyses. The procedure proposed by the authors integrated the linear method by Fenves and Chopra in the definition of the parameters of a new equivalent non-linear SDOF system.

In order to define the non-linear model it is worth to notice that a new variable must be introduced, which is the resistance of the dam to the base sliding. Starting from the dynamic balance equation, where every element was divided for $\widetilde{M}$:

$$\ddot{y}(t) + 2\tilde{\xi}\tilde{\omega}\dot{y}(t) + \tilde{\omega}^2 y(t) = -\frac{\tilde{\omega}_f{}^2}{\tilde{\omega}^2}\frac{\tilde{L}}{\tilde{M}}\, a_g(t).$$

If the participation factor and the equivalent mass to the Dam-foundation-reservoir system are the following:

$$p = \frac{\tilde{\omega}_f{}^2}{\tilde{\omega}^2}\frac{\tilde{L}}{\tilde{M}}$$

$$M_{dw} = -\frac{\tilde{\omega}_f{}^2}{\tilde{\omega}^2}\tilde{L}$$

If the equation is divided for p and then is multiplied for M_{dw}, stating that

$$D(t) = \frac{y(t)}{p}$$

Where D(t) is the displacement response of the SDOF system associated to the equivalent system, which is described by the following equivalent parameters: M_{dw}, $\tilde{\xi}$, $\tilde{\omega}$.

The equation is:

$$M_{dw}\ddot{D}(t) + 2\tilde{\xi}\tilde{\omega}M_{dw}\dot{D}(t) + \tilde{\omega}^2 M_{dw}D(t) = -M_{dw}\, a_g(t)$$

The shear resistance is evaluated using a Mohr-Coulomb law:

$$\tau = c + \sigma tan\phi$$

which can be rewritten in terms of forces as:

$$R_y = R_{yc} + R_{y\phi} = cA + (P_d - U_w)tan\phi$$

The response of the above described SDOF system can be split into a linear elastic response D(t) and in a non-linear response coincident with the displacement at the foundation level D_f. Starting by an equivalent SDOF system capable to take into account the interactions with reservoir and foundation, it is possible to evaluate the equivalent fundamental period and the spectral acceleration, which will cause a certain value of shear at the base of the dam.

When the shear force acting on the dam is minor than R_y the rock behaves as a linear elastic material. When the shear force is equal to R_y, a plastic displacement raises and there is a dissipation of the energy produced by the earthquake thus causing a permanent displacement. In this case the acceleration is constant during time and equal to the limit acceleration, corresponding to the limit shear. This behavior is depicted in Fig. 7.4.

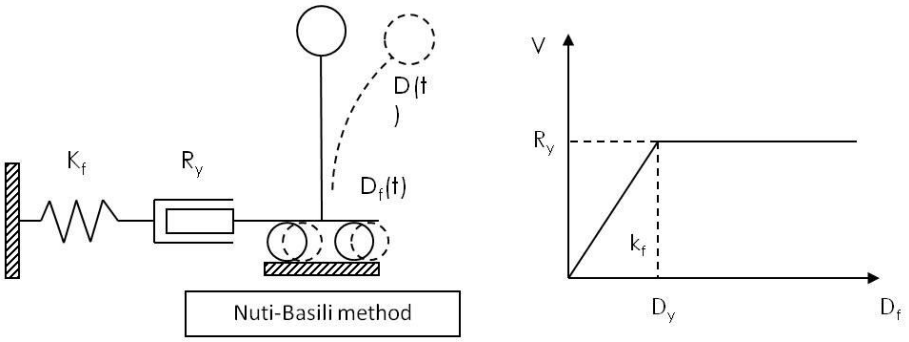

Fig. 7.4 Nuti-Basili model for SDOF non-linear system (Nuti and Basili, 2009)

The base displacement can be therefore expressed by the following equation:

$$D_f = \begin{cases} \frac{V}{K_f} & per\ V < R_y \\ \frac{V}{K_f} + \Delta\ per\ V = Ry \end{cases}$$

Where V is the base shear force and K_f is the foundation stiffness. The latter was evaluated on the basis of the work by Nuti and Pinto [63].

7.2.2 Simplified method: parameters used

Starting from the model which has been described in the previous section, it is useful to define some parameters which are able to synthesize the results obtained with non-linear analyses.

The limit acceleration a_L is the acceleration for which there is the first base displacement, and it is defined as:

$$a_L = \frac{\tilde{R}_y - \tilde{P}_w}{M_{dw}}$$

Where M_{dw} is the equivalent oscillator mass which takes into account the interaction of the dam with the foundation and the reservoir, $\widetilde{R_y}$ is the base shear resistance and $\widetilde{P_w}$ is the net force of the hydrostatic pressure in the equivalent system.

β is defined as the ratio between the limit acceleration and the acting acceleration:

$$\beta = \frac{a_L}{a(\bar{T})}$$

The acceleration a(T) is the spectral acceleration obtained from a spectrum with a 5% damping ratio. This parameter can give a measure of whether the sliding resistance has been exceeded and how large is this difference. If β is greater than unity, the dam behaves in linear elastic field, when β is less or equal to unity, the base sliding begins.

μ is defined as the ratio between the maximum displacement at the crest of the dam and the displacement for which there is a base sliding.

$$\mu = \frac{D_{max}}{D_y} = \frac{y_{max}}{y_y}$$

On the basis of non-linear analyses Nuti and Basili plotted the ductility factor μ versus the parameter β for four dams which had different heights. A correlation was found between this values, showing that for $0{,}5<\beta<1$ the equation:

$$\mu = \frac{1}{\beta}$$

allows to estimate in a conservative way the coefficient of ductility. For values of β less than 0,5, corresponding to a greater risk for the dam, results are more dispersed and can therefore bring to wrong evaluations of

the residual displacement. An application of this method is discussed in the next section, which also explains how the non-linear analyses were performed.

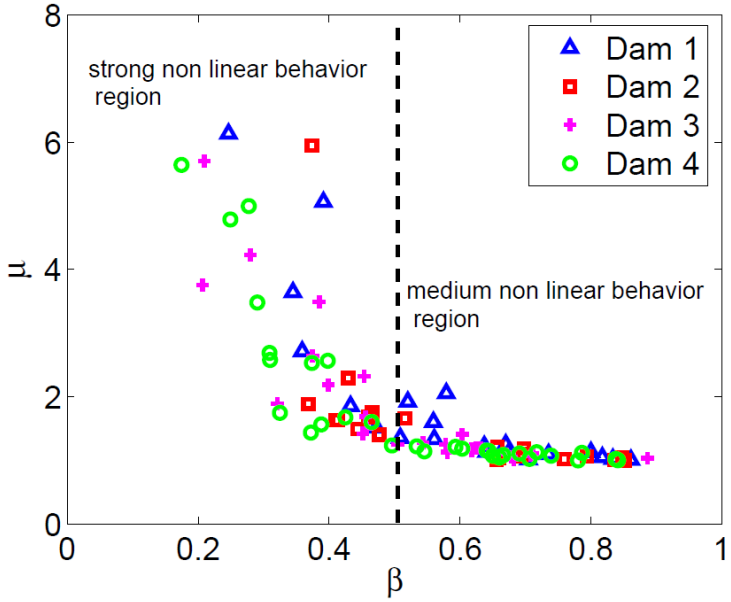

Fig. 7.5 Plot of μ vs β as presented by Nuti and Basili (Nuti and Basili, 2009)

7.3 Application of the method to a case study

7.3.1 Definition of the Case study

The dam considered for these simplified analyses is a concrete gravity dam, with a total height of the highest block of 87 m (H_D), a crest width of 5 m and an inclination of the downstream wall of 0,7 (α). The model of the dam in depicted in Fig. 7.6.

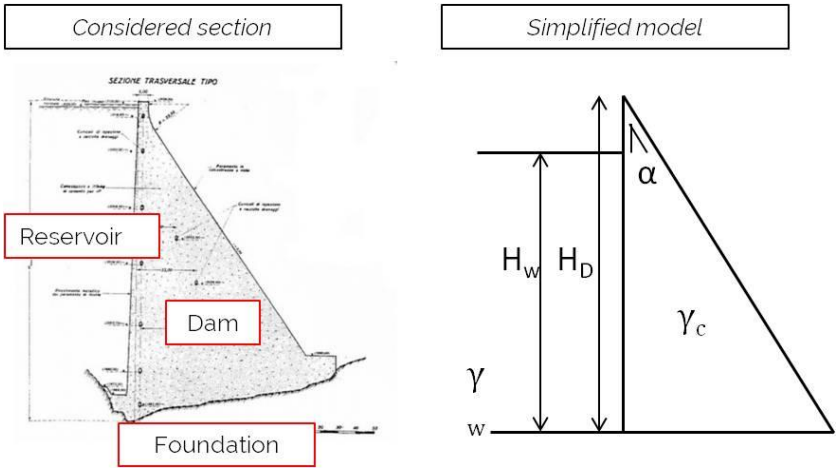

Fig. 7.6 Highest block of the gravity dam (left) and simplified model (right)

It is important to highlight that all the simplified analyses come from the hypothesis that the behavior of the blocks forming the gravity dam is independent from one to another. In fact, since the blocks of a gravity dam resist by their weight, they have a mainly cantilever behavior, as discussed in a previous section.

7.3.2 Application of the simplified method

The dam was modeled as a SDOF system, with parameters defined by the theory of Fenves and Chopra [60] which as seen in section 7.1 allows to evaluate the interaction between fluid, foundation and structure.

The mass of the system has been increased to take into account the effect of the water in the reservoir, the stiffness was modified to simulate the effects of the interaction with the foundation and the damping was increased in order to consider the contribution of the fluid and of the soil.

To evaluate the residual displacement produced by the seismic event a perfect elasto-plastic behavior was introduced between the base node and the foundation, capable to produce a Coulomb-type friction behavior.

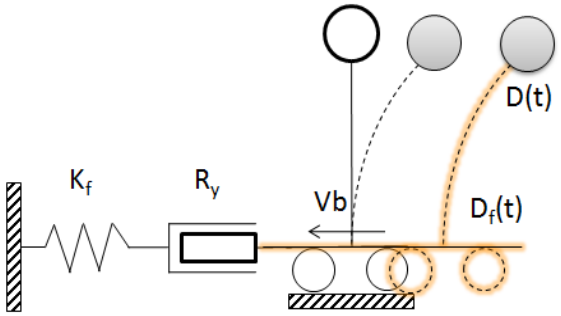

Fig. 7.7 SDOF equivalent system proposed by Nuti and Basili (2009).

When the base shear produced by the earthquake exceed the sliding resistance there is a base sliding at the base of the dam. With the purpose to highlight the differences between the effects of the accelerograms defined previously, a friction angle of 45° was considered, while the cohesion was neglected. The model was implemented in Opensees [64] software, with the fundamental support of a Matlab program.

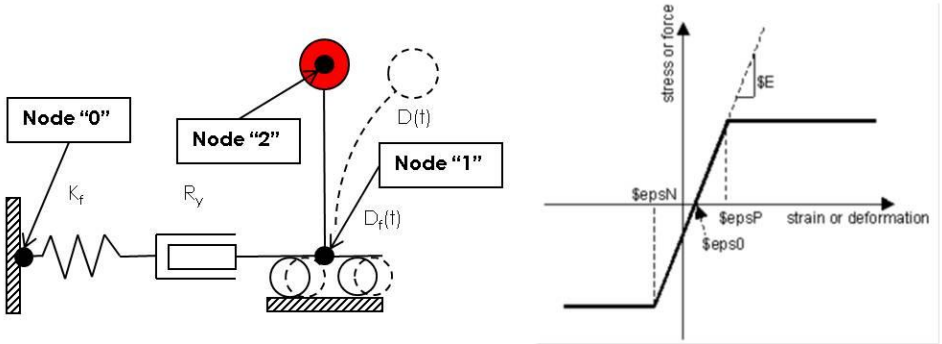

Fig. 7.8 SDOF system modeled in Opensees

In Opensees, the dam was modeled as an "elasticBeamColumn" element, while the non-linearity and the deformability of the foundation were modeled using a "zeroLength" element (See Fig. 7.8).

56 non-linear analyses were performed with this programs, 14 analyses for each of the four sites selected, changing the input accelerograms but maintaining the same dam model. The fundamental period of the dam when the reservoir is empty is resulted to be T_1=0,21 s. Considering the mass of the reservoir for the maximum water level the period obtained is T_1=0,29 s and the damping ratio is around 7%, parameters that are close to the results obtained with the accurate finite element model, which will be discussed in next sections.

7.3.3 Results

Fig. 7.9 shows the maximum response of the equivalent SDOF system for the accelerograms that produced the largest base sliding, which is reported in Fig. 6.27 and it is signal 006335 recorded in South Iceland. On the top of Fig. 7.9 is reported the relative displacement, which is the difference between the displacements at the crest and at the base of the dam, and this is reported for linear and non-linear SDOF system.

When this displacement reaches the sliding displacement threshold, which value is 56 mm (dotted red line), the dam slides as depicted in the lower part of the figure. As described in Nuti and Basili work (2010), this displacement is also associated with the sliding resistance R_y=64022 kN and the limit acceleration a_L=3.80 m/sec^2. Knowing this, the nonlinear behavior of the structure, evaluated in terms of base sliding, is strongly influenced by the shape of the signals used.

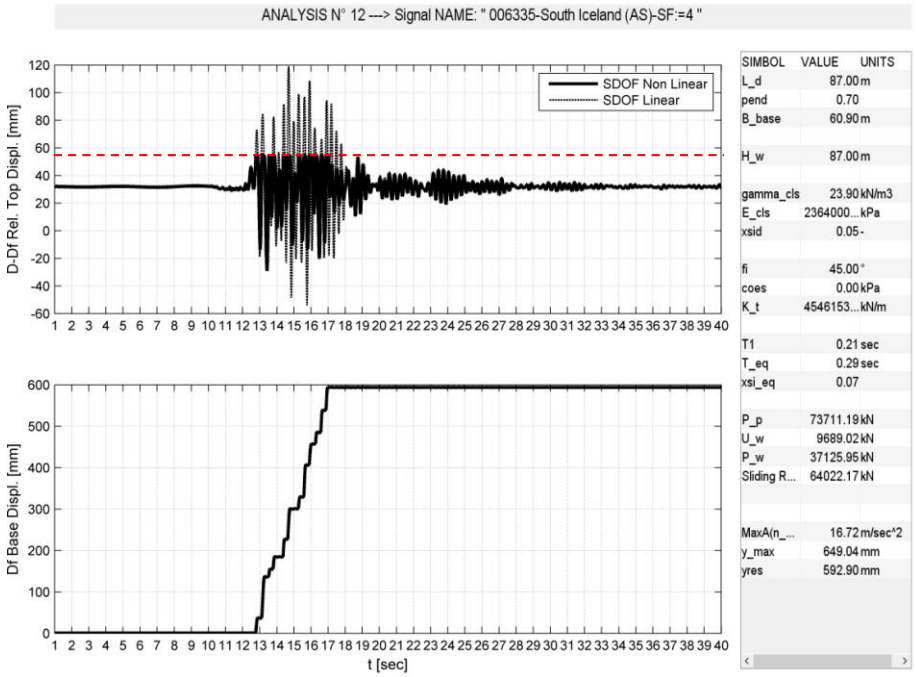

Fig. 7.9 Response for the accelerogram 006335: (top) relative displacement of nonlinear SDOF compared with a linear one; (bottom) plot of the base sliding.

The most important provision given by the Codes about the safety of a dam is that the uncontrolled release of water must be avoided, so there is the need to limit the base displacement, which cannot reach values that are incompatible with the hydraulic seal of the vertical joints between the blocks of the dam. It is worth to note that the base sliding can also produce a beneficial reduction of the stresses in the dam: actually it is possible to think at the base sliding as a damper for the dam.

In Fig. 7.10 are depicted the results in terms of base displacement for the selected sites A, B, C, D. It is possible to highlight that the displacement is larger for higher levels of seismicity, as expected, and the trend of the

dynamic responses shows that the highest values in terms of response are obtained with scaled records. The maximum base displacement is achieved as depicted in the previous figure for signal 006335 for site D.

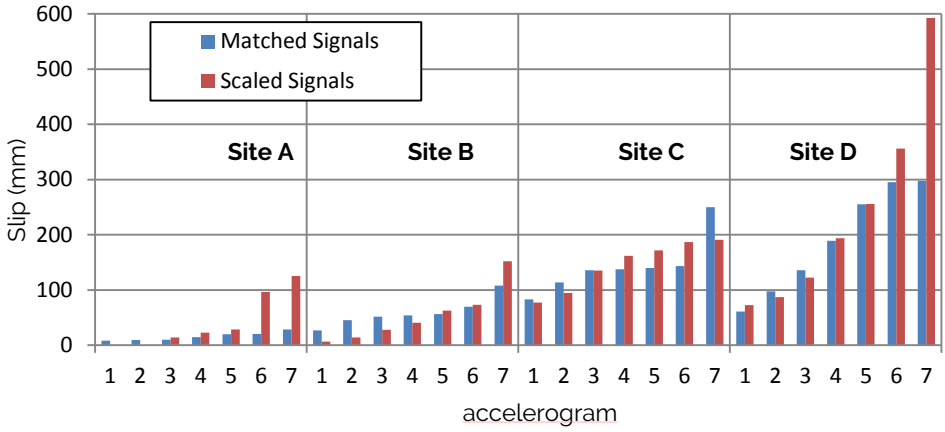

Fig. 7.10 Base displacement obtained with the 56 analyses for sites A, B, C, D

Tab. 7.1 Results of simplified analyses

	MATCHED SIGNALS					SCALED SIGNALS			
	N	**CODE**	**$S_e(T)$ [m/sec^2]**	**D_{max} [mm]**	**Slip [mm]**	**CODE**	**$S_e(T)$ [m/sec^2]**	**D_{max} [mm]**	**Slip [mm]**
Site A (PGA=0.25 g)	1	000055x-EQ:=22	5.3	66	10	000055-Friuli-SF:=0.7	6.1	79	23
	2	000368x-EQ:=23	6.6	65	9	000368-Lazio - Abruzzo-SF:=3.9	5.6	70	14
	3	000661x-EQ:=28	5.5	65	9	000661-Umbria - Marche-SF:=2.3	7.1	84	28
	4	006327x-EQ:=28	6.2	76	20	006327-South Iceland (AS)-SF:=2	3.1	50	0
	5	006333x-EQ:=106	6.1	76	20	006333-South Iceland (AS)-SF:=9	3.3	52	0
	6	006335x-EQ:=106	6.9	85	29	006335-South Iceland (AS)-SF:=2.2	9.1	182	126
	7	007142x-EQ:=111	6.3	71	15	007142-Bingol (Turkey)-SF:=0.8	8.6	153	96
		AVERAGE			**16**	AVERAGE			**41**
Site B (PGA=0.35 g)	1	000055x-EQ:=22	7.7	110	54	000055-Friuli-SF:=1	8.4	129	73
	2	000604x-EQ:=23	8.1	101	45	000604-Umbria Marche-SF:=16.1	7.6	97	41
	3	006270x-EQ:=28	8.6	83	27	006270-South Iceland-SF:=5.2	7.0	70	14
	4	006332x-EQ:=28	7.6	112	56	006332-South Iceland (AS)-SF:=0.7	9.3	119	63
	5	006349x-EQ:=106	7.9	164	108	006349-South Iceland (AS)-SF:=0.4	7.0	62	6
	6	007142x-EQ:=106	7.4	126	70	007142-Bingol (Turkey)-SF:=0.7	6.8	84	28
	7	007187x-EQ:=111	6.3	108	52	007187-Avej (Iran)-SF:=0.8	8.6	208	152
		AVERAGE			**59**	AVERAGE			**54**
Site C (PGA=0.42 g)	1	000055x-EQ:=22	10.8	170	114	000055-Friuli-SF:=1.2	12.6	228	172
	2	000198x-EQ:=23	11.4	139	83	000198-Montenegro-SF:=2.3	14.0	247	191
	3	000234x-EQ:=28	10.7	196	140	000234-Montenegro (AS)-SF:=6.1	9.9	218	162
	4	004674x-EQ:=28	9.8	193	137	004674-South Iceland-SF:=1.3	11.5	243	187
	5	006332x-EQ:=106	11.0	192	136	006332-South Iceland (AS)-SF:=0.8	11.1	151	95
	6	006333x-EQ:=106	11.2	200	144	006333-South Iceland (AS)-SF:=20.5	7.6	191	135
	7	007142x-EQ:=111	11.5	306	250	007142-Bingol (Turkey)-SF:=0.8	8.1	133	77
		AVERAGE			**143**	AVERAGE			**146**
Site D (PGA=0.46 g)	1	000198x-EQ:=22	12.0	154	98	000198-Montenegro-SF:=2.6	15.6	312	256
	2	000410x-EQ:=23	11.5	192	136	000410-Golbasi (Turkey)-SF:=11.9	10.3	143	87
	3	004675x-EQ:=28	7.6	117	61	004675-South Iceland-SF:=3.5	8.5	129	73
	4	006277x-EQ:=28	10.7	311	255	006277-South Iceland-SF:=1.3	17.6	412	356
	5	006335x-EQ:=106	11.2	245	189	006335-South Iceland (AS)-SF:=4	16.7	649	593
	6	006500x-EQ:=106	10.4	351	295	006500-Duzce (Turkey)-SF:=0.9	10.4	250	194
	7	007142x-EQ:=111	10.6	354	298	007142-Bingol (Turkey)-SF:=0.9	9.1	179	122
		AVERAGE			**190**	AVERAGE			**240**

In Tab. 7.1 are shown the results in terms of maximum crest displacement (D_{max}) and residual base displacement (slip) produced by the selected accelerograms. For each site are listed the results for the two sets of matched and scaled signals. It is also reported the scale factor for scaled accelerograms and the spectral acceleration $S_e(T)$. For each site and set of accelerograms the average values of the sliding displacement are shown.

As remarked before, results are strongly affected by the signal shape. As shown in Figure 4 the 006335 code signal, associated to the "South Iceland" earthquake, has a great number of peaks close to the PGA value. Conversely the signal that produces the lower effects for scaled Site D records is the 004675 signal, another South Iceland record.

In order to evaluate the safety requirements of the dam in accordance with the Code, the average values of the results obtained for the 7 set of ground motion are taken as reference. These values have to be compared with the minimum sliding that can affect the hydraulic seal of the vertical joints. In absence of indications 100 mm is assumed. Considering this and the preliminary analyses results, only Site C and Site D earthquakes seem capable to produce uncontrolled release of water and for these reason they need more advanced analysis.

The selection of the accelerograms strongly influences the results of non linear analyses. The 7 signals derived from the matching obtained with Seismomatch software, are closer to the target spectrum and the results obtained are also closer.

It is interesting to compare the average, standard deviation and covariance (COV) obtained for all the groups of spectrum compatible signals used. Tab. 7.2 suggests that the matched signals exhibit a significantly lower COV than the scaled signals.

Tab. 7.2 Statistical parameters of the base residual displacement for the different groups of signals

Set of accelerograms	Average [mm]	σ [mm]	COV
Sito A - 7 Matched Signals (NTC)	16	7	0.47
Sito B - 7 Matched Signals (NTC)	59	25	0.43
Sito C - 7 Matched Signals (NTC)	143	52	0.36
Sito D - 7 Matched Signals (NTC)	190	96	0.50
Sito A - 7 Scaled Signals (NTC)	41	50	1.21
Sito B - 7 Scaled Signals (NTC)	54	50	0.92
Sito C - 7 Scaled Signals (NTC)	146	45	0.31
Sito D - 7 Scaled Signals (NTC)	240	185	0.77

The results confirm the great influence of signal selection on non-linear behavior. This is only partially reduced considering matched instead of scaled signals.

Simplified analyses present the advantage to be faster than more complex analyses, and allow to understand which input records are more damaging for the considered structure. This fact can be useful also to understand in which cases it is necessary to perform more accurate analyses. These latter are essential to study with precision the evolution of the dam response in the time domain.

7.3.4 Application of the Nuti-Basili curve

As it was stated before, there are simplified methods in literature based on equivalent static forces which can avoid the use of dynamic nonlinear analyses. The example of the Nuti and Basili simplified method [62], discussed in section 7.2, is reported here.

Fig. 7.11 shows the results obtained with this method for the 56 analyses performed in this study for the four sites A, B, C, D. The demand, the

capacity and the response of the dam are synthesized in the β-μ chart, where β represent the ratio between the acceleration that produces sliding a_L and the spectral acceleration $S_e(T)$ and μ is the ratio between maximum absolute displacement D_{max} and D_y. The results obtained for all the analyses done are reported in terms of β-μ points in Figure 5.

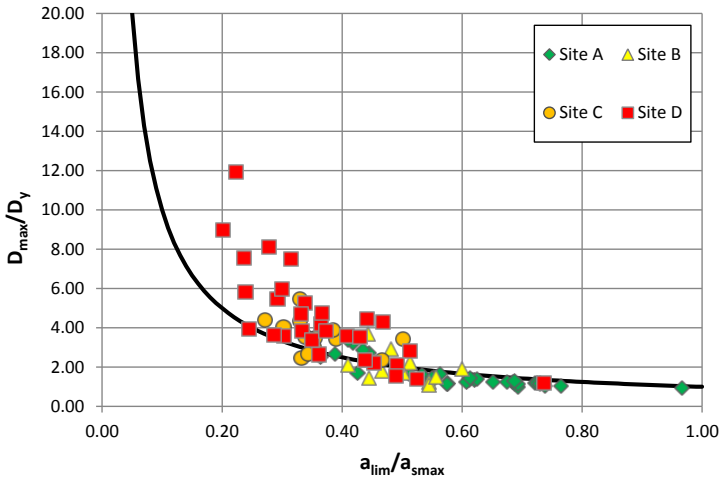

Fig. 7.11 β-μ points compared with the Nuti and Basili correlation curve.

The method, discussed in section 7.2.2 states that for values of β between 0.5 and 1 the sliding displacement can be evaluated from the regression curve μ=1/β. Knowing β it is possible to evaluate the residual displacement with the following equation:

$$D_{res} = D_y (1 - \mu)$$

If β is less than 0.5, more advanced analyses are required. It is possible to notice that in this range of values the results are more dispersed, therefore it is not possible to evaluate the base sliding with the regression curve. In fact, Fig. 7.11 shows that accurate analyses are necessary for Site C and Site D, confirming what deducted by the results of simplified dynamic nonlinear analyses. Making a comparison between this figure and Fig.

7.5, it is possible to highlight that while that plot was obtained for dams with different heights, here the difference between the case studies is represented by the intensity of the seismic input, which is higher for sites C and D and lower for A and B. Therefore it is possible to state that the higher are the dam and the seismic intensity, the higher is the risk to have a base sliding.

8 SafeDam

8.1 A probabilistic program to evaluate dam base sliding

An application of the procedure for defining the seismic input and the simplified method to rapidly evaluate the seismic input was developed, considering the provisions of many national codes which require to take into account all the uncertainties in the model using characteristic values and safety factors.

In this work, and in other works by other authors on the topic of the dynamic response of dams, the input variables of the problem are considered deterministically. Some examples of these variables are the mechanical parameters as elastic modulus E, water level H_w and angle fo friction between the dam and the rock foundation. While generally these parameters are considered as fixed and constant, these can actually change in time, like the water level in a time window of a year, and in space: dams are very large structures, and parameters like the strength and the elastic modulus can change from one point to another of the dam, depending on the conditions of concrete casting.

At this purpose this part of the work, tries to take into account for the uncertainties in the definition of these parameters using a Monte Carlo simulation method in order to find possible combination of the random variables which can bring to the collapse of the dam.

Programs as CADAM [65] already permit to compute the probability that the Sliding Safety Factor (SSF) is smaller than 1, however CADAM does not perform dynamic analyses and it is not possible to obtain the actual value of the residual slip. In order to understand how the dam behaves during earthquakes it is necessary to perform non-linear dynamic

analyses. In agreement with the procedure and seismic input results proposed in section 7.3.

The aim of this work was to develop a program capable to evaluate the probability to have a sliding at the base of a concrete gravity dam, to compute the probability to have a non-zero base displacement and to evaluate if this could lead to damage or collapse of the dam.

The program was developed using an increasing degree of complexity of analysis, starting from equivalent static analyses to understand which combinations of values of the input variables could lead to a Sliding Safety Factor SSF<1. Then these combinations were assigned to a simplified SDOF system to perform nonlinear dynamic analyses using acceleration time histories. Knowing the evolution of the base displacement it is possible to understand if there could be failure of some part of the dam due to the base sliding.

8.2 Selection of random variables

The variables considered in Monte Carlo simulation analysis are the water level H_w, angle of friction ϕ and the Young modulus of elasticity E of the concrete. All variables have a lognormal probability distribution.

The water level rules the design of the dams. During an earthquake the level of the impounded water plays an important role acting with an additional hydrodynamic pressure, changing the modal periods of the structure and, as consequence of this, the seismic actions. Considering that the maximum flood has a little probability to occur together with the earthquake, it is useful to take into account the probability associated to the water level.

In the present study, on the basis of some water level recordings, reporting the daily variation in a 5 years of observation, it is assumed that

the maximum level is equal to the total height of the dam and the minimum level is 75% of the total height. The friction angle variation was chosen after an evaluation of the experimental values found in literature. The average value chosen was 40° with a minimum of 35° and a maximum of 45°. The associated standard deviation was 1,5°. The contribution given by cohesion was neglected.

For the Young modulus, referring to real data observed on existing dams, the average value chosen was $24,7x10^6$ kN/m^2, the minimum value $18,78x10^6$ kN/m^2 and the maximum $29,08\ x10^6$ kN/m^2. Standard deviation was chosen as $1,5x10^6$ kN/m^2.

The other variable considered is the seismic intensity level, which is defined for the four sites A, B, C, D as reported in chapter 6.

8.3 Equivalent static analysis

8.3.1 Monte Carlo method

In the Monte Carlo method a distribution of probability which characterizes the epistemic uncertainty and the variability of the parameter in space and time is associated to each random variable. The output of the analysis is than computed n times through the random extraction of input variables obtaining n values of the response of the system. Given a large number n it is possible to obtain the probability distribution of the output variable, and to calculate the statistic moments of the distribution.

According to the law of large numbers as the number of experiments or simulations increases the average of the results should be closer to the expected value. It is therefore necessary to define a minimum number of analyses to perform in order to obtain a stable solution. In this work a

criteria suggested by Melchers is used, so a minimum of 20.000 analyses is adopted.

Latin Hypercube sampling method was used to exclude values with no physical meaning (e.g. height of impounded water bigger than the height of the dam) limiting the sample within a specific interval of the probability distribution.

8.3.2 Sliding Safety Factors

The aim of the simplified static analysis is to rapidly identify the input data combinations which could be critical for the structure. The Sliding Safety Factor (SSF) is a parameter which can be useful to evaluate the probability of the base sliding of the structure. The SSF is defined as the ratio between the sum of the stabilizing forces and the sum of the destabilizing forces. There is a possibility of sliding when SSF<1. In this work three different SSF were considered:

1. Static SSF: is the most simple SSF because depends only on static forces, easy to evaluate. Remembering that cohesion was neglected, it is possible to write:

$$SSF_{st} = \frac{(W - U_P) \cdot tg\varphi}{P_W} \qquad (1)$$

   Where W is the weight of the dam, Up is the uplift pressure, tgφ is the tangent of the friction angle. Pw is the hydrostatic pressure on the upstream wall of the dam.

2. Dynamic SSF - 1° vibration mode: this SSF considers the dynamic contribution of the first mode of vibration, as proposed by Fenves and Chopra [60].

$$SSF_{dyn1} = \frac{(W - U_P) \cdot tg\varphi}{P_W + f_1(y)} \qquad (2)$$

Where f1(y) is the seismic force acting on the dynamic system formed by the dam and the impounded water, for the first vibration mode.

3. Dynamic SSF - 1° vibration mode and higher modes: this SSF considers the dynamic contribution of the first mode of vibration and the contribution of the higher modes.

$$SSF_{dyn2} = \frac{(W - U_P) \cdot tg\varphi}{P_W + f_1(y) + f_d(y)} \qquad (3)$$

This factor was considered to obtain the failure set to be analyzed in the second part of the program.

For each value of SSF the failure probability of exceedance has been obtained.

8.3.3 Static analyses output

Fig. 8.1 shows the results of the Monte Carlo analysis for the three SSF obtained on the basis of a static analysis. For each SSF the histogram represents the values of SSF obtained with all the analyses. The values are displayed in green when the SSF>1, whereas the values for SSF<1 are displayed in red. A table reporting the number of failures for each SSF factor and the probability that each SSF could be minor than 1 is given.

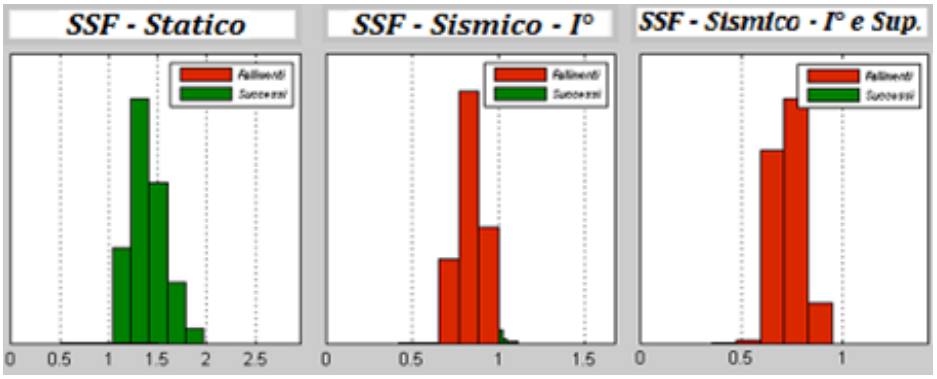

Fig. 8.1 Relative frequency of Sliding Safety Factors

8.4 Dynamic analyses

The dam was modeled as an equivalent SDOF system defined by the Nuti-Basili method. The system is analyzed using the open source program "Opensees" using a set of 7 accelerograms for each of the four sites scaled in order to match the response spectra chosen as target. In static analyses there is a base sliding only if SSF<1, but when dynamic analyses are performed it could be possible to have base sliding also for SSF major than 1. For this reason for dynamic analyses all SSF minor than 1,1 were considered. The second output includes all the statistical parameters of the analysis with the purpose to correlate the SSF values with the base sliding values.

It is possible to perform the dynamic analyses considering different initial values. There are three options:

- Only values of the basic variables that lead to SSFmin, SSFmax, SSFav (average SSF).
- All the initial values that brought to a base sliding are considered.
- All the initial values are considered.

Fig. 8.2 shows the response to a single accelerogram obtained for site 1, where PGA=0,46g. Top part of the figure shows the comparison between linear and non-linear displacement at the top of the 100 meters dam, while at the bottom the residual base displacement is reported.

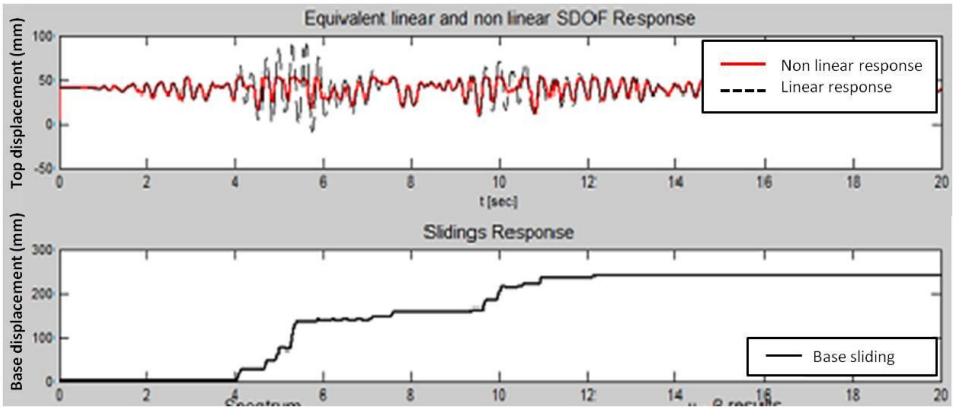

Fig. 8.2 Equivalent linear and non-linear response (top), residual base sliding (bottom)

8.5 Application to the Case study

The two stage procedure is applied to three concrete gravity dams with different height: 100 m, 75 m and 50 m using the seismic input of the 4 sites studied defined above. The failure probability of the three structures is computed taking into account the results of simplified static analyses and the dynamic nonlinear analyses.

Fig. 8.3 shows how the combinations of Hw, E and ϕ are chosen after equivalent static analysis. In fact, the figure reports the probability to have a sliding at the base considering the three SSF defined above, for the different case studies and the seismic intensity levels defined for the four cases A, B, C and D. From the figure it is clear that the taller is the dam, the higher is the probability of sliding p_f. Analyzing the different SSF

defined it is possible to notice that the probability of failure is higher when considering the contributions of higher modes.

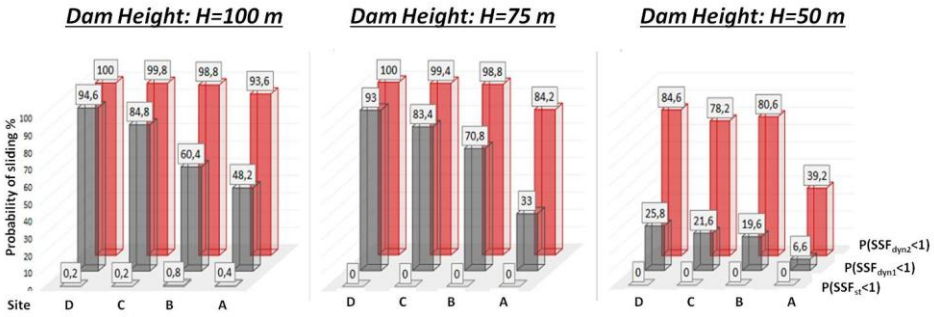

Fig. 8.3 Synthetic results of equivalent static analyses

Fig. 8.4 shows for the three case studies and for four seismic intensity levels the probability to have base displacements larger than 0, 10 cm and 1 meter, obtained with the non-linear dynamic analyses. δ=10 cm is the displacement which can cause the opening of the vertical joint and so the uncontrolled release of water, while for δ=1 m there could be the collapse of the dam.

The probability rapidly decreases in the dynamic case if the probability to have a base sliding capable to trigger the collapse of the structure (δ>1 m) is considered. In fact, if we consider the 100 meters dam at site D, the probability to have base sliding is 100%, the probability to have a sliding major than 10 cm is 64,4% and the probability to have a sliding major than 1 m is only 13,4%.

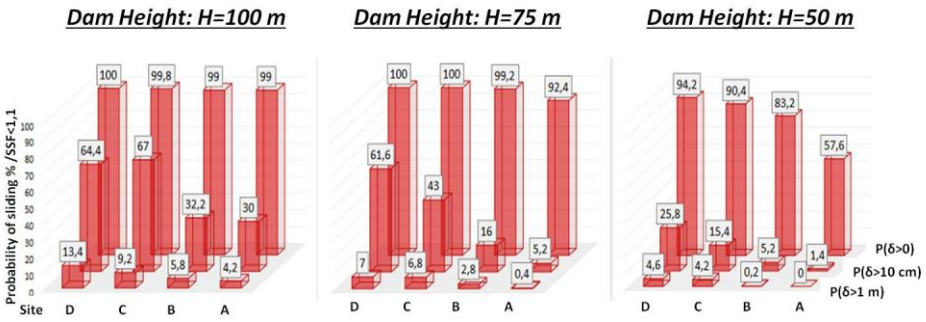

Fig. 8.4 Synthetic results of dynamic analyses

Comparing the static case $P_{fsismico}1$ or 2 with the dynamic case one notes that the latter is slightly larger. The static cases in which higher modes are included are very similar to the dynamic for $\delta>0$.

If one accept to have $\delta=0{,}10$ m as a failure the dynamic values are smaller than the static even with a single mode ($P_{fsismico}1$). Higher modes give a substantial contribution for all cases, especially when the probability of sliding is smaller: see for example site 4, dam H=75 m and site 1, dam H=50 m.

8.6 Considerations

In this work a procedure to study the base sliding taking into account the uncertainty of the input parameters is presented. As preliminary check the Sliding Safety Factor (SSF) of static or response spectrum analysis is evaluated using a Monte Carlo simulation procedure. If the SSF<1 it is necessary to carry out nonlinear dynamic analyses to evaluate the residual slip after the earthquake. In this work the base sliding is obtained using the Nuti-Basili simplified method [62] which evaluates it by means of nonlinear dynamic analysis of an equivalent SDOF system that takes into account the interaction of the structure with the foundation and with the impounded water. The two stage assessment procedure was implemented

in a Matlab software and applied to four dams with different heights considering four levels of seismic hazard.

The results obtained demonstrate the effectiveness of the method and the useful information given to rapidly estimate the risk connected to the sliding of a concrete gravity dam, considering the main parameters at hand and their dispersion. It represent a powerful tool for a preliminary but meaningful analysis of concrete gravity dams.

9 Accurate analyses

Accurate analyses have to be performed when the results of the simplified analyses highlight that the dam considered can have an excessive sliding or can arrive to the collapse.

In this study Finite Element analysis could be seen as the most complex tool to investigate the dynamic behavior of dams in a step-by-step analysis, which starts from static analyses, continues with simplified analyses which can help to find the most weak case studies, then the safety assessment has to be carried out with analyses that model the dam in the best possible way.

Finite element analyses have been the object of ICOLD Bulletin 155 [66]. The availability of new methods to assess the dynamic response of dams and the advances in computation speed of modern calculators has made these methods widely used. The finite elements models allow to perform linear and non-linear analyses. Linear analyses give informations on the maximum stresses on the dam walls, and can be obtained for example with response spectra analyses. When the stresses exceed the concrete strength there is the possibility that the dam is not safe. In order to better understand the behavior of the structure and assess the material behavior (for example, the presence of cracking on the dam) it is necessary to perform dynamic analyses in time domain.

In this chapter the accurate analyses of two dams, a concrete gravity dam and an arch-gravity dam are performed in order to arrive to an evaluation of the damage on the upstream and downstream walls of the dams. For arch and arch-gravity dams it is necessary to take into account the behavior of the dam in the three directions, while for gravity dams in large valleys it is possible to consider the sections of the blocks of the dam and so performing a 2D analyses. In this work the Finite element

analyses are performed with 3D models, with the purpose to make a comparison between the behavior of the different dams.

9.1 Case studies

The gravity dam, depicted in Fig. 9.1 analyzed is formed by 19 blocks with a constant width of 20.0 m and with height ranging from 20.0 to 87.0 m. All the blocks have a crest width of 5 m with inclinations of the upstream and downstream walls that are respectively 0.03 and 0.7. Excluding the spillways sections the base width of the sections of the dam range from 13.0 m to 62.0 m. The crest has a length of 380 m.

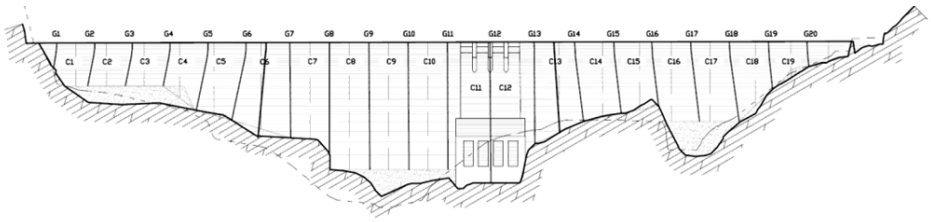

Fig. 9.1 Front view of the gravity dam

Principal features of concrete are the following:

- Elastic modulus: E=23.64 Gpa;
- Mass density:

For the modeling of the foundation the elastic modulus is E_f=41.55 GPa.

The arch gravity dam selected as case study has a maximum height of 100.0 m and a crest length of 250.0 m. The dam is formed by 11 monolithic blocks separated by vertical joints. There are three central blocks with a section more similar to gravity dams, while the external blocks of the structure (close to the abutments) have a shape closer to arch dams, with thickness ranging from 4.0 to 21.0 m. The thickness of the

central blocks ranges from 100 m at the base to 10 m at the crest. The material properties of the concrete are the following:

- Elastic modulus: E=31.47 GPa
- Concrete mass density ρ=2390 kg/m^3

Elastic modulus of the foundation is E_f=30 GPa

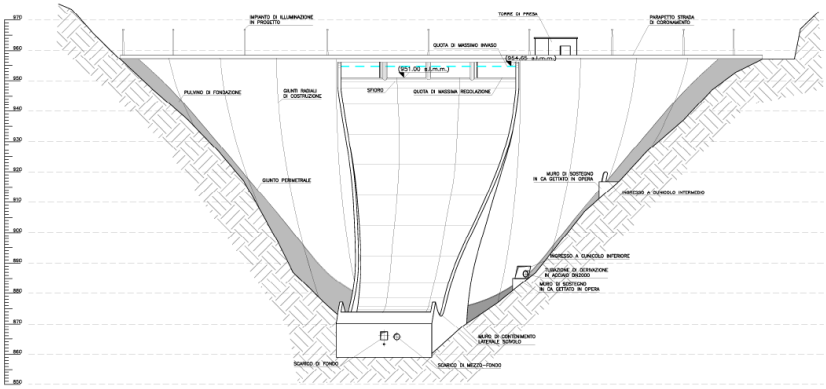

Fig. 9.2 Front view of the arch-gravity dam

9.2 Finite element model

9.2.1 Dam modeling

The FE (Finite Element) models of the dam presented as case studies in this work are built making some simplifications in the dam geometry in Abaqus [67]. Therefore, some details are not considered: for example the spillways and the appurtenant structures are replaced by equivalent loads or forces.

The minimum dimension of the mesh is one of the parameters which characterizes the numerical model. The features of the FE model of the case studies presented are discussed. In both cases the elements used were 4-nodes tetrahedrons. For the 3D model of the gravity dam (See Fig. 9.3)

a total number of 32.007 elements were used, with an average dimension of the elements of 5 m.

Fig. 9.3 Finite element model of the gravity dam

Fig. 9.4 shows the Finite element model used in Abaqus for the arch-gravity dam, which has 4.787 elements, also with an average dimension of the elements of 5 m.

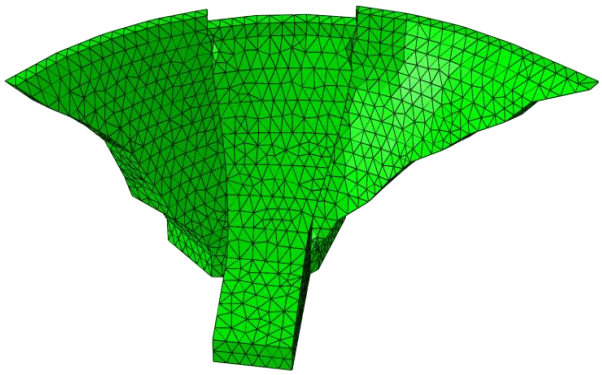

Fig. 9.4 Finite element model of the arch-gravity dam

regarding the modeling of the interfaces between different materials, there is the necessity to define the contact between the blocks of the dams, that is to model the vertical construction joints of the dams.

In studies which aim to study the seismic response of dams, it is needful to define the behavior of vertical joints, which can be modeled with a frictional surface. Such behavior can be modeled using the "*surface to surface interaction*" method, which is described in the Abaqus manual [67]. In this method a given relation between force and displacements is assigned to a couple of surfaces, and the contact surface has to simulate sliding between the blocks.

Regarding tangential direction, it is possible to find a relation between the relative tangential displacement and the tangential and normal forces acting on the blocks. In this study the Coulomb friction method is used, in which the displacement between the surfaces in equal to zero until the shear resistance, computed as the product between the friction angle and the normal pressure is exceeded. In this study a friction angle of 45° is assumed.

9.2.2 Dam - Foundation interaction

It is important to consider the interaction between the foundation and the structure in all the cases in which the foundation could not be considered as rigid, as described by many authors including Chopra (See [68]). In those cases the deformability of the rock underlying and surrounding the structure could have relevant effects on the behavior of the dam during earthquakes.

An ideal model of foundation has an infinite extension or includes all the geological features of the foundation rock, or has an extension so large that the boundary effects on the stresses on the dam are negligible.

There are two main approaches to define the soil-structure interaction: the indirect method and the direct method. In the first one, the foundation volume is replaced with boundary conditions applied directly to the base of the structure or to a transition element. In the direct method the volume of the foundation material is modeled together with the structure. This latter method has a greater computational cost, also if only a portion of foundation is modeled.

In this study a direct method is applied, modeling a part of the foundation rock. Regarding the interfaces, the contact surfaces between foundation rock and dam concrete are modeled using a frictional Coulomb method. For all these surfaces a friction angle of 45° is assumed.

In both cases the foundation was considered by assigning a null mass of the rock foundation. The approach consisting in considering the flexibility of the foundation and neglecting the mass and damping is popular because the stiffness matrix of the foundation is very difficult to determine without making these assumptions

The input signal is then applied to the boundary of the foundation model. In fact using a mass-less foundation and taking into account only the deformability of the rock the problem of the radiation damping could be avoided.

The geometry of the foundations were modeled considering a simplified geometry. For the arch-gravity dam (See Fig. 9.6), the foundation is modeled considering an extension of the foundation which is around two times the height of the dam, and a rock element which reproduces the rock-dam connection was modeled, obtaining a total of 16.282 elements for the foundation and 13.012 elements for the connection element. An elastic modulus of 30 GPa was considered for the foundation rock.

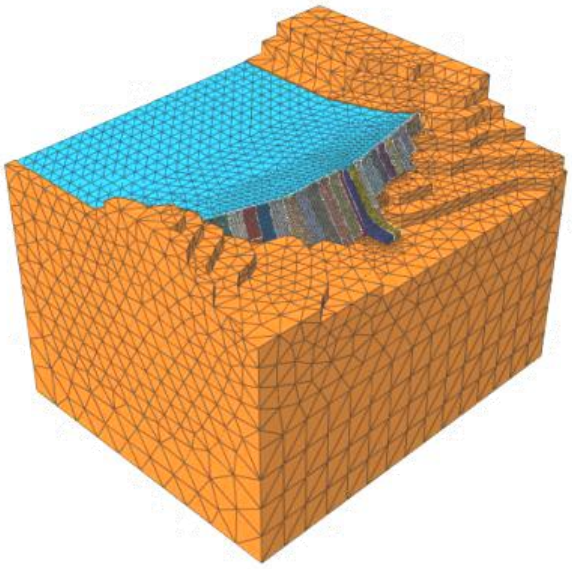

Fig. 9.5 Model of the gravity dam including the foundation

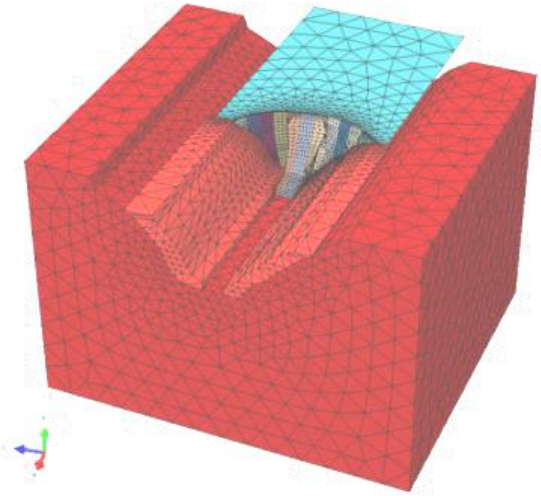

Fig. 9.6 Model of the arch-gravity dam including the foundation

9.2.3 Dam - Reservoir interaction

The approach used in this work to model the water in the reservoir is one of the most used methods to take into account the hydrodynamic pressure effects on the dam. The reservoir was modeled with the acoustic elements available in Abaqus, which are AC3D4, *linear acoustic tetrahedron.*

These elements allow to simulate the pressure distribution in the fluid medium neglecting viscosity and considering the compressibility of the fluid through the Bulk Modulus, which for water has a value of 2,2 GPa. Very important to correctly model the fluid-structure interaction is to consider the correct boundary condition at the interface between water and the structure.

The simulation of the physical behavior of the reservoir attached to the dam permits to take into account the compressibility of water and the radiation damping, that is the dissipation of seismic waves on the reservoir bottom. In general, if the reservoir is considered non-absorptive (rigid), this could bring to an unrealistically large response for dams with impounded water, as reported in a work by Chopra [68].

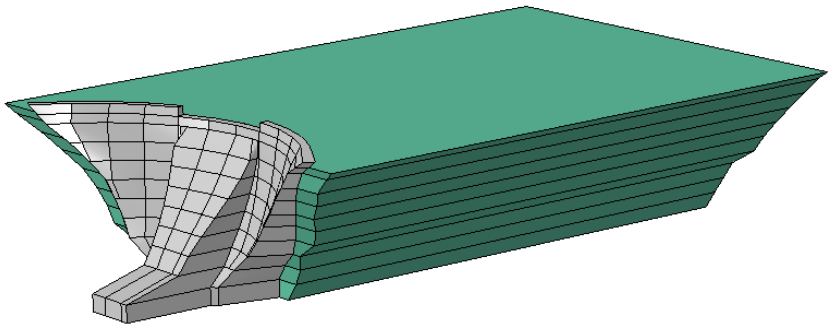

Fig. 9.7 Reservoir model for arch gravity dam in Abaqus

The reservoir model is extended in upstream direction for a length which is around 3 times the height of the dam. On the upstream face of the

reservoir, which has to simulate an infinite extension of the reservoir, it was set up the non-reflecting condition. On the side and bottom of the reservoir it was set up the condition of the partial absorption of the waves to take into account the dissipation caused by the deformability of the deposits which lie on the bottom of the reservoir.

9.3 Pre-seismic state

Before the execution of the seismic response analyses it is necessary to perform an evaluation of the pre-seismic state. For normal buildings, which have mainly vertical loads, this step is done combining loads in order to consider their concurrence.

When dams are considered, this evaluation is complicated by the presence of the water in the reservoir and by the uplift pressure caused by the underground water, depending on the water level in the reservoir, on the efficiency of the drainage system, and on thermal effects. The Italian Code on Dams defines the actions to be considered simultaneously.

The evaluation of pre-seismic state can require analyses which as complex as the seismic analyses. This section describes briefly the effects produced by the main static actions which act on the dam.

The self-weight may cause, depending on the geometry of the dam, and upstream displacement which can cause tension on the downstream wall. This effect is more evident in arch dams, as it will be discussed in the next sections. Conversely for the self-weight, the hydrostatic pressure causes a downstream displacement and tension on the upstream wall.

Some parts of the concrete of the dam are subjected to interstitial pressure due the porosity of concrete, which must be evaluated with specific permeability studies. The uplift pressure raises from this effect and can be

accounted for with a simplified method that models it as a linear distribution.

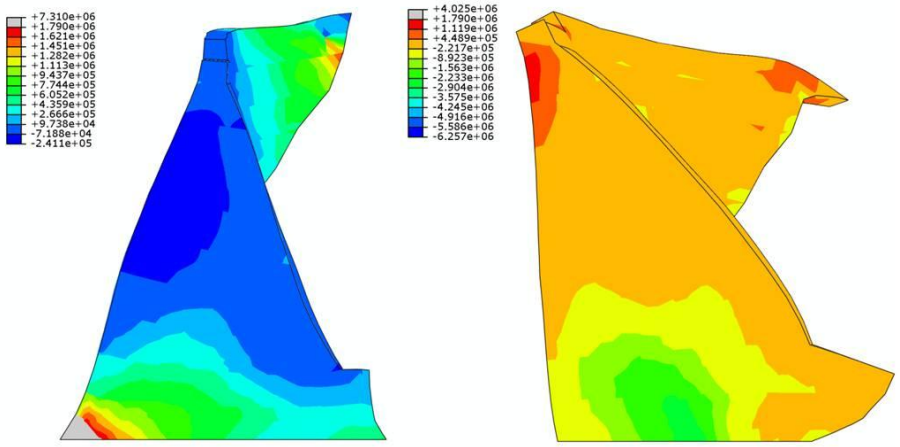

Fig. 9.8 Winter (left) and summer (right) thermal effects for the arch-gravity dam

The thermal variations can cause important effects on the dam. Generally positive thermal variations, associated to summer periods, produce a volumetric expansion and therefore the closure of vertical joints between blocks. In gravity dams this fact can cause the passage from a 2D behavior (independent blocks) to a 3D monolithic behavior. Conversely, negative variations bring to a shrinkage which in arch dams can have the effect to eliminate the arch effect. The estimate of the closure temperature of the joints is very important to correctly assess these variation. The temperature distribution inside the dam can be evaluated by thermal analyses, in which on the exposed parts of the dam are applied sinusoidal variations of temperature.

For seismic analyses, in cases of important thermal effects (arch and arch-gravity dams) it is necessary to consider two conditions, namely for winter and summer (Fig. 9.8).

The combinations of all these effects can bring to a state of tensions and deformations which can have significant variations and can affect seismic assessment of dams. In the following figures are reported the pre-seismic conditions considering the self-weight and the hydrostatic pressure.

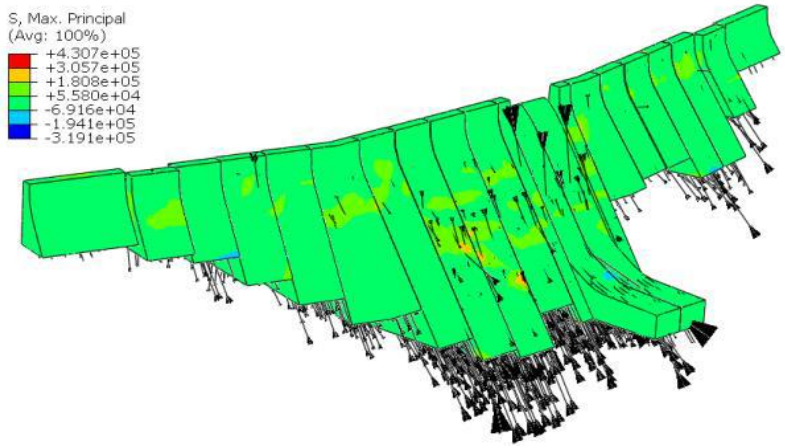

Fig. 9.9 Pre-seismic state for the gravity dam

Fig. 9.9 shows the pre-seismic state for the gravity dam. In this condition the maximum principal stresses are limited, reaching a value of σ=0.43 MPa. In the figure are also reported the isostatic compression lines, which show clearly how the hydrostatic pressure is transmitted at the base of the blocks, with a mainly vertical pattern which demonstrates the cantilever behavior of the blocks.

The maximum displacement at the crest is obtained for the highest block and it has a value of δ_{crest}=19.0 mm.

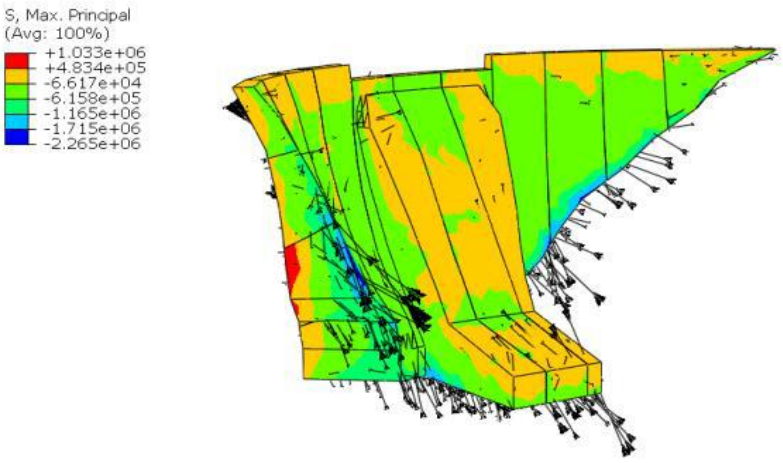

Fig. 9.10 Pre-seismic state for the arch-gravity dam

The pre-seismic condition for the arch-gravity dam is reported in Fig. 9.10. Also for this dam the stresses in the pre-seismic condition are moderate, with a maximum tensile stress σ=1.0 MPa.

9.4 Linear analyses

The safety assessment of existing dams has to be performed for different Limit States. In the following sections the Collapse Limit State will be considered, for which it is necessary to avoid the uncontrolled release of impounded water. This fact can be confirmed by demonstrating that the maximum stresses in all the elements of the dam are lower than the concrete strength, and if the stresses have greater values it has to be demonstrated that this condition has a limited extension in time and space.

When the stress limits are not verified, it is needful to deepen the analyses in non-linear field. In these cases resulting stresses are not interesting for the evaluation of the Collapse Limit state, so it is better to identify some

parameters which are typical of the non-linear field and that are connected with the residual deformations.

9.5 Choice of acceleration time histories

On the basis of the results of the simplified analyses obtained in section 7.3.3 a selection of two records for the accurate analyses was done. Those results have shown that for sites A and B, characterized by low-medium seismicity, the base sliding was not large enough to cause major damaging or the collapse of the dam.

Conversely, for sites C and D the average of the maximum displacements obtained with the sets of selected accelerograms was greater than the limit displacement of 100 mm, which represents the value for which it is possible to have opening of the vertical joints and consequently the uncontrolled release of water from the reservoir.

With the purpose to highlight the differences in the response between a site with low seismicity and one with high seismicity, in order to perform non-linear analyses two accelerograms were chosen, the first taken from site A, and the second from site D set. The signals selected are shown in Fig. 9.11.

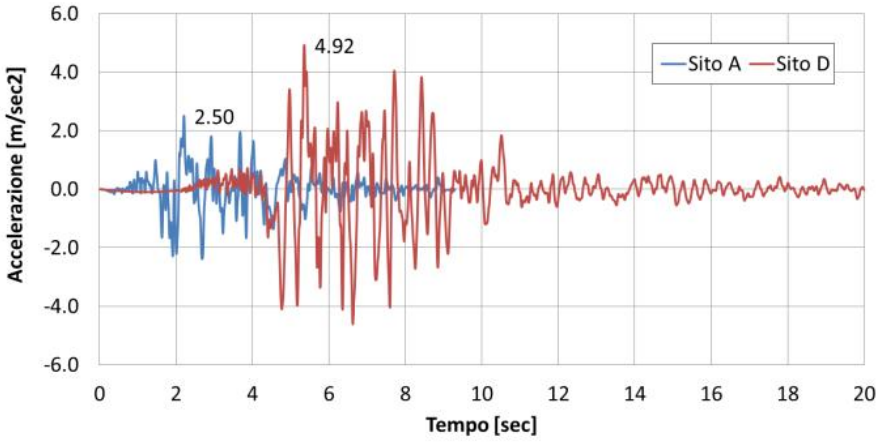

Fig. 9.11 Selected accelerograms for accurate analyses

9.6 Displacement time histories comparison

In order to represent the different responses in time of the considered structures subjected to the same input ground motions in Fig. 9.12 and Fig. 9.13 are shown the displacements time histories obtained with the non-linear analyses performed on the 3D finite element models of the two dams.

Per rappresentare le differenti risposte delle strutture rispetto agli stessi terremoti viene riportata di seguito la storia degli spostamenti relativi registrati sul concio più alto della diga a gravità e al centro del coronamento della diga ad arco-gravità.

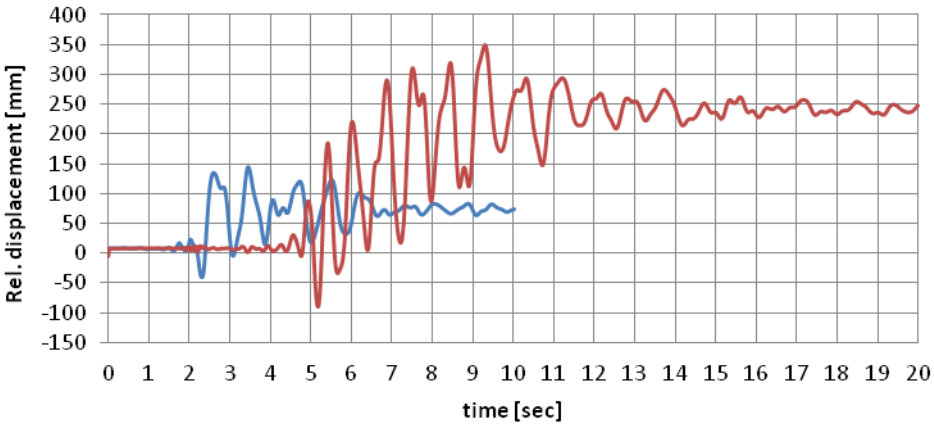

Fig. 9.12 Crest Displacement time histories for central block of gravity dam

Fig. 9.12 shows the response of the gravity dam. it is possible to notice that both accelerograms cause a residual displacement in downstream direction, as result of the non-linear behavior of the material introduced in the model.

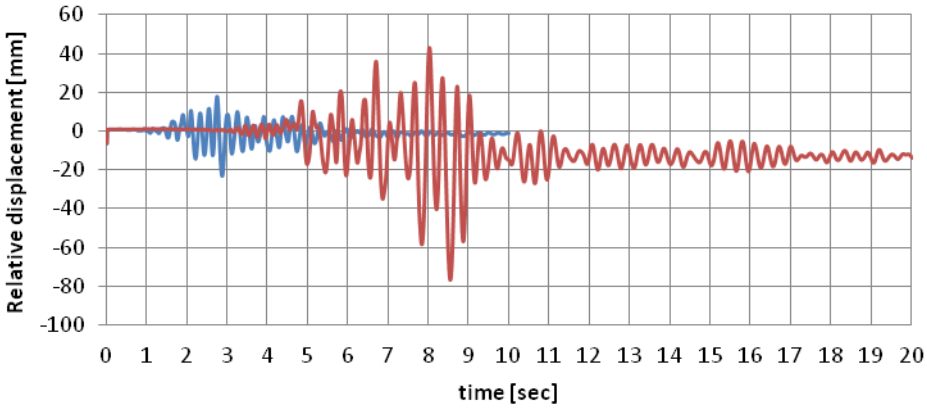

Fig. 9.13 Crest Displacement time histories for central block of arch-gravity dam

The oscillations in displacement are in the range of 100 mm for Site A signal and in the range of 200 mm for Site D signal. The final residual displacement has the value δ=250 mm for Site D signal and δ=73 mm for Site A.

Fig. 9.13 shows the response of the arch-gravity dam, which is much more rigid than the gravity dam as it can observed by the displacement plot. First it is possible to point out that also for this dam there is a residual displacement, but this happens in upstream direction., and this is mainly due to the fact that when the earthquake occurs the dam has a rocking motion in upstream and downstream direction. When the dam is moving in downstream direction, each block transmits compressive forces to the other blocks, behaving as a monolithic body, so that in this case there is an arch effect acting on the blocks of the dam which stops the motion in downstream direction. When the motion is in upstream direction, the blocks separate, so there is no more contact between the blocks that have an independent behavior, and the blocks are like cantilevers when moving in upstream direction. In this case the residual displacement for Site A signal is very small, in fact δ=1 mm, while the maximum residual displacement obtained with Site D signal is δ=14 mm.

9.7 Expected damage

9.7.1 Damage Plasticity model for concrete

The evaluation of the cracks openings is one of the phenomena which implies a very high computational cost. Despite the great number of studies existing on the topic, it is very difficult to accurately estimate the effective value of the crack opening. The *Damage Plasticity model*, introduced by Lee and Fenves [70] allows to introduce in the non-linear analyses the evolution of the plastic deformation and the gradual

deterioration of the mechanical properties of the concrete caused by seismic cyclic actions.

Elasto-plastic models are useful when in the unloading phase the stiffness of the material is constant. In this case the descending branch of the curve is parallel to the initial loading path. Conversely, Damage models can be used when in the unloading phase there is a stiffness decrease. In real materials can occur both permanent deformations and stiffness reductions, therefore it is necessary to use methods which combine plasticity and damage models. A parameter called *d* controls the stiffness reduction in the material, as reported in Fig. 9.14. In case of seismic actions there are cyclic loads acting on the dam. In this case the model has to be corrected in order to take into account the opening and closure of the cracks and their interaction. It was observed that there is a stiffness recovery effect when the load changes direction during a cyclic load.

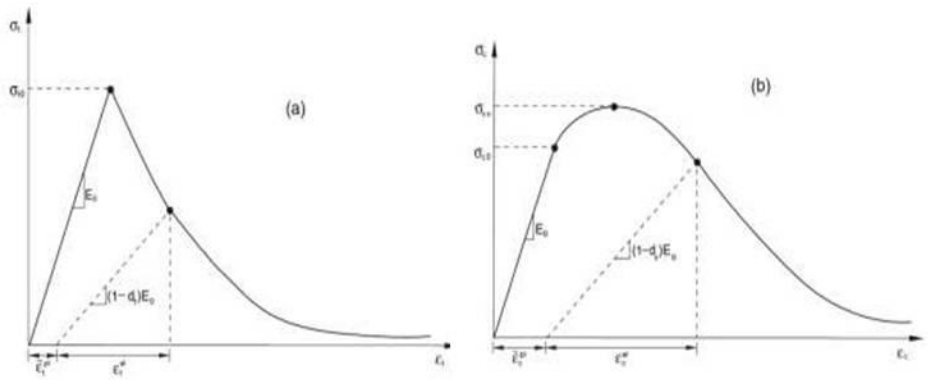

Fig. 9.14 Tensional (a) and compressive (b) behavior of the material (Lee and Fenves, 1998)

This method is implemented in Finite Element programs such Abaqus. Parameters used in this work were selected from the analyses performed

by Lee and Fenves for Koyna dam assuming as tensile strength the value of 1.3 MPa.

9.7.2 Results

On the basis of the above defined model to estimate the damage in concrete dams, in order to identify the critical areas of the dam in the following figures are reported the maps of damage variables at the end of the seismic event.

The red color indicates the areas where the concrete has lost its tensile strength. First, the case of the gravity dam is discussed.

In Fig. 9.15 and Fig. 9.16 are depicted the results of the damage analysis respectively for Site A and Site D seismic inputs. As expected the dam located in a site with major seismicity is more damaged than the other one. Most damaged areas are located in the central part of upstream and downstream walls. The figure shows the deformed shape (10 times larger than real) of the dam, and it can be observed that there is a sliding in downstream direction of the lateral blocks.

The maximum sliding between blocks is 550 mm for site A and 560 mm for site D, while the maximum joint opening is 17.7 mm for site A and 49 mm for site D.

Maximum plastic deformation is $3.73\ 10^{-3}$ for site A and $14.6\ 10^{-3}$ for site D. Considering the fact that the mesh of the dam model has an average size of the elements of 5.0 m it is possible to obtain an evaluation of the cracks opening, which are 19 mm for site A and 73 mm for site D, measured in the central part of one of the spillway blocks.

At the end of the seismic event there is no presence of hinges which can bring the structure to the collapse. On the basis of these results it is

possible to state that the dam can withstand to the Collapse Limit State seismic event without causing an uncontrolled release of water.

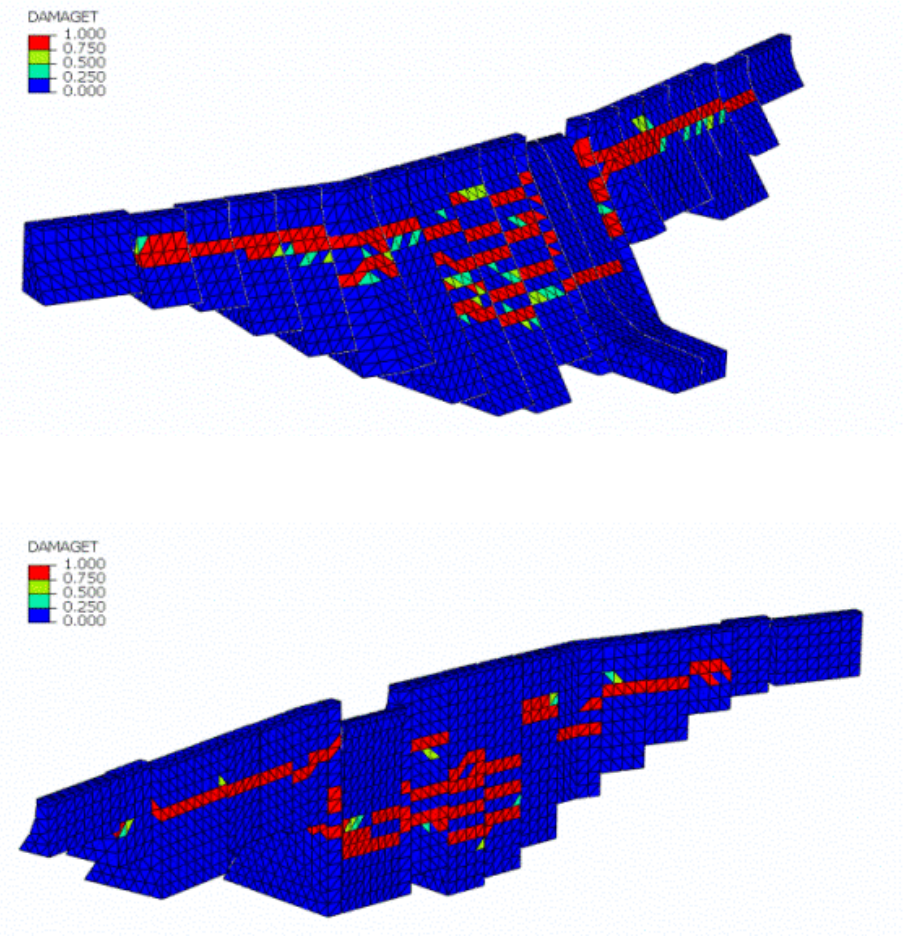

Fig. 9.15 Damage on the gravity dam - Site A: DS wall (top) and US wall (bottom)

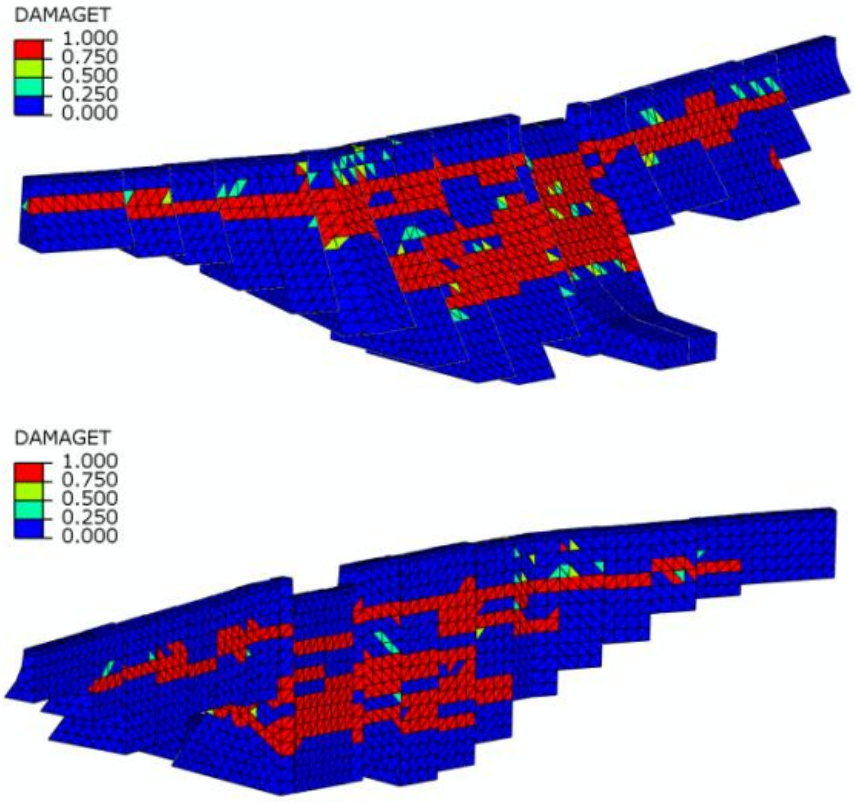

Fig. 9.16 Damage on the gravity dam - Site D: DS wall (top) and US wall (bottom)

Fig. 9.17 and Fig. 9.18 report the damage of the arch-gravity dam for site A and site D. The entity of damages is lower for this dam than for the gravity dam. The areas which are more subjected to damage are located in the central part of the walls, and there is also damage at the base of the dam.

For site A, joint sliding reaches a maximum of 15 mm for site D while maximum joint opening is 8.3 mm. The maximum crack opening is equal to 3.2 mm. For site D damages are more extended on the upstream and on

the downstream walls. Joint sliding arrive to a maximum value of 57.7 mm and joint openings are of 26.7 mm. The crack opening reaches the value of 16,7 mm.

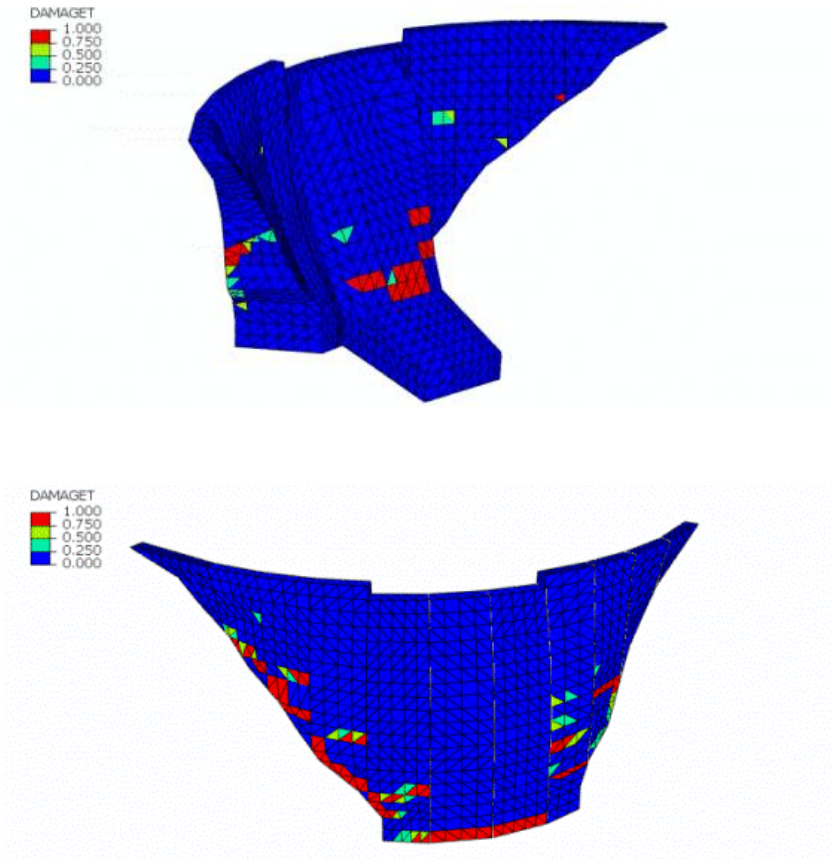

Fig. 9.17 Damage on the arch-gravity dam - Site A: DS wall (top) and US wall (bottom)

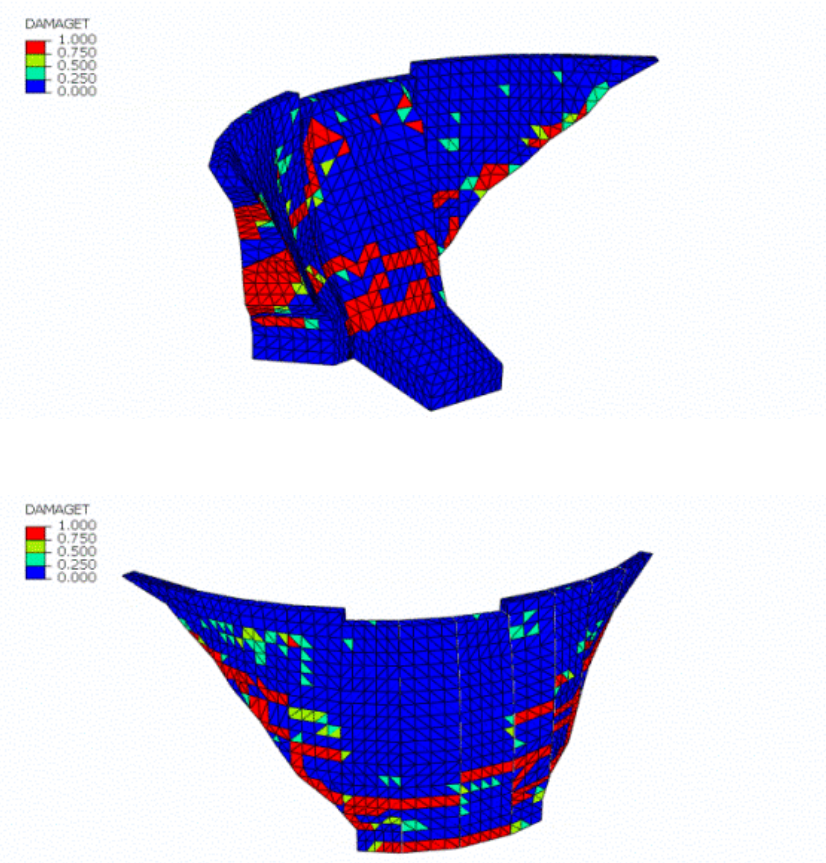

Fig. 9.18 Damage on the arch-gravity dam - Site D: DS wall (top) and US wall (bottom)

The damages which take place on the downstream wall are caused by the displacement of the arch gravity dam in upstream direction and so it is confirmed the "independent cantilever" behavior. This fact remarks the importance to model the vertical joints between the blocks. Regarding the safety of the dam, it is possible to state that despite the damages occurring on the dam, when the hydrostatic pressure is applied.

Part III - Dynamic soil-structure interaction of the leaning Tower of Pisa

10 Introduction

10.1 Aim of this part

Piazza del Duomo in Pisa, as known as Piazza dei Miracoli (Square of Miracles) from a novel by Gabriele D'Annunzio, is the most important architectural complex in the town of Pisa. The square is a World Heritage Site of UNESCO since 1987. In the square there are four religious buildings: The Cathedral of Santa Maria Assunta, The Camposanto Monumentale (Monumental Cemetery), the Baptistry and the Bell Tower.

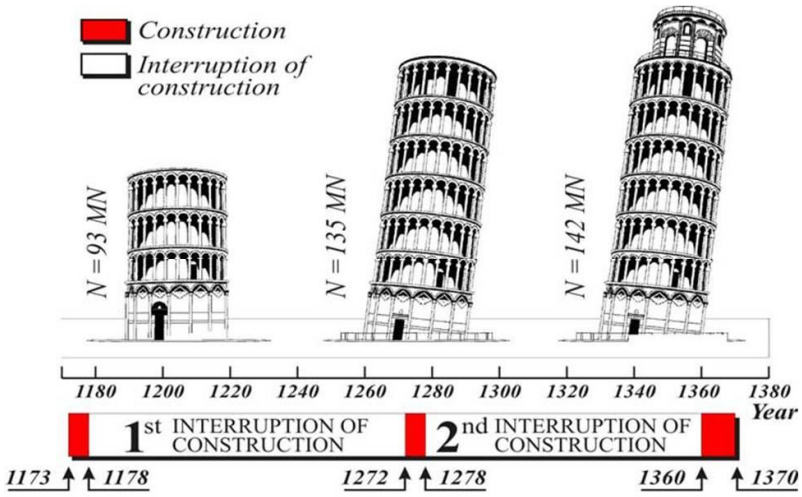

Fig. 10.1 History of the inclination of the Tower (Burland 2009)

The latter was built between 1173 and 1340, and many interventions were made during the construction in order to alleviate the undesired inclination, as shown in Fig. 10.1. Extensive instrumental investigations started only in 20th century, as illustrated in [71].

The Tower has become very popular because of its characteristic inclination, which proves the role of the underlying soil deformability on the behavior of the monument. The direction of the maximum inclination lies in the North-South plane. In 1993, a temporary stabilization was accomplished by posing 600 t lead weights on the north side of the foundation. From the beginning of 1999 until the first half of 2001, an extensive intervention of under-excavation was also made – which stopped the increment of Tower's tilt – and the "Catino" was connected to the foundation.

In April/May 2002, a drainage system was set up to lower the underground water level, whose fluctuations were considered the main cause of variations in the inclination of the Tower. The history of the interventions is described in [72].

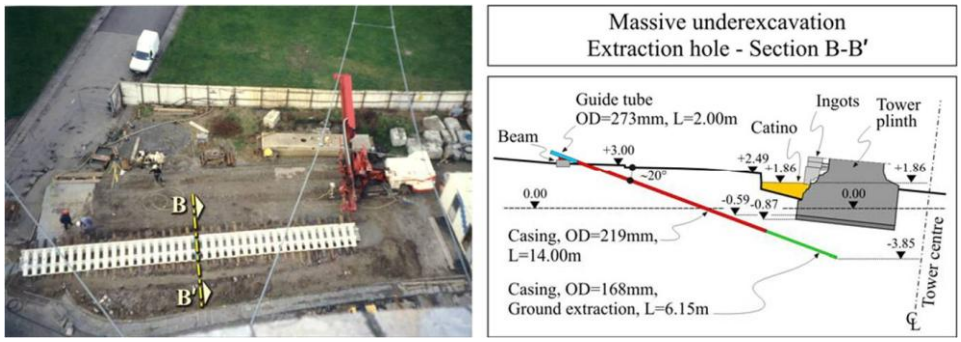

Fig. 10.2 Intervention of under-excavation under the Tower (Burland 2009)

The first study that took into account the soil-structure interaction was presented by Grandori and Faccioli [73]. In that work, the tower was modeled by means of a 2D model without considering the inclination of the structure. So doing, they obtained a fundamental period equal to 1.36 s. It is worth noting that this period is considerably longer than the period experimentally measured in other researches. A second study was made

by ISMES [74]. They identified experimentally bending and torsional modes, and thus it was not possible to calibrate the vertical foundation impedance. The aims of this study are to update and improve the characterization of the dynamic behavior of the Leaning Tower of Pisa, on the basis of the analysis of the earthquake-induced experimental response which allowed to identify the vibration frequencies of the Tower. With regard to the soil-structure interaction, special attention has been paid on the identification of the parameters that regulate the dynamic response of the foundation, calibrated using the results of the available geophysical tests. An Array 2D was performed to investigate at major depths the soil underlying the Tower.

A simplified model of the soil on the basis of its dynamic properties has been elaborated using the relations available in literature for the definition of dynamic impedances and then, a finite element (FE) model that takes into account the inclination of the structure has been elaborated, by assuming the position of the centroids reported in the work by Macchi and Ghelfi [76]. The numerical values of the impedances have been calibrated in order to reduce the differences between the natural frequencies identified experimentally and those obtained from the Finite Element analysis. A synthetic evaluation of the seismic input by means of a hybrid method that combines the Probabilistic and the Deterministic Seismic Hazard Assessments has been done, finding some controlling earthquakes for two different return periods of the expected local intensity, and selecting two sets of accelerograms on rigid soil (A and B EC8 classes). These has been reported to the ground level through a site response analysis, then the ground motions have been applied to the Tower, allowing to find the dynamic response in terms of acceleration and displacement.

Most of the historical data and informations included in this work have been taken from the works of the Committee for the Safeguard of the Tower of Pisa and of the Polvani Commission, which are reported respectively in [77] and [78]. Some of the figures are taken from the technical drawings made during architectural surveys [79].

10.2 Geometry of the Tower

The Tower has a total height of 58.4 from the base foundation, so that the height from the ground level to the top is about 55 m. The total diameter of the foundation is 19,6 m, while the width of the ring is 7,54 m, and the opening at the basement has a radius of 4,5 m (See Fig. 10.3).

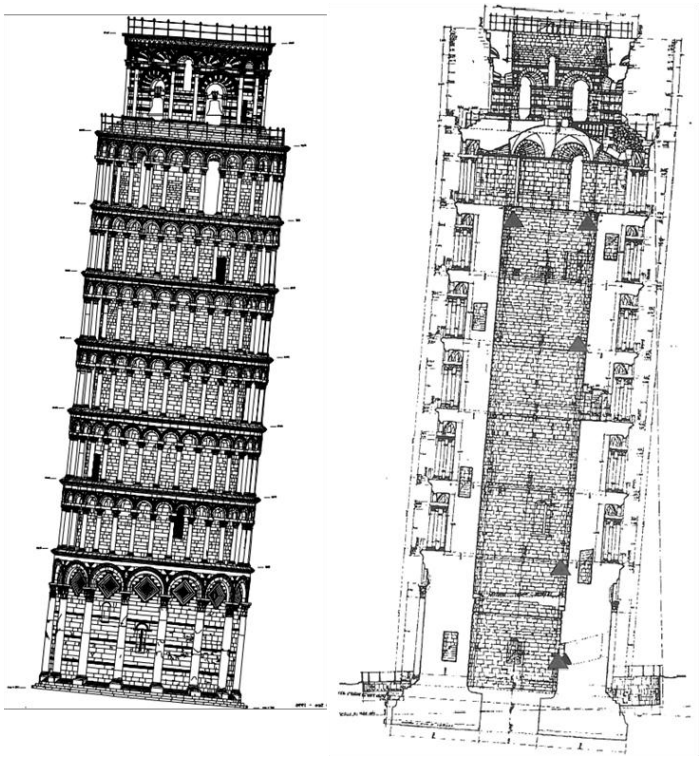

Fig. 10.3 Elevation and section of the Tower, N-S direction ([74][79])

The diameter of the elevation of the Tower is around 16 m considering also the external lodges, around 12 m without the lodges, and the central opening ranges from 7,3 to 7,7 m. Inside the external walls there is a spiral staircase which connects the levels of the Tower. There are eight levels called *Ordine*.

The Tower has an estimated weight of 14.453 tons, and the height of the center of mass from the base foundation is 22,6 m.

The tilt of the Tower is about 5,5° with respect to the vertical axis: the inclination is along the N-S direction whereas a modest tilt angle exists in the E-W direction. Therefore, the maximum drift of the top of the Tower in comparison with the base is around 5 m.

10.3 Italian guidelines - reduction of risk of cultural heritage

The Italian guidelines on the evaluation and reduction of the seismic risk of the cultural heritage [11] dedicated a chapter on towers, bell towers and other high structures which form a relevant part of the Italian cultural heritage. According to the guidelines, the seismic behavior of this type of buildings depends on some specific factors: the slenderness of the structure, the quality of the joint between walls and the possible presence of adjacent lower structures. Other factors are the presence of weak elements on the top of the building, like belfries. These elements could be particularly vulnerable because wide windows are present with slender columns, with shear ruptures for sliding, and because of the amplification of the seismic motion in the high parts of the construction.

Vulnerability is also influenced by the presence of damage states caused by other factors, due to the vibrations caused by the bells or to foundation problems.

The slenderness of towers is a very variable parameter, going to very squat structures (e.g. Renaissance bastions) to very slender structures. These structures can be considered as mono-dimensional structures, with a cantilever behavior. A recent study by de Silva et al. [80] reported a classification of the main Italian towers on the base of the slenderness ratio H/B of the height H and the base width, B, of the structure, distinguishing three classes:

- Very slender towers, with H/B>6;
- Slender towers, with H/B ranging from 3 to 6;
- squat towers, H/B<3.

According to this classification, the Leaning Pisa Tower is classified by the authors as a slender tower with a H/B ratio of 3,77: the Tower of Pisa is a clear example of a slender structure on a deformable subsoil.

10.4 Seismic Safety assessment according to Italian Guidelines

10.4.1 Definition of seismic input

In chapter 3 of the Guidelines it is stated that the Ground Motion is strongly influenced by the geological, stratigraphic and topographic local conditions. In presence of deformable and heterogeneous soils and depending on the different stiffness and on the possible topographic irregularities, there could be amplification effects of the Ground Motion, both in terms of maximum acceleration and in frequency content. In those cases it is necessary to **perform specific analyses of the local seismic response**, taking into account, as mentioned, the available studies of local seismic response and micro-zonation.

In the cases where the conditions could be classified in the categories defined by the Italian Code for standard buildings, also for the cultural heritage it is possible to evaluate the local seismic response using the same soil and topographic categories, defined in section 3.2.2 of NTC08.

11 Past studies on the seismic response of the Tower

11.1 Grandori & Faccioli (1993)

In their study published in 1993 in the framework of the studies made by the Committee for the safeguard of the Tower of Pisa, Grandori and Faccioli [73] presented a model to evaluate the soil-structure interaction. They considered two types of soil modeling: the first with a homogeneous elastic half-space, the second with an upper homogeneous layer over a rigid half-space. The two approaches produced similar results, therefore they used the dynamic impedances computed with the first model. The values of the dynamic impedances were estimated in the first method using the theory by Veletsos et al. [81]. The parameters of the model evaluated by Grandori and Faccioli are shown in Tab. 11.1.

Considering the results of geophysical tests performed in the Square of Miracles, which will be discussed in section 12.2, they assumed that the upper layer had a thickness of 39 m and a shear wave velocity equal to 200 m/s. As we will see this is a good estimate of the soil properties for this layer.

Tab. 11.1 Parametri terreno Grandori e Faccioli (1993)

Parametro	Valore
Spessore strato	39 m
V_{s1}	200 m/s
γ	17 kN/m^3
$G_0=G_{max}$	68000 kN/m^2
V_{s2}	350 m/s

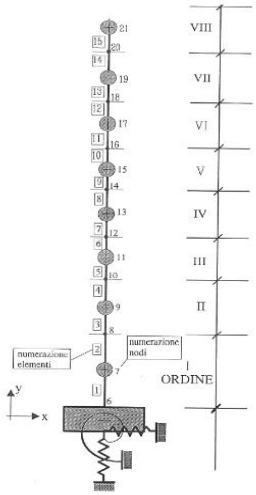

Fig. 19 - Modello dinamico.

Fig. 11.1 Finite element model (Grandori e Faccioli 1993)

In their study, the Tower was modeled in a Finite Element program with a *stick model*, defining the value of the concentrated masses connected by vertical elements with distributed stiffness. An important drawback of their study is that they did not modeled the inclination of the Tower, as it is possible to observe in Fig. 11.1. Moreover, at the base it was considered the ring foundation of the Tower, without taking into account the contribution to the stiffness given by the Catino, the concrete ring at the base of the building. The geometric parameters of each "Ordine" (storey) of the Tower are reported in Tab. 11.2.

The model considered only two dimensions, and did not take into account the off-plane and the torsional modes. From the modal analysis resulted a structural period equal to **T_1=1,36 s**.

Tab. 11.2 Caratteristiche meccaniche del modello (Grandori e Faccioli 1993)

Ordine	Massa (t)	M. d'inerzia (tm^2)	Area sezione (m^2)	M. d'in. sezione (m^4)
0	2396.	63495.	---	---
I	3738.	105272.	35.68	763.6
II	1371.	23504.	28.34	442.8
III	1362.	23390.	28.34	442.8
IV	1227.	20975.	21.44	388.4
V	1192.	20228.	21.44	388.4
VI	1175.	19894.	21.44	388.4
VII	1267.	23038.	20.37	352.0
VIII	725.	11695.	16.5	230.0

The results of the analysis are shown in Tab. 11.3. As it will be discussed later, this estimate seems to be excessive for the Tower, as all the experimental studies proved that the fundamental frequency of the Tower is around 1 Hz.

Tab. 11.3 Numerical results by Grandori e Faccioli (1993)

Modo	Frequenza (Hz)	Periodo (s)
1	0.731	1.368
2	2.333	0.429
3	3.336	0.300
4	10.75	0.093

11.2 ISMES (1995)

Another study which had the purpose to identify the vibration modes of the Tower, this time with an experimental test, was done by ISMES in January 1995 [82]. They performed a dynamic test with a vibrodyne, which had a rotating motion in the horizontal plane (See Fig. 11.2).

Fig. 11.2 Vibrodyne used by ISMES for the test (1995)

Tab. 11.4 shows the results in terms of vibrations modes. The first mode identified was a bending mode with a frequency f_1=1,08 Hz, while the second was a torsional mode with frequency f_2=6,2 Hz. Fig. 11.3 shows the first four modal shapes obtained by ISMES. It must be highlighted that the modal shapes were evaluated using seismometers (velocity sensors) for each *Ordine* of the Tower.

Tab. 11.4 Results of dynamic test by ISMES (1995)

Mode	Frequency (Hz)	Period (s)	Type
1	1.08	0.926	1° bending
2	6.2	0.161	1° torsional
3	6.8	0.147	2° bending
4	13.88	0.072	3° bending

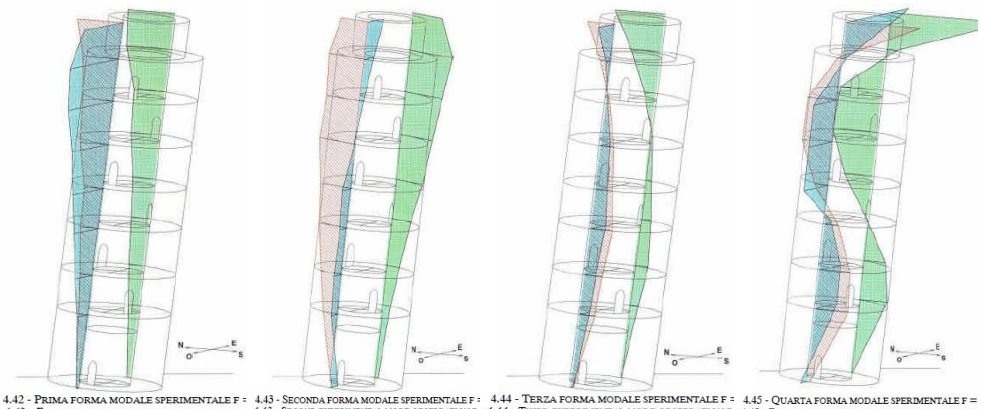

Fig. 11.3 Modal shapes obtained by ISMES (1995)

On the basis of these results, three *stick models* were built in a program using a finite element method (See Fig. 11.4): the first model with a fixed joint at the base, the second with nominal values of the spring stiffness and of the elastic modulus of the materials and the third with the value of springs and elastic moduli calibrated in order to obtain the modal shapes obtained with the dynamic test. The calibration was performed for the first eight modes obtained with the modal analysis, indicated in Tab. 11.5. However, the 3,7 Hz vertical mode obtained with the numerical model was excluded (in red in the Table), which was not identified in the experimental test, as explicitly highlighted in ISMES report.

The mechanical parameters which were modified in the calibration are the following: the modulus of elasticity of the masonry of the foundation basement and of the body of the Tower made in marble of S.Giuliano and of the columns, the stiffness of the horizontal E-W and N-S foundation springs and of the rotational spring N-S of the foundation.

Tab. 11.5 Results obtained with two numerical models by ISMES

Periods and frequencies				
Modal shape	**Model 1 (nominal)**		**Model (calibrated)**	
	T(s)	**f(Hz)**	**T(s)**	**f(Hz)**
1° modo	1.021	0.979	0.923	1.084
2° modo	1.016	0.984	0.920	1.087
3° modo	**0.270**	**3.708**	**0.269**	**3.715**
4° modo	0.186	5.364	0.175	5.715
5° modo	0.182	5.488	0.153	6.550
6° modo	0.126	7.923	0.147	6.818
7° modo	0.077	12.950	0.072	13.880
8° modo	0.075	13.290	0.072098	13.870

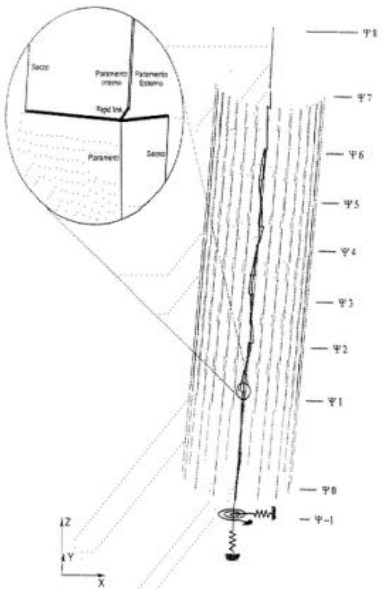

Fig. 11.4 Finite element model built by ISMES (1995)

11.3 Macchi & Ghelfi (2006)

In the publication *La Torre restituita* Macchi and Ghelfi [83] dealt with the survey and the study of the geometry of the Tower for the diagnostics of the structural damages and to optimize a 3D Finite Element Model. For the purpose of the present study the results of this publication were used to have data on the exact positions of the centroids of each storey of the Tower, reported in Tab. 11.6. These were evaluated by putting the origin at the center of lower circle of the foundation ring.

Tab. 11.6 Position of the centroids of each *Ordine*, after Macchi e Ghelfi (2002)

Element	X (m)	Y (m)	Z (m)
Foundation	0,015	0,176	1,761
Ordine 1	0,009	0,938	9,388
Ordine 2	0,212	1,697	17,898
Ordine 3	0,207	2,454	23,787
Ordine 4	0,134	2,676	29,691
Ordine 5	0	3,717	35,404
Ordine 6	0,06	3,793	41,091
Ordine 7	0,180	4,822	47,92
Ordine 8	0,118	5,019	55,263

12 Geophysical tests

12.1 The ground underlying the Tower

The ground underlying the Square of Miracles is formed by geologically recent deposits (Pleistocene - Olocene) of paludal origin: there are silts, clays and fine sands, with intercalation of eolian sands which formed ancient coastal dunes.

According to the definitions made the Polvani commission [78], the ground under the Tower is formed by three principal formations, as reported also in [84]:

- Horizon A: has a thickness of about 10 m, composed by "soft estuarine deposits of sandy and clayey silts laid down under tidal conditions";
- Horizon B: "soft sensitive normally consolidated marine clay extending to a depth of about 40 m". In this formation it is possible to identify:
  - Superior clays or *Pancone,* between 10 and 21 m. These are clays with low or medium consistency, going from slightly over-consolidated to normal-consolidated;
  - Intermediate clays, between 21 and 25 m, are over-consolidated with high consistency;
  - Intermediate sands, between 25 and 27 m;
  - Inferior clays, between 27 and 40 m depth. These are normal-consolidated clays with medium to high consistency;
- Horizon C: "dense marine sand" which arrives to a depth of about 60 m.

As depicted in Fig. 12.1, in proximity of the Tower foundation the interface between superior sands and Pancone clays lies on a almost

horizontal plane, except for a depression under the Tower: in fact the weight of the Tower had caused a lowering of around 2 meters.

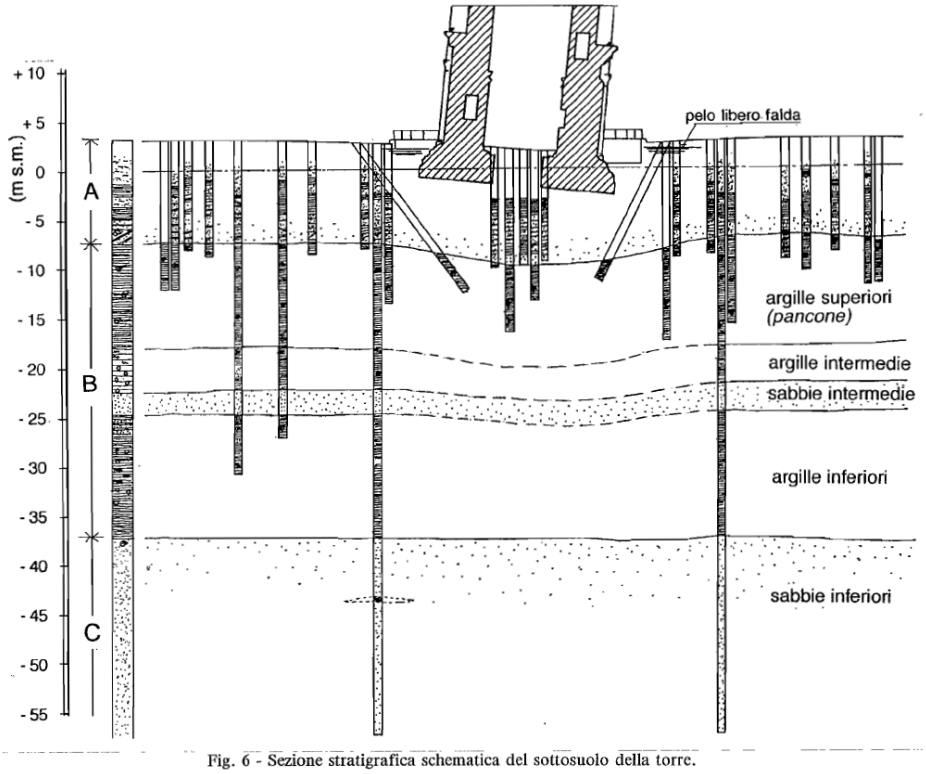

Fig. 6 - Sezione stratigrafica schematica del sottosuolo della torre.

Fig. 12.1 Soil profile of the ground underlying the Tower (Burland, 1994)

12.2 Existing tests

During the last 25 years many geophysical tests, mainly Down-Hole and Cross-Hole tests, were performed in order to assess the shear wave velocity in the layer of the soil underlying the Tower.

In the Cross-Hole test is measured the time needed by body waves (P, S) to move from two points inside the ground. Knowing the distances, measuring travel times the velocities are computed. The test is repeated at

various depths. The tri-axial sensors are located at the same depth in adjacent and in-line holes. The need of 2-3 boreholes implies an higher cost, but the quality of the results could be very good.

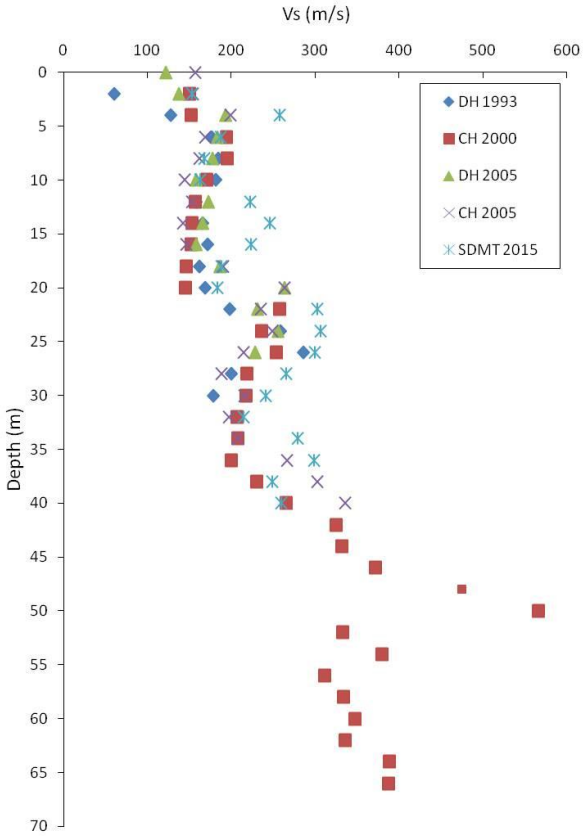

Fig. 12.2 Comparison of Vs obtained with geophysical tests in the last 25 years

In a Down-Hole test the time needed by seismic waves to move from a point at the ground level to a point inside the Borehole is measured. The necessity of a single borehole makes this test less expensive than a Cross-Hole test. The source is a plate which is hit in horizontal direction,

capable to generate SH waves. There could be two types of test: In Down-Hole mode, the source is fixed while the sensors in the borehole are moved up and down. In Up-Hole mode, the sensors are fixed at the ground level while the source moves along the borehole. The reliability of this type of test goes from medium to good, the test is limited to depths of 50-60 m. A variation of the DH is SDMT test, in which the source is located at the ground level and two sensors are located on a dilatometer. In this case a borehole is not needed.

Fig. 12.2 shows a comparison between the measures of the shear waves velocity Vs obtained with the geophysical tests performed in the last 25 years: Down Hole (DH) test [73] done in 1993, Cross Hole (CH) test done in 2000 [82], DH and CH tests done in 2005 [85], SDMT test performed in 2015 [86].

All the tests arrived at a maximum depth of 40 m, except for the Cross Hole test of 2000, which arrived at a depth of 70 meters. None of the tests was successful in identifying a bedrock, therefore there was the need to investigate at major depths, and in the framework of the Convention between the University of Roma Tre and the Opera della Primaziale Pisana an Array 2D test was programmed in november 2015 in the Square of Miracles in order to discover something new in the ground underlying the Tower.

It can be pointed out that other research groups have been performed geophysical tests, CH, DH, and also SASW and MASW tests. For example, Foti [87] and Castellaro and Mulargia [88] report the results of their tests. These tests are not discussed in this thesis.

12.3 Ambient vibration tests

12.3.1 Surface waves

In a linear elastic and homogeneous medium there two types of body waves propagating:

- Compression waves (P): the motion of the particles is parallel to the direction of propagation. This is more influenced by the compressibility of the water in the voids than by the soil particles.
- Shear waves (S): the motion of particles in orthogonal to the direction of propagation. The influence of the water on V_S is negligible, so shear waves can be used to provide informations on the solid part of the soil.

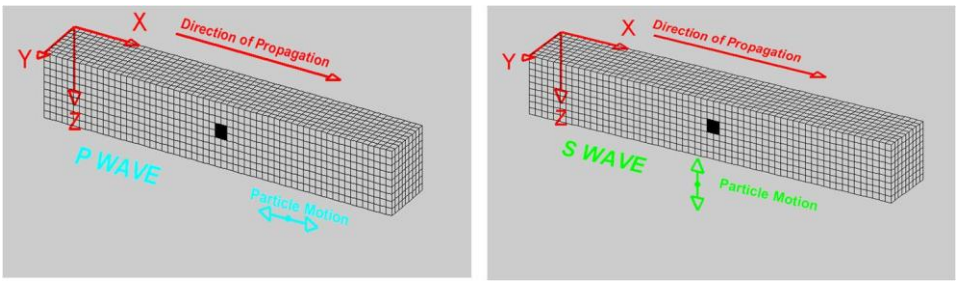

Fig. 12.3 Propagation of body waves in a linear elastic medium

Surface waves, namely Love waves and Rayleigh waves, are caused by the disturbance between body waves, and are slower than body waves. They propagate in upper layers, with amplitude decreasing with depth. These waves are characterized by *Dispersion*, meaning that waves with different frequencies travel at different speed. Meanwhile, they have less *Attenuation* than body waves.

In fact, while body waves attenuate with distance following a $1/R^2$ law, surface waves attenuate with $1/R^{0,5}$. Also Rayleigh waves can give

informations on the parameters of the solid structure of the soil. In fact, V_R can be expressed as function of V_S and Poisson ratio. It ranges from 0,874 V_S to 0,955 V_S depending on ν.

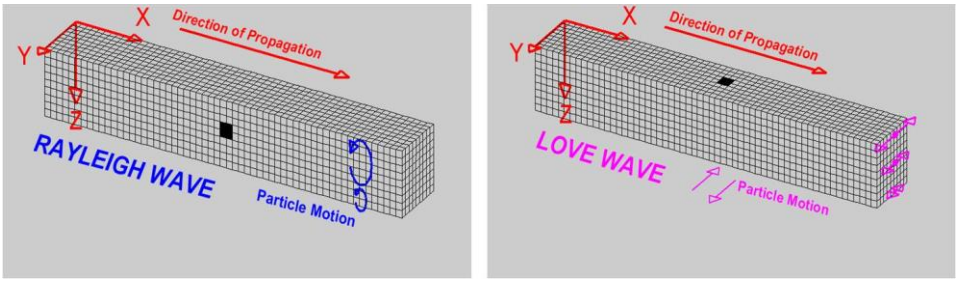

Fig. 12.4 Propagation of surface waves in a linear elastic medium

12.3.2 Ambient vibration tests

Ambient vibration tests are based on the geometric dispersion of the surface waves, used to investigate the relevant properties of the soil medium by solving an inverse problem for the parameters identification.

Ambient vibration, as known as microtremors, are mainly formed by surface waves, and can be generated by very different sources: natural sources like wind, sea waves, or anthropic sources, like the motion produced by machinery, car traffic, railways etc…

All these sources are called *passive sources*, and can give useful informations for the characterization of grounds arriving to hundreds of meters of depth. Conversely, the resolution of these tests close to the ground surface is low, because ambient vibration are poor at high frequencies.

In november 2015 two ambient vibration tests were executed in the Square of Miracles:

– An Array 2D test

– An H/V test

The following sections aim to describe these type of geophysical tests and to discuss the results obtained.

12.3.3 Geometric dispersion of Rayleigh waves

The Dispersion phenomenon characterizing the surface waves is depicted in Fig. 12.5, taken by [91]. At a distance of one or two wavelength λ from the source the contribution of body waves is negligible, and the wave-field is dominated by surface waves.

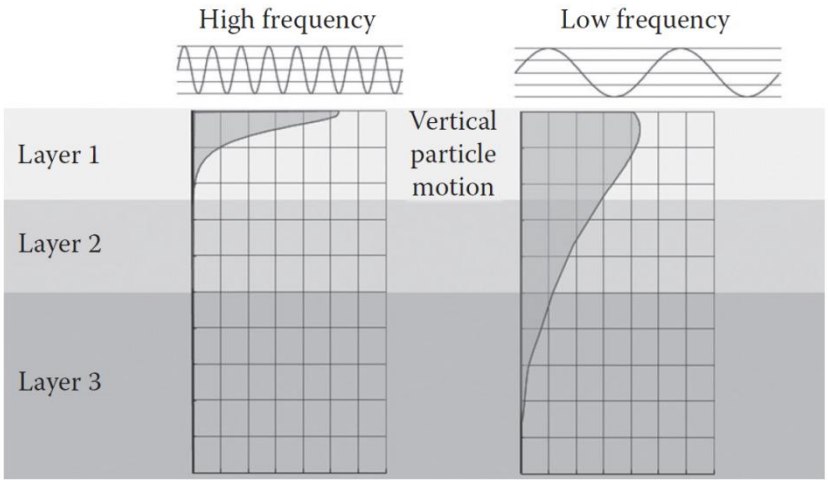

Fig. 12.5 Geometric dispersion of Rayleigh waves (Foti et al. 2015)

The majority of the energy of deformation associated to the wave motion is confined at a depth around one wavelength **λ** from the ground level. Therefore, Rayleigh waves with a larger λ (and minor frequency f) reach major depths than Rayleigh waves with a smaller λ (and higher frequency f) which are confined in upper layers of the ground.

Rayleigh waves in a linear elastic and homogeneous medium are non-dispersive: velocity is not dependent on the wave frequency but only on the medium properties. In stratified media there is dispersion and the wave velocity depends on the frequency content of the waves:

- High frequency waves: are confined in Layer 1, therefore the wave velocity is influences only by mechanical properties of Layer 1. (Fig. 12.5 - left)
- Low frequency waves: the wave velocity is controlled by a certain combination of the properties of the three layers (Fig. 12.5 - right).

In general, deeper layers has greater values of wave velocity, so low frequency waves usually have a resulting velocity which is greater than that of high frequency waves. This condition can be represented by a plot of the wavelength versus phase velocity of the waves. Then, remembering the close relation between the wavelength and the frequency, a dispersion curve, showing the trend of the phase velocity with frequency can be obtained.

If data are available on the soil profile, it is simple to build the dispersion curve. Conversely, if the purpose is to find a soil profile starting from an experimental dispersion curve the problem is more complex because it is needful to solve an inverse problem, as depicted in Fig. 12.6. In these case there is an infinite number of soil profiles which can match the dispersion curve, therefore it is necessary to introduce some constraints to limit the problem, as it will be discussed in the next section.

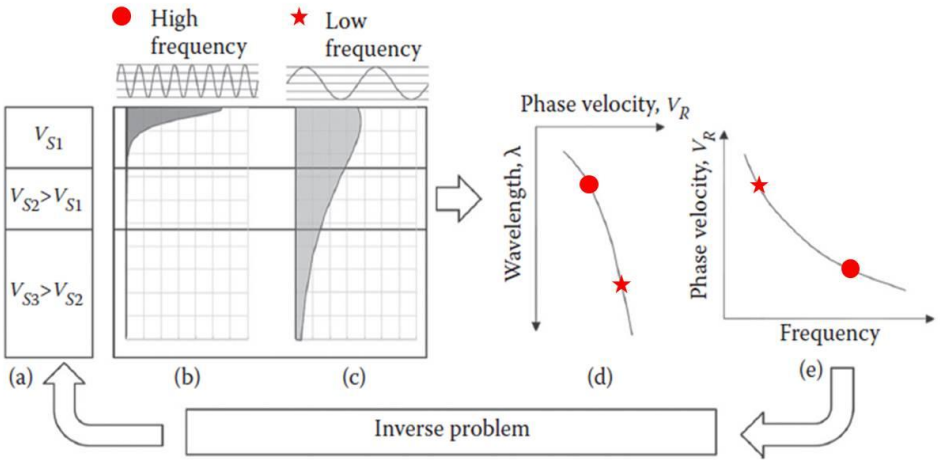

Fig. 12.6 Inverse problem (modified from Foti et al. 2015)

12.3.4 Array 2D test: Execution and results

An Array 2D test (F-K method) was performed in November 2015 in order to investigate the soil underlying the Tower at major depths, with the purpose to identify a more rigid layer than those identified in the past geophysical tests. The results of the tests elaborated with the software Geopsy [89] are taken from the report of the test written by Della Monica et al. [90].

Two pictures taken during the execution of the tests are reported in Fig. 12.9 and Fig. 12.10, showing respectively the phase of the synchronization of a station clock with the GPS system, and the phase of acquisition for station A, located close to the western walls of the Square.

The tests were performed by night to avoid undesired point sources of ambient noise. The Array was formed by 9 seismic stations with a triangle

geometry and a central station. The geometry of the Array (Fig. 12.8) was calibrated to maximize the resolution of the test.

The sensors used for the test are three components Le 3D 5s Lennartz velocimeters. These instruments were chosen because, due to the large period, they are able to catch very low frequency ground motions. The acquisition system was completed by a seismic recorder Reftek 130, a Gps antenna and a 12 V battery. Each sensor is equipped with a GPS in order to guarantee that the reference time is the same for all the sensors. Fig. 12.7 shows the components of the acquisition system and the type of sensor used.

Fig. 12.7 Acquisition system for the Array 2D test

Fig. 12.8 Array 2D test performed in the Square of Miracles, November 2015

Fig. 12.9 installation of a seismic station close to the Tower

Fig. 12.10 Acquisition phase for station A

Seismic Array is a geophysical technique which allows to obtain a vertical profile for the shear wave velocities at a given site. A seismic Array is formed by a certain number of seismic stations which are capable to record the ambient vibrations based on the same reference time.

The Array technique is based on the MASW analysis (Multichannel Analysis of Surface Waves), which is a non-destructive technique to determine the shear waves velocity. The method consists in the spectral analysis of Rayleigh waves recorded from ambient vibrations. From the definition of dispersion of Rayleigh waves, discussed in section 12.3.3, it is possible to obtain from experimental recordings the dispersion curve, which is a plot of the phase velocity (i.e. propagation velocity) of Rayleigh waves versus the frequency or the wavelength. The curve gives informations on the stiffness of the different soil layers. The MASW method allows to evaluate the phase differences of the armonics forming

the wave groups propagating between two receivers. These differences can be used to build the experimental dispersion curve.

The resolution of the Array characterized by the selected geometry is given by the Array Transfer Function (See Fig. 12.9): according to some authors the resolution of the Array depends not only on its maximum length or distance between sensors, but also on the spatial distribution of the sensors. This distribution can be modified in the phase of design of the Array in order to maximize the resolution, obtaining the maximum number of frequencies.

The experimental dispersion curve obtained with the software Geopsy, shown in Fig. 12.11 allows to identify, into the range of spatial resolution, a velocity spectrum with a minimum value of 220 m/s, corresponding to a frequency of around 4 Hz, and a maximum of 400 m/s, corresponding to 1,5 Hz. Nevertheless, it can noticed that for frequencies f<2 Hz the curve has a recognizable trend. Therefore it is possible to extend the results down to a frequency of around 1 Hz, corresponding to a shear wave velocity of around 500 m/s, remembering that the resolution of the instrument can arrive to very low frequencies (0,2 Hz which corresponds to 5 s, maximum period of the sensor).

As discussed in a previous section, the experimental dispersion curve can correspond to an infinite number of soil profiles. For this reason it is necessary to impose some constraint to the inversion process, for which are needed:

- The number of layers of the model. The hypothesis is that the layers are horizontal and parallel, condition verified by the H/V test that will be discussed in the next section;
- The ranges of velocities of compression and shear waves;
- The Poisson ratio;

– The densities of the layers.

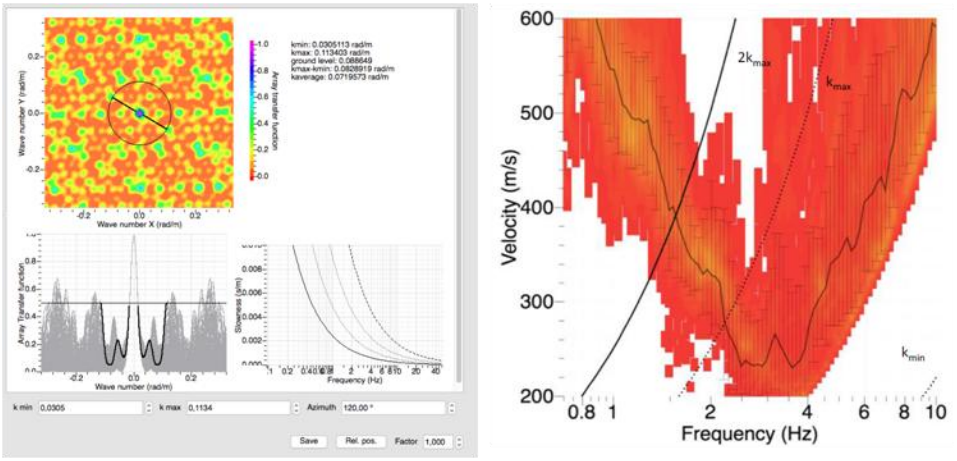

Fig. 12.11 Array Transfer function (left) and experimental dispersion curve (right)

For the first 40 meters of the inversion process were used the results of the Cross-Hole and Down-Hole tests. The parameters of the inversion process are shown in Tab. 12.1. The results of the inversion process are reported in Fig. 12.12. The figure represents the vertical profile of compression and shear waves velocities, with the relative misfit between the experimental and theoretical curves.

Tab. 12.1 Ranges of parameters to constraint the problem

Layer	V_P(m/s)	V_S (m/s)	Density	Thickness (m)
1	1350-1500	150-200	17	18-22
2	1500-1600	200-270	17.5	18-22
3	1600-1800	270-380	18	28-60
4	1800-2000	400-500	19-20	halfspace

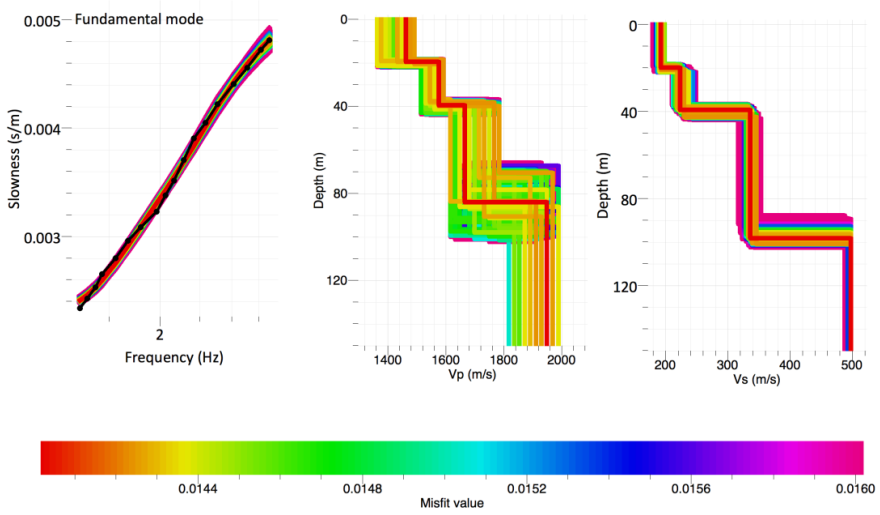

Fig. 12.12 Soil profile and dispersion curve obtained with Geopsy

It is clear from the figure that the maximum misfit obtained with these soil profile is around the 1,8%, therefore the results obtained have a resolution. From these plots it is possible to derive the minimum misfit curve, in red in Fig. 12.12, represented in Fig. 12.13 in comparison with the older geophysical tests made on the ground underlying the Tower.

This plot shows the presence of a more rigid layer, characterized by a $V_S \simeq 500$ m/s at a depth of about 100 m. This is a new result since past tests arrived at a maximum depth of 65 m and did not identified this layer. Nevertheless, this soil cannot be associated to the *Seismic bedrock*, as it shows velocities typical of a Class B soil, according to EC8 classification. However, under certain hypothesis, the results obtained can be used to perform a site response analysis, which will be discussed in chapter 16.

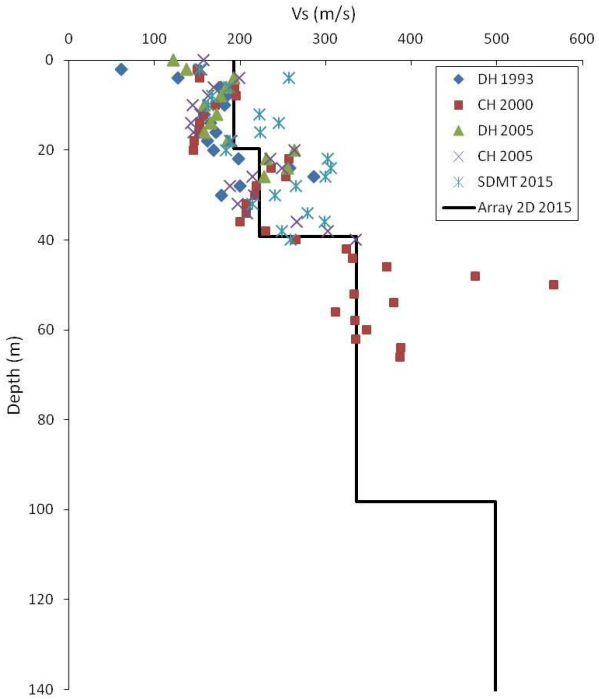

Fig. 12.13 Comparison between geophysical tests including Array 2D results

12.3.5 H/V test Execution and results

In layered grounds the Fourier Spectral ratio H/V or horizontal ellipticity depends on the frequency. The peaks of this ration are important because they depend on the thickness and on the velocity of the layers which lie on the bedrock, and they can give informations on the amplification given by the soft layers.

Considering the simplified model of uniform damped layer on a bedrock, it is thus possible to obtain an amplification function, which variates with the frequency, and has some local maxima, which correspond to the

natural frequencies of the deposit. The amplification factor is also equal to the ratio between the free surface motion to the bedrock motion.

The fundamental frequency and the corresponding characteristic site period of the layer could be expressed as:

$$\omega_0 = \frac{\pi v_s}{2H} \qquad T_s = \frac{4H}{v_s}$$

The characteristic site period depends only on the thickness and on the shear wave velocity of the soil, and can provide useful informations on the periods at which the major amplification are expected.

The technique named HVSR (Horizontal to Vertical Spectral Ratio) was widely used by Nakamura [92], and is based on the evaluation of the ratio between the horizontal (H) and vertical (V) Fourier spectral components of an ambient vibration (microtremors in Japan) recorded on the free surface. A typical H/V curve provides an amplification curve which has local maxima at some fundamental frequencies, exactly like the theoretical one but this can be obtained experimentally.

Single station analysis was performed within the same test in order to evaluate H/V spectral ratios. The position of the seismic station used for the test is reported in Fig. 12.14.

Fig. 12.14 H/V test performed in the Square of Miracles, November 2015

Fig. 12.15 and Fig. 12.16 show the output for the H/V test. The first depicts the Fourier spectra of the single components of the recordings (two horizontal and one vertical component).

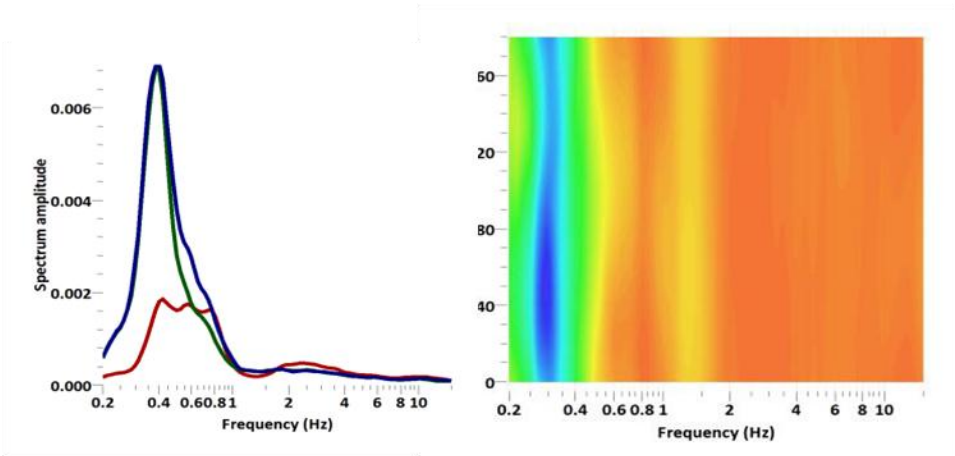

Fig. 12.15 Fourier spectra of records (left) Directionality of passive sources (right)

For some stations it was possible to notice that for certain values of frequency the vertical component is greater than the horizontal

components. This fact could be an indicator of the influence of a structure on the ground motion.

The second figure shows the directionality of the passive sources. It is possible to observe that for all directions, indicated by the Azimuth, the results do not highlight preferential source of noise.

Finally the H/V curve depicted in Fig. 12.16, where the red line is the resulting curve and the dotted lines are the minimum and the maximum value of amplification. In all cases the amplification factor is greater than 2.

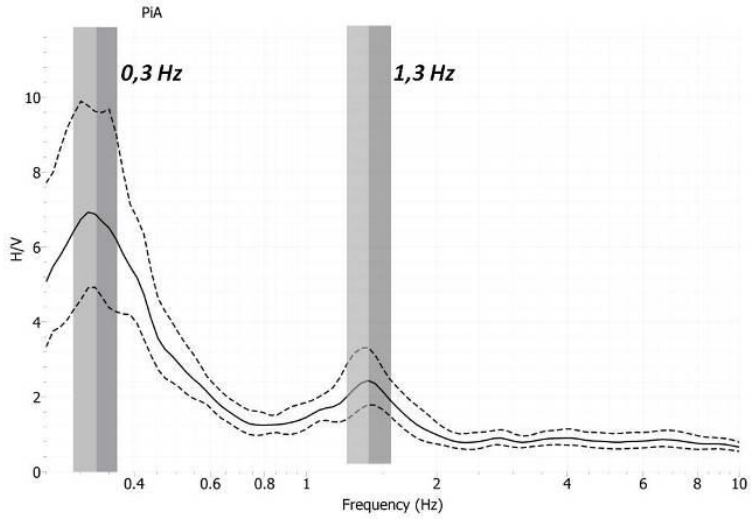

Fig. 12.16 Resonance peaks of H/V spectral curve for a single station

The single station analysis allowed to identify two different peaks of resonance frequency: one at 0.3 Hz, and the other at 1,3 Hz. Using the expression of the fundamental frequency discussed above, this peak can be related to the interface at 40 meters depth, which was identified with the Array test. The other peak is conversely related to a deeper layer, which could be located around 500 m depth. This layer is out of the

resolution of the Array, but it likely represents the *Seismic Bedrock* of the area. The resonance peaks are slightly different from a previous study carried on by Castellaro and Mulargia, which found a resonance peak at 1,1 Hz [88].

13 Foundation geometry and model

13.1 Introduction

The foundation of the Leaning Tower of Pisa has a ring shape with an external diameter of 19,6 meters. The central opening has a diameter of 4,5 m. The area of the foundation is around 285 m^2, and the average pressure on the ground is 497 MPa. Fig. 13.1 shows a section of the foundation ring. The external walls are made of San Giuliano marble, while in the internal part there is rubble stone fill while in a lower layer there is masonry which was object of an intervention of waterproofing through injections of mortar in 1935 [71].

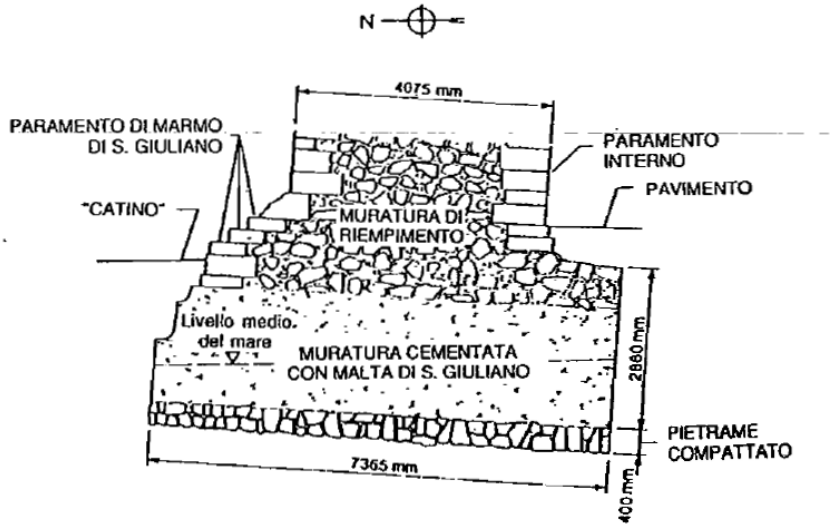

Fig. 13.1 Section of foundation ring (Burland 1994)

Until 19th century the foundation basement of the Tower was entirely underground as shown in some prints of that period (See Fig. 13.2), then in the years 1835-1836 the architect Gherardesca made a series of works

with the aim to dig up the basement of the Tower, forming the so-called *Catino*.

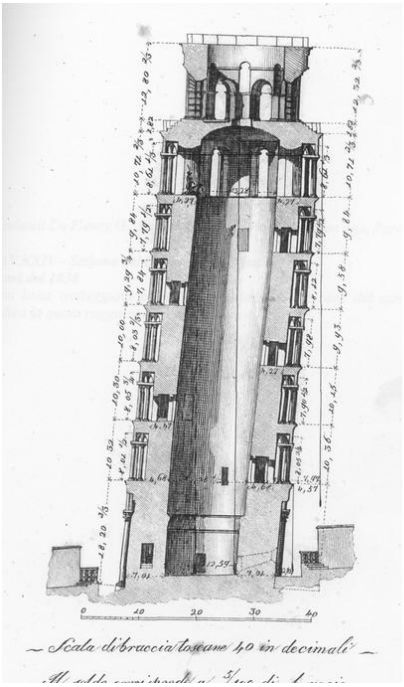

Fig. 13.2 Condition of the basement of the Tower before the works by Gherardesca (1838)

At the beginning of the 20th century the foundation of the Tower was completely open and it had the current shape, and at the base it was realized a ring-shaped concrete plate with a 80 cm thickness. In the years 1933-1935 the office of Genio Civile of Pisa prescribed some interventions of waterproofing and consolidation of the *Catino*, made by Rodio firm.

In recent times, some studies made in 1993-1994 demonstrated that the inclination of the Tower continued to increase during time, mostly because of the seasonal variation of the water table located a few meters

under the ground level, therefore the Committee for the safeguard of the Pisa Tower decided to intervene, initially by posing weights (900 tons) on the North side of the foundation and holding the Tower with tie rods. Then were executed two works of under-excavation, a preliminary intervention between February and October 1999 and the conclusive intervention between February 2000 and January 2001.

Fig. 13.3 Works for the consolidation of the *Catino*

Regarding the foundation, the concrete plate which lied on the basement of the *Catino* was rigidly connected to the foundation of the Tower using inox steel rebars and reinforced using post-tensioned rebars, as shown in Fig. 13.3 and Fig. 13.4. Therefore the section of the foundation changed significantly following these interventions.

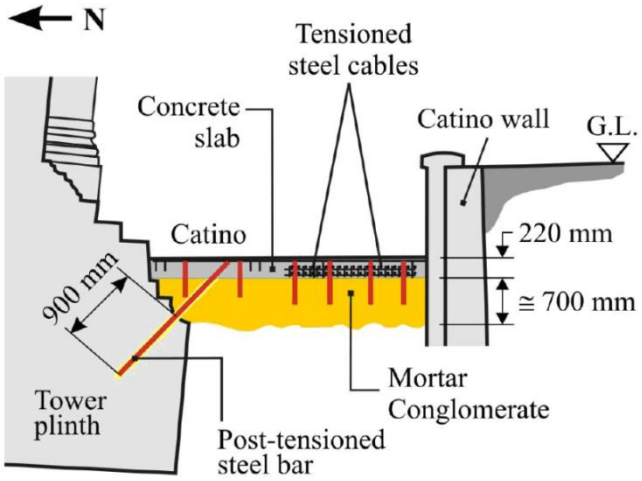

Fig. 13.4 Connection between the foundation and the *Catino* (Burland, 2009)

The foundation-*Catino* system has currently the aspect depicted in Fig. 13.5. it is possible to observe that the shape of the concrete ring at the base follows the different levels imposed by the Tower foundation.

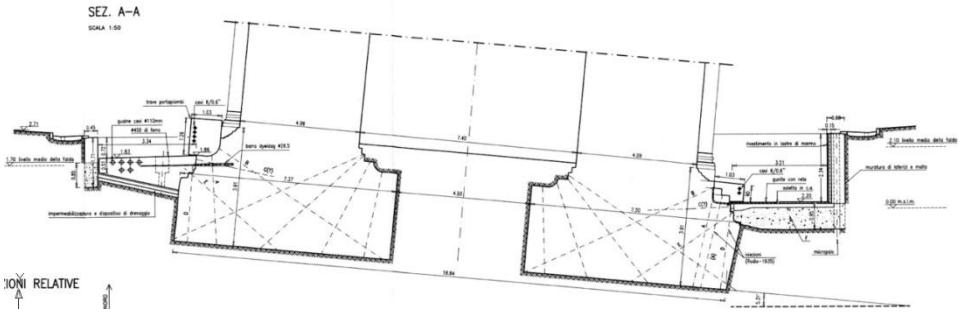

Fig. 13.5 Fondazione della torre e catino di base, configurazione attuale

This brief history of the works on the foundation of the Tower helps to reconstruct the current condition of the foundation, in order to better understand how to model the behavior of the Tower considering the soil-structure interaction.

13.2 Soil-structure interaction

The presence of the structure modifies the soil response in comparison with the free-field case. Theoretically, it could be possible to study the soil-structure system with a complete Finite Element model, but in this case the computational cost would be very high.

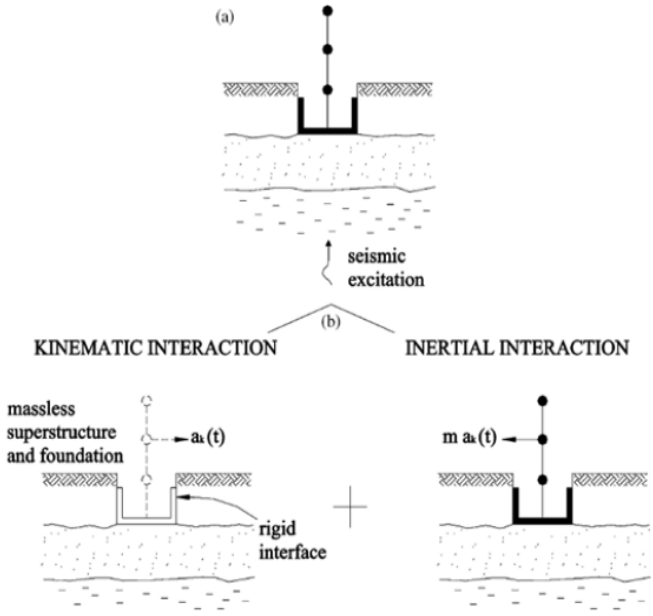

Fig. 13.6 Schematization of soil-structure interaction (Mylonakis, 2006)

Considering an elastic analysis, it is possible to analyze the structural response by dividing it in two parts, namely the cinematic and the inertial interactions (See Fig. 13.6, taken from [93]):

- *Cinematic interaction*: is the effect that the foundation has on the motion of the points which are in contact with the foundation structure and the soil considering a mass-less structure. If the structure had the same stiffness of the soil the cinematic

interaction would be zero because the motion would be equal to the Free Field motion.

– *Inertial interaction*: There is inertial interaction when the system formed by structure (with mass) and soil (mass-less) is subjected to seismic motion caused by the cinematic interaction.

If the structure has shallow foundations and the motion is essentially caused by S-waves propagating vertically the cinematic interaction is zero. In the case of the Pisa Tower the foundation is slightly embedded, so that it could be considered as a shallow foundation. Therefore, in this study only the inertial interaction was considered. The problem is then to assess the impedance matrix of the foundation.

There is another phenomenon which affects the seismic response of the soil-structure system and it is the *local amplification*: the seismic input which in general is assessed on bedrock must be modified in order to reproduce the Free Field motion at the base of the structure. For this reason a site response analysis must be performed, as discussed in chapter 16.

13.3 Experimental modal frequencies

During the last 20 years there were some dynamic monitoring-based studies, which had the purpose to identify the experimental frequencies, for example the work based on microtremors by Nakamura [94], the work by ISMES discussed in a previous section, Atzeni et al. [95] and Castellaro and Mulargia [88]. Some of these tests have been performed without providing enough informations on the methodologies used or in unsuitable conditions.

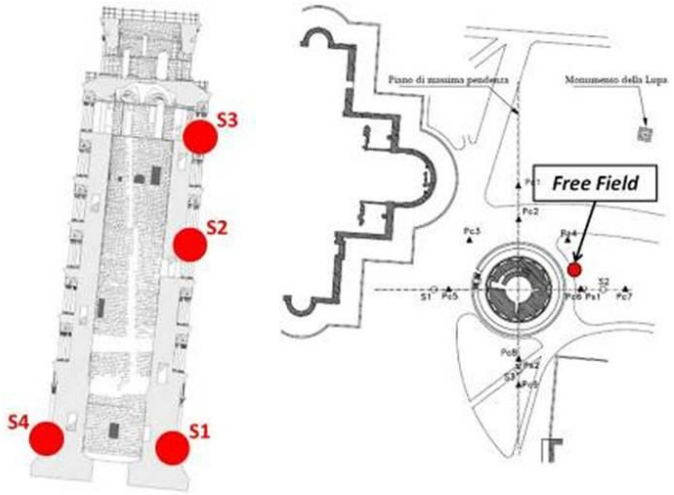

Fig. 13.7 Position of the sensors on the Tower (left) and on the ground (right)

In a work published at ACE2015 conference, held in Vietri sul Mare, Bartelletti et al. [97] presented an experimental assessment through dynamic monitoring which had the aim to identify the modal parameters of the Tower.

The Tower is provided with various instruments, Kinemetrics Episensor FBA ES-U, including three three-axial accelerometers (S1, S2, S3) indicated in Fig. 13.7 and one uni-axial accelerometer (S4), with his axis oriented in vertical direction. On the ground level, close to the *Catino*, there is a Free Field accelerometers, which is too close to the foundation of the Tower to be used as a real Free Field instrument. The list of the earthquakes recorded by the accelerometers in the years 2004-2015 is reported in Tab. 13.1. The ground motion intensity caused by these earthquakes was not important, because they were earthquakes with small Magnitude and large distances, in the majority of cases.

Tab. 13.1 List of the considered seismic events.

Event label	Date	Magnitude M_W	Distance from Pisa
150100023	2015-01-23	4.3	74
12010022	2012-01-27	5	94
12010015	2012-01-25	Not available	Not available
060400070	2006-04-17	4.2	33
050500025	2005-05-17	4	16
041100050	2004-11-24	5.06	214

The seismic records of the seismic event of 27 January 2012, depicted in Fig. 13.8 were analyzed using different techniques, such as Fast Fourier Transform (FFT), Continuous Wavelet Transform (CWS) and the Wavelet Cross Spectrum (WCS) [99]. Fig. 13.9 reports the CWT of a 3-component signal recorded during 2012 seismic event.

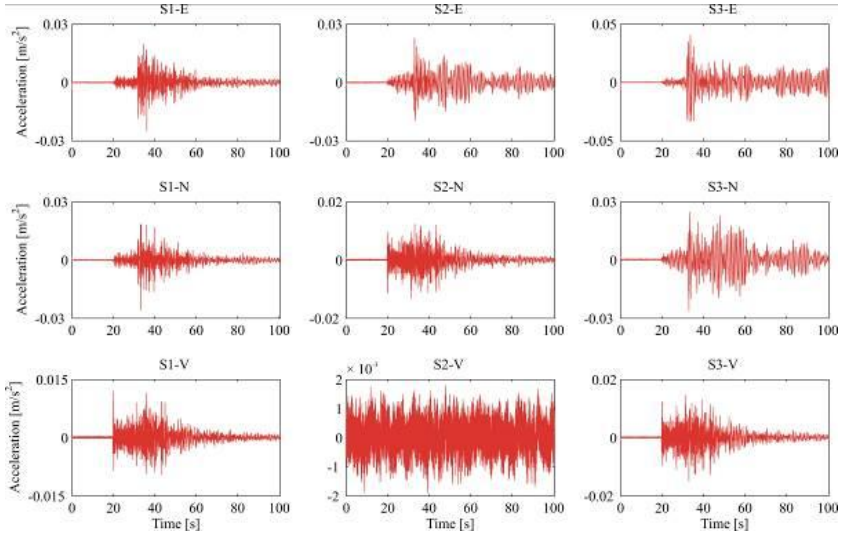

Fig. 13.8 Response recorded on the Tower by sensors S1, S2, S3

The analyses allowed to identify the modal frequencies of the first three modes of the Tower. The first two are bending modes in N-S and E-W direction, respectively, both with a frequency around 1 Hz. The third is a vertical mode with a frequency around 3 Hz.

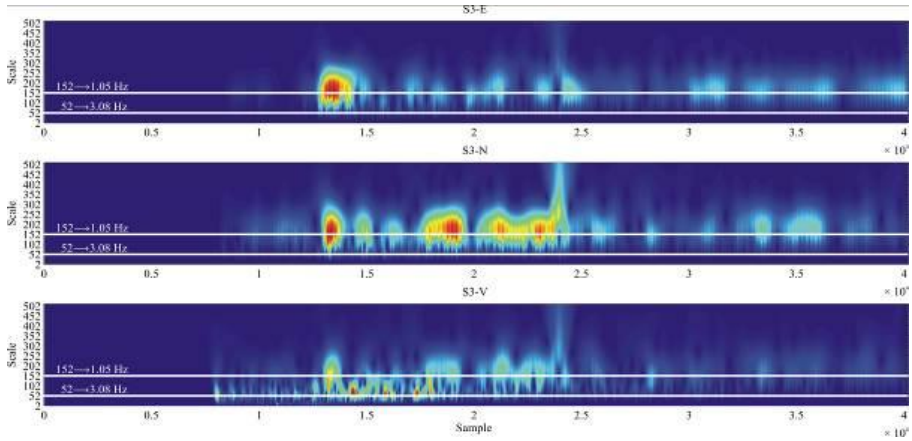

Fig. 13.9 CWT of the recorded tower response

This is a quite new result since the only evidence in literature in presented in Nakamura [94]. A comparison of the results on the main experimental studies conducted on the Tower. With the exception of the study by ISMES, all the other studies highlight that the frequency is slightly less for the N-S mode than for the E-W mode, and this is probably due to the inclination of the Tower.

Tab. 13.2 Comparison of results from different authors

Author	N-S freq.	E-W freq.	Vertical
ISMES (1995) – Forced Vibrations	1.08 Hz		-
Nakamura et al. (1999)	0.98 Hz	1.06 Hz	3 Hz
Atzeni et al. (2010)	1.01 Hz	1.04 Hz	-
Castellaro e Mulargia (2010)	1 Hz	1.1 Hz	-
Present work (2015)	**0.958 Hz**	**1.025 Hz**	**2,98 Hz**

Band pass filter analyses presented in the same work have shown that for a filter between 2 and 4 Hz the vertical mode does not cause rotation at the base (See Fig. 13.10). Conversely, for a filter 0,8-1,2 Hz corresponding to the Horizontal mode, the motion are in anti-phase, therefore the bending mode at 1 Hz is responsible of the rotation at the base of the Tower (See Fig. 13.11).

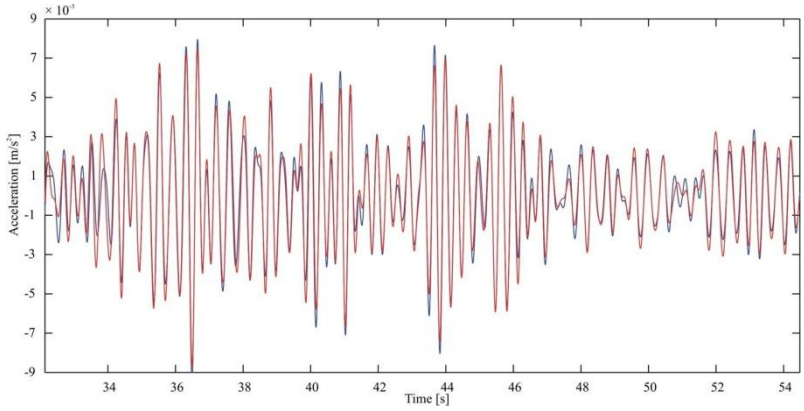

Fig. 13.10 Vertical response due to the vertical mode (Filter 2-4 Hz)

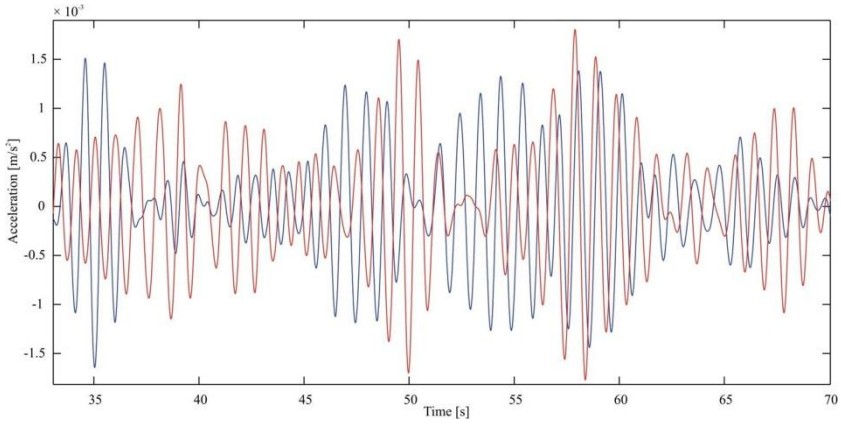

Fig. 13.11 Vertical response due to the bending mode (Filter 0,8-1,2 Hz)

13.4 Shear modulus at small deformations

The comparison between the geophysical tests highlights a satisfactory agreement, showing very close values of V_s. On the basis of these evidence, the soil underlying the Tower is modeled as homogeneous half-space. The parameters of the half-space, the mass density ρ of the soil and the V_s value are the average of the first 35 meters. The mass density of the soil is obtained by the specific weight reported in the study of Viggiani [85]. For small deformations, the shear modulus can be evaluated using the following equation, valid for small deformations:

$$G_0 = \rho \cdot V_s^2$$

which provides G_0=77326 kN/m^2 (ρ=18.7 t/m^3). Another important parameter of the soil is the Poisson coefficient. For dynamic conditions, when the soil is saturated by water, it is possible to assume v=0.5.

13.5 Wolf formulation

The model considered to evaluate the dynamic impedances at the base is the Standard Lumped parameter model, with Wolf formulation [100], which is depicted in Fig. 13.12.

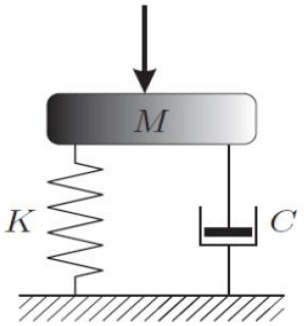

Fig. 13.12 Standard lumped parameter model - Wolf (1994)

The formulation used in the present work is the most simple proposed by Wolf. This model is based on a SDOF system formed by a mass M, a spring with stiffness K and a viscous damper with constant C. The stiffness K is equal to the static stiffness of the soil-structure system. The coefficients C and M are used to reproduce the real behavior of the soil-structure system, and depend on two adimensional coefficients μ e γ, which are evaluated using tables provided by the author together with K where m is the mass for the two translational DOF and the mass moment of inertia for rotation and torsion.

C expresses the dashpot coefficient and reflects two types of damping: radiation damping is due to the spreading of the seismic waves from the foundation while material damping comes from the dissipation of energy in the soil due to the hysteretic action. The formulae which allow to evaluate the static stiffness K and the adimensional coefficients for Dashpot and Mass are listed in Fig. 13.13, which reports a table from the work by Wolf [100].

Table II. Static-stiffness and dimensionless coefficients of spring-dashpot-mass model of Figure 6 for disk on half-space

	Static stiffness K	Dimensionless coefficients of Dashpot γ	Mass μ
Horizontal	$\frac{8Gr_0}{2-\nu}$	0·58	0·095
Vertical	$\frac{4Gr_0}{1-\nu}$	0·85	0·27
Rocking	$\frac{8Gr_0^3}{3(1-\nu)}$	$\frac{0{\cdot}3}{1+\frac{3(1-\nu)m}{8r_0^5\rho}}$	0·24
Torsional	$\frac{16Gr_0^3}{3}$	$\frac{0{\cdot}433}{1+\frac{2m}{r_0^5\rho}}\sqrt{\frac{m}{r_0^5\rho}}$	0·045

Fig. 13.13 Parameters of spring-dashpot-mass model (Wolf, 1994)

In the table G, ρ e ν are respectively the shear modulus, the density and the Poisson ratio of the soil. For the ground underlying the foundation it was used the model of homogeneous elastic half-space. Knowing γ and μ, it is possible to evaluate the mass M and the damping C of the system using the following equations:

$$C = \frac{R}{c_s}\gamma K \qquad M = \frac{R^2}{c_s^2}\mu K$$

An armonic excitation with ciclic frequency ω and amplitude P(ω) causes a displacement with an amplitude of u(ω). These two parameters are related by the equation:

$$P(\omega) = S(\omega) \cdot u(\omega)$$

Where

$$S(\omega) = K - \omega^2 M + i\omega C$$

It is possible to introduce an adimensional ratio dependent on frequency, defined as:

$$a_0 = \frac{\omega \cdot R}{c_s}$$

Where

$$c_s = \sqrt{G/\rho}$$

So doing, S can be expressed as function of a_0:

$$S(a_0) = K[k(a_0) + i a_0 c(a_0)]$$

K is the static stiffness, therefore knowing the dynamic stiffness it is possible to obtain the dynamic one. The coefficients $k(a_0)$ and $c(a_0)$ can be expressed with the following equations:

$$k(a_0) = 1 - \mu \cdot a_0^2$$

$$c(a_0) = \gamma$$

The coefficient of dynamic stiffness $k(a_0)$ has a parabolic trend. The parabola is valid for low/medium frequencies, until a_0=1,5, corresponding to a frequency of 30 Hz for our case. A plot of $k(a_0)$ versus a_0 is depicted in Fig. 13.14 to Fig. 13.17.

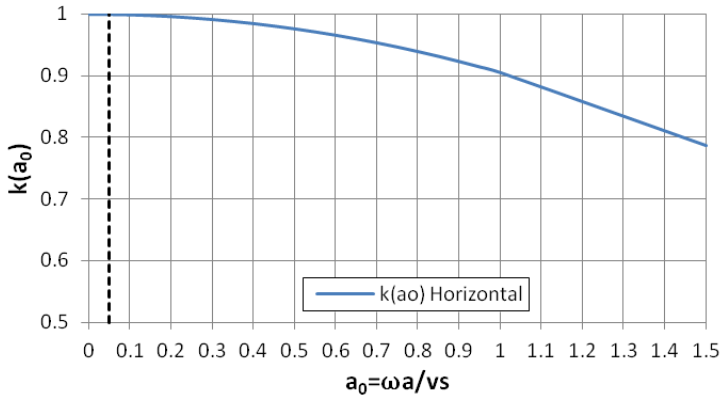

Fig. 13.14 Plot of $k(a_0)$ vs a_0 - Horizontal translation

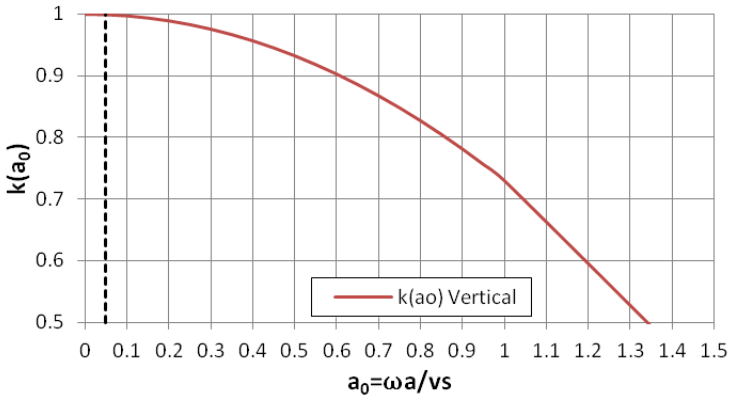

Fig. 13.15 Plot of $k(a_0)$ vs a_0 - Vertical translation

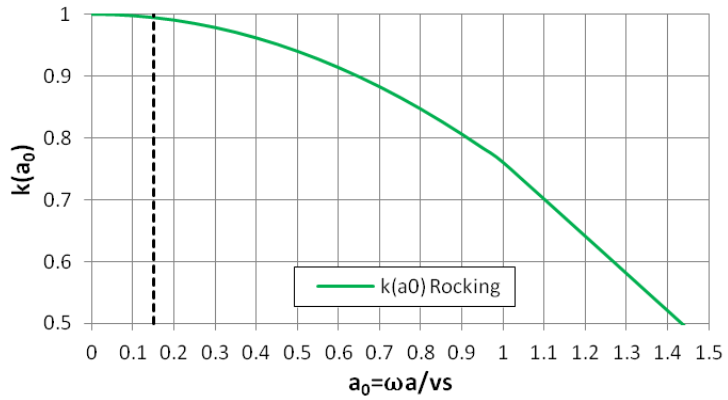

Fig. 13.16 Plot of $k(a_0)$ vs a_0 - Rocking

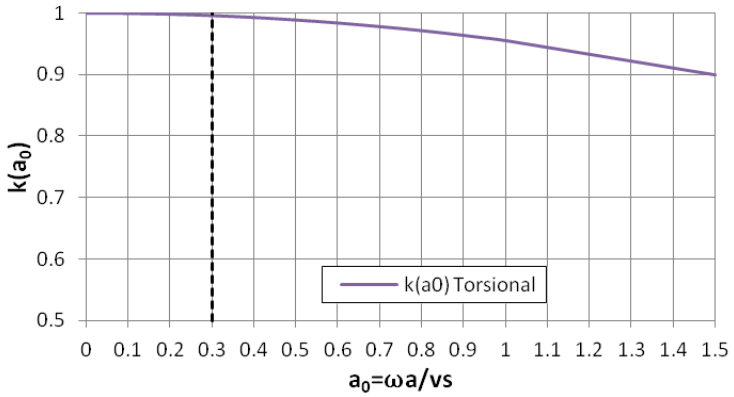

Fig. 13.17 Plot of $k(a_0)$ vs a_0 - Torsion

The dynamic stiffness, K(ω), can be computed by multiplying the static stiffness K for the coefficient depending on frequency $k(a_0)$.

For each identified mode it is possible to find the coefficient $k(a_0)$. As shown in Tab. 13.3 the values of coefficients are very close to unity, therefore it is possible to consider the dynamic stiffness K(ω) is equal to the static stiffness K.

Tab. 13.3 Values of $k(a_0)$ for the identified modes

Mode	Frequency (Hz)	a_0	$k(a_0)$
Horizontal N-S	1	0.05	0.9997
Horizontal E-W	1	0.05	0.9997
Vertical	3	0,15	0.9993
Torsional	6	0.3	0.978

In structures with embedded foundations, the horizontal forces cause rotational motion. In such circumstance, the off-diagonal elements of the impedance matrix *Kx-ry* and *Ky-rx* are no-null, as indicated in [93]. For shallow foundations, these off-diagonal elements are negligible. The aim of this part of the work is the evaluation of the diagonal elements of the impedance matrix.

13.6 Evaluation of dynamic impedances

In order to evaluate the impedance matrix, it is sufficient to compute the values of the static stiffness of the foundation. The expressions given in the literature [100] consider a disk foundation. There are two parameters that can affect the value of the impedances, which are the radius of the foundation *R* and the modulus of elasticity of the soil *G*.

The foundation of the Tower is ring-shaped, and the resulting impedances are obtained using an equivalent ring radius evaluated as the difference between the external and the internal radius.

In this work, two cases are considered, namely the ring foundation alone and the ring foundation with the *Catino*. The *Catino* is assumed rigidly linked to the foundation with regard to translation and torsion. It is important to highlight that the constraint between the *Catino* and the Tower is uncertain because it is basically due to the frictional contact

between the two bodies, but there is a tensioned radial system, as discussed in section 13.1. The *Catino* has a high stiffness in its own plane (with regard to translational and torsion) while it has a lower stiffness for out-of-plan rotations.

Two cases are considered for the estimation of *G*:

- In the first one, the modulus of elasticity is obtained with the nominal values reported within the Sub-section 13.3.
- In the second case, it is assumed G=95.000 kN/m^2, which allows to obtain numerical frequencies very close to those identified experimentally.

The Tab. 13.4 provides the obtained values of the dynamic impedances.

Tab. 13.4 Values of the dynamic impedances (units: kN/m^2)

		Foundation alone		Foundation with *Catino*	
Degree-of-freedom	G (kN/m^2)	77326	95000	77326	95000
Translation E-W	*Kux*	3.11E+06	3.83E+06	4.23E+06	5.19E+06
Translation N-S	*Kuy*	3.11E+06	3.83E+06	4.23E+06	5.19E+06
Vertical	*Kuz*	4.67E+06	5.74E+06	4.67E+06	5.74E+06
Rotation *x*	*Kϕx*	3.83E+08	4.71E+08	3.83E+08	4.71E+08
Rotation *y*	*Kϕy*	3.83E+08	4.71E+08	3.83E+08	4.71E+08
Torsion	*Kϕz*	3.83E+08	4.71E+08	8.01E+08	9.84E+08

14 Modal analysis

14.1 Simplified model (SAP 2000)

According to Italian guidelines on cultural heritage [11], considering that towers have minor geometric complexity than other structures, all the critical aspects can be studied using reliable structural models. In this case it possible to use also linear models, because the redistribution of stresses in a mainly isostatic structure is moderate. It is then possible to use the modal analysis to understand the above described effects of the amplification of motion. The relative simplicity of the structural scheme allows to use simple models.

A simplified FE model was elaborated using the program SAP2000 (Figure 3). It consists of 14 elements and 16 nodes, with 6 degrees of freedom per node. Assumptions and input data used for the model are the following:

- For each *Ordine* of the Tower, the coordinates of the centroid were defined according to the work by Macchi and Ghelfi [76]. Only the inclination in the North-South plane was considered whereas the inclination in the East-West direction was neglected;
- For each centroid, 3 translational masses and 3 rotational masses were defined;
- Area and moment of inertia were assigned to each level of the Tower. Geometric parameters are taken from the work by Grandori and Faccioli [73]. They are homogenized by assuming the whole sections made of marble of San Giuliano (the material of the walls of the Tower), which has a modulus of elasticity E=80,000 MPa;

– At the base of the model were assigned 3 translational springs and 3 rotational springs, for which the impedances reported in Tab. 13.4 are considered.

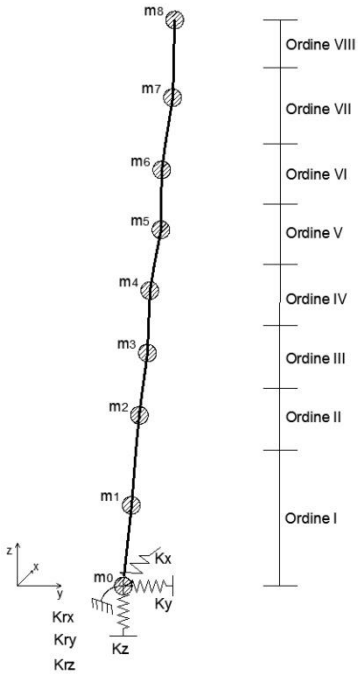

Figure 3.

Fig. 14.1 Scheme of the FE model

14.2 Modal frequencies

Four frequencies have been identified from the experimental dynamic response of the Tower under seismic loading. Table Tab. 14.1 shows the comparison between the results of the modal analysis and the frequencies obtained experimentally. It is possible to observe that, for a nominal value of G=77326 kN/m^2, the frequencies obtained by considering the

foundation alone and the foundation with the *Catino* are 0.873 Hz and 0.884 Hz, respectively.

Tab. 14.1 Comparison between numerical and experimental frequencies.

		Foundation alone		Foundation with *Catino*	
Experimental mode	Experimental frequency	G=77326 kN/m^2	G=95000 kN/m^2	G=77326 kN/m^2	G=95000 kN/m^2
Bending N-S	0.958 Hz	0.873 Hz	0.958 Hz	0.884 Hz	0.971 Hz
Bending E-W	1.025 Hz	0.873 Hz	0.958 Hz	0.885 Hz	0.971 Hz
Vertical	2.98 Hz	2.822 Hz	3.12 Hz	2.829 Hz	3.128 Hz
Torsional	6.29 Hz	4.309 Hz	4.729 Hz	5.925 Hz	6.432 Hz

A sensitivity analysis based on the modulus G has been performed to look for a better agreement with the experimental evidences. A satisfactory result was found for G=95.000 kN/m^2, which leads to a natural frequency equal to 0.958 Hz for the first and the second (bending) mode whereas the frequency calculated for the third (vertical) mode was found equal to 3.12 Hz.

14.3 Modal shapes

From Fig. 14.2 to figure Fig. 14.5 are shown the modal shapes relative to the case of the foundation without the *Catino* and with the elastic modulus of the soil calibrated in order to obtain the period experimentally identified for the first vibration mode.

The first and the second mode have a frequency of 0,958 Hz, the first has E-W direction with a participating mass of 64,6%, while the second has direction N-S (along the maximum inclination) with a participating mass of 64,1%. The third mode has a frequency of 3,12 Hz and a participating mass in vertical direction of 97,8%.

It is possible to highlight that the first two modes are characterized by the same frequency: this is caused by the fact that in this work the behavior of the foundation was considered as isotropic. The modal frequencies obtained with the numerical model can be updated using the results of the analyses of experimental records.

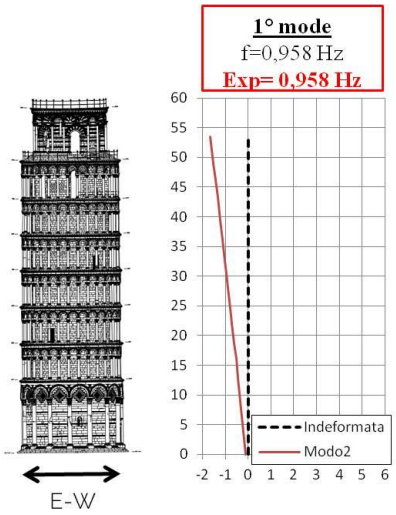

Fig. 14.2 First modal shape - Horizontal, direction E-W

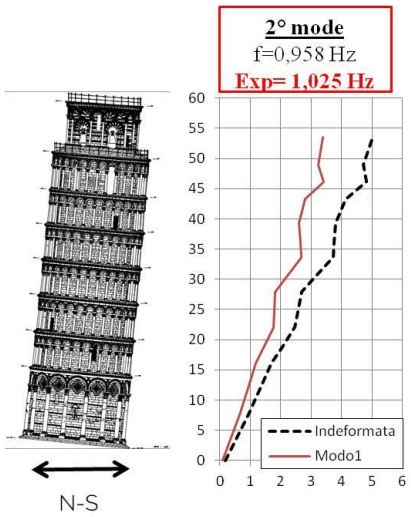

Fig. 14.3 Second modal shape - Horizontal, direction N-S

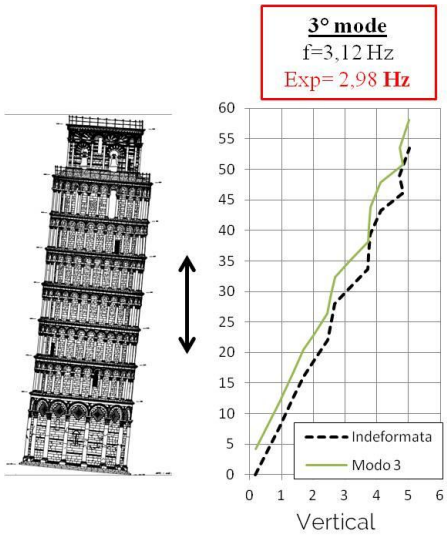

Fig. 14.4 Third modal shape - Vertical

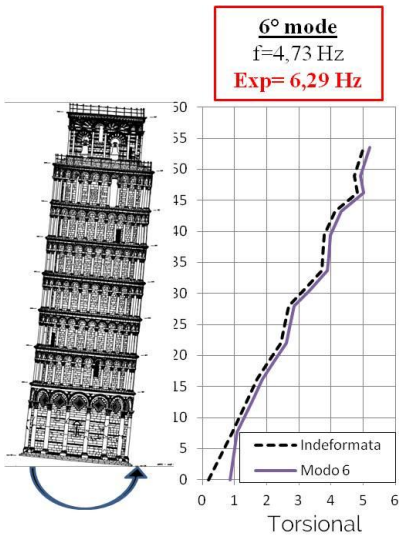

Fig. 14.5 6th modal shape - torsional

14.4 Model Updating

Under the hypothesis of linear elastic behavior of the structure it is possible to update the numerical model on the basis of the modal response of the structure evaluated experimentally.

Since there is a lack of reliable measures of the free field seismic input at the base of the Tower, the updating of the model was made on the base of the modal parameters. Due to the small number of measure points, for which was not possible to obtain the experimental modal shapes, in this case only the modal frequencies were used. For each vibration mode was imposed:

$$\frac{\phi_i^T K \phi_i}{\phi_i^T M \phi_i} = \omega_i^2$$

Only the values of the matrix K relative to foundation springs were optimized. The elements of K are given by SAP 2000. The initial values of the impedances are those defined in section 13.6.

Tab. 14.2 Comparison between experimental frequencies and numerical results after model updating.

Experimental mode	Experimental frequency	Case 1	Case 2
Bending N-S	0.958 Hz	0.950 Hz	0.963 Hz
Bending E-W	1.025 Hz	1.025 Hz	1.015 Hz
Vertical	2.98 Hz	2.964 Hz	2.980 Hz
Torsional	6.29 Hz	6.294 Hz	6.270 Hz

The model updating has been performed on the elements of the impedance matrix of the foundations in order to obtain an improved agreement between the natural frequencies estimated experimentally and those obtained from the modal analysis.

Tab. 14.3 Comparison between the results of numerical analyses by various authors

Author	N-S freq.	E-O freq.	Vertical
Grandori e Faccioli (1994)	0,735		-
ISMES (1995) – nominal values	0,979	0,984	3,708
ISMES (1995) – mod. updating	1.021	1.016	0.270
Present work – nominal values	0.873	0.873	2.822
Present work – sensitivity analysis	0,958	0,958	3,120
Present work - model updating	0,963	1,015	2,980
Present work - Exp. frequencies	0,958	1,025	2,980

These results are reported in Tab. 14.2. Tab. 14.3 shows a comparison between the results in terms of modal frequencies obtained with numerical models by various authors. The results obtained in the present work show a better agreement with the experimental frequencies reported in the last line of the table.

15 Seismic intensities expected in Pisa

15.1 Grandori & Faccioli (1993)

The seismic history of the Pisa's area was first studied by Grandori and Faccioli in 1993 [73]. First of all, the historical seismicity was studied, identifying all the seismic events from 1087 to 1984, in a period of around 900 years, which had produced a maximum epicentral intensity at the site of Pisa larger than the V degree of MCS scale.

Then it was pointed out that an intensity VI in the MCS scale (the maximum experienced by this area) occurred four times within a time window of 700 years (1280-1980) without causing major damages to the Tower and to other buildings. However, it was able to cause micro-damage to the masonry of the Tower.

Starting from the correlation between MCS intensity and return period, a return period of 130 years was stated for an intensity VI. This intensity corresponds to a peak ground acceleration (PGA) equal to 0.07g.

The relation between the MCS intensity and the PGA is confirmed also by more recent correlations, depicted in Fig. 15.1 (see for example Cause and Faccioli [25], Margottini et al. [102]). For the intensity VII – never occurred within the Pisa's area – the return period is 500 years and the PGA is 0.12g. The results of these correlations are shown in Tab. 15.1. It is possible to highlight that these values are compatible with the hazard maps for Italy discussed in the first chapter [16].

For the return period of 500 years the authors stated that a seismic event with such an intensity could result in a great risk for the safety of the Tower.

Tab. 15.1 Correlation between MCS intensity/T_R/PGA

MCS intensity	Return period	PGA (g)
VI	130 anni	0,07
VII	500 anni	0,12

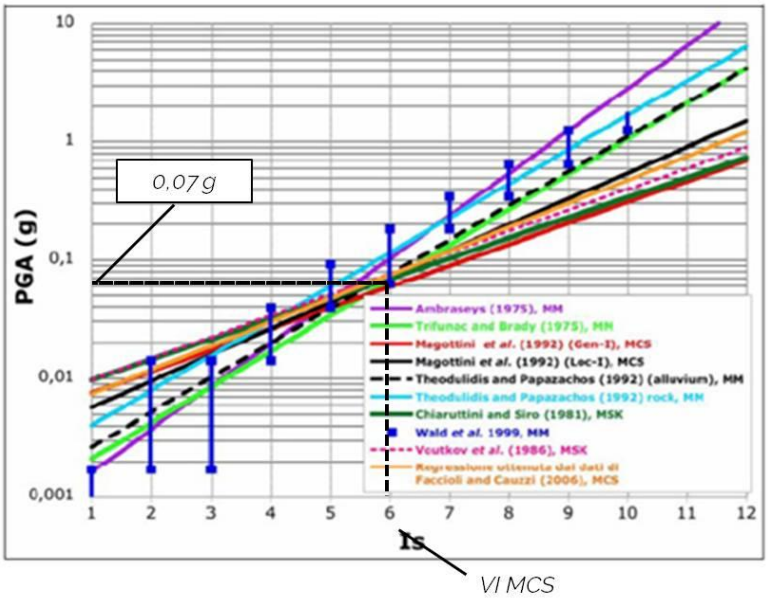

Fig. 15.1 Correlation between PGA and MCS intensity (modified from Sabetta)

On the basis of these results the authors defined a response spectrum to use as seismic input for the analysis. This was obtained from the envelope of response spectra of real accelerograms, extracted from the Italian Database. The selction of accelerograms was done taking into account the Magnitude of the events, ranging from M 5,4 to M 6,8, with a distance ranging from 24 to 53 km and similar geological and geotchnical conditions at the site. Choosing signals recorded on deep alluvium deposits.

Eight accelerograms were selected, each with two horizontal and one vertical component. Each record was scaled in order to obtain the same PGA of 0,07g. The average value and the standard deviation were evaluated, considering as the spectrum for the dynamic analyses the median value plus 1 sigma. The response spctrum obtained by Grandori and Faccioli is depicted in Fig. 15.2.

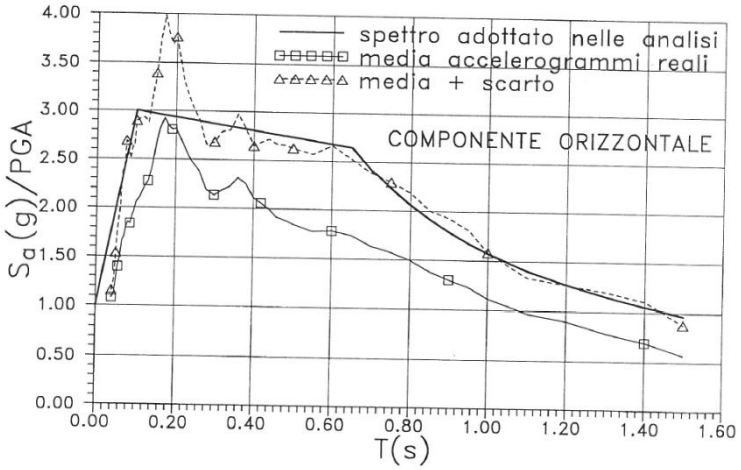

Fig. 15.2 Response spectrum obtained by Grandori e Faccioli (1993)

15.2 Scenario Earthquakes

15.2.1 Probabilistic response spectra

In this work, the seismic input has been studied by means of a much modern approach in terms of response spectrum and acceleration time histories. Initially, a probabilistic evaluation has been made. The ZS9 seismogenic zonation has been chosen, considering all the zones no farther than 100 km from Pisa. SP96 [19] and Akkar and Bommer 2010 [21] have been selected as Ground Motion Predictive Equations (GMPE). Uniform Hazard Spectra (UHS) were computed for return periods of 130

years and 500 years using these predictive equations. Fig. 15.3 and Fig. 15.4 show the results obtained in terms of Uniform Hazard Spectra, respectively for return periods of 130 years and 500 years. A comparison between spectra obtained with the two different GMPEs is reported.

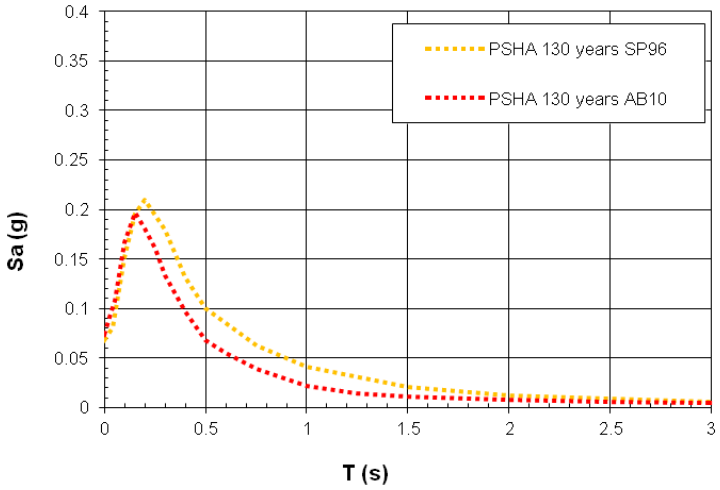

Fig. 15.3 Uniform Hazard Spectra - 130 years return period

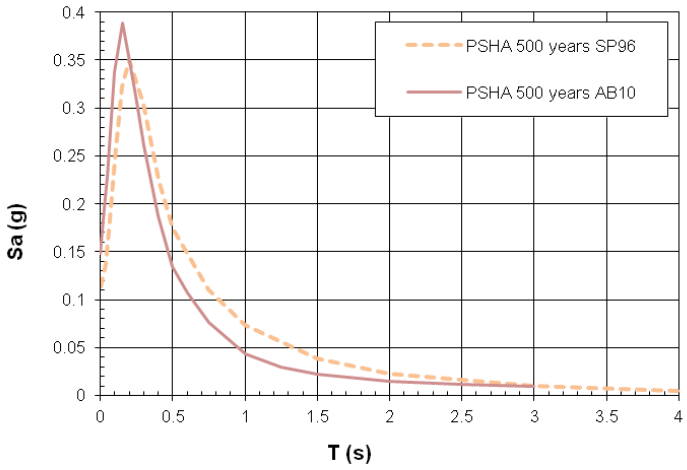

Fig. 15.4 Uniform Hazard Spectra - 500 years return period

In the case of safety assessment of a single monument the use of UHS spectra could be not appropriate, because the risk exists to estimate wrongly the expected intensities. Therefore, also in the case of the Leaning Tower of Pisa, it is necessary to apply the hybrid approach for the evaluation of the seismic input, by performing a disaggregation analysis to obtain the values of M and R useful for the selection of scenario earthquakes.

15.2.2 Disaggregation

Since the UHS does not give any information about magnitude *M* and distance *R* of the earthquake, the disaggregation of the hazard has been accomplished in order to look for seismic events (characterized by certain values of *M* and *R*) able to produce the expected intensities. The results of the disaggregation can be used to find controlling earthquakes.

Fig. 15.5 and Fig. 15.6 show the results of the disaggregation of the hazard for a return period of 130 years, respectively for the spectral periods of 1s, (first mode identified) and 0,3s (vertical mode). It is possible to notice that the maximum contribution to hazard is given by sources at distances in the range 10-25 km and with Magnitude ranging from M 4,6 to M 5,4.

Fig. 15.7 and Fig. 15.8 depict the results for a return period of 500 years. In this case there a slightly greater contribution of far sources, and Magnitude ranging from M 4,6 to M 5.7.

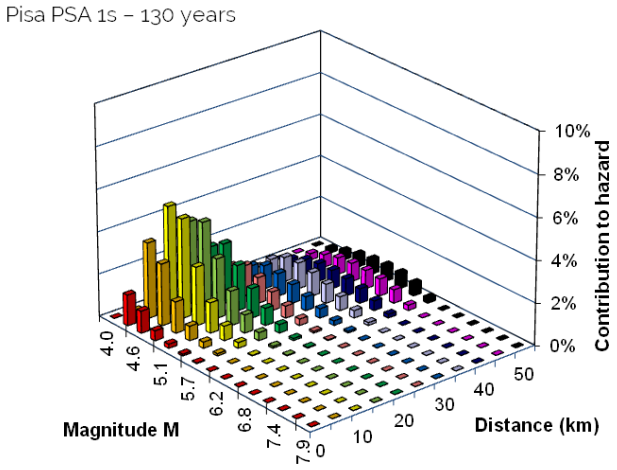

Fig. 15.5 Disaggregation for PSA 1s, TR=130 years

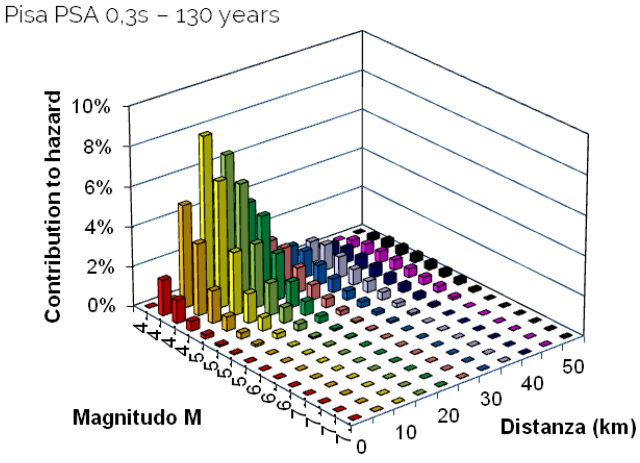

Fig. 15.6 Disaggregation for PSA 0,3s, TR=130 years

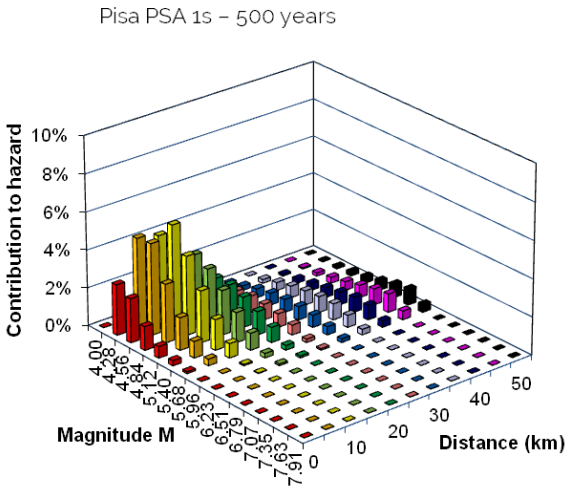

Fig. 15.7 Disaggregation for PSA 1s, TR=500 years

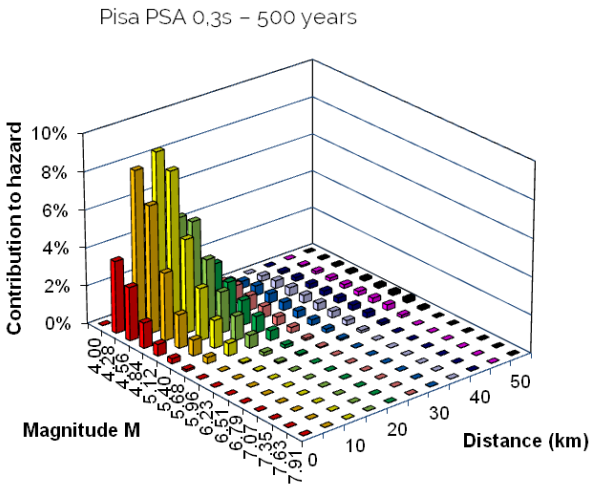

Fig. 15.8 Disaggregation for PSA 0,3s, TR=500 years

15.2.3 Deterministic response spectra

By studying the Italian seismic catalogue CPTI11 [58], it was possible to select two controlling earthquakes, chosen from various seismic events. They are reported in Tab. 15.2.

Tab. 15.2 Selection of controlling earthquakes

Event name	year	Mw	R (km)	T_R
Lucca	1306	4.83	16.8	
Livorno	**1742**	**5.15**	**19.0**	**130 years**
Livorno	1646	5.17	19.0	
Livorno	1814	5.22	9.2	
Alpi Apuane	1837	5.65	54.5	
Orciano Pisano	**1846**	**5.71**	**21.0**	**500 years**
Garfagnana	1914	5.79	27.2	
Lunigiana	1481	5.84	66.0	
Garfagnana	1920	6.48	53.0	

A further assessment of the return periods was done by doing a comparison between the return periods selected of 130 and 500 years and those obtained with the Gutenberg-Richter relation of the seismogenic zone ZS916, depicted in Fig. 15.9

At M 5.2 corresponds a value of $\log(f_c)$ of about -2,2, while for M 5.7 a value of $\log(f_c)$=-2,7, corresponding respectively to return periods of T_R=158 years and T_R=501 years. Therefore the Magnitudes of the scenario earthquakes are consistent with the selected return periods.

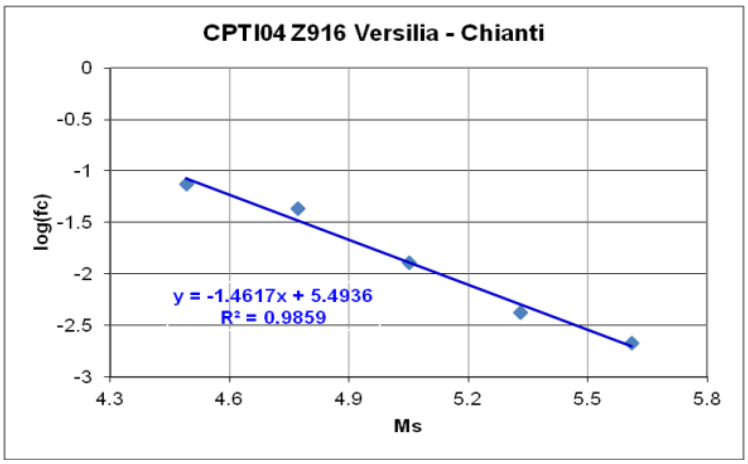

Fig. 15.9 Gutenberg-Richter relation for zone ZS916

Fig. 15.10 shows the comparison between probabilistic and deterministic spectra relative to the Livorno earthquake which had a M 5.15 and a source to site distance of 19 km obtained in this study for the return period of 130 years. It is possible to highlight a general good agreement between probabilistic and deterministic response spectra. The response spectrum which was then used as target spectrum to select the accelerograms was obtained by using the median value plus 1 standard deviation for the AB10 Ground Motion Predictive Equation. The figure shows also the results obtained by adding 0,5 sigma to the median value both for AB10 and SP96 GMPEs.

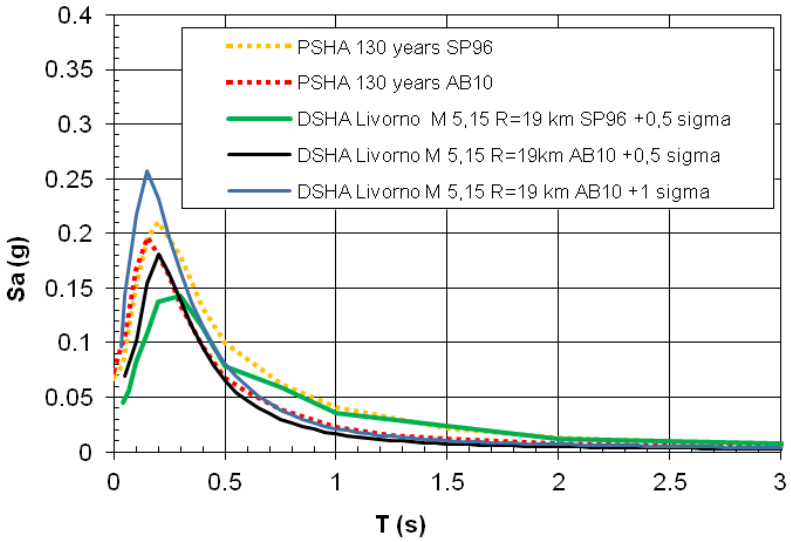

Fig. 15.10 Comparison between spectra - 130 years

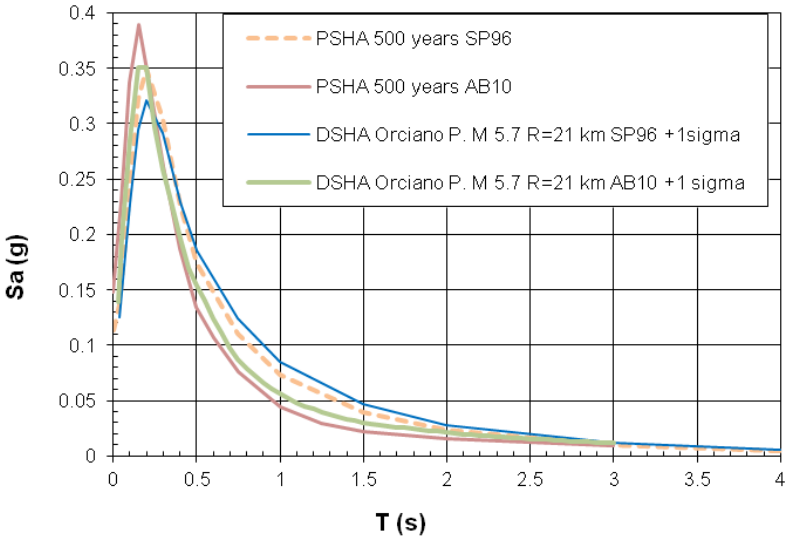

Fig. 15.11 Comparison between spectra - 500 years

Fig. 15.11 show the comparison between response spectra obtained for 500 years return period. These spectra show a better agreement than the spectra obtained with 130 years response spectra. The deterministic spectrum was obtained for the seismic event of Orciano Pisano, which had a M 5.7 and a distance R=21 km. The deterministic spectrum, later used as target spectrum, was obtained by adding 1 standard deviation to the median value both for AB10 and SP96 GMPEs.

All the response spectra obtained are relative to a soil class A according to EC8, which corresponds to compact rock. The seismic input to use in the analyses must take into account also the effects of local amplification due to the local features of the soil, and must be obtained with a site response analysis which will be discussed in chapter 16.

15.2.4 Vertical response spectra

The modal analysis highlighted the necessity to investigate the dynamic vertical behavior of the Tower. For this reason, a complete study on the seismic assessment for this building must include the evaluation of the vertical seismic input at the site.

As discussed in the first chapter, in section 3.8, in recent years it is preferred to use predictive equations to estimate V/H ratios instead of using predictive equations which give directly the vertical response spectra. In Fig. 15.12 is depicted a comparison between V/H ratios obtained with the geophysical parameters of the two scenario earthquakes selected in the previous section. It is possible to notice that the trend of V/H ratio with period is similar for both events, and it is always minor than unity, ranging from around 0,5 to 0,8.

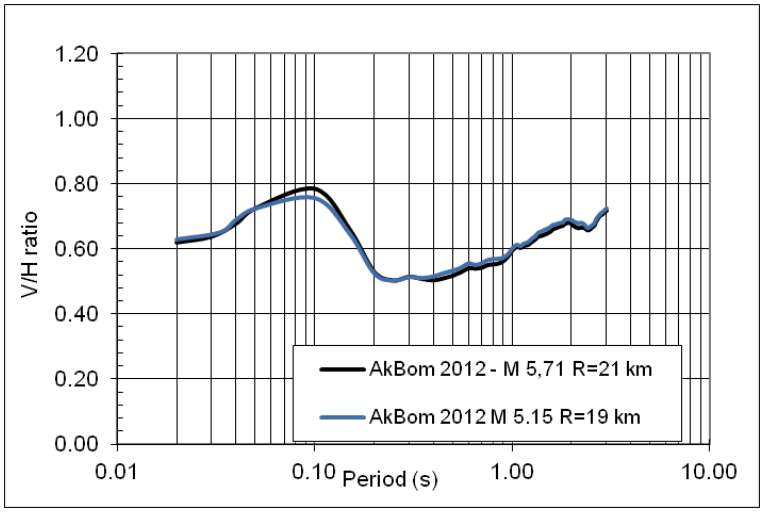

Fig. 15.12 V/H ratio for the response spectra of the Scenario earthquakes

Fig. 15.13 and Fig. 15.14 show the comparison between the vertical spectra obtained with the predictive equation by Akkar and Bommer [101], respectively for return periods of 130 years and 500 years showing major differences for periods from 0,2 to 0,5 and with a similar trend after 1s.

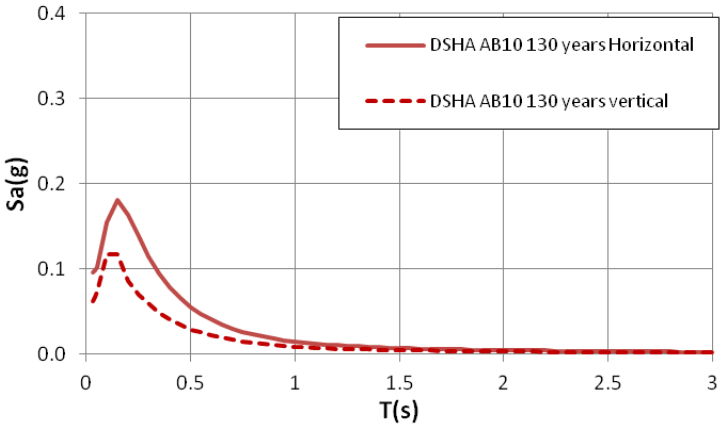

Fig. 15.13 Comparison Horizontal/vertical spectra - 130 years

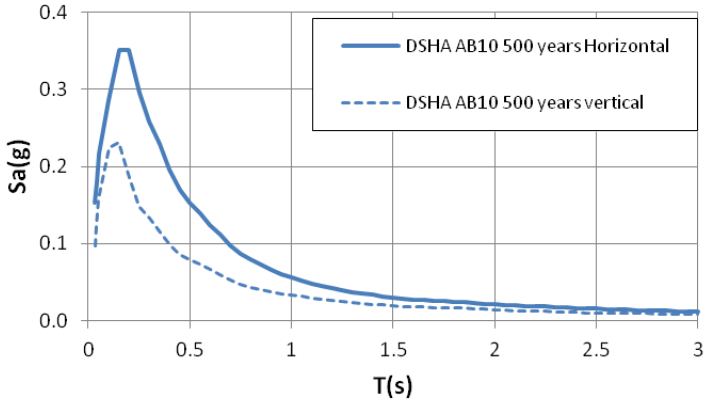

Fig. 15.14 Comparison Horizontal/vertical spectra - 500 years

15.3 Selection of accelerograms

The deterministic response spectra obtained in the previous section have been used as "target" spectra to select four sets of spectrum-compatible accelerograms, respectively for horizontal and vertical components and for both the chosen return periods.

A set of eleven time histories from ITACA-INGV database for class site A and B with V_s>600 m/s have been selected considering 5<M<5.5 for 130 years return period, while R ranges from 5 to 15 km.

For 500 years return period a set of eight time histories the parameters considered are 5.3<M<6.2 and distance 10<R<25, as described in Tab. 15.3.

Tab. 15.3 Search parameters for ITACA database

Return period	Range M	Range R (km)
130 anni	5-5,5	5-15
500 anni	5,3-6,2	13-25

Time histories have been scaled so that the average spectrum of each set of accelerograms well approximates the target spectrum. This task has been accomplished using In-Spector software, discussed in section 4.3.3.

The scaling was made in the range of the fundamental periods 0.3 s-1.1 s in order to take into account the periods of the first two bending modes (about 1 s) and that of the third (vertical) mode (about 0.3 s).

Fig. 15.15 and Fig. 15.16 show the comparison for 130 years return period between the response spectra of the accelerograms which were selected and scaled, the average spectrum (depicted in red) of the scaled accelerograms and the target spectrum (black dotted line). The two figures refers respectively to the Horizontal accelerograms and the vertical accelerograms.

In Fig. 15.17 and Fig. 15.18 are displayed the same results for the 500 years return period.

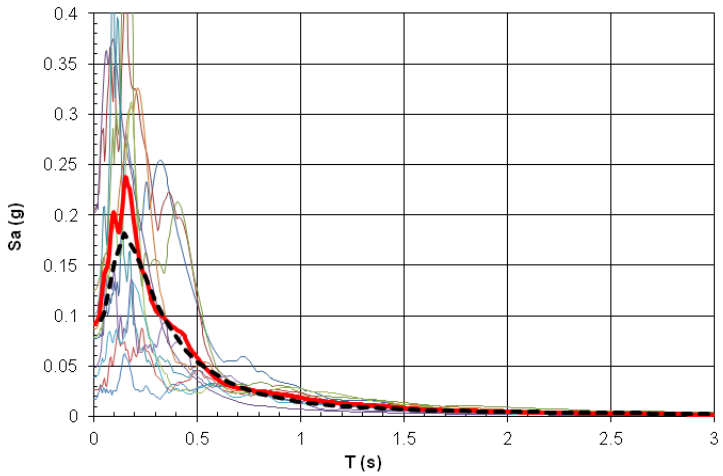

Fig. 15.15 Selected scaled accelerograms - Horizontal - TR=130 years

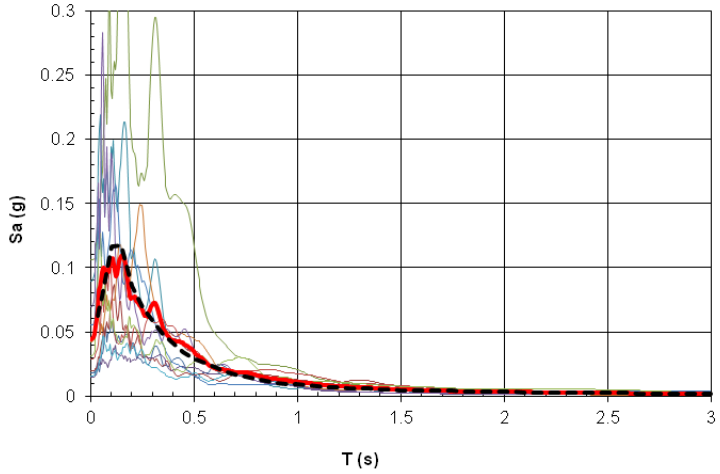

Fig. 15.16 Selected scaled accelerograms - Vertical- TR=130 years

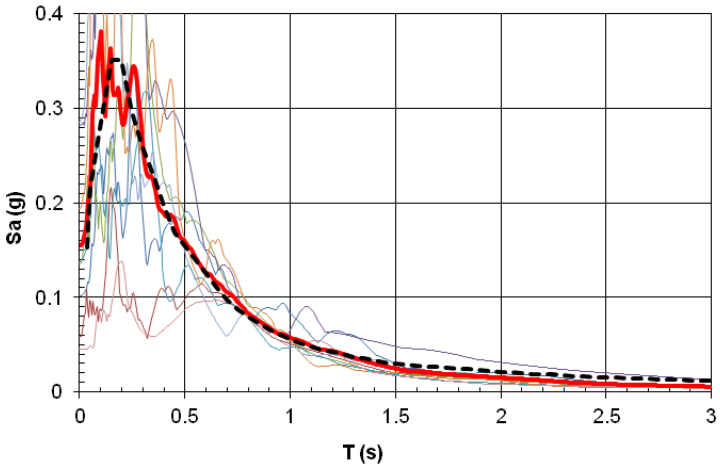

Fig. 15.17 Selected scaled accelerograms - Horizontal - TR=500 years

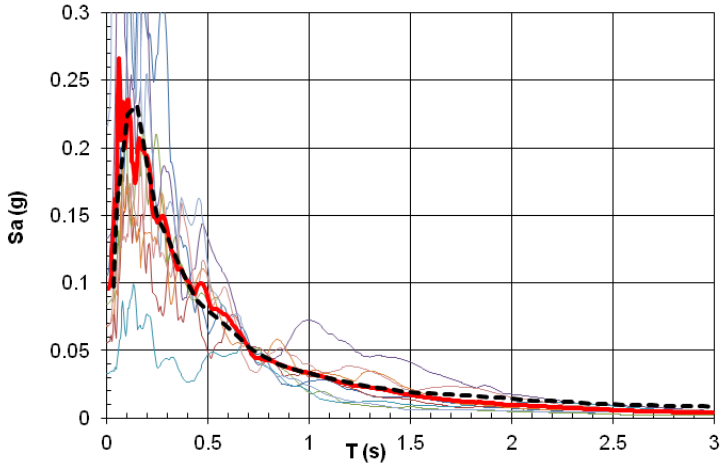

Fig. 15.18 Selected scaled accelerograms - Vertical - TR=500 years

Tab. 15.4 Parameters used for the scaled accelerograms - 130 years return period

Event and station	Date	MW	Ep.Dist [Km]	Soil	SF	Drms
App. Umbro-March. CESM	12/10/1997	5.2	9.8	A*	1.800	0.101
App. Umbro-March. CESM	21/03/1998	5	6.3	A*	2.698	0.015
L'Aquila AQP	09/04/2009	5.2	13.5	A	2.200	0.035
Friuli TRC	11/05/1976	5	13.4	A	2.200	0.037
Friuli TRC	11/09/1976	5.2	7	A	0.417	0.024
Garda Meridionale GVD	24/11/2004	5	14.5	A*	1.180	0.014
Gran Sasso AQG	09/04/2009	5.4	12.9	B	0.236	0.117
Gran Sasso AQP	09/04/2009	5.4	11.8	A	0.339	0.077
L'Aquila RM01	07/04/2009	5.1	7.8	A*	1.247	0.027
Lunigiana VGL	21/06/2013	5.4	13.3	A*	0.750	0.046
Pollino VGG	25/10/2012	5.3	10.1	A*	0.310	0.025

Tab. 15.4 and Tab. 15.5 report a list of the Seismic Events and records selected from ITACA database, together with some important parameters used in the selection process, respectively for 130 and 500 years of return

period. It is worth to notice that the scale factors used to modify the time histories range from 0,24 to 2,7 for T_R=130 yrs, while range from 0,34 to 4 for T_R=500 years.

Tab. 15.5 Parameters used for the scaled accelerograms - 500 years return period

Event and station	Date	MW	Ep. Dist. [Km]	Soil	SF	Drms
App. Lucano VGG	09/09/1998	5.6	13.5	A*	1.381	0.050
Gran Sasso AQG	09/04/2009	5.4	12.9	B	0.811	0.077
L'Aquila AQG	07/04/2009	5.5	14.6	B	1.000	0.037
L'Aquila AQP	07/04/2009	5.5	13.2	A	3.000	0.031
L'Aquila RM13	07/04/2009	5.5	15.6	A*	1.031	0.025
Lunigiana VGL	21/06/2013	5.4	13.3	A*	3.000	0.020
Umbria - Marche CAG	14/10/1997	5.6	16.2	A*	4.001	0.056
Umbria - Marche NRC	14/10/1997	5.6	20.5	B	0.338	0.105

Good results are obtained also form D_{RMS}, which maximum value is around 0,1 in both cases, which are consistent with the maximum value indicated by Bommer and Acevedo [43]. Fig. 15.19 shows the selected scaled acceleration time history for the signal of Umbria Marche earthquake recorded at CAG seismic station.

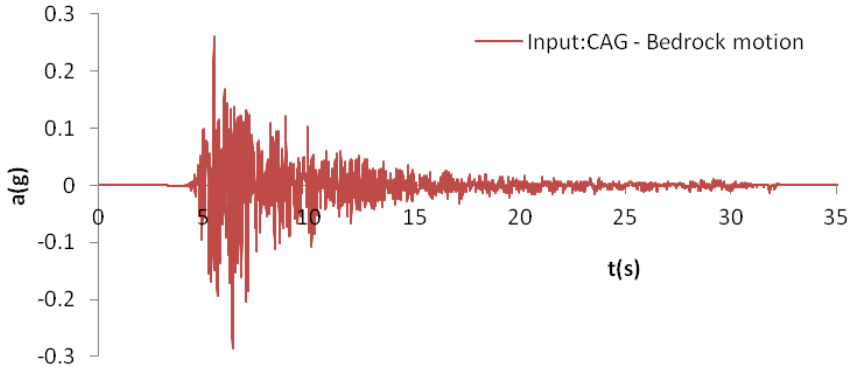

Fig. 15.19 Acceleration Time history on rigid soil - CAG

16 Site response analysis

16.1 Introduction

As discussed in some of the previous sections, the ground underlying the Tower is formed by many layers of alluvium deposits, which go from highly to barely deformable: a more rigid layer was found through an Array 2D test at around 100 m of depth, while the seismic bedrock lies at about 500 meters depth. The acceleration time histories found in the previous section were found on rigid soil, so the need exists to perform a site response analysis to obtain the ground motion at the ground level.

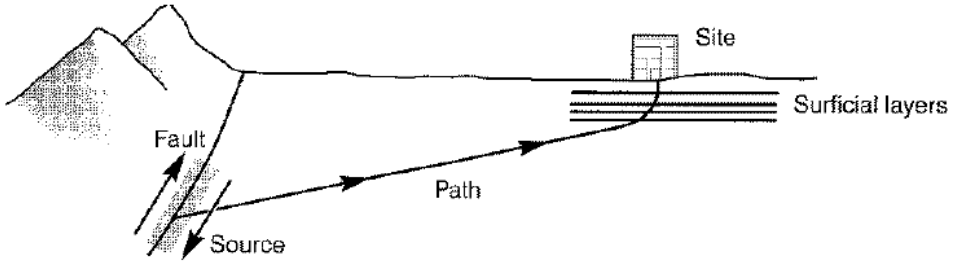

Fig. 16.1 Source-to-site travel path of body waves (Kramer, 1994)

Body waves are generated at deep distances from the ground level. In their path from the fault to the selected site, they cross many soil layers which have different dynamic features (in general shallow layers have lower velocities) therefore the inclined rays that cross the layers arrive with a nearly vertical direction to the site, as shown in Fig. 16.1, taken from Kramer [103]. In this model, the motion at the base of the soil deposit is defined as a *bedrock motion*, therefore the path of the body waves is formed by two parts, the bedrock motion and the soil deposit motion.

In this study a one-dimensional site response analysis is considered, and this is based on two hypothesis:

- The interfaces between different layers are horizontal, and have infinite extensions.
- the response of the soil deposit is mainly due to SH-waves which propagate vertically from the bedrock.

The procedure to evaluate the free surface ground motion is based on the computation of a transfer function which measures the amplification of each frequency of the input motion. In fact, starting from the input acceleration time history acting on the bedrock, the Fourier series using Fast Fourier Transform can be obtained. Then the transfer function which relates the ground surface at the bedrock, and the Fourier series of the Free surface (output) can be obtained as the product of the transfer function for the Fourier series of the motion at the bedrock (input). By inverting the Fourier series the output acceleration time history is obtained. The inverse procedure is called *deconvolution*.

As reported in a work by Yoshida [104], which discusses the approach followed in Japan, the path of the waves could be divided in three parts, namely the seismic bedrock (large depths), the *Engineering seismic base layer*, and the surface layer.

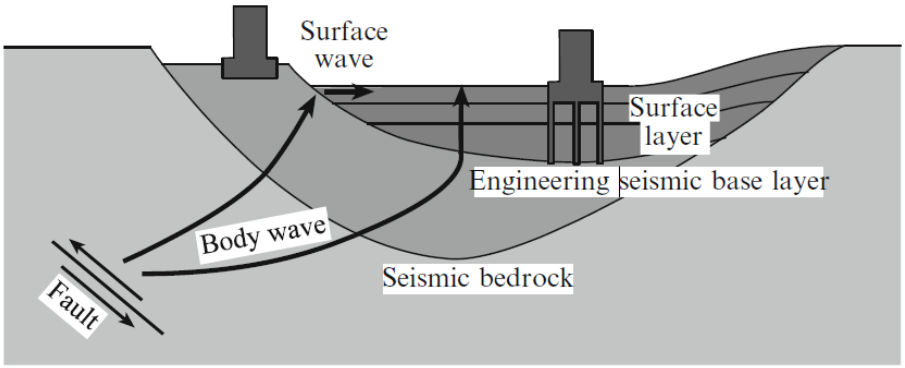

Fig. 16.2 Source-to-site travel path of body waves (Yoshida, 2015)

This concept is mentioned for the sake of completeness, as it will be put aside for the moment, but with this method it is possible to obtain the motion at the ground level by defining the input motion at the base of the *Engineering seismic base layer*. The advantage of this approach is that within this model it is sufficient to investigate the ground at a depth which is lower than the depth of the seismic bedrock-

16.2 Decay curves

The non-linear behavior of the soil can be described referring to the stress-strain behavior, by defining two parameters which describe the stiffness and the hysteresis of the soil in a load-unload cycle. These parameters are the shear modulus G and the Damping ratio D. The non-linear behavior of the medium is described by the evolution of these parameters, when γ increases 3 different behaviors could be defined.

Small deformations

The tangential stiffness, expressed by the secant shear modulus G, assumes a maximum value (G_0 o G_{max}) and then decreases when the deformation is higher. It must be pointed out that in soils the non-linearity raises also for small levels of deformations, both in monotonic that in cyclic field. It is possible to assume that $G(y)=G_0$ only for a very low level of deformation. Conventionally it is stated that there is a constant behavior until $G(y)=0.95\ G_0$, that is for values of γ in the range 0,00001% - 0,01%.

In this phase the τ - γ relation is linear and the response of the soil does not have hysteresis (D=0).

Medium deformations

When the threshold γ_l is exceeded, G decreases rapidly with γ and there is a non-linear behavior. When G decreases the energy dissipated in a cycle increases. In this field the material does not have memory of the previous cycles and in the unloading cycle the residual values of deformations are negligible.

Large deformations

When the cyclic loading increases, for example for large earthquakes, there is a level of deformations γ_v which if exceeded the soil has irreversible structural modifications. Over this threshold the deformability of the soils evolves with the number of loading cycles.

Fig. 16.3 and Fig. 16.4 show respectively the G/G_0 curve and the Damping curve obtained on the soil under the Tower by a research group from the Polytechnic University of Turin [105]. Undisturbed samples were taken at depths ranging from 13 m to 36 m.

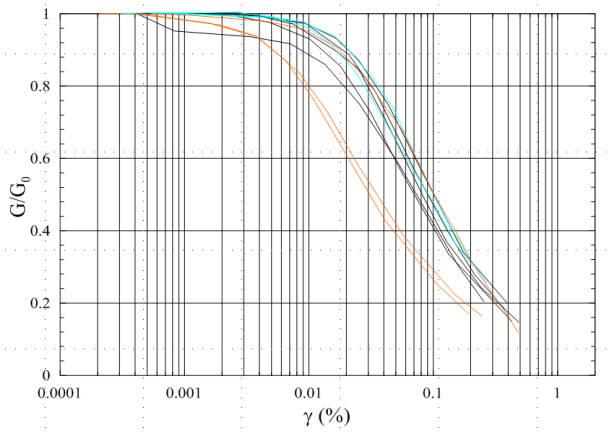

Fig. 16.3 G/G_0 decay curve for Pisa clays

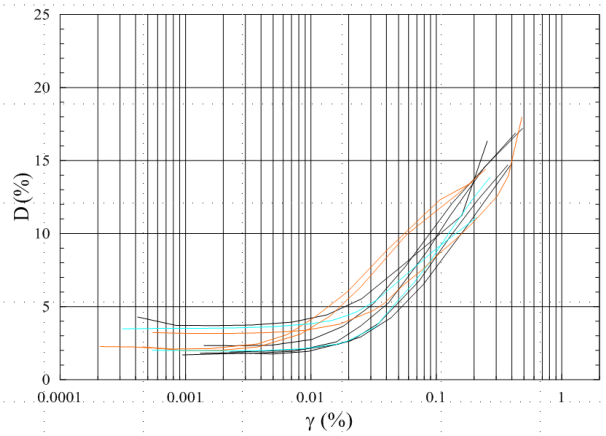

Fig. 16.4 D/γ curve for Pisa clays

16.3 Analysis results

For the case study of the Leaning Tower of Pisa, the model used must be take into account the multi-layer nature of the ground, and the damping associated to each layer. In this case the transfer function is more complex than for the case of a single soil layer, therefore compute programs are used in order to perform this type of analysis.

Site response analyses were performed referring to two hypothesis: the first with a rigid layer based at 95 m of depth from the ground level (shallow basement), and the second with the rigid layer at 520 m from the ground level (seismic bedrock).

The second hypothesis is justified by the resonance peak at 0.3 Hz identified in the H/V test. In order to perform the site response analysis it is needful to provide the following data: thickness of each layer, mass density, velocity of shear waves, and the decay curves of the soils of the different layers.

The amplification functions obtained with linear and non-linear methods of analysis, depicted in Fig. 16.5 [106] show that all the signals produce similar amplification, with a larger dispersion at higher frequencies. The amplification is high for low frequencies while for high frequencies tends to zero.

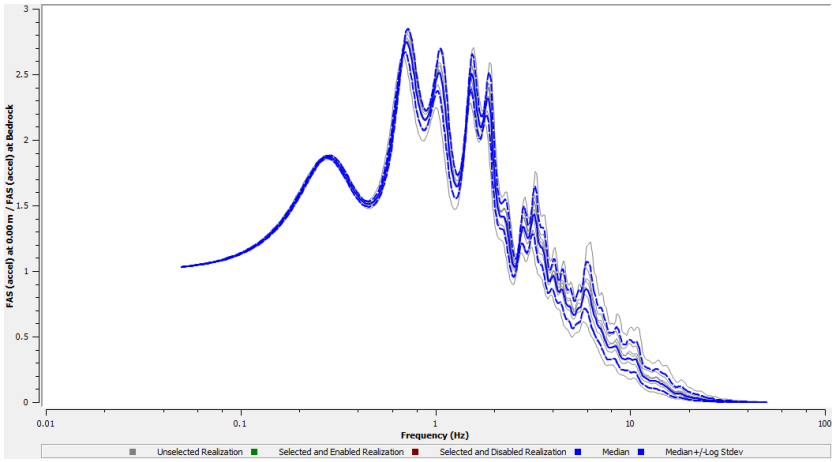

Fig. 16.5 Non-linear amplification function (Lanzo 2016)

Fig. 16.6 shows the results in terms of response spectra of the accelerograms at the ground level obtained with an analysis performed with DEEPSOIL. A comparison between the average spectrum of the accelerograms at the bedrock (See Fig. 15.17) shows that, in agreement with the amplification function, for periods 0<T<0,5s the average bedrock motion is higher than the ground level motion. In the range from 0,5s to 2s the bedrock motion is lower, and there are signals at the ground level that reach within this range of periods acceleration of 0,15 g (Umbria-Marche CAG signal), which are around 50% higher than for bedrock motion.

The acceleration time history of Umbria-Marche seismic event CAG reported at the ground level is shown in Fig. 16.7. It could be pointed out

that in comparison with the time history showed in Fig. 15.19 this acceleration time history presents large differences in frequency content, showing the presence of low frequency waves.

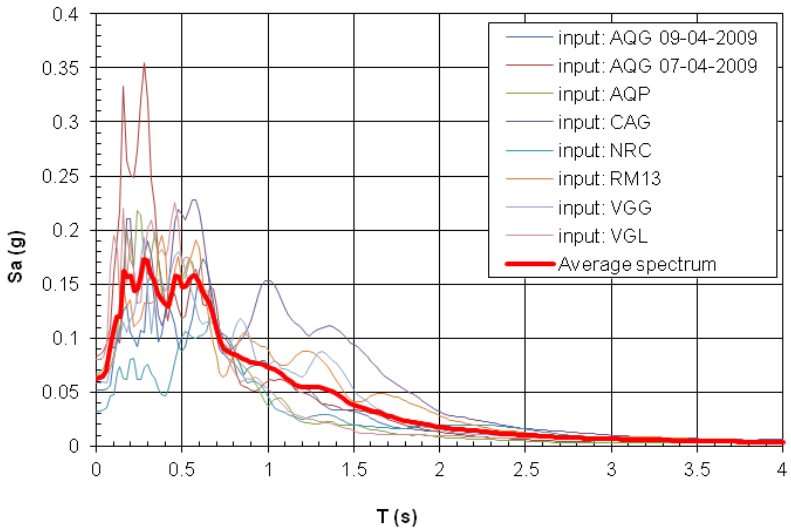

Fig. 16.6 Response spectra of the accelerograms at ground level - T_R=500 yrs

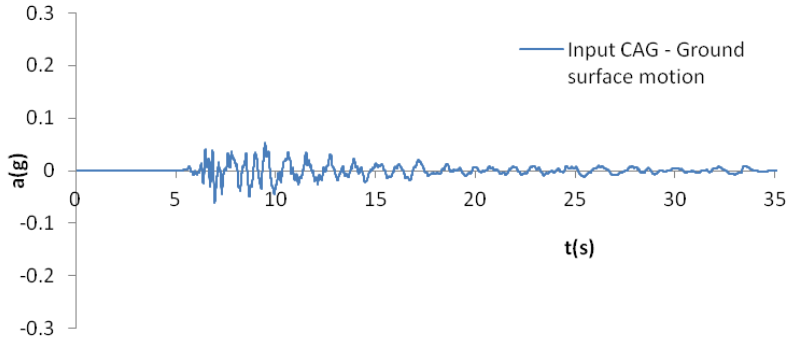

Fig. 16.7 Ground surface time history acceleration - Event Umbria-Marche CAG

17 Dynamic response of the Tower

17.1 Type of analysis and results

On the basis of the results obtained in section 14.4 with model updating, which allow to find a combination of foundation dynamic impedances that produced modal frequencies very close to the experimental values, the resulting values were assigned to the Finite Element Model in order to perform time history analyses.

For preliminary results, the input signals considered at the base of the Tower are the horizontal accelerograms selected and scaled for a 500 years return period. In SAP2000 a non-linear analysis for each selected record, including damping at the foundation was performed using Direct Integration method.

Tab. 17.1 Maximum acceleration and displacement results - 8th *Ordine*

Input	a_{max} (g)	D_{max} (mm)
AQG7	0.154	25.91
AQG9	0.144	30.95
AQP	0.112	17.11
CAG (max)	**0.245**	**64.2**
NRC	0.111	16.73
RM13	0.188	34.66
VGG	0.118	32.57
VGL	0.167	20.99
Average	**0.155**	**30.39**

Tab. 17.1 shows results obtained in terms of acceleration and displacement of the top node of the model, which represents the centroid of the 8th *Ordine* of the Tower. Highlighted in bold are the maximum

values obtained, which are relative to the signal of the Umbria Marche earthquake recorded at CAG seismic station, for which the maximum acceleration is 0,245g and the maximum displacement is 64,2 mm. The average values are smaller: for the displacement a value of 30,39 mm is obtained, while the average acceleration is 0,155g. The acceleration time history for CAG signal is depicted in Fig. 17.1.

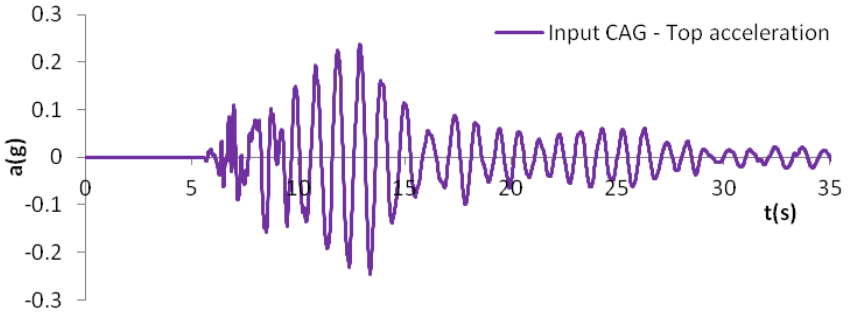

Fig. 17.1 Acceleration time history of node 30 - Event Umbria-Marche CAG

The displacement time history for CAG signal is depicted in Fig. 17.2.

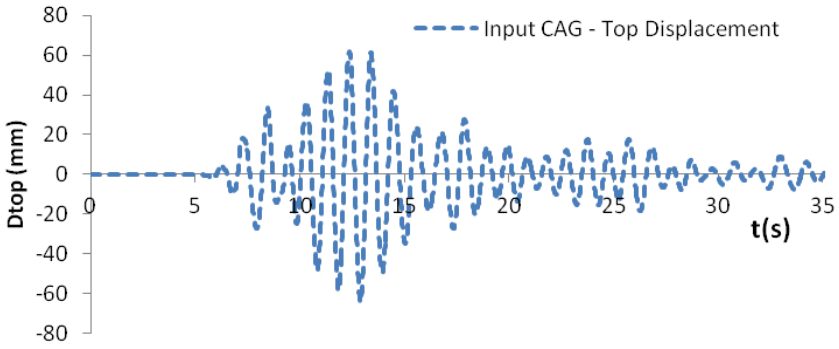

Fig. 17.2 Displacement time history of node 30 - Event Umbria-Marche CAG

18 Conclusions

The aim of this work is to discuss a procedure to evaluate the seismic input, and to discuss the application of this method to two actual case studies. In the first case two types of concrete dams were taken into account: in fact, the recent Italian Code on Large Dams requires the evaluation of the seismic input starting from a specific Seismic Hazard Assessment for areas characterized by a high level of seismicity. Moreover, for strategic structures the seismic actions have very large return periods (up to 10.000 years according to ICOLD). Therefore, assessing the seismic hazard with accurate methods can be beneficial to the seismic hazard assessment.

In the second case the procedure is applied to the Leaning Tower of Pisa. In the last thirty years Tower was the object of many interventions in order to stop the increasing inclination. These produced a modification in the conditions of the ground underlying the Tower. Moreover, the most recent studies about the expected seismic intensity in Pisa date back to 23 years ago. Meanwhile, there were advances in methodologies regarding the Seismic Hazard Assessment and the availability of a great number of new seismological records. In both case studies the final purpose was to select real ground motion accelerograms to perform non-linear analyses which could provide information on the seismic safety of these structures.

The main methods available today to assess the seismic intensities at a site, which are probabilistic (PSHA) approach and deterministic (DSHA) approach, can coexist by highlighting the differences between one method and the other and using their main advantages. This *hybrid* approach starts with a probabilistic evaluation based on the seismogenic zonation, then disaggregation is performed in order to find the controlling earthquakes; finally the local intensities with the Predictive Equations are evaluated.

The discussion of the procedure brought to the conclusion that the selection of upper bounds and the chosen Ground Motion Predictive Equation have a strong influence on the final value of intensity.

Some examples were presented in order to show the features of Uniform Hazard Spectra, the differences between the effects produced by close and far earthquakes and the comparison with the deterministic spectra. They highlighted the importance of the disaggregation in order to find the combinations of M and R which provide the largest contribution to hazard. Moreover, a comparison between the Italian Code Response spectrum and the response spectrum provided by the Hazard models MPS04 and SHARE was performed.

Finally, a discussion of the procedure for selecting accelerograms from the databases followed, in the attempt to understand which parameters are the most significant for the strong ground motion. Moreover, the methods used in this work to select and to modify accelerograms were presented to discuss the features of three softwares that will be used in further sections.

The second part of this doctoral dissertation presents the application of the procedure to the case of concrete dams. Referring to the Collapse Limit State four Italian sites with different levels of seismic intensity were identified. For these sites was conducted an assessment of the response spectra by using the method presented in the first part. On the basis of these results 56 accelerograms were selected and modified in order to match the target response spectra. Non-linear analyses were performed using a simplified method which allows to evaluate the base sliding of dams. This was done by applying the 56 signals at the base of a non-linear SDOF system, thus enabling the identification of the most damaging records among others.

Then two of the records selected were applied to two case studies, a gravity dam with a height of 87 m and an arch-gravity dam with an height of 100 m. The dynamic behavior of the two structures was investigated by performing non-linear analyses which took into account: the dam-reservoir interaction, the dam-foundation interaction, the presence of vertical joints for which it was modeled the frictional behavior, the possible sliding at the base and the crack opening.

The results demonstrated the capacity of simplified models to give a rapid prediction on the seismic behavior of dams, and to operate a distinction between the structures which have less probability to have damages or to collapse, and the structure for which this probability is larger, so that more complex analyses must be performed in order to evaluate the seismic safety.

The 3D models have great computational costs, but give the possibility of providing all the parameters necessary for the prediction of the structural safety of these structures. In particular, for the same seismic input, the response in terms of top displacement allowed to conclude that the gravity dam has a final residual displacement along the downstream direction which is higher than the displacement along the upstream direction suffered from the arch-gravity dam. Therefore the latter has a higher resistance to earthquakes. For the arch-gravity dam the 3D analyses are essential in order to evaluate the response, because these structures are characterized by a 3D motion due to the interaction between the arch effect and the cantilever behavior.

The third part reports the application of the method to the Tower of Pisa. The geophysical tests performed in the square of Miracles over the years have characterized very well the first 40 m of ground, arriving up to 70 m but without finding more rigid soil to apply accelerograms recorded on

rock. In this work are presented the preliminary results on the soil-structure interaction of the Leaning Tower of Pisa, including the results of new geophysical tests and the definition of the seismic input.

The analysis of seismic records allowed to identify three experimental vibration modes, namely two bending modes with a frequency of around 1 Hz in N-S and E-W directions, and a vertical mode with a frequency of 3 Hz. This result is quite new since only in Nakamura's study of 1999 a vertical mode was identified.

A Finite element model of the Tower was built, and with a sensitivity analysis on the value of the shear modulus G it was possible to evaluate the foundation impedances for which there is a good agreement between numerical and experimental values. The model was built considering the inclination of the Tower, and gave better results than the method used by Grandori and Faccioli which neglected it.

The model updating of the model allowed to obtain frequencies with a very good agreement with the experimental values; at the same time it has to be highlighted that a complete study should be based on re-designing the instruments network located on the Tower in order to provide enough data to build the actual modal shapes of the Tower.

The seismic input for the Pisa's area was defined in terms of response spectra using a hybrid approach combining the probabilistic and the deterministic one. The response spectra were obtained on rigid soil, while the Tower lies on soft deposits. Therefore, it is necessary to evaluate the seismic input at the ground level, using the available informations on the soil layers. Since the existing geophysical tests, mainly Down-Hole and Cross-Hole, did not allow to find a rigid layer to apply the accelerograms on rock, a new geophysical test was performed in November 2015. This was an Array test which permitted to find a more rigid layer (Vs=500

m/s) at a depth of around 100 m, while the analysis of the single stations provided results on the amplification of motion: two fundamental amplification peaks were found, one with a frequency of 1,3 Hz, corresponding to the interface between the layers at a depth of 40 m, and the second with a frequency of 0,3 Hz relating to a deeper interface, probably a seismic bedrock which lies at around 500 m of depth.

Under the hypothesis that the bedrock lies at this depth, the accelerograms at the ground level were evaluated through a site response analysis which allowed to evaluate the acceleration time histories at the ground level. These show major amplification at structural periods in the range 0,5s-2s (low frequencies). Non-linear dynamic analyses performed on the Tower with the selected records, allowed to evaluate the average displacement recorded on the top of the Tower, which has a value of 30,4 mm; the minimum and the maximum value of the top displacement are respectively 16,7 and 64,2 mm. The results of the preliminary analyses performed on the Tower permit to state that the effects of the horizontal seismic input is not critical for the Tower, because it does not cause a significant increase of the destabilizing vertical loads.

Future developments include the selection of new sets of accelerograms recorded on soil class B, which can be applied in a site response analysis directly on the *Engineering seismic base layer*, for which there are more data since it was identified in the geophysical test. Moreover, the Tower will be equipped with new instruments which will enable to perform a new dynamic identification in order to obtain modal shapes which will help to better re-assess the soil-structure interaction and to re-calibrate the numerical model.

References

[1] Daniell JE, Khazai B, Wenzel F, Vervaeck A. The CATDAT damaging earthquakes database. Nat Hazards Earth Syst Sci 2011;11:2235–51.

[2] Smith, K. (2013). Environmental hazards: assessing risk and reducing disaster. Routledge.

[3] Sandi H.; 1986: Report of the Working Group "Vulnerability and risk analysis for individual structures and systems" of the European Association of Earthquake Engineering. In: Proceedings of 8th European Conference on Earthquake Engineering, Lisbon.

[4] Japan Commission on Large Dams (JCOLD). 4th Quick Report on Dams, April 1, 2011.

[5] USGS MCS intensity map of Tohoku earthquake, 2011. http://earthquake.usgs.gov/earthquakes/

[6] Harder, Leslie F.; Keith I. Kelson; Tadahiro Kishida; Robert Kayen (6 June 2011). "Preliminary Observations of the Fujinuma Dam Failure Following the March 11, 2011 Tohoku Offshore Earthquake, Japan" . Geotechnical Extreme Events Reconnaissance (GEER). GEER Association. Retrieved 15 July 2011.

[7] UNESCO website, http://whc.unesco.org/en/statesparties/it.

[8] Parisi, F., & Augenti, N. (2013). Earthquake damages to cultural heritage constructions and simplified assessment of artworks. *Engineering Failure Analysis*, *34*, 735-760.

[9] Douglas, J., Seyedi, D. M., Ulrich, T., Modaressi, H., Foerster, E., Pitilakis, K., ... & Loli, M. (2015). Evaluation of seismic hazard for the

assessment of historical elements at risk: description of input and selection of intensity measures. *Bulletin of Earthquake Engineering*, *13*(1), 49-65.

[10] ANSA, "L'Aquila, ecco il più grande cantiere d'Europa", from Ansa.it, 7/04/2016.

[11] Direttiva Presidenza del Consiglio dei Ministri, 9 febbraio 2011, *Linee guida per la valutazione e la riduzione del rischio sismico del patrimonio culturale con riferimento alle Norme tecniche per le costruzioni di cui al decreto del Ministero delle Infrastrutture e dei trasporti del 14 gennaio 2008*.

[12] Norme Tecniche per le Costruzioni, Decreto 14/01/2008 del Ministero delle Infrastrutture: Norme Tecniche per le Costruzioni, GU n.29 del 04/02/2008.

[13] Julian J. Bommer (2002): Deterministic Vs. Probabilistic Seismic Hazard Assessment: An Exaggerated And Obstructive Dichotomy, Journal of Earthquake Engineering, 6:S1, 43-73.

[14] Sabetta, F. (2014). Seismic hazard and design earthquakes for the central archaeological area of Rome. Bulletin of Earthquake Engineering, 12(3), 1307-1317.

[15] C.A.Cornell, "Engineering seismic risk analysis", Bulletin of the Seismological Society of America, Vol. 58, No.5, pp. 1583-1606, October 1968.

[16] Meletti C, Galadini F, Valensise G, Stucchi M, Basili R, Barba S, Vannucci G, Boschi E (2008) A seismic source zone model for the seismic hazard assessment of the Italian territory. Tectonophysics 450: 85–108. ISSN 0040–1951: doi:10.1016/j.tecto.2008.01.003

[17] M.Ordaz, "Some integrals useful in probabilistic seismic hazard analysis", Bulletin of the Seismological Society of America, Vol. 94, No.4, pp. 1510-1516, 2004.

[18] Gutenberg, B. and C.F. Richter, Seismicity of the Earth and Associated Phenomena, Princeton, N.J.: Princeton University Press, 1954 (2nd ed.).

[19] Sabetta F., Pugliese A., "Estimation of response spectra and simulation of Non-stationary earthquake ground motion", Bulletin of the Seismological Society of America, Vol. 86, No.2, pp. 337-352, 1996.

[20] Bindi, D., Pacor, F., Luzi, L., Puglia, R., Massa, M., Ameri, G., & Paolucci, R. (2011). Ground motion prediction equations derived from the Italian strong motion database. Bulletin of Earthquake Engineering, 9(6), 1899-1920.

[21] Akkar, S., Bommer, J.J., "Empirical equations for the prediction of PGA, PGV, and spectral accelerations in Europe, the Mediterranean region, and the Middle East.", Seismological Research Letters, No.81 Vol.2, 2010, pp.195-206.

[22] Akkar S, Bommer JJ (2007a) Prediction of elastic displacement response spectra in Europe and the Middle East. Earthquake Eng Struct Dyn 36(10):1275–1301.

[23] Akkar S, Bommer JJ (2007b) Empirical prediction equations for peak ground velocity derived from strong-motion records from Europe and the Middle East. Bull Seism Soc Am 97(2):511–530.

[24] Akkar, S., Sandıkkaya, M. A., & Bommer, J. J. (2014). Empirical ground-motion models for point-and extended-source crustal earthquake scenarios in Europe and the Middle East. Bulletin of earthquake

engineering, 12(1), 359-387.

[25] Cauzzi, C., Faccioli, E., "Macroseismic intensities for seismic scenarios, estimated from instrumentally based correlations", First European Conference on Earthquake Engineering and Seismology, Geneva, Switzerland, 2006, pp.3-8.

[26] Luzi, L., S. Hailemikael, D. Bindi D, F. Pacor, F. Mele, F. Sabetta (2008), *ITACA (ITalian ACcelerometric Archive): A Web Portal for the Dissemination of Italian Strong-motion Data*, Seismological Research Letters, 79(5), 716–722. Doi: 10.1785/gssrl.79.5.716

[27] Ordaz, M., Martinelli, F., Agular, A., Arboleda, J., Meletti, C., & D'Amico, V. (2014). CRISIS 2014. Program for computing seismic hazard. Instituto de Ingeniería. Universidad Nacional Autónoma de México.

[28] Meletti, C., Calvi, G. M., & Stucchi, M. (2007). Project S1–Pursuing the assistance to DPC to complete and manage the Hazard Map of OPCM 3274/2003 and design of further development–Final Report, INGV (in Italian). Interactive Maps of Seismic Hazard (WebGis) on http://esse1.mi.ingv.it/.

[29] Pacor, F., Paolucci, R., Ameri, G., Massa, M., & Puglia, R. (2011). Italian strong motion records in ITACA: Overview and record processing. Bulletin of Earthquake Engineering, 9(6), 1741-1759.

[30] Final Report Volume 5 Elicitation Summaries Ground Motion Characterisation (SP2), "Probabilistic Seismic Hazard Analysis for Swiss Nuclear Power Plant Sites (PEGASOS Project)", Wettingen, 31 July 2004, 65-66.

[31] Sabetta F., Lucantoni A., Bungum H., Bommer J.J. (2005)

Sensitivity of PSHA results to ground-motion prediction relations and logic-tree weights. Soil Dyn. Earthq. Eng. 25:317–329.

[32] Krinitzsky, E. L. (2002). How to obtain earthquake ground motions for engineering design. Engineering Geology, 65(1), 1-16.

[33] Basili, R., et al. The European Database of Seismogenic Faults (EDSF) compiled in the framework of the Project SHARE. 2013.

[34] Meletti, C., Rovida, A., D'Amico, V., & Stucchi, M. (2014). Modelli di pericolosità sismica per l'area italiana:"MPS04-S1" e "SHARE". Progettazione Sismica.

[35] Robin K. McGuire, Probabilistic seismic hazard analysis and design earthquakes: Closing the loop, Bulletin of the Seismological Society of America, Vol. 85, No. 5, pp. 1275-1284, October 1995

[36] Bazzurro, P., & Cornell, C. A. (1999). Disaggregation of seismic hazard. Bulletin of the Seismological Society of America, 89(2), 501-520.

[37] Di Sarno, L., Elnashai, A. S., & Manfredi, G. (2011). Assessment of RC columns subjected to horizontal and vertical ground motions recorded during the 2009 L'Aquila (Italy) earthquake, Engineering structures, 33(5), 1514-1535.

[38] Newmark NM, Hall WJ. Earthquake spectra and design. EERI Monograph Series, Oakland (CA): EERI; 1982.

[39] Bozorgnia, Y., & Campbell, K. W. (2004). The vertical-to-horizontal response spectral ratio and tentative procedures for developing simplified V/H and vertical design spectra. Journal of Earthquake Engineering, 8(02), 175-207.

[40] Linda Al Atik and Norman Abrahamson, M.EERI An Improved Method for Nonstationary Spectral Matching, Earthquake Spectra: August 2010, Vol. 26, No. 3, pp. 601-617.

[41] Vanmarcke, E. H., Cornell, C. A., Gasparini, D. A., & Hou, S. (1976). SIMQKE: A program for artificial motion generation. Civil Engineering Department, Massachusetts Institute of Technology, 94720-1710.

[42] Mucciarelli M, Spinelli A, Pacor F (2004) Un programma per la generazione di accelerogrammi sintetici "fisici" adeguati alla nuova normativa. 11◦ Congresso Nazionale l'Ingegneria Sismica in Italia, Genova 25–29 gennaio 2004.

[43] Bommer, J. J., & Acevedo, A. B. (2004). The use of real earthquake accelerograms as input to dynamic analysis. Journal of Earthquake Engineering, 8(spec01), 43-91.

[44] Iervolino, I., Galasso, C., & Cosenza, E. (2010). REXEL: computer aided record selection for code-based seismic structural analysis. Bulletin of Earthquake Engineering, 8(2), 339-362.

[45] Smerzini, C., & Paolucci, R. (2011). Research Project DPC–RELUIS 2010-2013. SIMBAD: a database with Selected Input Motions for displacement-Based Assessment and Design–2nd release.

[46] Acunzo G., Pagliaroli A., Scasserra G., In-spector: un software di supporto alla selezione di accelerogrammi naturali spettro-compatibili per analisi geotecniche e strutturali, Proceedings of 33rd conference of GNGTS, Bologna, Italy, 2014.

[47] Shome, N., Cornell, C. A., Bazzurro, P., & Carballo, J. E. (1998). Earthquakes, records, and nonlinear responses. Earthquake Spectra, 14(3),

469-500.

[48] Seismosoft (2016) "SeismoMatch - A computer program for spectrum matching of earthquake records". Available from URL: www.seismosoft.com.

[49] Hancock, J., Watson-Lamprey, J., Abrahamson, N. A., Bommer, J. J., Markatis, A., McCOY, E. M. M. A., & Mendis, R. (2006). An improved method of matching response spectra of recorded earthquake ground motion using wavelets. Journal of earthquake engineering, 10(spec01), 67-89.

[50] Lilhanand, K., & Tseng, W. S. (1987). Generation of synthetic time histories compatible with multiple-damping design response spectra. In Structural mechanics in reactor technology.

[51] Website of ICOLD, International Commission On Large Dams, http://www.icold-cigb.org/.

[52] ITCOLD, Comitato Nazionale Italiano delle Grandi dighe, Rapporto finale della commissione "Riabilitazione delle dighe", 2012.

[53] Fiorentino G., Furgani L., Nuti C., Sabetta F., Seismic hazard and use of strong motion time histories for dam seismic analyses, Second European Conference on Earthquake Engineering and Seismology, 25-29 august, Istanbul (Turkey).

[54] Fiorentino G., Furgani L., Nuti C., Analisi dinamiche non lineari di dighe in calcestruzzo, Giornate AICAP 2014, 22-24 maggio, Bergamo (Italy).

[55] Norme Tecniche per la progettazione e la costruzione degli sbarramenti di ritenuta (dighe e traverse), Decreto 26/06/2014 del

Ministero delle Infrastrutture, GU n.156 del 08/07/2014.

[56] ICOLD, “Selecting seismic parameters for large dams”. Guidelines, Revision of Bulletin 72, Committee on Seismic Aspects of Dam Design, International Commission on Large Dams, Paris, 2010.

[57] DISS Working Group (2015). Database of Individual Seismogenic Sources (DISS), Version 3.2.0: A compilation of potential sources for earthquakes larger than M 5.5 in Italy and surrounding areas. http://diss.rm.ingv.it/diss/, © INGV 2015 - Istituto Nazionale di Geofisica e Vulcanologia - All rights reserved; DOI:10.6092/INGV.IT-DISS3.2.0.

[58] Rovida A, Camassi R, Gasperini P, Stucchi M (2011) CPTI11, the 2011 version of the Parametric Catalogue of Italian Earthquakes. Milano, Bologna, http://emidius.mi.ingv.it/CPTI.

[59] Quantum, G. I. S. (2013). Development Team, 2012. Quantum GIS geographic information system. Open source geospatial foundation project. Free Software Foundation, India.

[60] Fenves, G., & Chopra, A. K. (1986). Simplified analysis for earthquake resistant design of concrete gravity dams. Earthquake Engineering Research Center, University of California.

[61] Chopra A.K., Zhang L.. "Earthquake-induced base sliding of concrete gravity dams." Journal of structural Engineering 117.12 (1991): 3698-3719.

[62] Basili, M., & Nuti, C. (2009). A simplified procedure to estimate base sliding of concrete gravity dams induced by an earthquake. in Eccomas, Thematic Conference on Computational Methods in Structural Dynamics and Earthquake Engineering.

[63] Nuti C., Pinto P.E.. Analisi dell'interazione terreno struttura in condizioni sismiche. Roma : s.n., 1989.

[64] Mazzoni, S., McKenna, F., Scott, M. H., & Fenves, G. L. (2006). OpenSees command language manual. Pacific Earthquake Engineering Research (PEER) Center.

[65] Leclerc M., Léger P., Tinawi R.. "Computer aided stability analysis of gravity dams—CADAM." Advances in Engineering Software 34.7 (2003): 403-420.

[66] ICOLD. Bulletin 155 - Guidelines for use of numerical models in dams engineering. Paris : ICOLD, 2012.

[67] Dassault Systèmes Simulia Corp. Abaqus Analysis User's Manual, Abaqus 6.11.1993.

[68] Chopra, A. K. (2012). Earthquake analysis of arch dams: factors to be considered. Journal of Structural Engineering, 138(2), 205-214.

[69] ITCOLD, Italian Commission on Large Dams, Risk analysis - Applied researches and possible applications of risk analysis methods to Italian situation, 2004.

[70] Lee, J., & Fenves, G. L. (1998). A plastic damage concrete model for earthquake analysis of dams. Earthquake engineering & structural dynamics,27(9), 937-956.

[71] Burland J.B., Viggiani C.: Osservazioni sul comportamento della Torre di Pisa, Rivista Italiana di Geotecnica, N.3, 1994, pp. 179-200.

[72] Burland J.B; Jamiolkowski M.; Viggiani C, Leaning Tower of Pisa: Behaviour after Stabilization Operations, International Journal of

Geoengineering. Case Histories, 2009.

[73] Incarico Prot. n. JAM2763.32/tp del 29.01.1993; Studio per la definizione del terremoto di verifica per le analisi sulla Torre di Pisa; Relazione finale a cura di: prof. G. Grandori e prof. E. Faccioli.

[74] Incarico Prot. n. JAM4804.158/tp del 09.12.1999; Approfondimento degli studi sul problema sismico; Relazione a cura di: prof. G. Grandori, prof. E. Faccioli e ing. R. Paolucci.

[75] Incarico Prot. n. JAM2660.12 tp del 11.03.1992, Modellazione numerica della struttura della Torre – calibrazione dello stick model dell'elevazione e analisi a spettro di risposta; Doc. RAT-DMM-1340/95.

[76] Macchi G., Ghelfi S. (2005) , Problemi di consolidamento strutturale, Bollettino d'arte "La torre di Pisa. gli studi e gli interventi che hanno consentito la stabilizzazione della Torre di Pisa", Volume III, parte II.

[77] Settis, Salvatore. La torre restituita: gli studi e gli interventi che hanno consentito la stabilizzazione della Torre di Pisa. Istituto poligrafico e Zecca dello Stato, 2006.

[78] Polvani G. et al. - "Ricerche e Studi sulla Torre Pendente di Pisa" - Istituto Geografico Militare. Firenze 1971.

[79] Incarico Prot. n. JAM2660.1/tp del 11.03.1992 Rilevamento architettonico della Piazza dei Miracoli e della Torre di Pisa i risultati generali dell'attività sul campo, VOL. I.

[80] de Silva, F., Ceroni, F., Sica, S., Rosaria, P. M., & Silvestri, F. (2015). Effects of soil-foundation-structure interaction on the seismic behavior of monumental towers: the case study of the Carmine bell tower

in Naples. Rivista Italiana Di Geotecnica, 3, 3-27.

[81] Veletsos, A. S., & Wei, Y. T. (1971). Lateral and rocking vibration of footings.Journal of Soil Mechanics & Foundations Div.

[82] ISMES, "Indagini strutturali sulla Torre di Pisa: prove dinamiche"", Comitato per gli interventi di consolidamento e restauro della Torre di Pisa, Incarico Prot. n. JAM2660.9/tp del 11.03.1992.

[83] Macchi G, Ghelfi S (2006) Indagini strutturali. In: La Torre Restituita, vol III. Bolletino d' Arte, Ministry of Cultural Affairs, Rome, Italy.

[84] Cestelli Guidi, C., Croce, A., Skempton, A. W., Schultze, E., Calabresi, G., & Viggiani, C. (1971). Caratteristiche geotecniche del sottosuolo della Torre. Ricerche e studi sulla Torre pendente di Pisa ed i fenomeni connessi alle condizioni d'ambiente, 1, 179-200.

[85] Viggiani C., Pepe M. C. (2005), Il sottosuolo della Torre, Bollettino d'arte "La torre di Pisa. gli studi e gli interventi che hanno consentito la stabilizzazione della Torre di Pisa", Volume II.

[86] Prova con dilatometro sismico (SDMT), 16 marzo 2015, Opera della Primaziale Pisana.

[87] Foti, S. (2003). Small strain stiffness and damping ratio of Pisa clay from surface wave tests. Geotechnique, 53, 455-461.

[88] Castellaro, S., Mulargia, F. " How Far from a Building Does the Ground-Motion Free-Field Start? The Cases of Three Famous Towers and a Modern Building", Bulletin of the Seismological Society of America, 100(5A), 2080-2094, 2010.

[89] Wathelet, M. (2005). GEOPSY Geophysical Signal Database for Noise Array Processing. Software, LGIT, Grenoble, Fr.

[90] Della Monica G., Basile F., Carlucci G., Piersanti M., Relazione indagine sismica passiva Campo dei Miracoli (Pisa), Laboratory of Geophysics and Geotechnics (LGG), Department of Science, Roma Tre University, 2016.

[91] Foti, S., Lai, C. G., Rix, G. J., & Strobbia, C. (2014). Surface wave methods for near-surface site characterization. CRC Press.

[92] Nakamura, Y. (1989). A method for dynamic characteristics estimation of subsurface using microtremor on the ground surface. Railway Technical Research Institute, Quarterly Reports, 30(1).

[93] Mylonakis, George, Sissy Nikolaou, and George Gazetas. "Footings under seismic loading: Analysis and design issues with emphasis on bridge foundations." Soil Dynamics and Earthquake Engineering 26.9 (2006): 824-853.

[94] Nakamura, Y., Gurler, E. D., Saita, J., “Dynamic characteristics of leaning tower of Pisa using microtremor - Preliminary results”, Proceedings of the 25th JSCE Earthquake Engineering Symposium, Tokyo (Japan), Vol. 2, 1999, pp. 921–924.

[95] Atzeni, C., Bicci, A., Dei, D., Fratini, M., Pieraccini, M. “Remote survey of the leaning tower of Pisa by interferometric sensing”, IEEE Geoscience and Remote Sensing Letters, 7(1), 185-189, 2010.

[96] Duhamel, P., Vetterli, M. “Fast Fourier Transforms: A Tutorial Review and a State of the Art", Signal Processing, 19, 259-299, 1990.

[97] Bartelletti, R., Fiorentino, G., Lanzo, G., Lavorato, D., Marano, G.

C., Monti, G., Nuti, C., Quaranta, G., Sabetta, F., Squeglia, N., “Behavior of the leaning tower of Pisa: analysis of experimental data from structural dynamic monitoring”, Proceedings of the 2nd International Symposium “Advances in Civil and Infrastructure Engineering”, Vietri sul Mare (Italy), June 2015.

[98] Bartelletti R., Fiorentino G., Lanzo G., Lavorato D., Marano G. C., Monti G., Nuti C., Quaranta G., Sabetta F., Squeglia N., Behavior of the leaning Tower of Pisa: insights on seismic input and soil-structure interaction, ACE 2015 Advances in Civil Engineering, 12-13 giugno 2015, Vietri sul Mare (SA).

[99] Grinsted, A., Moore, J.C., Jevrejeva, S. "Application of the cross wavelet transform and wavelet coherence to geophysical time series”, Nonlinear Processes in Geophysics, 11, 561-566, 2004.

[100] Wolf J.P., Dynamic Soil-Structure Interaction, Prentice Hall, New York, NY, USA, 1985.

[101] Bommer, J. J., Akkar, S., & Kale, Ö. (2011). A model for vertical-to-horizontal response spectral ratios for Europe and the Middle East. Bulletin of the Seismological Society of America, 101(4), 1783-1806.

[102] Margottini, C., Molin, D., & Serva, L. (1992). Intensity versus ground motion: a new approach using Italian data. Engineering Geology, 33(1), 45-58.

[103] Kramer, S. L. (1996). Geotechnical earthquake engineering. Pearson Education India.

[104] Yoshida, N. (2015). Seismic Ground Response Analysis. Springer.

[105] Impavido M., Lancellotta R., Lo Presti D., Pallara R., Esecuzione di prove relative alla caratterizzazione del comportamento meccanico dell'argilla di Pisa, Department of Structural Engineering, Polytechnic University of Turin, March 1993.

[106] Lanzo G., Personal communication, 2016.

[107] Hashash Y.M.A., Groholski D.R., Philips C.A., Park D. (2015) – DEEPSOIL 6.1: User Manual and Tutorial. pp. 84.